Mathematical Model of Plant Nutrient Uptake

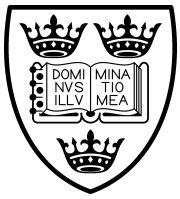

Tiina Roose

Linacre College

University of Oxford

A thesis submitted for the degree of

Doctor of Philosophy

Michaelmas 2000

Emale ja Mammile

To my mother and grandmother

Acknowledgements

I would like to thank my supervisors Dr. Andrew Fowler and Dr. Peter Darrah for supervising this thesis, Professor Jim Briden of the Environmental Change Institute for awarding me the Director's Studentship, my boyfriend Dr. David Smith for proof reading the manuscript and for the support throughout the years. I would also like to thank all the members of the Oxford Centre for Industrial and Applied Mathematics, the Oxford Centre for Mathematical Biology and Linacre College who made my stay at Oxford very enjoyable.

Abstract

This thesis deals with the mathematical modelling of nutrient uptake by plant roots. It starts with the Nye-Tinker-Barber model for nutrient uptake by a single bare cylindrical root. The model is treated using matched asymptotic expansion and an analytic formula for the rate of nutrient uptake is derived for the first time. The basic model is then extended to include root hairs and mycorrhizae, which have been found experimentally to be very important for the uptake of immobile nutrients. Again, analytic expressions for nutrient uptake are derived. The simplicity and clarity of the analytical formulae for the solution of the single root models allows the extension of these models to more realistic branched roots. These models clearly show that the "volume averaging of branching structure" technique commonly used to extend the Nye-Tinker-Barber with experiments can lead to large errors. The same models also indicate that in the absence of large-scale water movement, due to rainfall, fertiliser fails to penetrate into the soil. This motivates us to build a model for water movement and uptake by branched root structures. This model considers the simultaneous flow of water in the soil, uptake by the roots, and flow within the root branching network to the stems of the plant. The water uptake model shows that the water saturation can develop pseudo-steady-state wet and dry zones in the rooting region of the soil. The dry zone is shown to stop the movement of nutrient from the top of the soil to the groundwater. Finally we present a model for the simultaneous movement and uptake of both nutrients and water. This is discussed as a new tool for interpreting available experimental results and designing future experiments. The parallels between evolution and mathematical optimisation are also discussed.

Contents

List of Figures

List of Tables

Chapter 1

Introduction

The Industrial Revolution was made possible because of the intensification of farming that occurred as agriculture became progressively more scientific. The efficient production of food is required so that some of the population can concentrate on matters not directly related to producing their daily bread. The productivity of agriculturally important plants is often limited by the availability of essential mineral nutrients in the soil. In this thesis mathematical models for the uptake of nutrients by plants will be developed. Modelling of these processes is not just a matter of pure scientific interest, but will also help in the development of solutions to real life problems. One of the important developments in recent years has been the need to decrease the fertilisation of soils due to the excessive costs of such practices, popularity of organically produced crops and tighter legislation on environmental pollution. This has resulted in what is known as precision agriculture, which deals with the customisation of fertiliser application for individual fields. However, this can successfully be done only within a framework of sophisticated experimental and modelling initiatives.

Farmers have over 2000 years tried to improve the soil quality and resulting crop productivity by applying fertilisers to the soil. Initially they applied plant ash and lime [80]. In modern times the fertiliser industry provides them with a wide range of man-made fertilisers, since soils in different areas in the world have different problems. For example in Europe the limiting nutrient for crop productivity is often nitrogen due to large losses through leaching and volatilisation. However, in the areas of highly weathered soils like the West African Savannah, Malaya, and South Australia, phosphate is thought to be limiting [93]. High rates of fertilisation can lead to problems of groundwater pollution and surface runoff of fertilisers. The nutrient losses as high as 50% due to the irrigation have been recorded [17].

Recently non-food applications of plants, that utilise the property of plant roots to take up substances from the soil, have also started to emerge. For example, so called *hyper-accumulator plants* can take up large amounts of heavy metals from the

soil by essentially the same mechanism as they take up nutrients [82]. Problems that can be tackled using these plants include the removal of radioactive contamination and explosive residues from the soil and the mining of gold. Such use of plants is thought to be one of the most promising and cost effective techniques for cleaning large areas of moderately and heterogeneously contaminated soil [124].

Radioactive contamination of the environment is a very serious problem and can be very expensive to remove. In recent years British Nuclear Fuels Ltd. (BNFL) has started to use plants, more specifically sunflowers, spinach, sugar beet and Indian mustard, to remove radioactive residues from the soil [36]. BNFL hopes to reduce the radioactivity by $10-20\%$ using plants. A similar technique is used by the United States Army to remove explosive residues, more specifically TNT, from the soil at their firing ranges [124]. A novel plant-based method of gold-mining has been developed in New Zealand [4]. Although normal background levels of gold in plants hardly ever exceed 10 ng per g dry weight, hyper-accumulator plants can have levels as high as 1 mg per g dry tissue. This corresponds to a gold crop value of 16 000 dollars per hectare [4].

In this chapter a short introduction into the soil science and plant nutrition required for understanding this thesis will be presented. As Chapter 2 is an analysis of the current standard mathematical model of nutrient uptake by a single root, the Nye-Tinker-Barber model, this will not be discussed here. Instead this introduction will concentrate on the biology of plant nutrient uptake.

1.1 Plant Nutrients

In addition to water, plants require thirteen essential mineral nutrients to complete their full lifecycle. That is, although in the absence of an essential nutrient it may be possible for the plant to grow, it will definitely not be possible for it to reproduce successfully. Essential mineral nutrients can be divided into macro- and micro-nutrients depending on the amount required by plants. The macro-nutrients are: nitrogen, potassium, sulphur, phosphorus, magnesium and calcium, and micro-nutrients are: iron, zinc, manganese, copper, molybdenum, boron, and chlorine. Typical requirements for macro-nutrients are presented in Table 1.1. We will now discuss briefly the importance of the different macro-nutrients to plants based on the evidence presented by Marschner [80] and Barber [6].

Nitrogen is one of the most important nutrients for plants since it is a constituent of proteins and nucleic acids. Thus, large quantities of nitrogen are taken up by plant roots. However $50-70\%$ of the nitrogen available to the plant during one season will be available in the following season via plant residues. Therefore nitrogen is the

Nutrient	Requirement [% of dry weight]
N	2-5%
K	2-5%
S	0.1-0.5%
P	0.3-0.5%
Mg	0.15-0.35%
Ca	0.1-5%

Table 1.1: Typical agricultural plant nutrient requirements after Marschner [80].

limiting nutrient in areas where the soil is intensively farmed resulting in little of the crop being returned to the soil, e.g., Europe. Potassium is known to control the water potential in plant cells. Sulphur is a constituent of the amino acids cyteine and methionine and thus directly involved in metabolic reactions. It can also bond covalently to proteins and thus stabilise their structure. Phosphorus is another plant nutrient that is involved with metabolic functions. It is utilised in reactions where energy is transferred involving ATP, adenosine triphosphate, the principal energy-carrying molecule in cells. Magnesium is a necessary component of chlorophyll and cell membranes. Calcium promotes cell membrane integrity and is central to the strength of cell walls.

1.2 Soil

Soil is the natural, unconsolidated, mineral and organic matter occurring on the surface of the Earth [3], i.e., soil consists of mineral solid particles mixed with organic matter and water. The standard soil classification is carried out based on the size distribution of mineral solid particles which can be divided into three different categories; sand, silt and clay. The characteristic size distribution of sand, silt and clay particles is shown on Table 1.2.

Particle	Diameter [mm]	Number per 1 gramme of soil	Surface area [cm^2] per 1 gramme of soil
Sand	$0.05 - 2$	$89 \times 10^5 - 112$	$15 - 308$
Silt	$0.002 - 0.05$	2×10^7	888
Clay	< 0.002	4×10^{11}	4×10^5(non-swelling)
			8×10^6(swelling)

Table 1.2: Soil particle sizes [6].

The bigger particles, i.e., sand and silt particles are mostly responsible for providing anchorage to the plant (see Table 1.2). Due to their relatively large size they

also increase the porosity of the soil, hence enabling the air and water to move more easily. Clay particles are the smallest particles in the soil. Due to their chemical structure they are important in retaining plant nutrient ions in the soil.

Plants obtain most of their nutrients in the form of ions dissolved in the soil pore water [6], [95], [129], [104]. However large amounts of the nutrient ions in the soil can in fact be bound to soil particles, particularly clay particles. This binding is possible because the clay particle surface has a net negative charge, thus causing it to attract nutrient ions to the surface forming a diffuse double layer (see Figure 1.1). The nutrient ions in the soil solution and the ones bound to the charged soil particles can be shown to be in equilibrium, so that if the concentration of nutrients in the soil solution is reduced due to nutrient uptake by plants, the soil has the ability to resupply nutrients. This concentration stabilising effect is called buffering. Various excellent textbooks on soil science present the details of soil chemistry and nutrient buffering ([80], [95], [129] and many others).

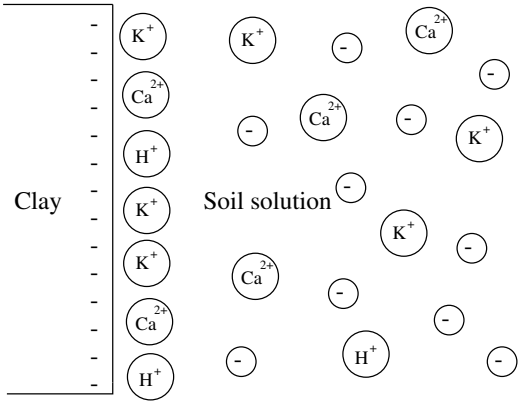

Figure 1.1: Electrical double layer. If a nutrient ion such as potassium is removed from the soil solution via plant uptake, it is replaced by the release of potassium ions from the clay surface. The free clay surface sites are then occupied by protons (hydrogen ions) or by other cations [104].

1.3 Root Structure and Nutrient Uptake

Anyone who has done any gardening or has grown pot-plants will know that plant roots form extensive branching structures in the soil (see Figure 1.2). It is the complexity of these structures which has limited the modelling of nutrient uptake by plants.

The root branching structure develops when roots emerging from the seed form lateral branches from their side. These lateral branches will in turn develop branches of their own. The branching occurs in the middle part of the root since near the base

Figure 1.2: Root branching structure. Photo of a tree root system from `http://community.webshots.com/photo/179628/179732` web community user `sam48`.

and tip of the root there are non-branching regions. These non-branching regions develop as a result of root internal hormones [80], although the exact biochemical mechanism of their formation still remains unknown. Typically, the roots emerging from the seed, the zero order roots, are the thickest roots in the system and they connect the root system to the stem of the plant. The radius of the higher order lateral branches is progressively smaller.

Many authors have tried to discover the branching rules that would mimic the root branching structures observed in nature. Therefore a wide range of branching models have been developed with the aim of visualising the evolution of the root branching structures since the observation of its development *in situ* is difficult. These models are based on sets of hypothetical heuristic branching rules to describe the development of branching structure in time.

One of the very first branching models was developed in the early seventies by Hackett and Rose [54], [55] with the aim of calculating the length and volume of different orders of sub-branches as a function of time. At that time it was of course difficult to visualise the results of these computations due to the very primitive computers available to soil scientists. Later, one of the very first attempts to visualise the two dimensional branching structure development was done by Lungley [77]. Now the

relatively wide availability of personal computers has brought forward more models of three dimensional branching structures [28], [115]. However, only very few of them have attempted to model water and nutrient uptake [23], [33], [78], [46], because the simultaneous computational treatment of a three dimensional branching structure and nutrient and water uptake is extremely difficult. Thus, most of these models, instead of calculating nutrient uptake by root branching structure, estimate the effectiveness of the simulated root structure by using the simplistic "nutrient depletion cylinder" approach [78]. The width of the nutrient depletion cylinders is taken to be equal to the diffusional length scale of the nutrient considered. By drawing these depletion cylinders onto a branching image the authors are able to estimate the amount of overlap between the nutrient depletion cylinders. Using this estimate on the nutrient depletion cylinder overlap the authors can classify the root structures for their ability to obtain nutrients without competition.

The structure of roots on the small, single root, scale is presented schematically in Figure 1.3. The outer layer of the root surface consists of the epidermal layer of small cells. This layer sometimes has structures known as root hairs which extend into the soil. Root hairs are long ($\approx 100-1500$ μm) and thin ($\approx 5-17$ μm). Because they extend the overall root surface area by over five times, they are thought to be very influential in nutrient uptake [6], [80]. Just inside the epidermis is the cortex, which makes up most of the root mass and consists of large cells with air between them. The endodermis is a thin dense layer of cells. It's function is to control the flow between the stele and the epidermis thus waterproofing the stele, since water and nutrients can only move through it via plasmalemma membranes. The stele contains the "piping" network for plant nutrient and water flow between leaves and roots. The flow of water and nutrients from the roots to the leaves takes place along the xylem vessels (see Chapter 7 and 8). Sugars, carboxylic acids etc. however are transported from the leaves along the phloem tubes to the roots.

There are essentially two different ways that nutrients can be moved from the root surface into the xylem vessels, from where they can move to the stems and leaves [80], [129]. The two different pathways are: the apoplasmic pathway which is passive, and the symplasmic pathway which is active. In the apoplasmic pathway, the nutrient ion movement is driven by diffusion or mass flow in inter-cellular spaces. In the inter-cellular spaces the nutrient ions can become bound to the cell membranes and thus leave the apoplasmic pathway. In the symplasmic pathway the nutrient ions are moved within the cytoplasm and possibly also the vacuole of the cortical cells. The two pathways merge at the endodermis where all the nutrient ions have to pass through the symplasmic pathway, because the dense tissue of the Caspian band has limited inter-cellular space.

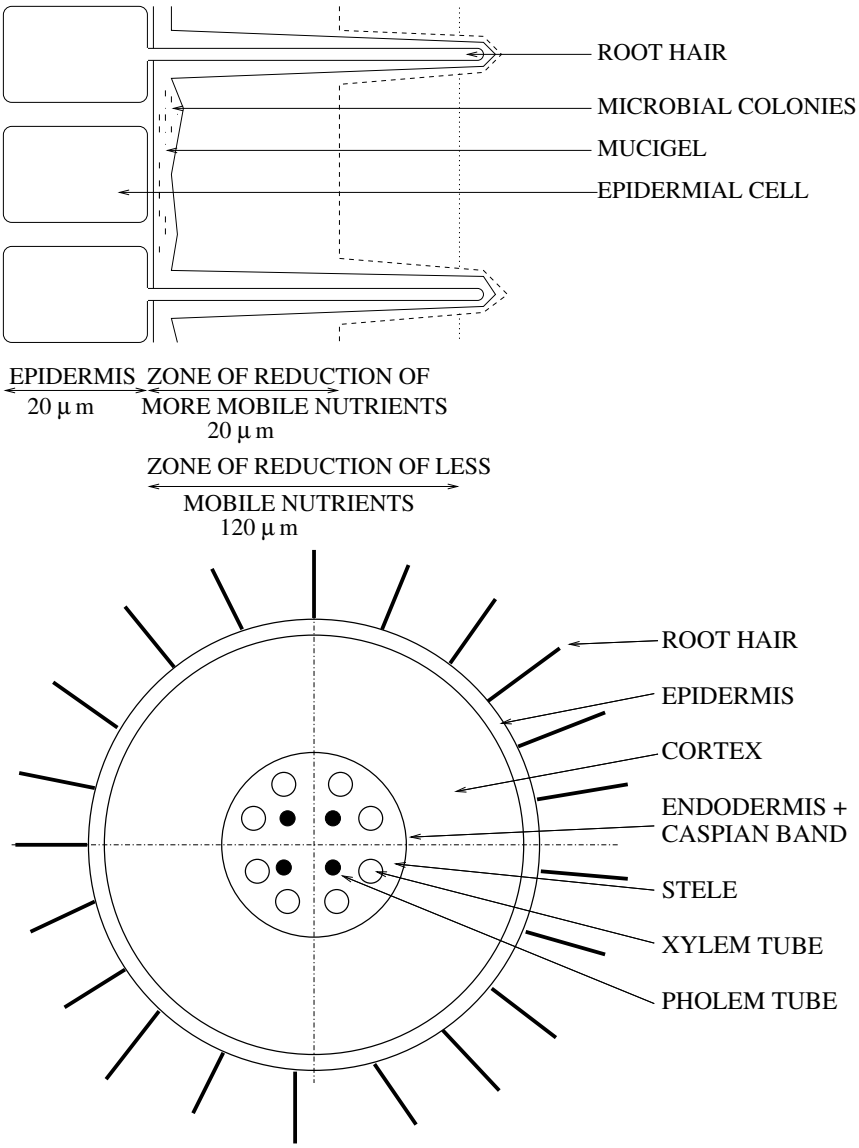

Figure 1.3: Simplified structure of the root surface and the soil around it; side-view after [22] and top-view after [80].

Although many fundamental biological experiments for quantifying the transport processes in each of the different pathways have been conducted, as yet no microscopic derivation of the relationship between extra-root nutrient concentration and nutrient uptake has been possible. However heuristic uptake-concentration relations have been determined experimentally. Typical relationships between the root surface concentration and nutrient uptake show a saturating uptake relation, i.e., when the root surface nutrient concentration increases indefinitely, the rate of nutrient uptake reaches a plateau after which the increase in root surface nutrient concentration is ineffective in increasing uptake. It is also observed that when the nutrient concentra-

tion is below some measured threshold value the nutrient uptake stops. It is this type of heuristic, experimentally measured, nutrient uptake law which is used in models for nutrient uptake, such as the Nye-Tinker-Barber model, that will be presented in Chapter 2.

Many scientists have come to a conclusion that the uptake of immobile ions like phosphate is enhanced by the existence of mycorrhizae in the soil. Mycorrhizal fungi can provide a parallel path for nutrient uptake and it has been found that the presence of mycorrhizal fungi can double plant growth [113], [110], [47]. Mycorrhizae are fungi that live in the soil and form symbiotic links with plant roots. They form extensive, but very fine, fungal networks that can cover large areas of soil. Indeed, the largest single living organism in the world is thought to be a mycorrhizal fungus *Armillaria ostoyae*, popularly known as the honey mushroom, one specimen of which is thought to be over 2400 years old and covers 890 hectares of soil in the Malheur National Forest in the Blue Mountains of eastern Oregon [29]. Mycorrhizae are particularly helpful to plants in taking up relatively immobile nutrients such as phosphate [80], [113], [127]. In fact some experimental studies have found that mycorrhizae increase the phosphate uptake by a factor of four [113], [110], [47].

1.4 Outline of the Thesis

In this thesis a systematic method for calculating simultaneous nutrient and water uptake by root branching structures will be presented. Our aim in this thesis is to first describe the processes on a small, single root scale, and then expand the modelling to a large, root branching structure scale. This technique is sometimes also known as upscaling. For the purposes of transparency and clarity, the model will be built up piece by piece. In Chapter 2 the Nye-Tinker-Barber model for nutrient uptake by a single cylindrical root in fully saturated soil will be presented and an approximate solution to the flux of nutrient into the root found using the method of matched asymptotic expansions. In Chapter 3, the single cylindrical root model will be expanded to include the effect of root hairs and mycorrhizae on nutrient uptake. In Chapter 4, a model for root branching structure development and nutrient uptake by it in the absence of competition will be presented. Chapter 5 presents the model for nutrient competition and uptake by a static root distribution that will serve as an introduction for the following Chapter 6, which deals with nutrient uptake by a root branching structure in the presence of competition and fertilisation. One of the conclusions in Chapters 5 and 6 is that fertiliser movement is highly restricted when the vertical water movement due to rainfall is neglected. Thus, in Chapters 7 and 8 a model for water movement in the soil and uptake by a root branching structures

will be developed with the aim of linking it to the nutrient uptake model. Finally a model for simultaneous water and nutrient uptake by a root branching structure is presented in Chapter 9.

Validation of theoretical models by comparison with experimental evidence is a central tenet of science. However, this has only been partially possible for the models presented in this thesis due to a lack of experiments in which all the relevant experimental conditions have been controlled. Where possible, comparison between theory and experiments has been made and one of the main successes of the models presented here is their ability to explain previously unresolved discrepancies between experiments and theory.

Chapter 2

Nye-Tinker-Barber Model

In this chapter the model for nutrient uptake by single cylindrical root first developed by Nye, Tinker [95], [129], and Barber [6] is presented. The parametrisation of the model and analysis of it at different parameter limits will also be carried out. The aim of the parametrisation is to find an analytical expression for nutrient uptake by the root as a function of time at all physiologically important parameter regimes. The validity of analytic approximations will be verified by comparison with numerical solutions of the full model.

2.1 Model for Soil-Root Interaction

2.1.1 Modelling Assumptions

The Nye-Tinker-Barber model for nutrient uptake by a single cylindrical root in an infinite extent of the soil was first developed in 1970s [6], [95], [129]. In that model the nutrient uptake by the root is considered to occur from the liquid (water) phase of the soil only. The soil is assumed to be homogeneous and isotropic, and the changes in the moisture conditions are assumed to be negligible since the soil is assumed to be fully saturated. The classical Nye-Tinker-Barber model also neglects the effect of root exudates, microbial activity, mycorrhizae etc. on the plant nutrient uptake and nutrient movement in the soil. The movement of nutrient to the root surface takes place by convection due to water uptake by the plant, and by diffusion of nutrient ions in the soil pore water.

The relation between the net influx of nutrients into the root and the concentration of nutrients at the root surface is described in the Nye-Tinker-Barber model by an experimentally measured heuristic Michaelis-Menten type uptake law. Classically the Michaelis-Menten kinetics (see Murray [88]) is derived from the most basic enzyme catalysed reaction. This is compatible with the nutrient "carrier" theory in which the nutrients are considered to be carried through the root surface cell membranes

by so called nutrient "carrier" proteins. Thus, the Michaelis-Menten uptake law appears to include the characteristics of symplasmic pathway of nutrients into the root. Alternatively, the Michaelis-Menten type uptake law could also be derived similarly to that of Langmuir adsorption isotherm in physical chemistry [7]. This describes the fraction of free and bound nutrient ion binding sites on a membrane or on a solid surface. This results in what looks like a Michaelis-Menten type equilibrium condition for the number of binding sites that are bound at any given time. However, as mentioned, the Nye-Tinker-Barber model does not consider the exact mechanism of nutrient uptake by the plant root, instead it uses an experimentally measured heuristic Michaelis-Menten nutrient uptake law.

2.1.2 Derivation of the Soil-Root Interaction Model

The soil volume surrounding the root can be divided into three different fractions: solid, liquid, and gas. We will define ϕ_s to be the volume fraction of the soil taken up by the solid (i.e. sand, silt and clay particles), ϕ_l the volume fraction of soil taken up by the liquid, and ϕ_g the volume fraction of gas (air) in the soil. In the absence of other phases, i.e., microbes, mucigel etc., the conservation of soil volume gives

$$\phi_s + \phi_l + \phi_g = 1. \tag{2.1}$$

The porosity ϕ of the soil is defined as

$$\phi_l + \phi_g = \phi \quad \text{or} \quad \text{alternatively} \quad \phi = 1 - \phi_s. \tag{2.2}$$

Soil is described as fully saturated if the pore space is full of water, i.e., $\phi = \phi_l$.

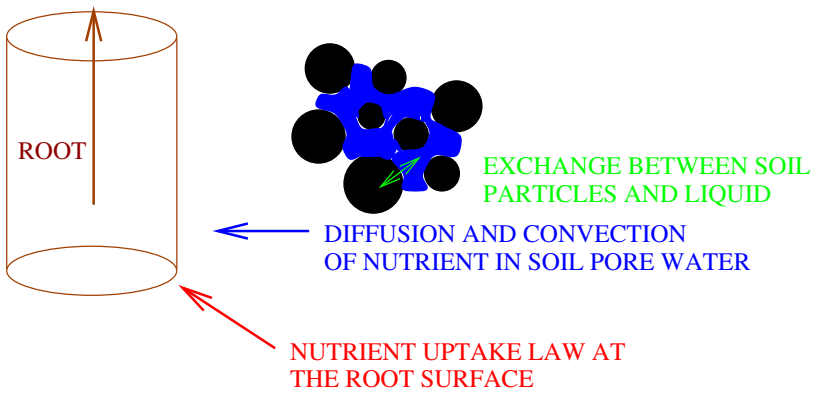

Figure 2.1: Movement of nutrients to the root surface.

Nutrients in the solid phase (see Figure 2.1) can be exchanged with the liquid phase, and can, in principle, also diffuse in the solid phase. However, the diffusion of

ions in this phase is usually very slow and from now on we will neglect it [95], [129]. Thus the equation for the ions in the solid phase in absence of diffusion within that phase is

$$\frac{\partial c_s}{\partial t} = d_s, \tag{2.3}$$

where c_s is the amount of ions in the solid form (mass per unit volume of soil), and d_s is the rate of liquid-solid inter-facial ion transport.

Nutrients in the liquid phase of the soil are carried to the surface of the root by water flow and also by diffusion in the soil pore water. Hence, the equation for ions in the liquid phase is given by

$$\frac{\partial}{\partial t}(\phi_l c_l) + \nabla \cdot (c_l \mathbf{u}) = \nabla \cdot (\phi_l D \nabla c_l) + d_l, \tag{2.4}$$

where c_l is the nutrient concentration in the liquid phase of the soil, d_l is the rate of solid-liquid inter-facial ion transport, $\mathbf{u}$ is the Darcy flux of water in the soil, i.e., volume flux of water, and D is the diffusion coefficient in the liquid phase of the soil. According to Nye and Tinker [95], [129] and Barber [6], the diffusion coefficient in the soil is thought to be equal to the diffusion coefficient in free liquid, D_f, times a tortuosity factor f, i.e., $D = D_f f$. The tortuosity factor can be taken to be $f \approx \phi_l^d$ with $1 \lesssim d < 2$, however, typically it is evaluated experimentally for different values of soil moisture [129].

By adding up the two previous equations for nutrient in liquid and solid phases, we obtain an equation for the overall amount of nutrient in the soil

$$\frac{\partial}{\partial t}(\phi_l c_l + c_s) + \nabla \cdot (c_l \mathbf{u}) = \nabla \cdot (\phi_l D \nabla c_l) + d_s + d_l. \tag{2.5}$$

Assuming mass conservation during the inter-facial transport of ions, i.e., the ions which leave the solid phase all enter the liquid phase, an instantaneous jump condition is given by

$$d_s + d_l = 0. \tag{2.6}$$

We call the attachment of ions to the solid particles *adsorption* and de-attachment of ions from the solid particles into the water *desorption*. We take the rates of adsorption and desorption from the solid phase to be proportional to the concentration of ions in the phases from which the ions are leaving. If the rate of adsorption from the liquid phase into the solid phase is k_a and the rate of desorption is k_d we have

$$d_s = k_a c_l - k_d c_s = \frac{(k_a/k_d)c_l - c_s}{(1/k_d)}, \tag{2.7}$$

where $1/k_d$ is the desorption time. Assuming that $1/k_d$ is very small, i.e., that the desorption is very fast, we obtain

$$c_s = \frac{k_a}{k_d} c_l = b c_l, \tag{2.8}$$

where $b = \frac{k_a}{k_d}$ is also called the soil buffer power [6], [75], [95].

Hence, the equation (2.5) in terms of c_l becomes

$$(b + \phi_l)\frac{\partial c_l}{\partial t} + \nabla \cdot (c_l \mathbf{u}) = \nabla \cdot (D\phi_l \nabla c_l). \tag{2.9}$$

Noting $c_l = c$ and writing equation (2.9) in radial polar coordinates we get

$$(b + \phi_l)\frac{\partial c}{\partial t} - \frac{aV}{r}\frac{\partial c}{\partial r} = D\phi_l \frac{1}{r}\frac{\partial}{\partial r}(r\frac{\partial c}{\partial r}), \tag{2.10}$$

where a is the radius of the root. The water flux is given by $\mathbf{u} = -aV/r$, which derives from the law of mass conservation for water, i.e., $\nabla \cdot \mathbf{u} = 0$. The quantity V is the Darcy flux of water into the root. The quantity $D_{\text{eff}} = \dfrac{D_f f \phi_l}{\phi_l + b}$ is called the effective diffusion coefficient [6], [95] and when $b >> 1$ it simplifies to $D_{\text{eff}} \approx \dfrac{D_f f \phi_l}{b}$.

2.1.3 Initial and Boundary Conditions

2.1.3.1 Boundary Condition at the Root Surface

Experiments show that the uptake of nutrients at the root surface is bounded above when the root surface concentration is increased indefinitely. The measurements also indicate that there is a critical level of root surface concentration below which the nutrient flux into the root stops and the plant will start bleeding out nutrients into the soil. The experimentally measured, heuristic Michaelis-Menten type nutrient uptake boundary condition is therefore given by

$$\phi_l D\frac{\partial c}{\partial r} + Vc = \frac{F_m c}{K_m + c} - E \quad \text{at} \quad r = a, \tag{2.11}$$

where c is the concentration of nutrient in the liquid phase of the soil, F_m is the maximum flux of nutrient into the root, K_m is the Michaelis-Menten constant that is equal to the root surface nutrient concentration when the flux of nutrient into the root is half of the maximum possible, $E = \dfrac{F_m c_{\min}}{K_m + c_{\min}}$, where $c_{\min}$ is the minimum concentration when the nutrient uptake by the roots stops, and a is the radius of the root.

2.1.3.2 Initial Condition and the Boundary Condition away from the Root

At the time $t = 0$ we will assume a uniform distribution of nutrients in the liquid phase of the soil. Hence, the initial condition can be written as

$$c = c_0 \quad \text{at} \quad t = 0 \quad \text{for} \quad a < r < \infty. \tag{2.12}$$

For all later times the boundary condition far away from the root surface[1] will be taken to be equal to the initial undisturbed concentration, i.e.,

$$c \to c_0 \quad \text{as} \quad r \to \infty \quad \text{for} \quad t > 0. \tag{2.13}$$

2.2 Non-dimensionalisation and Parameter Estimation

The Nye-Tinker-Barber model described above is a diffusion-convection equation with non-linear boundary condition. Because of this non-linearity Nye and Tinker [95], [129] and Barber [6] were forced to solve this model numerically. Numerical solution to this model is relatively straightforward using for example an implicit finite difference scheme [87]. However, the numerical solution needs to be calculated separately for each parameter configuration. This, in addition to being very time consuming, has been the limiting factor in expanding the model to include more realistic root structures, i.e., root branching structures. In this chapter we first non-dimensionalise the model to find out which parameter combinations influence the solution to the model and then find analytic approximations to the solution at various different parameter limits. Having an analytic formula will then enable us, in the following chapters, to expand the modelling from single cylindrical root scale to the root branching structure scale.

2.2.1 Non-dimensionalisation

Choosing time-, space-, and concentration-scale as follows

$$t = \frac{a^2(\phi_l + b)}{D\phi_l} t^*, \quad r = ar^*, \quad c = K_m c^*, \tag{2.14}$$

where c^*, t^* and r^* are dimensionless nutrient concentration, time, and radial variables, respectively, we obtain (after dropping *s) the following dimensionless model

$$\frac{\partial c}{\partial t} - Pe \frac{1}{r} \frac{\partial c}{\partial r} = \frac{1}{r} \frac{\partial}{\partial r} (r \frac{\partial c}{\partial r}), \tag{2.15}$$

[1] From now on we call this boundary condition the nutrient far-field boundary condition.

with boundary conditions

$$\frac{\partial c}{\partial r} + Pe\, c = \lambda \frac{c}{1+c} - \epsilon \quad \text{at} \quad r = 1, \tag{2.16}$$

$$c \to c_\infty \quad \text{as} \quad r \to \infty \quad \text{for} \quad t > 0. \tag{2.17}$$

The dimensionless initial condition is given by

$$c = c_\infty \quad \text{at} \quad t = 0 \quad \text{for} \quad 1 < r < \infty. \tag{2.18}$$

The dimensionless parameters in above equations are defined as

$$Pe = \frac{aV}{D\phi_l}, \quad \lambda = \frac{F_m a}{DK_m\phi_l}, \quad \epsilon = \frac{Ea}{DK_m\phi_l}, \quad c_\infty = \frac{c_0}{K_m}. \tag{2.19}$$

Hence instead of 8 dimensional parameters we are left with only 4 dimensionless parameters. The most important of those is the Péclet number, Pe, and it shows the balance between the water movement V, and diffusion $D\phi_l$ over the typical length-scale a [41]. The parameter λ is the dimensionless nutrient uptake parameter, c_∞ is the dimensionless nutrient far-field concentration, and ϵ is the parameter showing the minimum concentration when the nutrient uptake stops.

2.2.2 Parameter Estimation

The nutrient ion diffusion coefficient in free water, D, is the same for most nutrients and so also is the Darcy flux of water, V, at the root surface. Hence, the Péclet number, Pe, for the given soil moisture condition ϕ_l will vary mostly with the root radius a.

If $a << D\phi_l/V$, then the convection term in our model is negligible. Similarly, if $a >> D\phi_l/V$, then the diffusion is not important in our system and most nutrients are carried to the surface of the root by the mass flow. A typical value of nutrient diffusion in free water is $D_f \approx 10^{-5}$ cm^2 s^{-1} and Darcy's flux[2] is $V \approx 10^{-7}$ cm s^{-1}. The Péclet number is given in terms of D_f and V by the expression

$$Pe = \frac{aV}{D_f f \phi_l}, \tag{2.20}$$

where f is the nutrient diffusion impedance factor.

Typical values of the volume fraction of liquid in soils ϕ_l and impedance factor f suitable for crop growth are in the range 0.1 to 0.5 [67]. Thus, the Péclet number

[2]In reality the Darcy's flux varies with the water content of the soil ϕ_l, but the variation for current model is taken to be small since the soil is assumed to be fully saturated and typically $\phi_l = 0.1 - 0.5$.

satisfies $0.02[\text{cm}^{-1}]a[\text{cm}] < Pe < 0.3[\text{cm}^{-1}]a[\text{cm}]$, where a is the root radius in centimetres. Hence, in order to have a Péclet number of order 1 or bigger the radius of the root would have to be of order 3 cm or bigger. Typical root radius of agricultural plants, such as maize, beans, wheat etc., are $0.0005 - 0.06$ cm. Hence, the Péclet number is of order $10^{-5} - 10^{-2}$, i.e., very small.

Péclet number terms can also almost always be neglected compared to the terms containing λ, since λ depends linearly on root radius a. In order to have $aV/D\phi_l = Pe < \lambda = F_m a/(DK_m\phi_l)$ we need to have $V < F_m/K_m$. This is the case for typical agricultural plants (see Table 2.2) for all nutrients, except calcium in which case $\lambda \sim Pe$. Thus, in the case of calcium, one can neglect the $O(Pe)$ terms in the main diffusion-convection equation, but not in the root surface boundary condition.

2.2.3 Dimensional Parameter Estimation for Maize

In Table 2.1 the nutrient dependent coefficients for the maize plant, *Zea mays* L., are presented after [6], [111]. Non SI units are used because of their relative popularity in the soil science textbooks.

Nutrient	c_0	b	F_m	K_m	$c_{\min}$	$\frac{a^2(\phi_l+b)}{D\phi_l}$
Unit	μmol cm^{-3}	-	μmol cm^{-2}s^{-1}	μmol cm^{-3}	μmol cm^{-3}	s
N	5	1.0	10^{-5}	0.025	0.002	578
K	0.046	39	3×10^{-5}	14×10^{-3}	1.6×10^{-3}	17467
S	0.1	2	3×10^{-7}	10^{-2}	≈ 0	1020
P	2.9×10^{-3}	239	3.26×10^{-6}	5.8×10^{-3}	9×10^{-5}	10^5
Mg	10^{-3}	1.2	4×10^{-6}	0.15	≈ 0	666
Ca	0.8×10^{-3}	156	10^{-6}	4	≈ 0	69466

Table 2.1: Dimensional parameter estimation for maize. c_0 is the initial concentration of nutrient in the soil solution, b is the soil buffer power, F_m is the maximum rate of uptake, K_m is the Michaelis-Menten coefficient, $c_{\min}$ is the minimum level of concentration when the nutrient uptake stops, and $a^2(\phi_l + b)/D\phi_l$ is the relevant time-scale which corresponds to time 1 in dimensionless time units.

In Table 2.1 we also show the natural timescale of the model $[t] = a^2(\phi_l+b)/(D\phi_l)$ [s]. It shows the time when the diffusion profile has spread over length-scale proportional to the radius of the root. As we can see the natural timescales of the model are small, with the longest timescale being found for phosphorus and it is approximately 1 day. The shortest timescale is for nitrogen which is just around 10 minutes. When compared with the maize vegetative timescale (3 months), the natural timescales are relatively short and therefore the solutions of the greatest interest from the agricultural point of view are long time, i.e., dimensionless time $t >> 1$, solutions of the model.

2.2.4 Dimensionless Parameters for Macro-nutrients

The diffusion coefficient, D_f, of different nutrients in water is typically 10^{-5} [cm^2 s^{-1}]. We will take the root radius to be 0.02 [cm], which is the average root radius used by Barber [6]. Estimates of typical dimensionless parameter values for macro-nutrient uptake by maize plants are presented in Table 2.2.

Nutrient	λ	c_∞	ϵ
N	8.8	200	7.4×10^{-7}
K	47	3.28	5.7×10^{-7}
S	0.66	10	$<< 1$
P	12.32	0.5	4.98×10^{-8}
Mg	0.55	6.7×10^{-3}	$<< 1$
Ca	5.5×10^{-3}	2×10^{-4}	$<< 1$

Table 2.2: Dimensionless parameter estimation for maize where $D = D_f f$ with $D_f = 10^{-5}$ cm^{2}s^{-1} and $\phi_l = f = 0.3$.

The previous parameter estimation was given for maize, but in Table 2.3 the parameter estimation for phosphate uptake by different agriculturally important plants is shown after [6].

Plant	F_m	K_m	$c_{\min}$	λ	ϵ	c_∞
Soybean	6.4×10^{-7}	2.7×10^{-3}	0.04×10^{-7}	5.2	7.02×10^{-7}	1.07
Lettuce	10.6×10^{-7}	2×10^{-3}	0.24×10^{-7}	11.7	1.27×10^{-7}	1.45
Tomato	49.9×10^{-7}	6.1×10^{-3}	0.12×10^{-7}	18.2	3.22×10^{-7}	0.475

Table 2.3: Soybean, lettuce, and tomato dimensional and dimensionless parameters for phosphate [6].

2.3 Summary of the Dimensionless Model

We recall that the full dimensionless model was given by:

$$\frac{\partial c}{\partial t} - Pe\,\frac{1}{r}\frac{\partial c}{\partial r} = \frac{1}{r}\frac{\partial}{\partial r}(r\frac{\partial c}{\partial r}), \tag{2.21}$$

$$\frac{\partial c}{\partial r} + Pe\,c = \frac{\lambda c}{1+c} - \epsilon \quad \text{at} \quad r = 1, \tag{2.22}$$

$$c \to c_\infty \quad \text{as} \quad r \to \infty, \tag{2.23}$$

$$c = c_\infty \quad \text{at} \quad t = 0 \quad \text{for} \quad 1 < r < \infty. \tag{2.24}$$

We found that for most agricultural plants, the dominating mechanism for the transport of nutrient to the root surface was diffusion since $Pe << 1$. Hence, the

terms containing the Péclet number can be neglected in our system unless the far-field concentration $1 + c_\infty > \lambda/Pe$, or when $\lambda < Pe$ for $c_\infty << 1$, that is when convection becomes important in the root surface boundary condition. In the next few sections we will consider the cases when all Péclet number terms and also ϵ terms are neglected, since $\epsilon < Pe << 1$. We will then aim to derive an analytic expression to the nutrient flux, $F(t) = \dfrac{\partial c}{\partial r}|_{r=1}$ as a function of parameters λ, c_∞, and time t. However, we will return to discuss the solution to this problem for $Pe \sim O(1)$ later on in the chapter once we have analysed the $Pe << 1$ case.

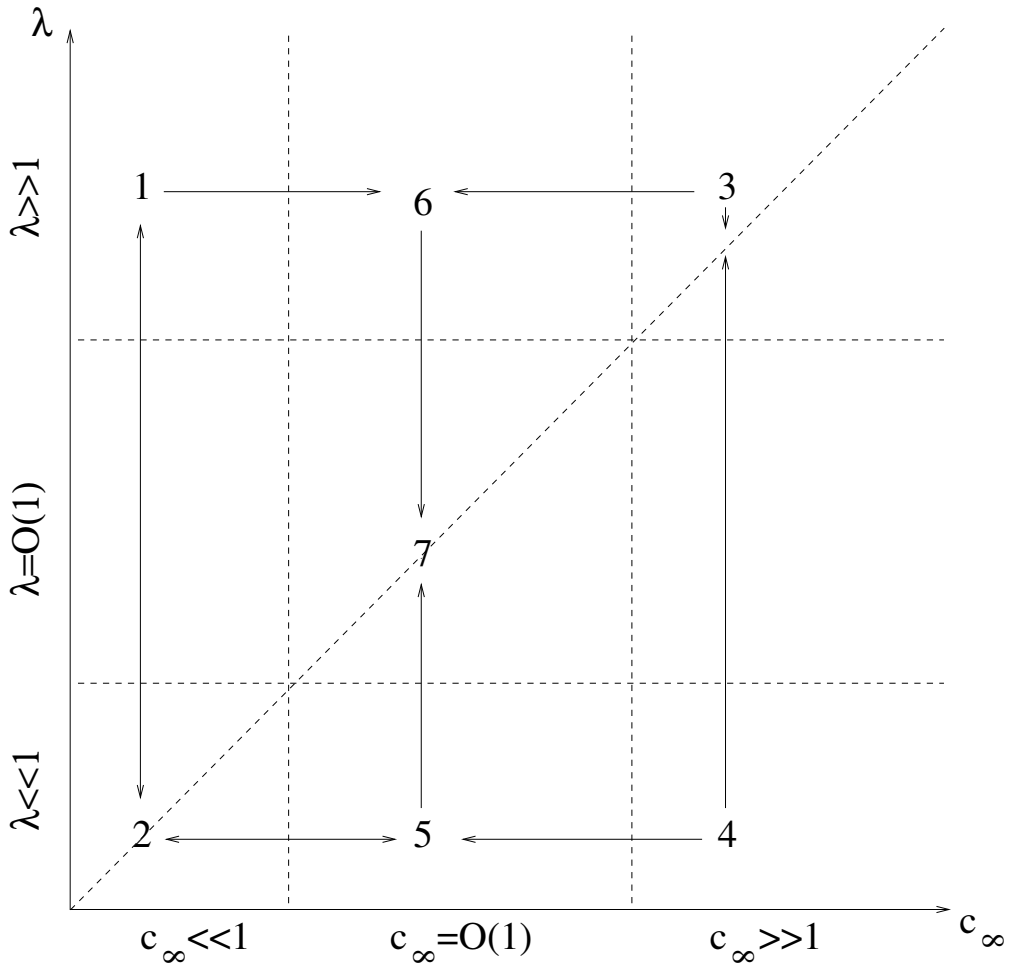

Figure 2.2: Strategy for analysing Nye-Tinker-Barber model. Numbers represent the order of approximation process.

The only environmental control variable in this system is the dimensionless far-field nutrient concentration c_∞, which depends on the nutrient level in the soil. It is therefore natural to consider the cases when c_∞ is large, small, or order one. In dimensional terms this corresponds to $c_0 >> K_m$, $c_0 << K_m$, or $c_0 = O(K_m)$. The

other principal parameter we vary, for these three cases of c_∞, is the nutrient uptake coefficient λ, which is mainly determined by the plant species.

Neglecting all terms which are of order Pe and ϵ, the system reduces to

$$\frac{\partial c}{\partial t} = \frac{1}{r}\frac{\partial}{\partial r}(r\frac{\partial c}{\partial r}), \tag{2.25}$$

$$\frac{\partial c}{\partial r} = \frac{\lambda c}{1+c} \quad \text{at} \quad r = 1, \quad \text{and} \quad c \to c_\infty \quad \text{as} \quad r \to \infty. \tag{2.26}$$

$$c = c_\infty \quad \text{at} \quad t = 0 \quad \text{for} \quad 1 < r < \infty. \tag{2.27}$$

The strategy for analysing this model will be to find the approximate model for c_∞ large and small. Then the solutions to those approximate models will be found together with the approximations for λ small and large. Then corresponding solutions at both c_∞ limits will be joined up to give the approximations for λ large and small for all values of c_∞. Finally, one is able to arrive at the expression for flux of nutrient into the root at all c_∞ and λ limits. A schematic presentation of this strategy is shown in Figure 2.2.

2.4 The Limit $c_\infty << 1$

Let us first consider the case when $c_\infty << 1$ which corresponds in dimensional terms to the Michaelis-Menten coefficient K_m being much larger then the far-field concentration c_0. Rescaling $c = c_\infty C$ we find that the model in terms of scaled concentration variable C becomes

$$\frac{\partial C}{\partial t} = \frac{1}{r}\frac{\partial}{\partial r}(r\frac{\partial C}{\partial r}), \tag{2.28}$$

$$\frac{\partial C}{\partial r} = \frac{\lambda C}{1+c_\infty C} \quad \text{at} \quad r = 1, \quad \text{and} \quad C \to 1 \quad \text{as} \quad r \to \infty. \tag{2.29}$$

For $c_\infty << 1$ we can approximate the the root surface boundary condition, using the binomial expansion, at the leading order by

$$\frac{\partial C}{\partial r} \approx \lambda C \quad \text{at} \quad r = 1. \tag{2.30}$$

The model with this boundary condition (2.30) is in soil science textbooks [129] known as the "root absorbing power" model, and it has been used extensively to simplify the calculation of phosphate and sometimes also potassium uptake [95], [129].

The solution to this model can be found using Laplace transforms and according to [19] it is given by the following integral formula

$$C(r,t) = \frac{2}{\pi}\int_0^\infty e^{-u^2 t}\frac{J_0(ur)[uY_1(u) - \lambda Y_0(u)] - Y_0(ur)[uJ_1(u) - \lambda J_0(u)]}{[uJ_1(u) - \lambda J_0(u)]^2 + [uY_1(u) - \lambda Y_0(u)]^2}du. \tag{2.31}$$

Clearly, this analytic solution (2.31) is quite complicated and thus it is also useful to know the approximation for flux at small and large times. A large time approximation has been obtained for this and some other problems in the case of cylindrical diffusion equation by Ritchie and Sakikura [105]. Their solution involves Bessel functions, thus the complexity of it is still relatively high. However, we will now proceed to derive asymptotic approximations to the solutions in λ large and small limits in order to illustrate the different behaviours of the model at different parameter limits.

2.4.1 Approximate Solution for $\lambda >> 1$

When $\lambda >> 1$, i.e., nutrient uptake is high, we expect the gradient of nutrient concentration near the root surface to be big, i.e., $\partial C/\partial r|_{r=1} \approx \lambda >> 1$ for $C \sim O(1)$. Thus, there is a boundary layer near $r = 1$ and by rescaling the independent variables r and t to stretched variables R and T, i.e., $r = 1 + R/\lambda$ and $t = T/\lambda^2$, the problem reduces to

$$\frac{\partial C}{\partial T} = \frac{\partial^2 C}{\partial R^2} + \frac{1}{R+\lambda}\frac{\partial C}{\partial R}, \tag{2.32}$$

which at the leading order simplifies to

$$\frac{\partial C}{\partial T} = \frac{\partial^2 C}{\partial R^2}, \tag{2.33}$$

since $1/(\lambda + R) << 1$ for $\lambda >> 1$. The rescaled boundary conditions are

$$\frac{\partial C}{\partial R} = C \quad \text{at} \quad R = 0, \quad \text{and} \quad C \to 1 \quad \text{as} \quad R \to \infty, \tag{2.34}$$

and the uniform initial condition is $C = 1$ at $T = 0$ for $0 < R < \infty$.

The solution to this leading order problem (2.33)-(2.34) is given by

$$C(R,T) = \text{erf}(\frac{R}{2\sqrt{T}}) + e^{R+T}\text{erfc}(\frac{R}{2\sqrt{T}} + \sqrt{T}), \tag{2.35}$$

with the flux, $F(T) = \dfrac{\partial C}{\partial R}\dfrac{\partial R}{\partial r}\Big|_{R=0}$, of nutrient into the root given by

$$F(T) = \lambda e^T \text{erfc}(\sqrt{T}). \tag{2.36}$$

As $T \to \infty$, the concentration of nutrient at the root surface $C \to 0$ and $F \to 0$, since $e^T\text{erfc}(\sqrt{T}) \to 0$ as $T \to \infty$.

We can see the comparison of the analytic solution against the numerical simulations with the full nonlinear model and conclude that they agree quite well (see Figure 2.3 (a)) while $c \approx c_\infty$ ($C \sim 1$) and $t < 1/\lambda^2$.

For $t >> 1/\lambda^2$ the nutrient uptake is no longer of order λ since $c(1,t)$ has become small and thus $\partial c/\partial r|_{r=1} = \lambda c << 1$. At long times we could use the Ritchie and

Sakikura [105] large time solution to equations (2.28)-(2.29) in terms of Bessel functions. However, it is reasonable to obtain the result similar to theirs by considering the problem where the concentration at the root surface has dropped approximately to zero, more specifically C has dropped to less than the order 1.

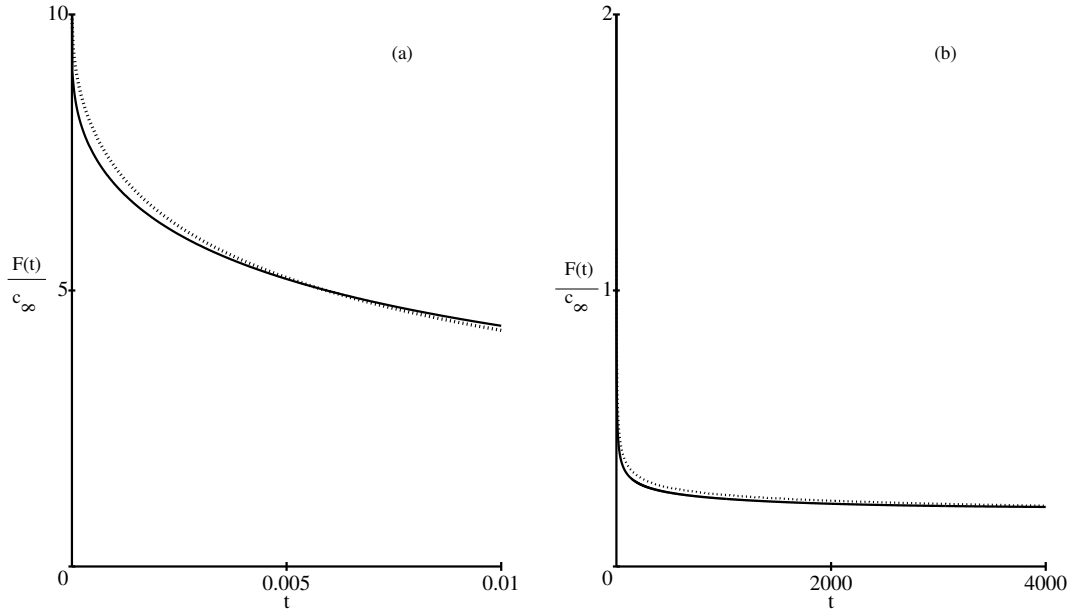

Figure 2.3: Comparison of numerical experiments (solid lines) for nutrient flux $F(t)$ for $\lambda = 10$ and $c_\infty = 0.1$ with the full non-linear model and asymptotic approximations (dashed lines). Analytic solution given by the equation (2.36) for short time (a), and by the equation (2.55) for long time (b).

2.4.1.1 Zero-sink Model

For $t > t_c \sim 1/\lambda^2$ the root surface nutrient concentration has dropped to a very low level and thus we can take the boundary condition at the root surface at the leading order to be $C = 0$ at $r = 1$, i.e., the problem to be solved is

$$\frac{\partial C}{\partial \tilde{t}} = \frac{1}{r}\frac{\partial}{\partial r}(r\frac{\partial C}{\partial r}), \tag{2.37}$$

$$C = 0 \quad \text{at} \quad r = 1, \quad \text{and} \quad C \to 1 \quad \text{as} \quad r \to \infty. \tag{2.38}$$

The initial condition for this problem would be given by the approximate solution (2.35) evaluated at $t_c \approx 1/\lambda^2$, i.e.,

$$C \approx \text{erf}(\lambda\frac{r-1}{2}) + e^{\lambda(r-1)+1}\text{erfc}(\lambda\frac{r-1}{2}+1) \quad \text{at} \quad \tilde{t} = t - t_c \approx t - \frac{1}{\lambda^2} = 0. \tag{2.39}$$

This initial condition has also a boundary layer at $r = 1$. We can approximate the initial condition by taking $C = 1$ at $\tilde{t} = 0$, since the region where $C << 1$ is very narrow. Thus the leading order initial condition is

$$C = 1 \quad \text{at} \quad \tilde{t} = 0 \quad \text{for} \quad 1 < r < \infty. \tag{2.40}$$

This model is in soil science commonly called the "zero sink" model and it is used to calculate the uptake of immobile nutrients, such as phosphate and potassium, in large scale crop models [50]. However, the justification of its applicability has not always been clearly stated. As discussed, the zero sink model with uniform initial condition is only valid when there is a fast transition in the root surface nutrient concentration to a very low level, i.e., when $t_c \sim 1/\lambda^2 << 1$. However, the region where $c << c_\infty$ must be very thin, i.e., there must be a boundary layer near the root surface, for the zero sink approximation to the full Nye-Tinker-Barber model to be valid.

The analytical solution to this zero sink model can be derived using Laplace transformations and it is, after [19], given by

$$C(r, \tilde{t}) = -\frac{2}{\pi} \int_0^\infty e^{-u^2 \tilde{t}} \frac{J_0(ur)Y_0(u) - Y_0(ur)J_0(u)}{J_0^2(u) + Y_0^2(u)} \frac{du}{u}. \tag{2.41}$$

The flux at the root surface $r = 1$ is given by

$$F(\tilde{t}) = \frac{4}{\pi^2} \int_0^\infty e^{-u^2 \tilde{t}} \frac{du}{u[J_0^2(u) + Y_0^2(u)]}. \tag{2.42}$$

According to [19] the small time flux approximation is given by

$$F_{\text{small}}(\tilde{t}) \approx (\pi \tilde{t})^{-1/2} + \frac{1}{2} + \ldots, \tag{2.43}$$

and large time flux approximation is given by

$$F_{\text{large}}(\tilde{t}) \approx 2[\frac{1}{\ln(4\tilde{t}) - 2\gamma} - \frac{\gamma}{(\ln(4\tilde{t}) - 2\gamma)^2} - O(\frac{1}{(\ln(4\tilde{t}) - 2\gamma)^3})]. \tag{2.44}$$

One could also combine in the equation (2.44) the terms containing $1/[\ln(4\tilde{t}) - 2\gamma]$ using the binomial expansion properties and the resulting approximation for large times would become

$$F_{\text{large}}(\tilde{t}) \approx \frac{2}{\ln(4\tilde{t}) - \gamma + O(\frac{1}{(\ln(4\tilde{t}) - 2\gamma)})}. \tag{2.45}$$

Hence at the leading order the approximation can also be written as

$$F_{\text{large}}(\tilde{t}) \approx \frac{2}{\ln(4e^{-\gamma}\tilde{t})}. \tag{2.46}$$

The zero-sink model has a singularity for flux at the time-origin[3] $t = 0$. However in our case the flux is finite at the time-origin, more specifically $F(0) = \lambda$. The heuristic procedure of introducing a small shift of the time origin would easily overcome this problem. This can be approximately done by writing the solution as $F(t + t_0)$, where we choose the small time shift t_0 such that the initial condition for the flux is satisfied.

Hence, we get from the small time flux approximation using two terms

$$\frac{1}{\sqrt{\pi t_0}} + \frac{1}{2} = \lambda, \tag{2.47}$$

which gives for the time-shift

$$t_0 = \frac{1}{\pi(\lambda - 1/2)^2}, \tag{2.48}$$

and the small time t flux becomes

$$F_{\text{small}}(t) = \frac{\lambda - 1/2}{\sqrt{\pi(\lambda - 1/2)^2 t + 1}} + \frac{1}{2}. \tag{2.49}$$

We notice that for very short times the large time solution (2.46) has a singularity at $t = 0$. Again to overcome this problem we use the heuristic procedure of introducing the time-shift $t_0 = (1/4)e^{\gamma}$. The large time approximation now becomes[4]

$$F_{\text{large}}(t) = \frac{2}{\ln(4e^{-\gamma}t + 1)}. \tag{2.50}$$

Knowing the solution to the zero model at large times and short times one can try and use a heuristic interpolation technique to find the solution that would approximate the integral (2.42) for all times. Multiplying the large and small time solutions and dividing by a weighting function, which would enable us to switch between the two limit solutions, we obtain one possible way of interpolating the solution. However, we must note that the interpolation found in this way is not unique, but for the purposes of current research possibly quite satisfactory. Hence we look at the uniform interpolation in the form

$$F(t) = \frac{F_{\text{small}}(t)F_{\text{large}}(t)}{[F^{\alpha}_{\text{small}}(t) + F^{\alpha}_{\text{large}}(t)]^{1/\alpha}}, \tag{2.51}$$

where α is some positive number. The comparison between the numerical experiment with zero model and large and small time approximations together with interpolation

[3] $\tilde{t} = t - 1/\lambda^2 \approx t$ for $\lambda >> 1$, thus $\tilde{t} \sim t$.

[4] The large time behaviour is clearly not affected by this introduction of the time-shift as for $t >> 1$ we have $(1/4)e^{\gamma}/t << 1$ and thus $\ln(4e^{\gamma}\tilde{t} + 1) \approx \ln(4e^{\gamma}\tilde{t})$.

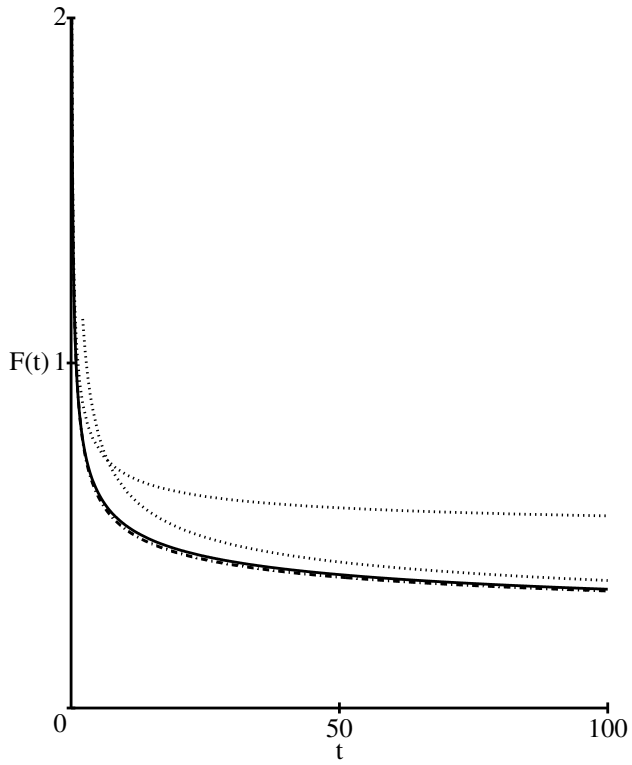

Figure 2.4: Comparison of numerical experiments with zero-sink model (solid line) and large (2.50) and small time (2.49) approximations (dashed lines) together with interpolation (2.51) for $\alpha = 3$ (dotted-dashed line).

(2.51) for $\alpha = 3$ is shown on Figure 2.4. We see that numerical solution agrees well with the uniform interpolation formulae (2.51).

In conclusion, we recall that when $c_\infty << 1$ and $\lambda >> 1$, the solution for $t << 1/\lambda^2$ is given by

$$c(1,t) \approx c_\infty e^{\lambda^2 t} \mathrm{erfc}(\lambda\sqrt{t}), \tag{2.52}$$

$$F(t) \approx \lambda c_\infty e^{\lambda^2 t} \mathrm{erfc}(\lambda\sqrt{t}). \tag{2.53}$$

For large time $t >> 1/\lambda^2$ the approximations to the root surface concentration and flux are

$$c(1,t) \approx 0, \tag{2.54}$$

$$F(t) \approx \frac{2c_\infty}{\ln(4e^{-\gamma}t + 1)}. \tag{2.55}$$

We notice that the time-range for the validity of short time solutions (2.52) and (2.53) is at most approximately 10 minutes (for phosphate $c_\infty = 0.5$ and $\lambda = 12.32$ resulting in $t_c = 6.58 \times 10^{-2}$ in dimensionless units, i.e., 11 minutes). After that the long time solutions (2.54) and (2.55) are satisfactory. In practice we are not concerned with the short time solution, although it is useful to know it.

2.4.2 Approximate Solution for $\lambda << 1$

We will now consider the case when $\lambda << 1$. For λ small we expect the region where C is less than order 1 to be larger. The asymptotic behaviour of this system turns out to be mathematically similar to that of Oseen type of problems (see [68] page 88) and is derived in terms of two length scales $r \approx 1$ and $r >> 1$. The classical Oseen problem is the problem of low Reynolds number flow past a cylinder. In this case the problem is, as will be shown also in our case, that the inner (near cylinder surface) expansion has $\ln r$ terms in it which makes it impossible to satisfy the finite far-field boundary condition. This is overcome by considering the outer variable such that to the first approximation the radius of the cylinder is negligible. Hence the first term in the outer expansion is the solution in the absence of the disturbance from the cylinder. The second term in the outer expansion represents now the disturbance to the far-field due to an infinitely thin cylinder. By matching the inner and outer solutions, one is able to arrive at a uniformly valid approximation. In this and in the following sections we will demonstrate the applicability of such Oseen approximations to the problem of nutrient uptake by cylindrical roots.

Outer Expansion

As mentioned before, we are interested in the long time solution to the nutrient uptake problem. Therefore, we rescale the time variable $t = \tau/\sigma^2$ so that τ is the long time variable since $\sigma << 1$. To find the concentration gradient far away from the root surface we now need to rescale also the space variable r to the large-scale space variable R, i.e., $r = R/\sigma$. We expect σ will be small, such that $\sigma << \lambda << 1$. We choose $\sigma = e^{-1/\lambda} << 1$ for $\lambda << 1$. The diffusion equation is invariant to this scaling and stays

$$\frac{1}{R}\frac{\partial}{\partial R}(R\frac{\partial C}{\partial R}) = \frac{\partial C}{\partial \tau}. \tag{2.56}$$

Since the root surface at $r = 1$ transforms into $R = \sigma << 1$ we find that far away from the root the root acts as an infinitely thin line sink at the origin. Thus, far away from the root the solution has no intrinsic length-scale. This suggests that we should look for a similarity type solution with similarity variable $\eta = R^2/(4\tau)$. The solution satisfying the far-field boundary condition $C \to 1$ as $\eta \to \infty$ is given by

$$C = 1 + BE_1(\eta) = 1 + BE_1(\frac{R^2}{4\tau}) \tag{2.57}$$

where $E_1(\eta) = \int_\eta^\infty (e^{-y}/y)\, dy$ is the exponential integral. The unknown coefficient B must be determined from the solution that is valid in the near root surface region. However, we will not take B to be a constant, but allow it to be a slowly varying

function in time. In other words, we allow $B'(\tau)/B(\tau) << 1$, so as to enable us to match the outer solution to the inner solution.

Inner Expansion

Rescaling back to the near root surface region, i.e., $r = R\sigma$, the long time-scale τ equation transforms to

$$\frac{1}{r}\frac{\partial}{\partial r}(r\frac{\partial C}{\partial r}) = \sigma^2\frac{\partial C}{\partial \tau}. \tag{2.58}$$

The leading $O(\sigma^0)$ solution satisfying the root surface boundary condition at $r = 1$ is given by

$$C \approx C(1,\tau) + F(\tau)\ln r + O(\sigma^2) \tag{2.59}$$

where we allow the root surface concentration $C(1,\tau)$ and flux $F(\tau)$ to depend on time τ and parameter λ, bearing in mind that σ is small, more specifically $\sigma << \lambda << 1$.

Thus,

$$\frac{\partial C}{\partial r} \approx \frac{F(\tau)}{r}, \tag{2.60}$$

and in order to satisfy the boundary condition at the root surface we have to choose

$$F(\tau) = \lambda C(1,\tau). \tag{2.61}$$

$C(1,\tau)$ and $F(\tau)$ should be determined via matching with the outer solution.

Matching

To match the inner and outer solution in the overlap region, we first have to expand the outer solution at the small, near root surface, limit. The expansion of the exponential integral at small argument η limit is given, after [1], by

$$E_1(\eta) \approx -\gamma - \ln\eta + O(\eta), \quad \text{for} \quad \eta << 1. \tag{2.62}$$

Thus, the outer solution at the inner limit is given by

$$C \approx 1 + B[-\gamma - 2\ln(\frac{R}{2\sqrt{\tau}}) + O(\frac{R}{\sqrt{\tau}})]. \tag{2.63}$$

The outer expansion in the inner limit should however be equal to the inner solution. Thus, matching the $O(\ln R)$ terms in the expansions we find that

$$-2B(\tau) = F(\tau) \quad \text{i.e.} \quad B(\tau) = -\frac{F(\tau)}{2}, \tag{2.64}$$

and matching the remaining leading order terms we get

$$C(1,\tau) = 1 - \frac{F(\tau)}{2}[-\gamma - 2\ln(\sigma) + 2\ln(2\sqrt{\tau})]. \tag{2.65}$$

Since the flux of nutrient F into the root can be written in terms of root surface nutrient concentration $F(\tau) = \lambda C(1,\tau)$, the equation above has only one unknown variable in it. Thus, the root surface nutrient concentration is given by

$$C(1,\tau) = \frac{1}{1 - \lambda(\frac{\gamma}{2} + \ln(\sigma) - \frac{1}{2}\ln(4\tau))} \tag{2.66}$$

Scaling back into the natural time variable $\sigma^2\tau = t$, after introducing the small time-shift $t_0 = (1/4)e^{\gamma}$ such that $C(1,t) = 1$ at $t = 0$, we get

$$C(1,t) = \frac{1}{1 + \frac{\lambda}{2}\ln(4e^{-\gamma}t + 1)}. \tag{2.67}$$

Since $C(1,t)$ is clearly a slowly varying function in time, then B is also slowly varying. Hence this assumption made in matching procedure holds.

To obtain the approximation to the flux we will use this approximation to the root surface concentration and substitute it into the full non-dimensional flux condition $F = \lambda c_1/(1 + c_1)$ where $c_1 = c_\infty C(1,t)$. Hence we obtain

$$c(1,t) \approx \frac{c_\infty}{1 + \frac{\lambda}{2}\ln(4e^{-\gamma}t + 1)}, \tag{2.68}$$

$$F(t) \approx \frac{\lambda c_\infty}{1 + c_\infty + \frac{\lambda}{2}\ln(4e^{-\gamma}t + 1)}. \tag{2.69}$$

The results of numerical experiments in comparison to the approximations derived, are shown in Figure 2.5. As we can see the solution agrees reasonably well with the numerical experiments conducted with the full non-linear model. The slight error at larger times is due to the leading order approximation of the non-linear boundary condition. However, we will not consider higher order terms in the approximation of the boundary condition. Instead we will tackle the problem in the following Section 2.6, when considering the large time solution at all values of c_∞ and λ.

2.5 The Limit $c_\infty >> 1$

We will now investigate the case when the nutrient far-field concentration is large, i.e., $c_\infty >> 1$ and thus $c_0 >> K_m$. We rescale $c = c_\infty C$, and the equation and boundary conditions become

$$\frac{\partial C}{\partial t} = \frac{1}{r}\frac{\partial}{\partial r}(r\frac{\partial C}{\partial r}), \tag{2.70}$$

$$\frac{\partial C}{\partial r} = \frac{\lambda}{c_\infty}\frac{C}{(C + 1/c_\infty)} \quad \text{at} \quad r = 1, \tag{2.71}$$

and

$$C \to 1 \quad \text{as} \quad r \to \infty. \tag{2.72}$$

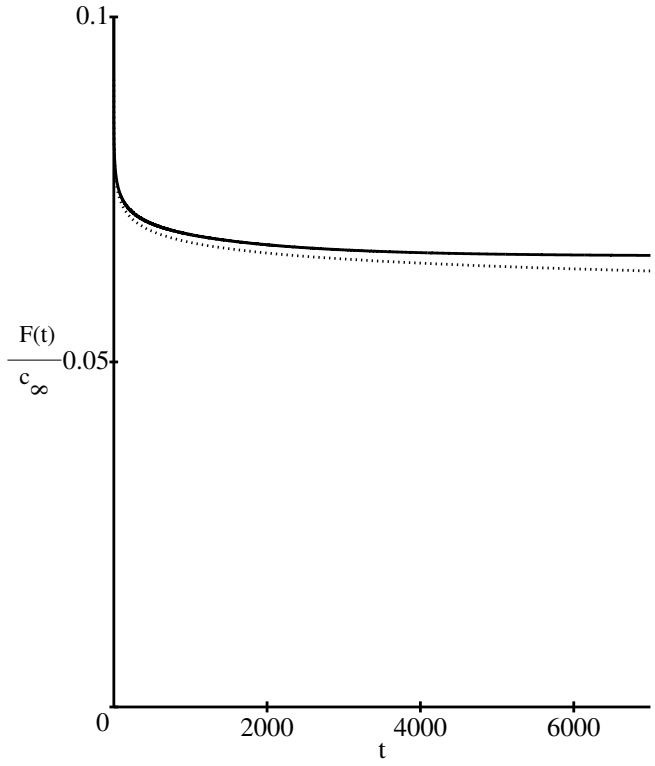

Figure 2.5: Comparison of numerical experiments (solid line) with the full non-linear model and asymptotic approximation (dashed line) given by (2.69) for $c_\infty = 0.1$ and $\lambda = 0.1$. $F(t)$ is the rate of nutrient uptake.

When $c_\infty >> 1$, i.e., $1/c_\infty << 1$, the boundary condition (2.71) can be approximated by

$$\frac{\partial C}{\partial r} = \frac{\lambda}{c_\infty} = \Lambda \quad \text{at} \quad r = 1. \tag{2.73}$$

For this case we have to solve the diffusion equation (2.70) with boundary conditions (2.72) and (2.73) together with the initial condition $C = 1$ at $t = 0$ for $1 < r < \infty$.

The solution to this model can be found using Laplace transformations [19] and it is given by the following integral formula

$$C(r,t) = 1 + \frac{2\Lambda}{\pi}\int_0^\infty (1 - e^{-u^2 t})\frac{J_0(ur)Y_1(u) - Y_0(ur)J_1(u)}{u^2[J_1^2(u) + Y_1^2(u)]}du. \tag{2.74}$$

with small time approximation given by

$$C(r,t) = 1 - 2\Lambda\sqrt{\frac{t}{r}}[\text{ierfc}\frac{r-1}{2\sqrt{t}} - \frac{(3r+1)\sqrt{t}}{4r}\text{i}^2\text{erfc}\frac{r-1}{2\sqrt{t}} + \ldots], \tag{2.75}$$

where $\text{i}^n\text{erfc}(x) = \int_x^\infty \text{i}^{n-1}\text{erfc}(\xi)\, d\xi$ are the repeated integrals of the complementary error function, i.e., $\text{ierfc}(x) = \frac{1}{\sqrt{\pi}}e^{-x^2} - x\text{erfc}(x)$, $\text{i}^2\text{erfc}(x) = \frac{1}{4}[\text{erfc}(x) - 2x\text{ierfc}(x)]$.

Large time approximation is given after [19] by

$$C(r,t) = 1 + \gamma - \frac{\Lambda}{2}\ln\frac{4t}{r^2} + O(\tfrac{1}{t}); \tag{2.76}$$

where $\gamma \approx 0.57722..$ is Euler's constant.

This solution is valid up until $C \approx 0$ at $r = 1$ and $t = t_c$, at which point terms containing $1/c_\infty << 1$ are no longer negligible in comparison to C. This critical time t_c after which $C \approx 0$ at $r = 1$ can be found from the equation (2.74) evaluated at $r = 1$ with the left hand side equated to zero. This would give us the integral relationship for t_c. If t_c is large, we can compute it using the first two terms in (2.76), hence

$$t_c \approx \frac{1}{4}e^{\gamma+2/\Lambda}, \tag{2.77}$$

and we see that Λ has to be very small for t_c to be large.

Conversely, for a very small t_c we have to have Λ very large and we can find the value for it from equation (2.75). Using a one term approximation at $r = 1$ and noting that $2\,\mathrm{ierfc}(0) = 2/\sqrt{\pi}$ we find that

$$t_c \approx \frac{1}{\Lambda^2(2\mathrm{ierfc}(0))^2} = \frac{\pi}{4\Lambda^2}. \tag{2.78}$$

When $t > t_c$ the concentration of nutrient at the root surface $r = 1$ has dropped approximately to zero, more specifically $C(1,t)$ is one order of magnitude less than order 1. Hence we now approximate the non-linear model at the leading order by

$$\frac{\partial C}{\partial t} = \frac{1}{r}\frac{\partial}{\partial r}(r\frac{\partial C}{\partial r}), \tag{2.79}$$

with approximate boundary conditions

$$C = 0 \quad \text{at} \quad r = 1, \tag{2.80}$$

$$C \to 1 \quad \text{as} \quad r \to \infty. \tag{2.81}$$

The initial condition at $t = t_c$ will be given by the constant flux solution, i.e.,

$$C(r,t_c) = f(r), \tag{2.82}$$

where $f(r)$ is equation (2.74) evaluated at $t = t_c$.

The solution to this model when $f(r) \approx 1$ for $1 < r < \infty$ at $t = t_c$, i.e., the so called "zero-sink" model, was discussed in Section 2.4.1.1.

2.5.1 Approximate Solution for $\Lambda >> 1$

In the first part of section 2.5 we presented the large and small time approximation, which in turn corresponded to solutions for $\Lambda << 1$ and $\Lambda >> 1$ respectively. In this and the following sub-section we will re-derive these results in order to gain a better understanding of the physical processes exhibited by the system. We begin by considering the case when Λ is large, i.e., the case when the uptake of nutrients is very large compared to the far-field concentration, $\lambda >> c_\infty$.

If $\Lambda >> 1$ then equation (2.73) suggests that there is a boundary layer near the root surface $r = 1$ where $\partial C/\partial r >> 1$. Therefore, we define $t = T/\Lambda^2$ and $r = 1 + R/\Lambda$. Hence, the equations (2.70), (2.72), and (2.73) now become

$$\frac{\partial C}{\partial T} = \frac{1}{R+\Lambda}\frac{\partial C}{\partial R} + \frac{\partial^2 C}{\partial R^2}, \tag{2.83}$$

together with the boundary conditions

$$\frac{\partial C}{\partial R} = 1 \quad \text{at} \quad R = 0, \quad \text{and} \quad C \to 1 \quad \text{as} \quad R \to \infty, \tag{2.84}$$

and the initial condition

$$C = 1 \quad \text{at} \quad T = 0 \quad \text{for} \quad 0 < R < \infty. \tag{2.85}$$

If $\Lambda >> 1$ then $1/(R+\Lambda) << 1$, and hence the equation (2.83) reduces at leading order to

$$\frac{\partial C}{\partial T} = \frac{\partial^2 C}{\partial R^2}. \tag{2.86}$$

The solution to equations (2.84)-(2.86) is given by

$$C(R,T) = 1 - 2(\sqrt{\frac{T}{\pi}}e^{-R^2/4T} - \frac{R}{2}\,\text{erfc}\frac{R}{2\sqrt{T}}). \tag{2.87}$$

In particular, at $R = 0$, i.e., $r = 1$, we have $C = 1 - 2(T/\pi)^{1/2}$, which implies that $C = 0$ when $T_c = \pi/4$ and hence $t_c \approx \pi/(4\Lambda^2)$ for $\Lambda >> 1$, as before.

Figure 2.6 shows the results for root surface concentrations obtained from the numerical experiments conducted with the full non-dimensional model given by equations (2.25)-(2.27), and the approximation given by (2.87).

The numerical experiments conducted with the full non-linear model show that the actual value of the root surface nutrient concentration when the approximation becomes invalid, i.e., $C \approx 0$, is when C has dropped by one order of magnitude. One would expect this, since we have used only leading order approximation, which by definition is valid only up to the order 1 root surface concentration (see Figure 2.6).

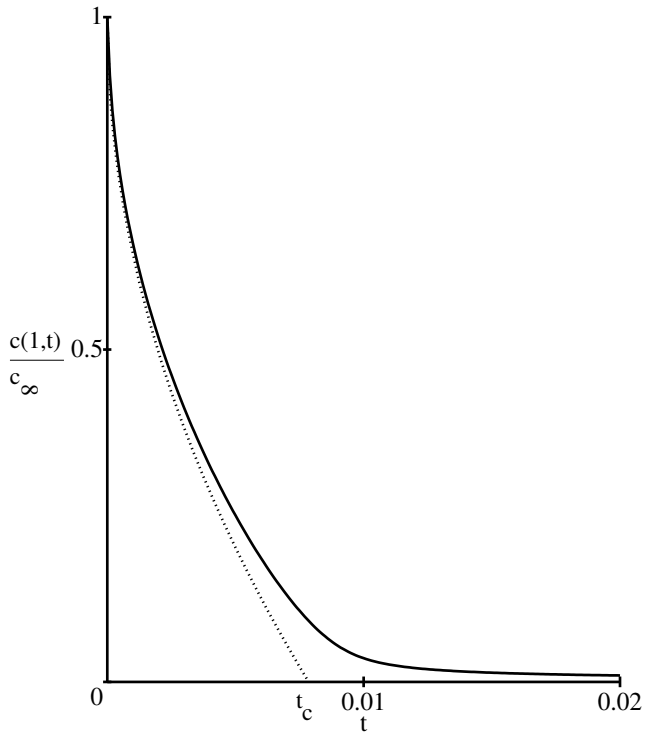

Figure 2.6: Comparison of numerical experiments (solid line) with the full non-linear model and asymptotic approximation (dashed line) given by (2.88) for $c_\infty = 100$ and $\lambda = 1000$ ($\Lambda = 10$). $c(1,t)$ is the root surface nutrient concentration.

Hence, we have found the approximations for the nutrient concentration and the flux for the time $t < t_c \approx \pi/(4\Lambda^2)$, and these are

$$c(1,t) \approx c_\infty(1 - 2\Lambda\sqrt{\frac{t}{\pi}}), \tag{2.88}$$

$$F(t) \approx c_\infty\Lambda = \lambda. \tag{2.89}$$

For $t > t_c$ the boundary condition at the root surface can be taken to the leading order to be $C = 0$ at $r = 1$. The initial condition would be given by the approximate solution (2.87) evaluated at t_c given by (2.78). Hence we have

$$C \approx 1 - \sqrt{\pi}\text{ierfc}\frac{\Lambda(r-1)}{\sqrt{\pi}}, \quad \text{at} \quad \tilde{t} = t - t_c = 0. \tag{2.90}$$

This initial condition has also a boundary layer at $r = 1$. We can approximate the initial condition by taking $C = 1$ at $\tilde{t} = 0$, since the region of $C << 1$ is very narrow. Thus, for $t > t_c$ the problem reduces to the "zero-sink" model, the solution of which was discussed in Section 2.4.1.1.

On Figure 2.7 (b) there are three different graphs shown and, as we can see, the numerical solutions to the full non-linear problem mostly overlap with the zero

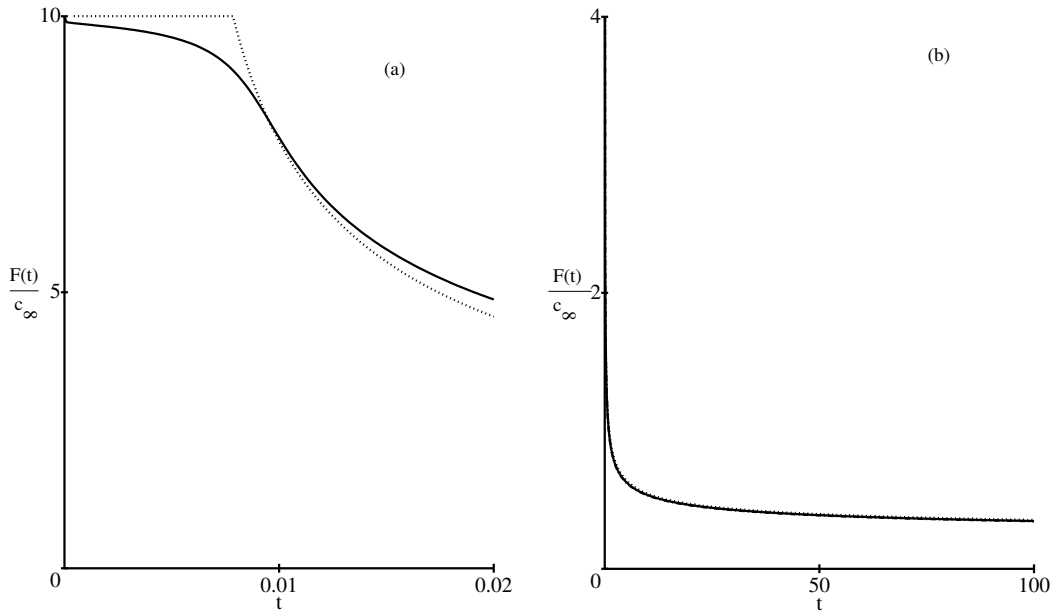

Figure 2.7: Comparison of numerical experiments (solid lines) for $c_\infty = 100$, $\lambda = 1000$, and $\Lambda = 10$ with the full non-linear model and asymptotic approximations (dashed lines) of nutrient flux into the root given by the equation (2.89) for short time (a), and the approximation to zero sink model given by the equation (2.51) with $\alpha = 2.5$ for long time (b). On (b) there is also a dotted-dashed line overlapping the solid line. This is the numerical solution to the cylindrical diffusion equation with the boundary condition at the root surface being $C = 0$ at $r = 1$.

boundary condition numerical solution except in the very thin region near the time origin where the zero boundary condition model has a singularity. We can see in Figure 2.7 (a) the comparison between numerical solutions and approximations near the critical time t_c. It must also be noted that the small time solution valid for $t < t_c \approx \pi/(4\Lambda^2)$ corresponds to non-dimensional time of order 66 seconds for potassium when $\Lambda = \lambda/c_\infty = 47/3.28 \approx 14.33$. This is a very short time and no experimental data for this time are available. Hence we conclude that the zero sink model provides a satisfactory approximation to the nutrient uptake when $c_\infty >> 1$ and $\lambda >> 1$ for times of practical importance.

2.5.2 Approximate Solution for $\Lambda << 1$

Now we will consider the case when $\Lambda << 1$. Since $\partial C/\partial r|_{r=1} \approx \Lambda << 1$ we expect the region where C is less than order 1 to be larger. Similarly to Section 2.4.2 we use the Oseen type expansion to find the approximate solution. Thus, after rescaling to large time and space variables τ and R, i.e., $t = \tau/\sigma^2$ and $r = R/\sigma$ with $\sigma << \Lambda << 1$ and $\sigma = e^{-1/\Lambda}$, we find that the outer similarity solution satisfying the

far-field boundary condition is given by

$$C(R,\tau) \approx 1 + BE_1(\frac{R^2}{4\tau}), \tag{2.91}$$

where $E_1(x) = \int_x^\infty e^{-y}\frac{dy}{y}$ is the exponential integral, and the coefficient B should be determined by matching the outer solution with the inner solution.

Similarly to the $c_\infty << 1$ case, the inner long time solution is given by

$$C(r,\tau) \approx C(1,\tau) + \Lambda \ln(r) + O(\sigma^2). \tag{2.92}$$

By expanding the outer solution for small argument and matching $\ln(R)$ terms in the inner and outer expansions we find that $B = -\Lambda/2$. The matching of the leading order terms gives

$$C(1,t) \approx 1 - \frac{\Lambda}{2}\ln(4e^{-\gamma}t). \tag{2.93}$$

Thus, the critical time when the root surface nutrient concentration has reached zero is given by $t_c \approx \frac{1}{4}e^{\gamma+2/\Lambda}$, i.e., the concentration at the root surface drops to zero on an exponentially large time-scale.

The approximation becomes invalid when $\tau \lesssim \sigma^2 = e^{-2/\Lambda}$. However, the invalidity is over an exponentially small range, and a heuristic procedure which enables the outer solution to satisfy the initial condition is to add a small shift of time t_0 to the time t; in other words we choose $C(1,t) = 1$ for $t = 0$, i.e., $t_0 = (1/4)e^\gamma$ and hence we arrive at

$$c(1,t) = c_\infty[1 - \frac{\Lambda}{2}\ln(4e^{-\gamma}t + 1)]. \tag{2.94}$$

The approximation to the flux, which is given in this approximation by $F(t) = \Lambda c_\infty$, is even worse than the approximation to the root surface concentration (see Figure 2.8). This is due to the leading order approximation of the nonlinear boundary condition. One way of improving our approximation for $\Lambda << 1$ when $c_\infty >> 1$ would be to consider further terms in the boundary condition approximation (2.73). However, we will not proceed in this way. Instead we will tackle this problem later in section 2.6.1 when we carry out the asymptotic expansion for all values of c_∞ when $\lambda << 1$. The comparison of numerical simulations for flux will also be presented in that section.

2.6 The Regime $c_\infty = O(1)$

When $c_\infty = O(1)$ we can still look for the solution in the limit when λ is small and large. We can also use the results of the c_∞ large and small limits to determine the behaviour at $c_\infty = O(1)$.

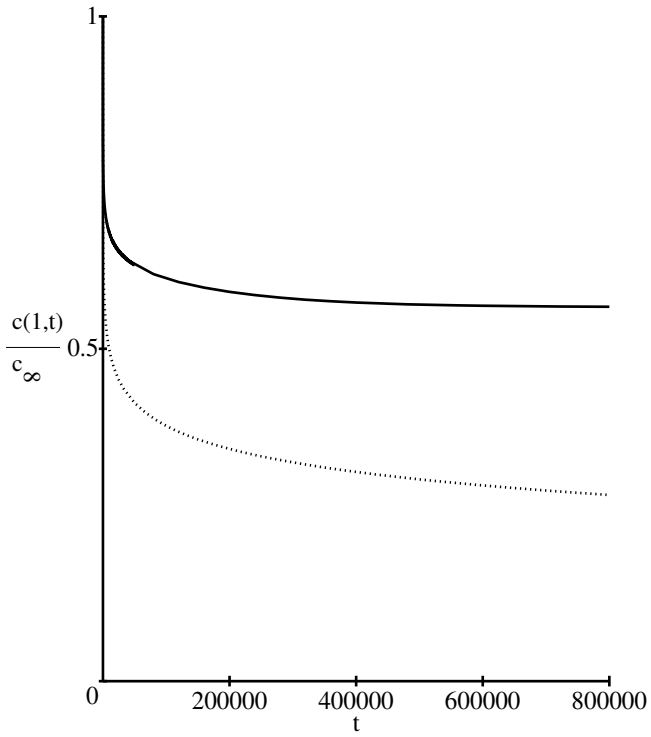

Figure 2.8: Comparison of numerical experiments (solid line) with the full non-linear model and asymptotic approximation (dashed line) given by (2.94) for $c_\infty = 10$ and $\lambda = 1$ ($\Lambda = 0.1$). We see that the approximation does not agree well with the numerical solution to the full non-linear model. However, in Section 2.6.1 this will be improved.

2.6.1 Approximation for $\lambda << 1$

As in previous sections for λ small we can also follow the procedure of asymptotic Oseen expansion for $\lambda << 1$ in the general case of c_∞. In this case the outer solution can be found for the long time and space scaling $r = R/\sigma$ and $t = \tau/\sigma^2$, with $\sigma << \lambda << 1$, to be given by

$$c(R,\tau) \approx c_\infty + BE_1(\frac{R^2}{4\tau}). \tag{2.95}$$

Similarly the leading order long time inner solution (after rescaling back with $R = \sigma r$) is given by

$$c(r,\tau) \approx c(1,\tau) + F(\tau)\ln r. \tag{2.96}$$

As before we assume that B is slowly varying in time. After expanding the exponential integral for small argument and matching $O(\ln r)$ terms we get that $B = -F(t)/2$, and matching leading order terms gives

$$c(1,t) = c_\infty - \frac{F(t)}{2}\ln(4e^{-\gamma}t). \tag{2.97}$$

However, we also know that $F(t) = \lambda c(1,t)/[1 + c(1,t)]$. Eliminating the singularity at $t = 0$ (as in previous sections) by introducing the small time shift $t_0 = (1/4)e^{\gamma}$, such that $c(1,t) = c_\infty$ at $t = 0$ (since $F(0) \neq 0$), we arrive at the following equation for $c(1,t)$

$$c(1,t) = c_\infty - \frac{1}{2}\frac{\lambda c(1,t)}{1 + c(1,t)} \ln(4e^{-\gamma}t + 1). \tag{2.98}$$

Alternatively we can write the equation (2.98) in terms of flux $F(t)$, i.e., in this case we get the following quadratic for $F(t)$

$$F^2(t)\frac{1}{2}\ln(4e^{-\gamma}t + 1) - F(t)(c_\infty + \frac{\lambda}{2}\ln(4e^{-\gamma}t + 1) + 1) + c_\infty\lambda = 0. \tag{2.99}$$

Use of the Descartes Rule of Signs indicates that there are at most 2 real positive roots for this quadratic (two sign changes in the coefficients). Using a substitution $F(t) = -G(t)$ and applying the Descartes Rule of Signs again, we find that there are no negative roots to this quadratic (zero sign changes in coefficients of quadratic). The roots are given by

$$F_\pm(t) = \frac{1}{\ln(4e^{-\gamma}t + 1)}\Big\{1 + c_\infty + \frac{\lambda}{2}\ln(4e^{-\gamma}t + 1) \pm \sqrt{4c_\infty + [1 - c_\infty + \frac{\lambda}{2}\ln(4e^{-\gamma}t + 1)]^2}\Big\}. \tag{2.100}$$

Clearly the argument under the square root is always positive and hence one has exactly two real roots. However, since at the time-origin the multiplier of the highest power of $F(t)$ in the quadratic vanishes, we have one of the roots of this quadratic being infinite at the time-origin. The other root has the finite value of the required initial nutrient uptake $F(0) = \lambda c_\infty/(1 + c_\infty)$. Our aim is now to determine at which one of the roots, square root negative or square root positive, we should be looking. We begin by using the property of quadratic solutions

$$F_+F_- = \frac{2\lambda c_\infty}{\ln(4e^{-\gamma}t + 1)}, \tag{2.101}$$

which gives using the solution of the quadratic the following formula

$$F_\pm(t) = \frac{2\lambda c_\infty}{1 + c_\infty + \frac{\lambda}{2}\ln(4e^{-\gamma}t + 1) \mp \sqrt{4c_\infty + (1 - c_\infty + \frac{\lambda}{2}\ln(4e^{-\gamma}t + 1))^2}}. \tag{2.102}$$

Clearly at the time-origin $F_- = \lambda c_\infty/(1 + c_\infty)$, but $F_+ = 2\lambda c_\infty/0 = \infty$. Hence the flux of nutrient into the root is given by

$$F(t) = \frac{2\lambda c_\infty}{1 + c_\infty + \frac{\lambda}{2}\ln(4e^{-\gamma}t + 1) + \sqrt{4c_\infty + (1 - c_\infty + \frac{\lambda}{2}\ln(4e^{-\gamma}t + 1))^2}}. \tag{2.103}$$

Comparison between exact numerical solutions and solutions for the quadratic are shown in the Figure 2.9. We see that this approximation agrees well with the numerical experiments with the full non-linear model.

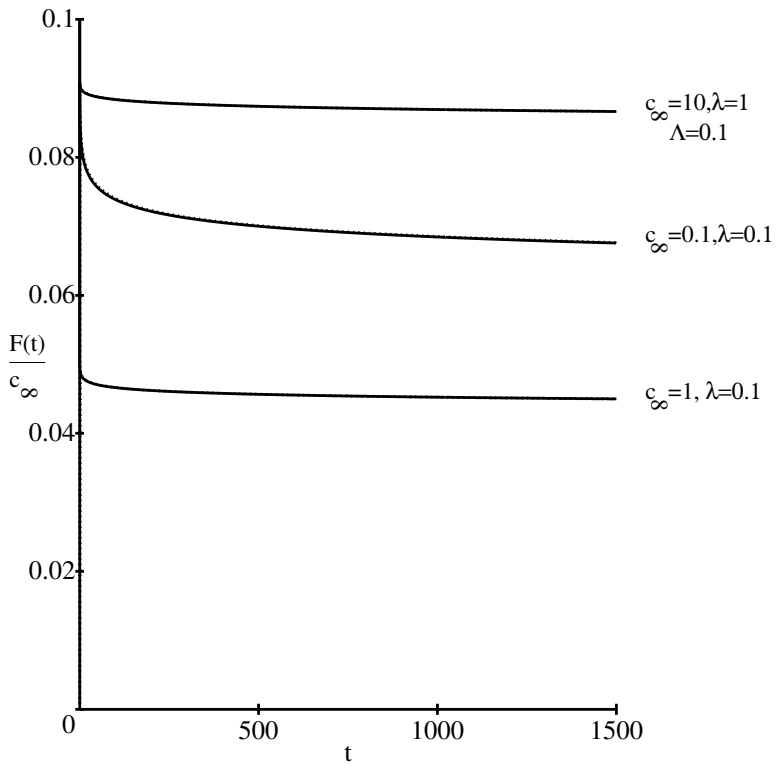

Figure 2.9: Comparison of numerical experiments (solid line) with the full non-linear model and asymptotic approximation (dashed line) given by (2.103). $F(t)$ is the rate of nutrient uptake.

2.6.2 Approximation for $\lambda >> 1$

At short times the previous two cases for $\lambda >> 1$, i.e., when $c_\infty << 1$ and $c_\infty >> 1$, we found that there was a boundary layer near the surface of the root. Thus for $c_\infty = O(1)$ and $\lambda >> 1$, such that $\partial c/\partial r|_{r=1} >> 1$ we rescale to the boundary layer variables $r = 1 + R/\lambda$ and $t = T/\lambda^2$ and transform the equations (2.25)-(2.27) at the leading order into

$$\frac{\partial c}{\partial T} = \frac{\partial^2 c}{\partial R^2}, \tag{2.104}$$

i.e., neglecting $1/(R+\lambda) << 1$ terms. The boundary conditions become

$$\frac{\partial c}{\partial R} = \frac{c}{1+c} \quad \text{at} \quad R = 0, \quad \text{and} \quad c \to c_\infty \quad \text{as} \quad R \to \infty. \tag{2.105}$$

This is a nonlinear model, and the exact solution to it is not available. We only notice that this approximation is valid until $t << 1/\lambda^2$.

We recall the results for the $c_\infty >> 1$ and $c_\infty << 1$ for $\lambda >> 1$, whose derivation was presented in the previous sections. For $c_\infty >> 1$ we had

$$c(1,t) \approx c_\infty - 2\lambda\sqrt{\frac{t}{\pi}}, \tag{2.106}$$

and for $c_\infty << 1$ we had the solution given by

$$c(1,t) \approx c_\infty e^{\lambda^2 t}\text{erfc}(\lambda\sqrt{t}). \tag{2.107}$$

Expanding the equation (2.107) for $\lambda^2 t$ small, i.e., in the region of validity of that approximation, we get

$$c(1,t) \approx c_\infty(1 - 2\lambda\sqrt{\frac{t}{\pi}} + \cdots). \tag{2.108}$$

For $c_\infty \sim O(1)$ both solutions are approximately the same, except for the c_∞ term multiplying the $\sqrt{t}$ in (2.108). We can try to interpolate both limit solutions using the function $f(c_\infty)$ such that when $c_\infty >> 1$ we have $f \approx 1/c_\infty$, and when $c_\infty \lesssim 1$ then $f = O(1)$. The function which would exhibit such behaviour could be

$$f(c_\infty) = \frac{1}{1 + c_\infty}. \tag{2.109}$$

Hence, the solution which would have the required limiting behaviours will be given by

$$c(1,t) \approx c_\infty e^{\lambda^2 f^2 t}\text{erfc}(\lambda f\sqrt{t}). \tag{2.110}$$

The flux into the root can now be calculated using the full nonlinear flux condition. The comparison between the numerical experiments and approximation for flux is shown in Figure 2.10. As we can see this formulae, which is valid for the times $t << 1/\lambda^2$, interpolates the solution in that time-region reasonably well. The biggest break down occurs for c_∞ being large, but even then the interpolation is reasonably good in the region of the validity, i.e., for $t << 1/\lambda^2$.

The expansion of $e^T\text{erfc}(\sqrt{T})$ for large T can be obtained using integration by parts, i.e., we get

$$e^T\text{erfc}(\sqrt{T}) \approx \frac{1}{\sqrt{\pi}}\Big[\frac{1}{\sqrt{T}} - \frac{1}{2T^{3/2}} + \ldots + (-1)^n\frac{1\cdot 3\cdots(2n-1)}{2^n}\int_{\sqrt{T}}^{\infty}\frac{e^{-\xi^2}}{\xi^{2n}}\,d\xi\Big], \tag{2.111}$$

where $T = \lambda^2 f^2 t$. Hence we also know now that as $T = \lambda^2 f^2 t \to \infty$ the surface concentration, and hence also flux, approaches zero. We also notice that for our parameter values presented in Section 2.2.3 the values of $\lambda \sim O(10)$ is for potassium and phosphorus. Thus the validity of the small time approximation is over dimensionless time-range of less than 10^{-2}, which in turn corresponds in dimensional terms to the time-range 1-10 minutes. In the current experiments there is no experimental data collected over so short a time period. So from the point of view of experiments the short time solution is not important, but it is useful to know it in case more accurate measurements become available.

The time-range we are interested in is larger than one day and hence we have to find the long time solution to the flux. When $t > 1/\lambda^2$ the concentration of the

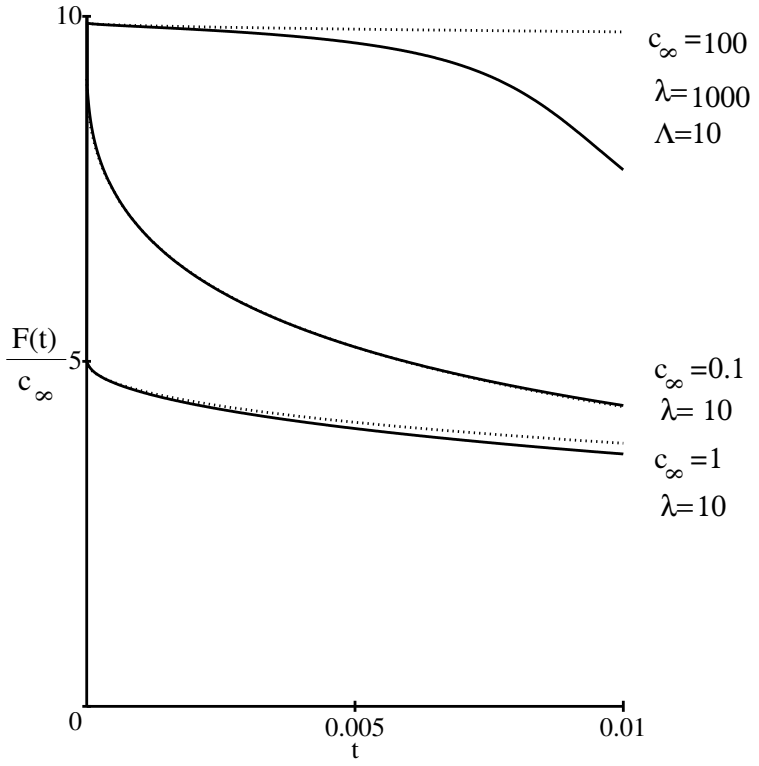

Figure 2.10: Comparison of numerical experiments (solid line) with the full non-linear model and asymptotic approximation (dashed line) given by $F(t) = \lambda c(1,t)/[1 + c(1,t)]$ with $c(1,t)$ given by (2.110).

nutrients at the surface of the roots has dropped approximately to zero, and hence, as before in previous sections, we will approximate the model by

$$\frac{\partial C}{\partial t} = \frac{1}{r}\frac{\partial}{\partial r}(r\frac{\partial C}{\partial r}), \tag{2.112}$$

$$C = 0 \quad \text{at} \quad r = 1, \quad \text{and} \quad C \to 1 \quad \text{as} \quad r \to \infty, \tag{2.113}$$

where $c = c_\infty C$.

The initial condition for this can be taken to be similar to the large and small far-field c_∞ concentration, i.e., we assume that as before there is a small region (order $1/\lambda$) where the concentration is less than order 1. Hence we can approximate the initial condition for this solution by taking $C = 1$ at $t = 0$. The large time approximation to this solution was found in section 2.4.1.1 to be given by

$$F(t) = \frac{2c_\infty}{\ln(4e^{-\gamma}t + 1)}. \tag{2.114}$$

However we can use the quadratic approximation, derived in section 2.6.1 for the general case of $\lambda << 1$, also for $\lambda >> 1$ at large times since in the approximation

procedure for this parameter range we assumed that the scaling factor σ was much smaller than λ. Therefore by repeating this procedure for λ large and choosing $\sigma = 1/\lambda << 1$, since $\lambda >> 1$, we would arrive at the same quadratic equation for the flux (2.99). This quadratic would now be valid for the times $t >> 1/\lambda^2$. We need to demonstrate that the solution to this quadratic for large λ does not contradict the approximation (2.114) derived for the zero-sink model. Let us first recall the quadratic

$$F^2(t)\frac{1}{2}\ln(4e^{-\gamma}t+1) - F(t)[c_\infty + \frac{\lambda}{2}\ln(4e^{-\gamma}t+1)+1] + c_\infty\lambda = 0, \tag{2.115}$$

but we can rewrite this quadratic as

$$F^2(t)\frac{1}{\lambda} - F(t)[\frac{1+c_\infty}{(\lambda/2)\ln(4e^{-\gamma}t+1)}+1] + \frac{2c_\infty}{\ln(4e^{-\gamma}t+1)} = 0. \tag{2.116}$$

Since $\lambda >> 1$ and $1/\lambda << 1$ we get by neglecting $O(1/\lambda)$ terms, that flux is approximately given by

$$F(t) \approx \frac{2c_\infty}{\ln(4e^{-\gamma}t+1)}, \tag{2.117}$$

which is the same as (2.114). As we can see from Figure 2.11 the approximation given by the quadratic agrees well with the numerical solution to the full non-linear model for $t >> 1/\lambda^2$. Hence we have found the approximation to the solution at large times.

2.6.3 Regime $\lambda = O(1)$

We have now seen in the previous two sections that the equation (2.103) satisfies the solutions in the case of large and small λ. Hence it is reasonable to assume that it is also valid for $\lambda = O(1)$. We will now present a comparison between the analytical approximation and numerical experiments for $\lambda = 1$ and $c_\infty = 0.1, 1$ and 10 (see Figure 2.12).

We see that numerical experiments and analytical approximation are in good agreement except for a short time, when analytical approximation slightly overestimates the flux. The invalidity is over a small time-range (as mentioned before up to $O(1)$ dimensionless time corresponding to a couple of minutes in dimensional time) which is of no current interest to us. Hence we take the flux into the root to be given by the solution to the quadratic (2.99), i.e.,

$$F(t) = \frac{2\lambda c_\infty}{1+c_\infty+\frac{\lambda}{2}\ln(4e^{-\gamma}t+1)+\sqrt{4c_\infty+[1-c_\infty+\frac{\lambda}{2}\ln(4e^{-\gamma}t+1)]^2}}. \tag{2.118}$$

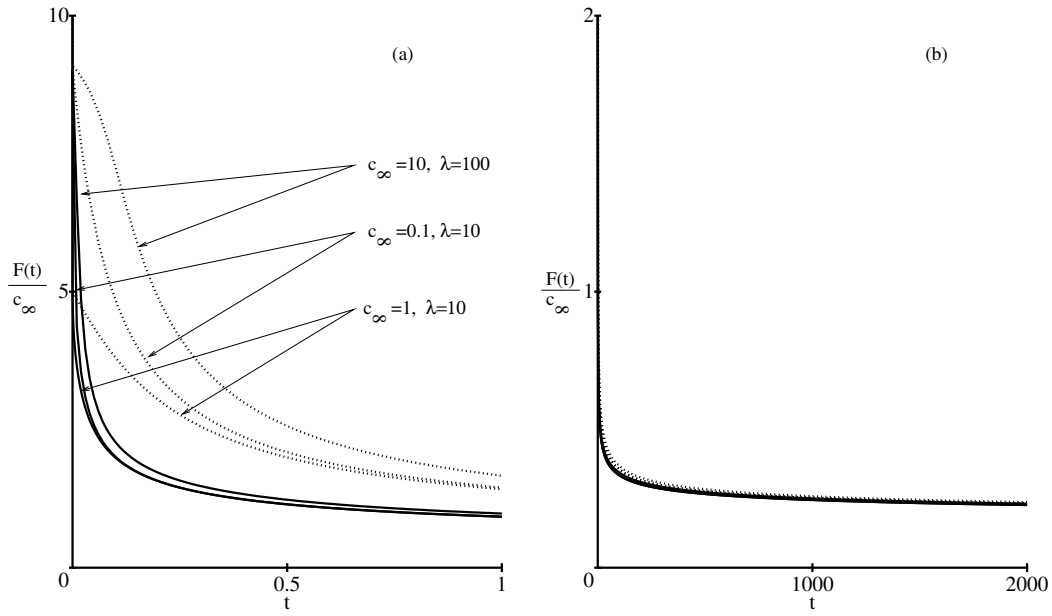

Figure 2.11: Comparison of numerical experiments (solid lines) with the full non-linear model and asymptotic approximations (dashed lines) of nutrient flux $F(t)$ into the root given by the equation (2.103) for short time (a), and for long time (b). $c_\infty = 10$ and $\lambda = 100$; $c_\infty = 1$ and $\lambda = 10$; $c_\infty = 0.1$ and $\lambda = 10$. (a) shows the discrepancy between the numerical approximation of the full non-linear model and the large time approximation (2.103) at short times. However, because the short time corresponds there to times less than couple of minutes, a time region of no real interest.

2.7 Summary of Approximate Solutions

The aim of this chapter was to find an expression for the nutrient uptake by a single cylindrical root as a function of time t, uptake coefficient λ, and far-field nutrient concentration c_∞. Most experimental data are available for vegetative time-periods which are from 1 day to 3 months, i.e., approximately 100 days. This dimensional time region corresponds to a dimensionless time-range 10 to 10^4. Hence, for this so called large time-range, the solution to the flux $F(t)$ for all values of λ and c_∞ is found from the quadratic expression

$$F^2(t)\frac{1}{2}\ln(4e^{-\gamma}t+1) - F(t)(c_\infty + \frac{\lambda}{2}\ln(4e^{-\gamma}t+1)+1) + c_\infty\lambda = 0, \qquad (2.119)$$

and it is

$$F(t) = \frac{2\lambda c_\infty}{1+c_\infty+\frac{\lambda}{2}\ln(4e^{-\gamma}t+1)+\sqrt{4c_\infty+[1-c_\infty+\frac{\lambda}{2}\ln(4e^{-\gamma}t+1)]^2}}. \qquad (2.120)$$

For $\lambda << 1$ this solution is invalid over an exponentially small time-range proportional to $e^{-2/\lambda}$. This time-range is of no real interest to us since in dimensional terms it

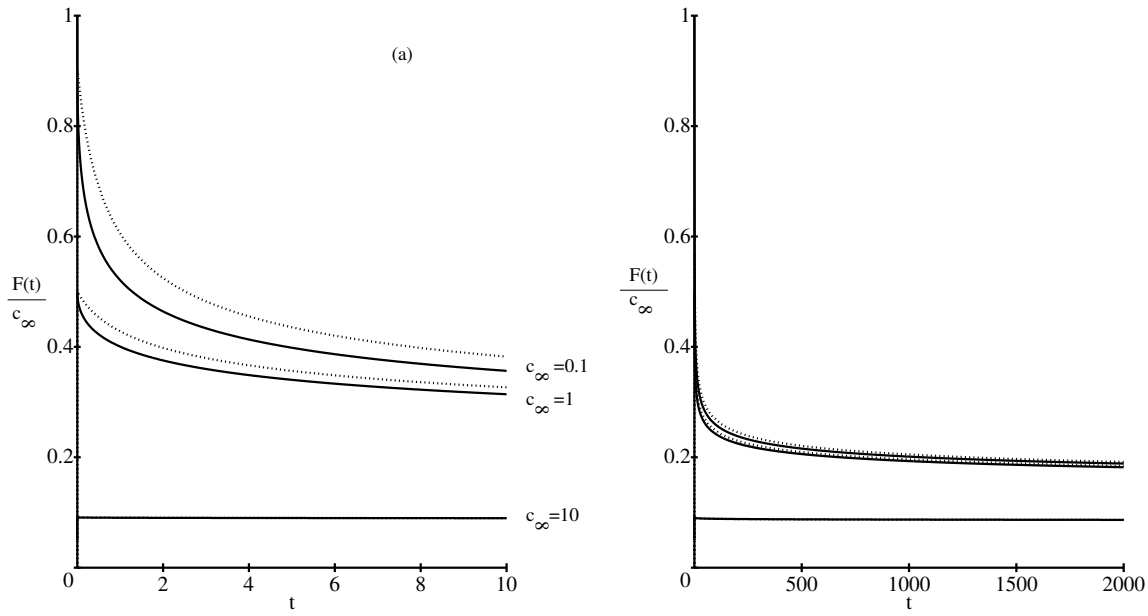

Figure 2.12: Comparison of numerical experiments (solid lines) with the full non-linear model and asymptotic approximations (dashed lines) of nutrient flux into the root given by the equation (2.103) for short time (a), and long time (b). $\lambda = 1$ for various values of c_∞.

corresponds to times less than a couple of seconds.

In the case of λ being large, the solution is invalid when there is a boundary layer solution for $t << 1/\lambda^2$, i.e., in the dimensional time-range up to 10 minutes. Hence the short time solution is of no current interest. Nevertheless the flux in that case was found to be given by

$$F(t) = \frac{\lambda c(1,t)}{1 + c(1,t)}, \tag{2.121}$$

with $c(1,t)$ given by

$$c(1,t) = c_\infty e^{\lambda^2 t/(1+c_\infty)^2} \text{erfc}(\frac{\lambda}{1+c_\infty}\sqrt{t}). \tag{2.122}$$

Thus, we have found the expressions for the dimensionless flux $F(t)$ as a function of dimensionless time t. Dimensional time t_{dim} can be written in terms of dimensionless time t according to the non-dimensional scaling which was carried out in Section 2.2.1 and it is $t = \dfrac{D\phi_l}{a^2(\phi_l + b)} t_{\text{dim}}$. In a similar way we find that dimensional flux $F_{\text{dim}}(t_{\text{dim}}) = \dfrac{F_m}{\lambda} F(t_{\text{dim}})$, where F_m is the dimensional uptake coefficient and λ is dimensionless uptake coefficient.

2.8 Pore Water Convection, i.e., Péclet Number Revisited

In the previous section we found that the flux of nutrient into a cylindrical root for $t >> 1$ for all values of λ and c_∞ was given by equation (2.120) provided the Péclet number is sufficiently small, more specifically after the boundary condition and the asymptotic matching conditions

$$Pe << \frac{\lambda}{1+c_\infty}. \tag{2.123}$$

When the Péclet number is still small, but does not satisfy the above condition it cannot be neglected in the boundary condition. Hence, $F = \partial c/\partial r|_{r=1}$ is given in this case by

$$F = \frac{\lambda c}{1+c} - Pe\, c \quad \text{at} \quad r = 1. \tag{2.124}$$

Solving the radial diffusion equation with this boundary condition we find that the overall flux into the root is given by

$$\begin{aligned} F_{\text{tot}} &= Pe\, c(1,t) + F(t), \qquad (2.125)\\ &= \frac{2\lambda c_\infty}{1 + c_\infty + \frac{L(t)}{2}(\lambda - Pe) + \sqrt{4c_\infty(1 - \frac{L(t)}{2}Pe) + [1 - c_\infty + \frac{L(t)}{2}(\lambda - Pe)]^2}}, \end{aligned}$$

where $L(t) = \ln(4e^{-\gamma}t + 1)$.

We can also extend the asymptotic expansion techniques for the case when $Pe \sim O(1)$. In this case we cannot neglect Pe terms in the diffusion-convection equation. However, we can still find the outer similarity type solution with similarity variable $\eta = R^2/4\tau$ (as before in previous sections), which is valid far away from the root, i.e, the outer solution is given by

$$c = c_\infty - B\int_{R^2/4\tau}^{\infty} \frac{e^{-\eta}}{\eta^{1+Pe/2}} d\eta. \tag{2.126}$$

The inner long time solution for $Pe \sim O(1)$ is given by

$$c = c(1,t) + \frac{F(t)}{Pe}(1 - r^{-Pe}), \tag{2.127}$$

where $F(t) = \partial c/\partial r|_{r=1}$.

We can now expand the outer solution, after writing the above integral in terms of Whittaker M functions and using the Handbook of Mathematical Functions [1], at the limit where $R^2/4\tau \to 0$. Matching order 1 and order r^{-Pe} terms in resulting

outer and inner expansion, we will arrive at the following quadratic equation for the root surface nutrient concentration $c_1 = c(1,t)$

$$c_\infty = c_1 + [\frac{\lambda c_1}{1+c_1} - Pe\, c_1]\beta, \tag{2.128}$$

where

$$\beta = \frac{Pe - 2 + 2[4(t+t_0)]^{-Pe/2}\Gamma(2-Pe/2)}{Pe(Pe-2)}, \quad t_0 = \frac{1}{4}\Big(\frac{2\Gamma(2-Pe/2)}{2-Pe}\Big)^{Pe/2}, \tag{2.129}$$

with t_0 being the time-delay such that $c_1 = c_\infty$ at $t = 0$, since $F(0) \neq 0$. The solution for $\lambda = 1$, $c_\infty = 1$ for different values of Péclet number Pe is shown on Figure 2.13. We see that as Péclet number becomes smaller the solution approaches the solution found in the previous sections for $Pe = 0$ (red line on the figure).

We can also ask a question for which value of Pe would the root surface concentration start to increase in time as oppose to decreasing. For that we need to calculate the gradient at the root surface concentration at time $t = 0$. Hence by solving the equation $\partial c(1,t)/\partial t|_{t=0} = 0$ we find that this occurs at $Pe_{\text{crit}} = \lambda/(1+c_\infty)$ (as can be observed also on Figure 2.13 for $\lambda = 1$ and $c_\infty = 1$, $Pe_{\text{crit}} = 0.5$).

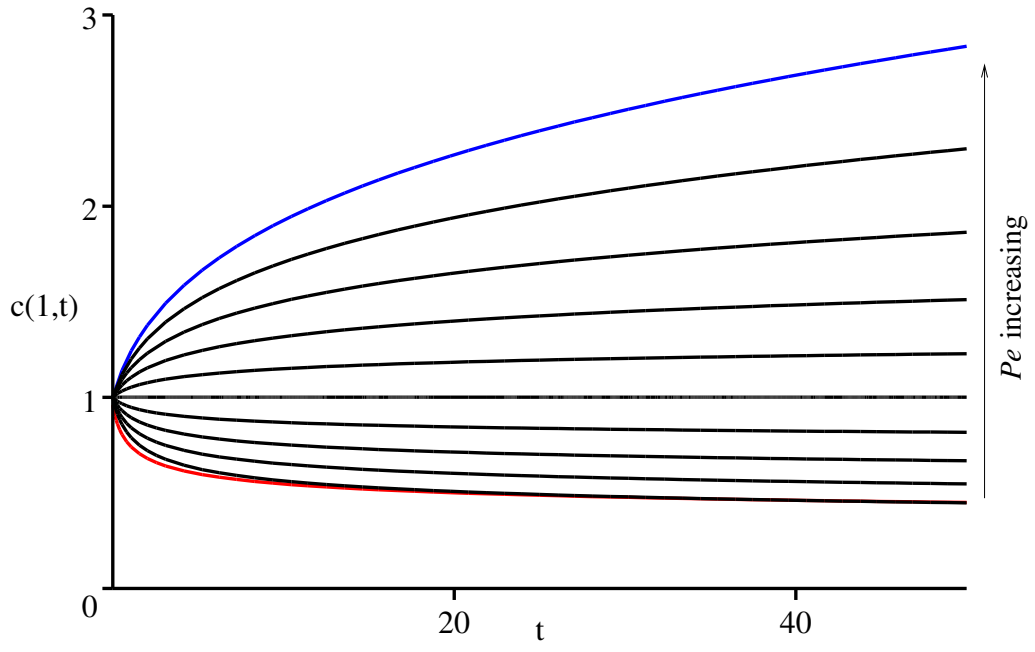

Figure 2.13: Root surface nutrient concentration $c(1,t)$ for $\lambda = 1$ and $c_\infty = 1$ as a function of time given by a positive square root solution to the equation (2.128). Black lines correspond to Péclet number values $Pe = 0.1$, 0.2, 0.3, 0.4, 0.5, 0.6, 0.7, 0.8, 0.9, and blue line corresponds to $Pe = 1$. Red line corresponds to $Pe = 0$ solution given by equation (2.120).

Hence, we can also calculate the flux of nutrient into the root when Pe is not small. However, we point out that $Pe \sim O(1)$ corresponds to the root radius of order 3 cm. Therefore this solution presented above is irrelevant for calculating nutrient uptake by agricultural plants which in general have roots at least an order of magnitude finer than that.

2.9 Conclusions

In this chapter the derivation of the model initially developed by Nye, Tinker and Barber was presented together with its non-dimensionalisation and mathematical analysis at different dimensionless parameter limits. We found the estimate for the critical time t_c after which the nutrient flux into the root starts actively decreasing due to the deficiency of nutrients at the root surface. This critical time was found to be relatively large for the case when the far-field concentration c_0 is much larger than the Michaelis-Menten uptake coefficient K_m, and also when the dimensionless nutrient uptake coefficient $\lambda = \dfrac{F_m a}{D K_m \phi_l}$ is very small compared to the far-field concentration $c_\infty = c_0/K_m$.

In the case when the nutrient uptake coefficient λ is large compared to the far-field concentration c_∞, the flux starts decaying very rapidly after a short transition time, which is approximately of order $1/\lambda^2$, corresponding to times of order 10 minutes. In the case of the small uptake coefficient $\lambda << 1$, the decrease in root surface nutrient concentration takes place over the exponentially large time-scale, more specifically of order $e^{2/\lambda}$ corresponding to times larger than the average vegetative period of agriculturally important plants.

Hence, in this section we have described and approximated the Nye-Tinker-Barber model at all possible parameter ranges. This will enable us in the following chapters to expand the modelling from a single cylindrical root to a more realistic root morphology, i.e., branched root structure.

Chapter 3

Root Hairs and Mycorrhizae

In Chapter 2 we considered a model for nutrient uptake by smooth cylindrical roots in homogeneous soil. However, roots are not perfect cylinders. As discussed in Chapter 1, many roots have root hairs extending out from the root surface cells and mycorrhizal fungi living on and in the root surface epidermal cells. These fungi grow hyphal extensions out to the surrounding soil and are thought to aid the nutrient uptake by the root. In this chapter we aim to develop a framework for modelling the influence of root hairs and mycorrhizae on nutrient uptake.

3.1 Root Hairs

The surface of a root consists of epidermal cells. Some of those epidermal cells form extensions out into the soil, known as root hairs (see Figure 1.3 in Chapter 1). Root hairs are part of the root surface cells and one can consider the mechanism of nutrient uptake by them to be similar to that responsible for the uptake at the root surface. However, due to their small radius and high density it is thought that their presence can increase the nutrient uptake by up to 78% [6]. The number of root hairs varies with the levels of nutrients in the soil. For example, at high phosphorus concentrations the number of root hairs per centimetre of root length (for maize) is approximately 500, but at low phosphorus concentration this number can increase up to 2000 [80]. The development of root hairs is therefore thought to be an adaptive plant response to the deficiency of nutrients in the soil. In addition to the number of root hairs varying with the nutritional status of the plant, their length can also increase with nutrient deficiency. This effect has been measured in rape, where the root hair length can vary between 0.3 and 3 mm depending on the level of nitrogen and phosphorus in the soil [80].

Root hairs extend the total root surface area quite considerably. For the average maize root with radius 2×10^{-2} cm, and root hairs with length 0.1 cm, radius 10^{-3}

cm, and number density of 1000 root hairs per centimetre of root length, the increase in the total root surface area is approximately 500%. At the same time the increase in the volume of root tissue is 25%. This implies that with the relatively small increase in the volume, i.e., commitment of resources, the increase in nutrient absorbing root surface area is large.

The contribution of the nutrient uptake by the root hairs has been formerly calculated merely by using the cylindrical root model, presented in Chapter 2, with the root radius taken to be the root radius plus the root hair length [95]. This is motivated by the fact that the concentration of nutrients in the root hair region is thought to relax rapidly to the time equilibrium [95]. In the classical Nye-Tinker-Barber sense this would lead, in the case of root hair length being 10 times the radius of the root, to 10 times increase in the dimensionless nutrient uptake coefficient λ. However, this method does not take into account the dramatic increase of root surface area. The experimental observations also contradict this approach [11].

Another popular approach in modelling root hair nutrient uptake is to consider them to be a volume sink with finite thickness extending from the root surface [12], [25], [60]. Calibration of those models is usually very complex, since in general they contain large numbers of independent parameters (in some cases up to 16 different parameters). All those parameters need to be determined from experiments. It has been extremely difficult to constrain these parameter values since experiments in the absence of root hairs have been nearly impossible due to a lack of plants that have hairy and hairless genotypes. The main difficulty with those two approaches is that the parameter values derived for hairless root (Chapter 2), root hair cylinder and root hair volume sink model are not consistent and interchangeable. However, with the advancement in genetic engineering, it will be possible to carry out more accurate calibration of the models using hairless and hairy mutants [30], [32].

Another possible way of tackling the modelling of root with root hairs would be to calculate an *effective root radius* corresponding to the total root surface area including the contribution from root hairs, i.e., given a root radius a, hair radii a_h, hair length l, and the number of root hairs per unit length of the root n, the effective root radius r_e is calculated as $r_e = a + a_h nl$. To our knowledge there is no indication in the literature that this approach has been used in the past.

In this section we aim to establish a more detailed dependence of the rate of nutrient uptake by the cylindrical root on the length and density of root hairs. We will consider the specific geometrical properties of root hairs, in particular their radius and density in order to approximate their influence on nutrient uptake.

3.1.1 Modelling the Influence of Root Hair Uptake on Total Nutrient Uptake by the Root

Root hairs can be considered to be cylinders that extend perpendicularly from the root surface. The root hair density n is the number of root hairs per unit length of the root and it varies from species to species. For maize plants a typical range is from 100 to 2000 root hairs per centimetre of the root [6], [57], [80].

The mechanism of nutrient uptake at the root hair surface is thought to be the same as on the root surface, and hence the model presented in Chapter 2 is applicable also for root hairs. By modifying the boundary surface to include root hairs one would obtain the following dimensional model

$$(b+\phi_l)\frac{\partial c}{\partial t}+\nabla\cdot(c\mathbf{u})=D\phi_l\nabla^2 c, \tag{3.1}$$

with boundary conditions

$$\mathbf{n}\cdot(D\phi_l\nabla c_l+\mathbf{u}c_l)=\frac{F_m c}{K_m+c}-E, \quad \text{on} \quad \partial H, \tag{3.2}$$

where ∂H is the root and root hair surface. The root surface is defined by $r=\sqrt{x^2+y^2}=a$, with a being the dimensional root radius. Any particular root hair surface is given by $\rho=\sqrt{y^2+z^2}=a_{h,d}$, where $a_{h,d}$ is the dimensional radius of the root hair, i.e., the root hair is placed along the x-axis. r and ρ are radial coordinates associated with the root and root hair respectively. The corresponding angle variables for root and root hair are $\theta=\arctan(y/x)$ and $\phi=\arctan(z/y)$ (see Figures 3.1 and 3.2). $\mathbf{n}$ is the unit normal to the root and root hair surface. In order to include inter root hair competition in the model, one would also need to impose a zero flux boundary condition at the half way distance between two neighbouring root hairs. Hence we require

$$\frac{\partial c}{\partial\theta}=0 \quad \text{at} \quad \theta=\pm\frac{d_d}{a}, \quad \text{and} \quad \frac{\partial c}{\partial z}=0 \quad \text{at} \quad z=\pm d_d, \tag{3.3}$$

where d_d is the dimensional half distance between the two root hairs. We use the same far-field boundary condition as before, i.e.,

$$c\to c_0 \quad \text{as} \quad r\to\infty, \tag{3.4}$$

with the initial condition

$$c=c_0 \quad \text{at} \quad t=0. \tag{3.5}$$

As in Chapter 2, we now non-dimensionalise this model by putting

$$t=\frac{a^2(\phi_l+b)}{D\phi_l}t^*, \quad \mathbf{r}=a\mathbf{r}^*, \quad c=K_m c^*. \tag{3.6}$$

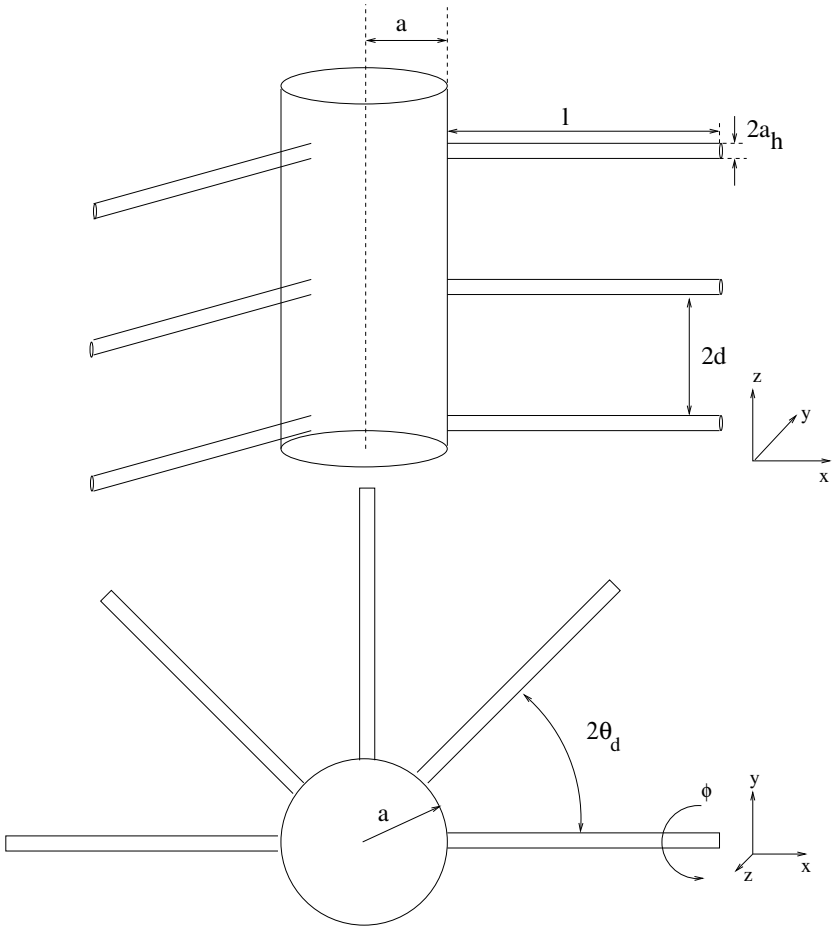

Figure 3.1: Root with root hairs. Parameter d is the half distance between the root hairs, a_h is the root hair radius, a is the root radius, l is the length of the root hair, and $\theta_d = d_d/a$ is the angle corresponding to the half distance between the root hairs.

Our dimensionless model is, after neglecting the $Pe, \epsilon << 1$ terms[1] and dropping $*$s, given by

$$\frac{\partial c}{\partial t} = \nabla^2 c, \tag{3.7}$$

with the boundary condition is given by

$$\mathbf{n} \cdot \nabla c = \frac{\lambda c}{1+c} \quad \text{on} \quad \partial H, \tag{3.8}$$

where $\mathbf{n}$ is the unit outward normal to surface ∂H. The far-field nutrient boundary condition is

$$c \to c_\infty \quad \text{as} \quad r \to \infty, \tag{3.9}$$

and the initial condition is

$$c = c_\infty \quad \text{at} \quad t = 0. \tag{3.10}$$

[1]We also neglected these terms in Chapter 2 Section 2.2.

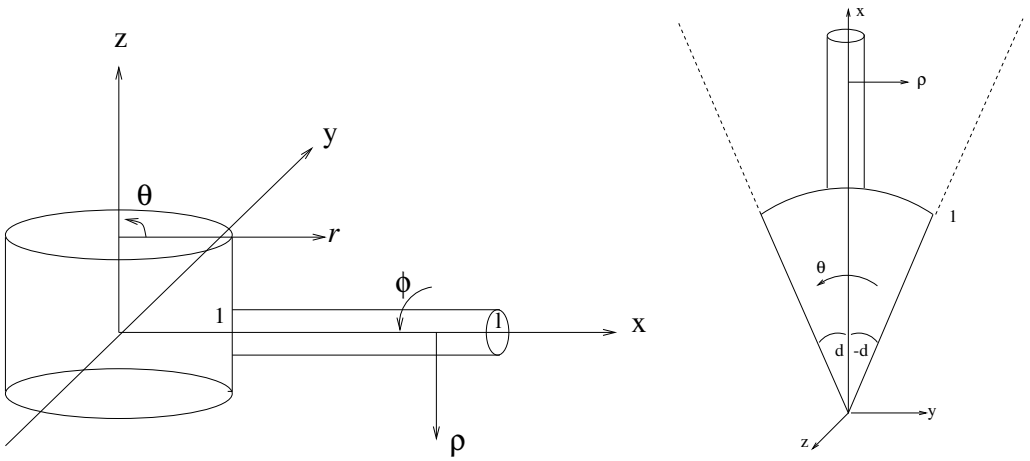

Figure 3.2: Dimensionless root and root hair surface. ∂H is given by $r = 1$ and $\rho = a_h$, where r and θ are the radial root surface coordinates, and ρ and ϕ are the radial coordinates associated with the root hair. $r^2 = x^2 + y^2$, $\tan(\theta) = y/x$, and $\rho^2 = y^2 + z^2$, $\tan(\phi) = z/y$.

The boundary surface ∂H is given as a combination of two intersecting cylinders (see Figure 3.2) characterised with corresponding cylindrical coordinate systems. The root surface is characterised by $r = \sqrt{x^2 + y^2} = 1$, and $\theta = \arctan(y/x)$. Root hair surface is characterised by $\rho = \sqrt{y^2 + z^2} = a_h$, where $a_h = a_{h,d}/a$ is the dimensionless root hair radius, with $a_{h,d}$ [cm] being the dimensional root hair radius, and a [cm] the dimensional root radius. Similarly, we have the angle variable $\phi = \arctan(z/y)$ associated with the root hair, and the root hair length variable x.

Zero flux boundary conditions at the halfway distance between the two neighbouring root hairs are given by

$$\frac{\partial c}{\partial \theta} = 0 \quad \text{at} \quad \theta = \pm d, \quad \text{and} \quad \frac{\partial c}{\partial z} = 0 \quad \text{at} \quad z = \pm d, \tag{3.11}$$

where d is the dimensionless half way distance between the root hairs.

3.1.1.1 Non-dimensional Parameter Estimation

As reported in [6] and [80], there are approximately 500 to 2000 root hairs per cm of root length. Hence, the average distance between the root hairs can be calculated in following way: if the number of root hairs per unit length [cm] of the root is n, then the number of root hairs per unit root surface area is $n/(2\pi a)$, where a is the radius of the root [cm]. Thus, the average half distance d [cm] between the root hairs at the root surface is $\sqrt{\pi a/(2n)}$ [cm]. The dimensionless distance between the root hairs is then given by $d = d[cm]/a[cm] = \sqrt{\pi/(2na)}$.

In the following sections we will use this parameter estimation to derive an approximation to the root hair nutrient uptake. The dimensionless parameters are presented

Parameter	Dimensional	Dimensionless
Root radius (a)	2×10^{-2} [cm]	1
Root hair radius (a_h)	$2.5 \times 10^{-4} - 10^{-3}$ [cm]	$(1-5) \times 10^{-2}$
Length of the root hair (l)	$10^{-2} - 3 \times 10^{-1}$ [cm]	$0.5 - 10$
Number of root hairs per unit of root length (n)	$500 - 2000$ [cm^{-1}]	$10 - 40$
Number of hairs per unit root surface area (m)	$3978 - 15915$ [cm^{-2}]	$1.59 - 6.39$
Half distance between root hairs (d)	$3.9 \times 10^{-3} - 10^{-2}$ [cm]	$0.19 - 0.39$

Table 3.1: Root and root hair dimensional and dimensionless parameters.

in Table 3.1. The same parameter ranges as in Table 3.1 for maize are also applicable for wheat, lettuce, russian thistle, tomato, onion, and carrot [6]. The nutrient uptake parameters λ, ϵ etc. are the same as presented in Chapter 2 Section 2.2, since we have used the same non-dimensional scaling. As we can see the distance between root hairs is at least one order of magnitude larger than the root hair radius, i.e., $d >> a_h$. We will use this information to find the approximations to the solution of this model at limit of large time.

3.1.2 Model Approximations

Sufficiently far away from the root and root hairs, i.e., in the outer region, the model of nutrient uptake by root and root hair is expected to be the same as in the absence of root hairs (see Chapter 2). This is because far away from the root the influence from the root and root hair length scales can be considered negligible. Hence, as before in Chapter 2, far away from the root we find that the concentration profile is given by the similarity solution

$$c(r,t) = c_\infty + BE_1(\frac{r^2}{4t}), \tag{3.12}$$

where B is allowed to be a slowly varying function of time, $B'(t)/B(t) << 1$ (as in Chapter 2), and it is to be determined by matching the outer solution with the inner solution that is valid near the root surface. The variable r is the radial distance from the root centre, i.e., the radial coordinate associated with the root. Given a particular position (r, θ, z) associated with the root, the corresponding Cartesian coordinates are $x = r\cos\theta$, $y = r\sin\theta$, and z (see Figure 3.2). Equivalently, in terms of radial coordinates (ρ, ϕ, x) associated with the root hairs, these are x, $y = \rho\cos\phi$, and $z = \rho\sin\phi$. Hence, we can write $r^2 = x^2 + \rho^2\cos^2\phi$, which implies that using

root hair coordinates the outer solution becomes

$$c(x,\rho,\phi,t) = c_\infty + BE_1(\frac{x^2+\rho^2\cos^2\phi}{4t}). \tag{3.13}$$

Near the root and root hair surface the diffusion profile clearly has quite a complex structure. There is a diffusional gradient in the direction of the root surface at $r = 1$ and also in the direction of the root hair surface $\rho = \sqrt{y^2+z^2} = a_h$. However, we can approximate the solution when the inter root hair distance is much bigger than the root hair radius, $d >> a_h$, and the root hair radius is very small, $a_h << 1$ (we can see from Table 3.1 that this is the case).

First we look for the solution near the root hair surface. The solution in this region can be calculated using an appropriate rescaling of the space variable. We introduce the space variable $\widehat{\rho} = \rho/a_h$ (remembering $\rho = \sqrt{y^2+z^2}$ is the radial coordinate associated with root hair), and then the diffusion equation written in the radial coordinates $(x,\widehat{\rho},\phi)$, associated with root hairs, becomes

$$\frac{\partial^2 c}{\partial\widehat{\rho}^2} + \frac{1}{\widehat{\rho}}\frac{\partial c}{\partial\widehat{\rho}} + \frac{1}{\widehat{\rho}^2}\frac{\partial^2 c}{\partial\phi^2} = a_h^2(\frac{\partial c}{\partial t} - \frac{\partial^2 c}{\partial x^2}), \tag{3.14}$$

in which $a_h << 1$. At the leading order this reduces to

$$\frac{\partial^2 c}{\partial\widehat{\rho}^2} + \frac{1}{\widehat{\rho}}\frac{\partial c}{\partial\widehat{\rho}} + \frac{1}{\widehat{\rho}^2}\frac{\partial^2 c}{\partial\phi^2} = 0. \tag{3.15}$$

The solution of (3.15) independent of ϕ is

$$c = A_1(x) + A_2(x)\ln\widehat{\rho}, \tag{3.16}$$

where A_1 and A_2 depend on the distance from the root surface along the x axis. The root hair surface boundary condition is

$$\frac{\partial c}{\partial\widehat{\rho}} = \frac{a_h\lambda c}{1+c} \quad \text{on} \quad \widehat{\rho} = 1. \tag{3.17}$$

However, $x^2 = r^2 - a_h^2\widehat{\rho}^2\cos^2\phi$, i.e., $A_1(x) = A_1(\sqrt{r^2 - a_h^2\widehat{\rho}^2\cos^2\phi}) \approx A_1(r)$ since $a_h << 1$. Hence, $A_2 = \partial c/\partial\widehat{\rho}$ and $A_1 = c$ at $\widehat{\rho} = 1$, which implies that $A_2 = a_h\lambda A_1(r)/[1+A_1(r)]$. Therefore the solution near the root hair is in the form

$$c = A_1(r) + \frac{a_h\lambda A_1(r)}{1+A_1(r)}\ln\widehat{\rho}. \tag{3.18}$$

When $a_h\lambda << 1$ (our estimated parameters show that this is mostly the case) the root hair influence on the general diffusion profile around the root is small, which implies that the diffusion profile around and between the root hairs is "flat". In [60] Itoh and

Barber conclude the same, but their justification is inaccurate. They thought that the diffusion profile around the root hairs is flat because of the "small distance between the root hairs". In fact the distance between the root hairs compared to their radius is large, $a_h << d$. However, we have shown that the concentration profile around the root hairs is flat because the dimensionless root hair nutrient uptake coefficient $a_h\lambda$ for root hairs is small, i.e., root hairs are very weak sinks in the soil because of their very small radius.

We can neglect the zero flux boundary conditions between the neighbouring root hairs since the root hair radius is much smaller than the half distance between the root hairs, $a_h << d$.

For $a_h\lambda << 1$, the diffusion profile in r is the same as in absence of root hairs, i.e., $A_1(r)$ is given by the uniform approximation found in Chapter 2, more specifically by

$$A_1(r,t) = c_\infty - \frac{F(t)}{2}E_1(\frac{r^2}{4t}), \tag{3.19}$$

where $F(t)$, the nutrient uptake by the root, is given in this case by equation (2.120):

$$F(t) = \frac{2\lambda c_\infty}{1 + c_\infty + \frac{\lambda}{2}\ln(4e^{-\gamma}t + 1) + \sqrt{4c_\infty + [1 - c_\infty + \frac{\lambda}{2}\ln(4e^{-\gamma}t + 1)]^2}}. \tag{3.20}$$

However, $F(t)$ is only the amount of nutrient taken up by the root. The nutrient uptake by the root hairs, $F_h(t)$, will be given by integrating the diffusion profile over the root hair length, i.e., from $r = 1$ to $l+1$, and around it, times the number of root hairs per unit root surface area. Hence we have

$$F_h(t) = 2\pi a_h\lambda m\int_1^{l+1}\frac{A_1(r,t)}{1 + A_1(r,t)}\,dr, \tag{3.21}$$

where m is the number of root hairs per unit of dimensionless root surface area. Taking $A_1(r)$ to be given by the inner approximation, i.e., $A_1(r,t) = c(1,t) + F(t)\ln r$ by expanding (3.19) for small r, and $m = n/2\pi$ (n is the number of root hairs per unit of dimensionless root length), we get

$$F_h(t) = na_h\lambda\int_1^{l+1}\frac{c(1,t) + F(t)\ln r}{1 + c(1,t) + F(t)\ln r}\,dr. \tag{3.22}$$

This gives, using the fact that $c(1,t) = F(t)/(\lambda - F(t))$, the expression for $F_h(t)$:

$$F_h(t) = a_h n\lambda\Big[l + \frac{e^{-\frac{\lambda}{F(\lambda-F)}}}{F}\Big\{E_1\Big(\ln(\frac{1}{1+l}) - \frac{\lambda}{F(\lambda-F)}\Big) - E_1\Big(-\frac{\lambda}{F(\lambda-F)}\Big)\Big\}\Big]. \tag{3.23}$$

This solution is valid for the times $t >> (l+1)^2/4$ such that $\eta = r^2/(4t) << 1$ in the root hair region so that the approximation of the exponential integral $E_1(\frac{r^2}{4t})$ for small argument is valid. This corresponds to dimensional time more than 2 hours.

When $\eta = r^2/(4t) >> 1$ in the root hair region, i.e., $t << (l+1)^2/4$, we can approximate the exponential integral using Watson's Lemma [56] and find that at the leading order $E_1(\eta) \sim e^{-\eta}/\eta$, when $\eta >> 1$.

Hence the integrand in (3.21) becomes, using the binomial expansion,

$$\frac{A_1}{1+A_1} = \frac{c_\infty - \frac{F}{2\eta}e^{-\eta}}{1+c_\infty - \frac{F}{2\eta}e^{-\eta}} \approx \frac{c_\infty - \frac{F}{2\eta}e^{-\eta}}{1+c_\infty}[1+\ldots], \tag{3.24}$$

and the uptake of nutrient by root hairs is given by

$$\begin{aligned} F_h(t) &= a_h n \lambda \Big\{ \frac{c_\infty}{1+c_\infty} l + \frac{2tF(t)}{2(1+c_\infty)} \Big[\frac{e^{-(1+l)^2/4t}}{1+l} - e^{-1/4t} \\ &+ \frac{1}{2}\sqrt{\frac{\pi}{t}} \Big(\mathrm{erf}\Big(\frac{1+l}{2\sqrt{t}}\Big) - \mathrm{erf}\Big(\frac{1}{2\sqrt{t}}\Big)\Big)\Big]\Big\}. \end{aligned} \tag{3.25}$$

For root hairs with length 14 mm, this solution is valid for times of order 2 hours to 1 day or less. However, the vegetative time-scale of the roots and root hairs is of order 10 days or more. Hence, except in very short time experiments, the use of (3.23) is appropriate.

The results for calculating the nutrient uptake by root and root hairs (given by equation (3.23)) are shown on Figure 3.3 up to time $t = 10^5$, which in dimensional terms corresponds to a time of order 20 days.

As we can see, the nutrient uptake in this regime is strongly dominated by the presence of root hairs. The nutrient uptake by the root hairs is approximately 5-6 times that of the root. With the root hair parameters $a_h = 0.01$, $l = 10$, and $n = 40$ the total root surface area has also increased by 5 times.

This result suggests that it would be instructive to revise the estimates of nutrient uptake parameters F_m and K_m derived from experiments which omit the effect of nutrient uptake by root hairs. As one can see from Figure 3.4, the length of the root hairs influences the cumulative nutrient uptake by the root almost linearly. The number of root hairs has a similar effect on the nutrient uptake. Figure 3.4 should give one extra tool for estimating the nutrient uptake parameters from experiments in which the number and length of root hairs has been measured in addition to the nutrient uptake. With the aid of modern genetic engineering techniques this is now possible, however no results on this have been published so far.

3.1.3 Conclusions on the Root Hair Model

In the first part of this chapter we have developed a model for approximating the nutrient uptake by a complete root and root hair assembly. There are two main conclusions we can derive from this study.

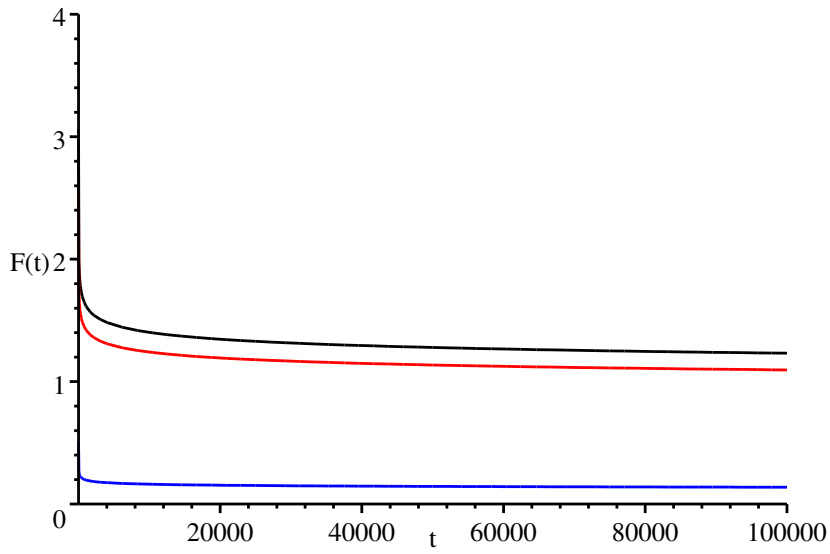

Figure 3.3: The dimensionless nutrient uptake by the root and root hair. The red line shows the uptake of nutrients by the root hair given by (3.23), the blue line shows the nutrient uptake by the root, and the black line shows the total nutrient uptake by the plant. Parameters are $\lambda = 1$, $c_\infty = 1$, $n = 40$, $a_h = 0.01$, and $l = 10$. $t = 10^5$ corresponds to ≈ 20 days.

Firstly, the influence of root hairs can be, crudely speaking, divided into two different situations. When root hair length is of the order of the root radius or less, their effect is purely to extend the root surface area. This can be seen in Figure 3.4 where in the region of $l < 1$, F_c/S is approximately constant indicating the linear relationship between the increase in root surface area and nutrient flux[2]. Longer root hairs however, can take up substantially more nutrients since they extend into soil with higher concentration.

Secondly, we would like to suggest the revision of experimental estimation of the nutrient uptake parameters F_m and K_m with the view of including the effect of root hairs. In the current parameter estimation the roots are considered to be smooth cylinders, however, in experiments roots clearly do have root hairs. The neglect of root hairs in the parameter estimation results in higher values of F_m and also K_m. The adjustment of the estimation procedure to include root hairs would lead to smaller values of F_m and K_m, and hence also λ, making the current calculation applicable for most of the parameter ranges.

[2] l is non-dimensional root hair length. $l = 1$ corresponds to the root hair length equal to the root radius.

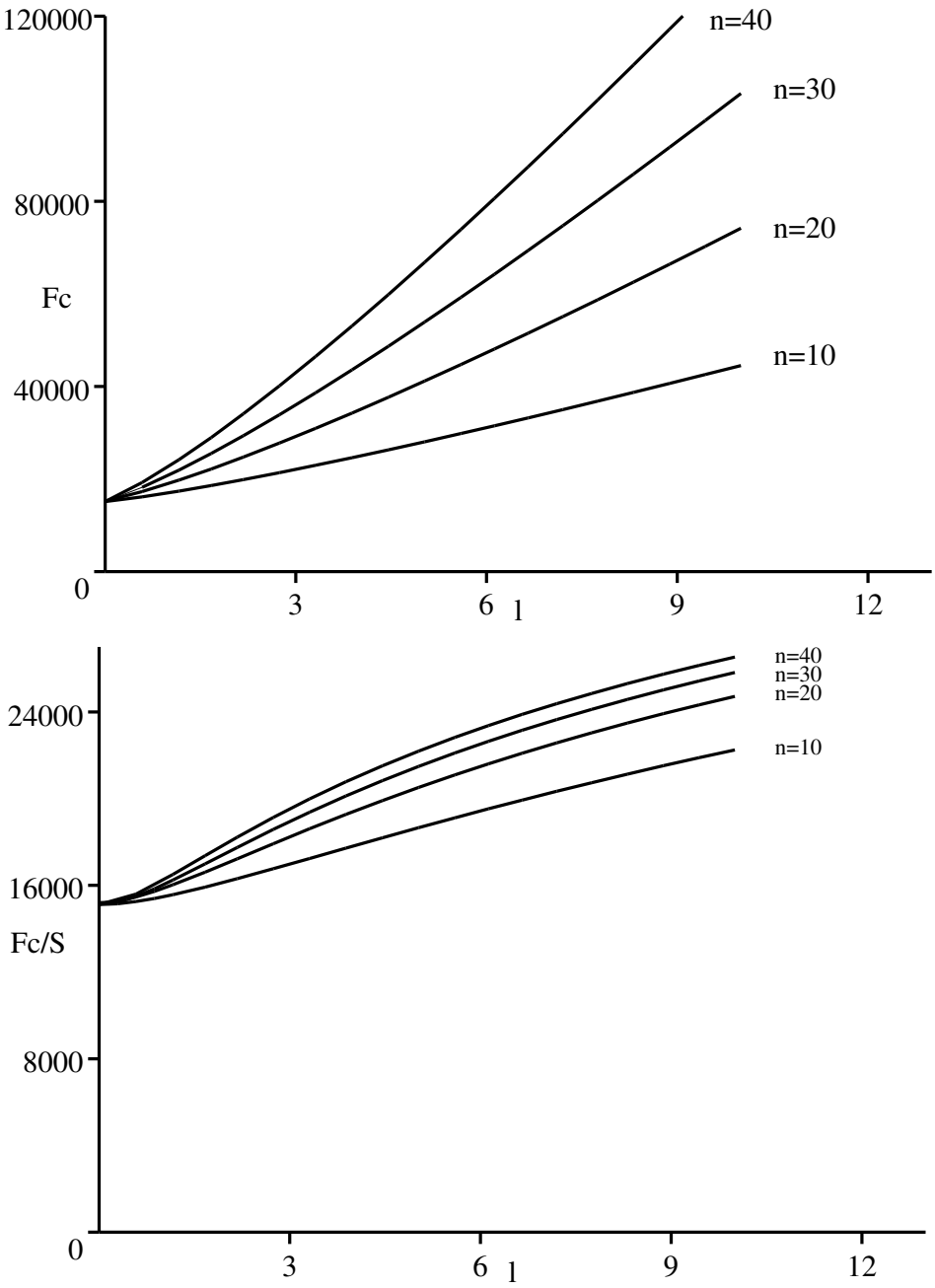

Figure 3.4: The cumulative uptake $F_c = \int_{t_1}^{t_2} (F(t)+F_h(t))\, dt$ with $t_1 = 50$ and $t_2 = 10^5$ (corresponding dimensionally approximately to $1 - 20$ days), depending on the root hair length l for different numbers of root hairs, n, per unit (non-dimensional) root length (typically n ranges from 10 to 40). Cumulative uptake is calculated using the trapezoidal rule in the symbolic mathematical package *xMaple*. Top graph shows the cumulative uptake F_c as a function of root hair length, bottom graph shows F_c/S where S is the total root surface area including the root hair surface area. Parameters $\lambda = 1$, $c_\infty = 1$, and $a_h = 0.01$.

3.2 Mycorrhizae

As discussed before in Chapter 1, roots form a symbiotic link with fungi, called mycorrhizae. Mycorrhizae can be divided into two main categories: (1) ectotrophic mycorrhizae that form a fungal sheath with thickness ~ 40 μm, which completely encloses the root (this is more common in trees); and (2) endotrophic mycorrhizae, which live inside the root, between and inside the cells and extend out to the surrounding soil. Endotrophic mycorrhizae belong to the genus *Endogone* L. and are found in the roots of most agriculturally important plants such as rubber, tobacco, and cereals.

The existence of mycorrhizae is thought to be very beneficial to plants which grow in nutrient deficient environments as they aid nutrient uptake. It has been demonstrated that the phosphorus uptake in the presence of mycorrhizae is two to three times higher than in its absence [80], [113]. The rate of infection of roots by mycorrhizal fungi is thought to saturate once the required uptake of nutrients is obtained. In addition it has been found that mycorrhizal infection does not develop in very dry, saline, or water logged soils [80], [16]. In cases where mycorrhizae are present, they may be extremely important to the nutrient uptake and thus must be taken into account in the model.

The branching structure of mycorrhizae outside the root and within the soil is very complex. It attaches into the root surface epidermal cells with hyphae whose diameter is in the range of 2-27 μm. Outside the root the mycorrhiza has external hyphae with diameter in the range of 20-150 μm. Mycelial hyphae (see Figure 3.5) form an extended branching network in the soil and can reach far out into the soil [14]. Nutrients taken up by the mycorrhizae are transported to the root surface where nutrient ions are released into the plant. In return the plant supplies carbohydrates which are needed by mycorrhizae for its growth and functioning. Hence, the plant needs the mycorrhizae to obtain nutrients, and the mycorrhizae need the plant to obtain carbohydrates. This forms the basis for the symbiotic link between the plant and fungus.

There has been some, small effort made to model the nutrient uptake by roots with mycorrhizal symbiosis. For example, Sanders [109] describes a phenomenological model for mycorrhizae-plant interaction and finds that it is able to capture the qualitative behaviour of phosphate uptake. However, the quantitative aspects of this type of model need to be derived more accurately from basic microscopic biological experiments and models.

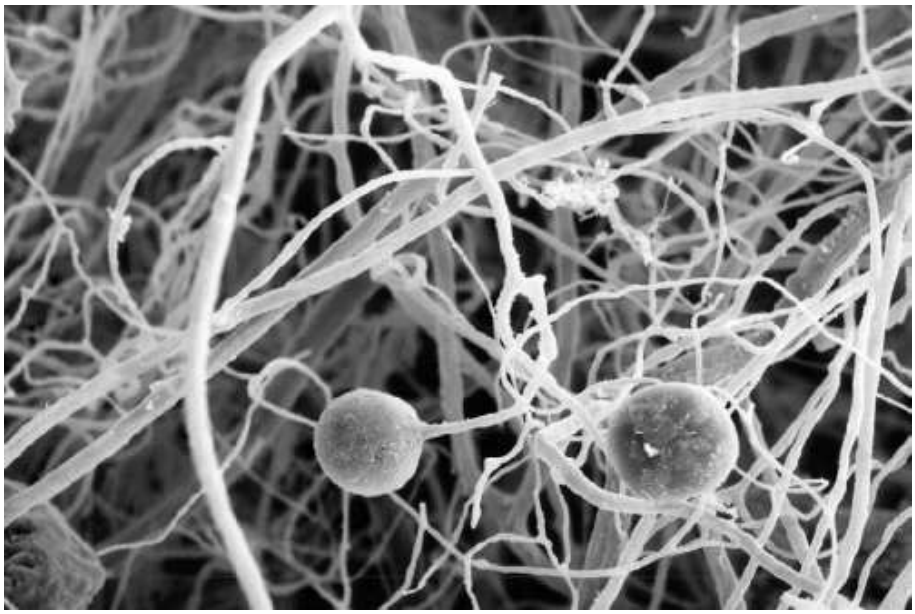

Figure 3.5: Picture of *Glomus deserticola L.* soil hyphae outside *Rosa hybrida L.* roots. Picture reproduced from `http://mycorrhiza.ag.utk.edu/`.

3.2.1 Mathematical Model for Nutrient Uptake by Roots with Mycorrhizal Infection

As mentioned before, the structure of the mycorrhizae is very fine. In order to model nutrient uptake by roots with mycorrhizal infection, we first divide the soil phase up into 2 volume fractions, i.e., ϕ_s is the volume fraction of the solid particles, and ϕ_l is the volume fraction of the liquid (as in Chapter 2 we are going to ignore the gaseous phase in the soil). That implies that for fully saturated soil $\phi_s + \phi_l = 1$. By doing this we are assuming that the presence of mycorrhizae in the soil does not influence the soil moisture conditions, i.e., the volume fraction of mycorrhizae is small.

As in Chapter 2, we consider the concentration of nutrient ions present in each fraction separately. The concentration of ions in the solid phase is considered to be changing in time only due to the exchange of ions with the liquid solution, i.e., we neglect the very slow diffusion of ions in the solid state; and so

$$\frac{\partial c_s}{\partial t} = d_s, \tag{3.26}$$

where d_s is the rate of liquid-solid inter-facial ion transport. We also assume that the mycorrhizae do not take up nutrients from the solid fraction in the soil. The actual source of mycorrhizal nutrient uptake is highly controversial with the soil solution, solid phase and nutrients immobilised in organic matter all being proposed. However, the only certain source is the soil solution and we will confine our attention to uptake only from this pool.

Ions in the liquid phase are considered to be diffusing and convecting towards the root (see Chapter 2). There is also the exchange of ions with the solid state and ion uptake by the mycorrhizae. Hence, assuming that nutrient uptake by mycorrhizae is described by a sink term F_{myc}, the equation for nutrient in the liquid fraction becomes

$$\frac{\partial \phi_l c_l}{\partial t} + \nabla \cdot (c_l \mathbf{u}) = \nabla \cdot (D \phi_l \nabla c_l) + d_l - F_{\text{myc}}, \tag{3.27}$$

where $\mathbf{u}$ is the Darcy flux of water, D is the diffusion coefficient in the liquid phase of the soil, d_l is the solid-liquid inter-facial ion transport ($d_s + d_l = 0$), and F_{myc} is the rate of nutrient ion uptake by the mycorrhizae per unit volume of soil.

By adding up the equations for the two phases and using the same buffer power arguments as in Chapter 2, equations (2.6), (2.7) and (2.8), the system reduces to

$$\frac{\partial (b + \phi_l) c_l}{\partial t} + \nabla \cdot (c_l \mathbf{u}) = \nabla \cdot (D \phi_l \nabla c_l) - F_{\text{myc}}, \tag{3.28}$$

where b is the so called buffer power of the soil, i.e., $c_s = b c_l$. Hence we are now left with the diffusion-convection equation (3.28) for c_l which has a sink term represented by F_{myc}.

3.2.1.1 The Rate of Nutrient Uptake by Mycorrhizae F_{myc}

The nutrient uptake per unit soil volume at distance r from the root centre clearly depends on the amount of mycorrhizae at this position, more specifically on the surface area of mycorrhizae per unit volume of soil $S_m(r)$. If the average mycorrhizae radius is a_m, and the length of mycorrhizae per unit volume of soil l_m, then the total mycorrhizal surface area per unit volume of soil is $S_m = 2\pi a_m l_m$. Almost no experimental measurements of the distributions of mycorrhizae in the soil have been performed. The best available measurements are by Jakobsen et al. [64], [65], [66]. They present experimental measurements on length of mycorrhizal hyphae per gramme of dry soil (1 gramme of dry soil corresponds to approximately $1-2$ cm^3 of soil) as a function of distance from the root surface. On Figure 3.6 the distribution profile for *Scutellospora calospora* L. is shown. The mycorrhiza radius a_m is very small, typically of order 20 to 150 μm [14], which in dimensionless terms (non-dimensionalising the length with respect to root radius $a = 0.02$ cm) corresponds to 0.05 to 0.37. Thus it is small compared to the root radius. Mycorrhizae attache to the root via the entry points on the root surface. There are approximately 2.6 to 21.1 mycorrhizae entry points per mm of root length. Therefore the average half distance of mycorrhizae at the root surface is approximately of order 0.61 to 1.7 (non-dimensionalised with respect to root radius). It is reasonable to assume that the mycorrhizae density is highest at the root surface. Thus, since the distance between the mycorrhizae is much larger than the

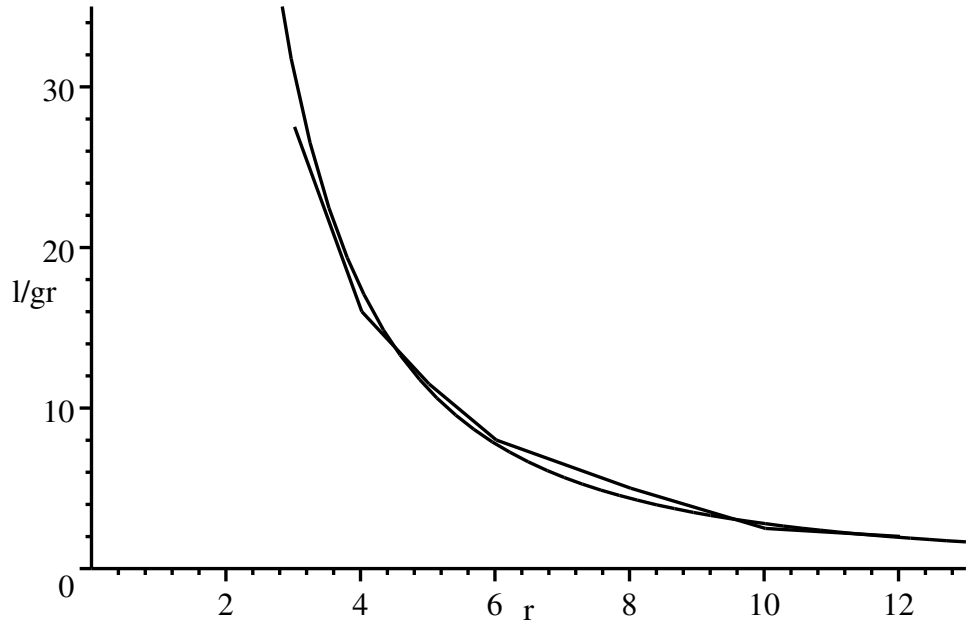

Figure 3.6: Mycorrhizae *Scutellospora calospora* L. profiles (length in meters per gramme of dry soil) after [64] which have been fitted using least squares fit with $l(r) = \kappa_{\text{dim}}^2/r^2$ [m g^{-1}], where $\kappa_{\text{dim}} = 16.7$ and r is measured in cm from the centre of the root. 1 gramme of soil corresponds to approximately $1 - 2$ cm^3 of soil.

mycorrhizae radius the same approximation applies as in the case of root hairs, i.e., the nutrient uptake by the mycorrhizae is not influenced by the competition between them, but is determined by the local concentration of nutrient. Because of their small uptake the concentration profile between the different mycorrhizal branches is flat. Hence we take

$$F_{\text{myc}} = S(r)\frac{F_m c}{K_m + c} = 2\pi a_m l_m(r)\frac{F_m c}{K_m + c}, \tag{3.29}$$

where a_m is the mycorrhizal radius [cm], F_m [μmol cm^{-2}s^{-1}] and K_m [μmol cm^{-3}] dimensional nutrient uptake coefficients, $l_m(r)$ is the total mycorrhizal hyphal lengths per unit of soil volume at position r [cm cm^{-3}], and c is the nutrient concentration at the radial position r.

3.2.2 Boundary Conditions

Now that we have written down the equation for the nutrient concentration in the soil including the mycorrhizal uptake, we need to apply some boundary conditions at the root surface and far away from the root. As before, at the root surface nutrients in the liquid phase get taken up according to a Michaelis-Menten type uptake law, i.e.,

$$\mathbf{n} \cdot [D\phi_l \nabla c_l + \mathbf{u} c_l] = \frac{F_m c_l}{K_m + c_l} - E, \quad \text{at} \quad r = a, \tag{3.30}$$

where F_m is the maximum flux of nutrients into the root, K_m is the Michaelis-Menten constant, $E = F_m c_{\min}/(K_m + c_{\min})$ with $c_{\min}$ being the minimum concentration when the nutrient uptake by the root still occurs, and a is the radius of the root.

The far-field nutrient concentration boundary condition is

$$c \to c_0 \quad \text{as} \quad r \to \infty. \tag{3.31}$$

3.2.3 Non-dimensionalisation

Using the same scales (2.14) as in Chapter 2 we arrive at the non-dimensional equation

$$\frac{\partial c}{\partial t} - Pe\frac{1}{r}\frac{\partial c}{\partial r} = \frac{1}{r}\frac{\partial}{\partial r}(r\frac{\partial c}{\partial r}) - F^*_{\text{myc}}, \tag{3.32}$$

where F^*_{myc}, non-dimensional uptake of nutrients by mycorrhizae, is given by

$$F^*_{\text{myc}} = \frac{a^2}{DK_m\phi_l}2\pi a_m l_m(r)\frac{F_m c}{1+c} = S(r)\frac{a_m\lambda c}{1+c}, \tag{3.33}$$

where c is the dimensionless nutrient concentration, a_m is the ratio of the mycorrhizae radius to the root radius, λ is the dimensionless nutrient uptake coefficient, and $S(r) = 2\pi a^2 l_m(r)$, where a is the root radius [cm] and l_m is the dimensional mycorrhizae length per unit of soil volume [cm cm^{-3}].

Since we have used the same non-dimensionalisation as in Chapter 2 the value of Péclet number Pe is the same as found there, i.e., $Pe << 1$. The dimensionless boundary condition at the root surface is given by

$$\frac{\partial c}{\partial r} + Pe\, c = \frac{\lambda c}{1+c} \quad \text{on} \quad r = 1, \tag{3.34}$$

and the dimensionless far-field boundary condition is

$$c \to c_\infty \quad \text{as} \quad r \to \infty. \tag{3.35}$$

3.2.4 Approximate Solutions

Generally, given a specific mycorrhizal surface area distribution $S(r)$, one would need to solve this problem numerically. However when $S(r) = 2\pi\kappa^2/r^2$ with $\kappa^2 = a^2\kappa^2_{\text{dim}}$, i.e. maybe for *Scutellospora calospora* L., we can approximate the solution analytically (see Figure 3.6). Note that κ is a dimensionless mycorrhizal profile coefficient. For $Pe << 1$ the leading order $O(Pe^0)$ model is given by

$$\frac{\partial c}{\partial t} = \frac{1}{r}\frac{\partial}{\partial r}(r\frac{\partial c}{\partial r}) - \frac{\alpha^2}{r^2}\frac{c}{1+c}, \tag{3.36}$$

where $\alpha^2 = 2\pi\kappa^2 a_m\lambda$ is the mycorrhizal profile dependent nutrient uptake coefficient.

3.2.4.1 The Small c_∞ Limit

Since mycorrhizae have been shown to be very important for plants growing in nutrient deficient soils, we consider the case where the far-field nutrient concentration is small. When $c_\infty << 1$, the mycorrhizal model equation (3.36) simplifies at leading order to

$$\frac{\partial c}{\partial t} = \frac{1}{r}\frac{\partial}{\partial r}(r\frac{\partial c}{\partial r}) - \frac{\alpha^2}{r^2}c, \tag{3.37}$$

where $\alpha^2 = 2\pi\kappa^2 a_m \lambda$, and boundary conditions are

$$\frac{\partial c}{\partial r} = \lambda c \quad \text{at} \quad r = 1, \quad \text{and} \quad c \to c_\infty \quad \text{as} \quad r \to \infty. \tag{3.38}$$

As in Chapter 2, we are interested in the long time solution to this model.

Outer Solution

By rescaling $r = R/\sigma$ and $t = \tau/\sigma^2$ with $\sigma << 1$, and looking for an outer solution with similarity variable $\eta = R^2/4\tau$, we find that the equation (3.37) transforms into the following ordinary differential equation for $c(\eta)$

$$4\eta^2\frac{\mathrm{d}^2 c}{\mathrm{d}\eta^2} + 4(1+\eta)\eta\frac{\mathrm{d}c}{\mathrm{d}\eta} - \alpha^2 c = 0. \tag{3.39}$$

The general solution to this equation is given by

$$c(\eta) = \frac{e^{-\eta/2}}{\sqrt{\eta}}\Big\{A_1 W_{-1/2,\alpha/2}(\eta) + A_2\eta[I_{-1/2+\alpha/2}(\frac{\eta}{2}) + I_{1/2+\alpha/2}(\frac{\eta}{2})]\Big\}, \tag{3.40}$$

where $W_{-1/2,\alpha/2}$ is the Whittaker W-function, and I is the modified Bessel I function. However, satisfying the outer boundary condition $c \to c_\infty$ as $r \to \infty$ we find that since

$$\lim_{\eta\to\infty}[e^{-\eta/2}\sqrt{\eta}I_\beta(\frac{\eta}{2})] = \frac{1}{\sqrt{\pi}}, \tag{3.41}$$

for all β, and

$$\lim_{\eta\to\infty}[\frac{e^{-\eta/2}}{\sqrt{\eta}}W_{-1/2,\alpha/2}(\eta)] = 0, \tag{3.42}$$

then parameter $A_2 = \sqrt{\pi}c_\infty/2$. As before in Chapter 2 we allow A_1 to be slowly varying in time, i.e., $A_1'(t)/A_1(t) << 1$; the precise form of A will be determined from matching the outer solution with the inner solution.

Inner Solution

In order to find the inner solution we transform back to inner variable $r = R/\sigma$, but keep the long time variable τ, since as in Chapter 2, we are interested only in the long time behaviour of the system. Thus we get

$$\sigma^2 \frac{\partial c}{\partial \tau} = \frac{1}{r}\frac{\partial}{\partial r}(r\frac{\partial c}{\partial r}) - \frac{\alpha^2}{r^2}c. \tag{3.43}$$

The leading order $O(\sigma^0)$ solution to this equation is given by

$$c(r,\tau) \approx B_1(\tau)\sinh[\alpha \ln(r)] + B_2(\tau)\cosh[\alpha \ln(r)] + O(\sigma^2). \tag{3.44}$$

By applying the boundary conditions at $r = 1$, we find that

$$c(r,\tau) \approx \frac{1}{2}r^{-\alpha}(c_1 - \frac{F}{\alpha}) + \frac{1}{2}r^{\alpha}(c_1 + \frac{F}{\alpha}) + O(\sigma^2), \tag{3.45}$$

where $F = \frac{\partial c}{\partial r}|_{r=1}$ and $c_1 = c|_{r=1}$.

Matching

In order to match the inner solution to the outer solution we expand the outer solution, given by (3.40), for the small argument and thus the leading order terms (see [1] for the expansions of Whittaker W functions and Bessel functions) are given as a series in powers of r, i.e.,

$$c(r,t) \approx \frac{A_1\Gamma(-\alpha)r^{\alpha}}{\Gamma(1-\alpha/2)(4t)^{\alpha/2}} + \frac{A_1\Gamma(\alpha)r^{-\alpha}}{\Gamma(1+\alpha/2)(4t)^{-\alpha/2}} + \frac{c_\infty\sqrt{\pi}r^{\alpha}}{2}\frac{1}{(4t)^{\alpha/2}}\frac{1}{4^{(\alpha-1)/2}}\frac{1}{\Gamma(\frac{1+\alpha}{2})}, \tag{3.46}$$

where $\Gamma(x) = \int_0^\infty t^{x-1}e^{-t}\,dt$ is the Gamma function.

Matching $O(r^{-\alpha})$ terms leads to

$$A_1 = \frac{\Gamma(1+\frac{\alpha}{2})}{2(4t)^{\alpha/2}\Gamma(\alpha)}(c_1 - \frac{F}{\alpha}), \tag{3.47}$$

and matching $O(r^{\alpha})$ terms leads to

$$\frac{1}{2}(c(1,t) + \frac{F(t)}{\alpha}) = \frac{A_1\Gamma(-\alpha)}{\Gamma(1-\alpha/2)(4t)^{\alpha/2}} + \frac{c_\infty\sqrt{\pi}}{2^{\alpha}(4t)^{\alpha/2}\Gamma(\frac{1+\alpha}{2})}. \tag{3.48}$$

Substituting the definition of A_1 given by equation (3.47) and using $c(1,t) \approx F(t)/\lambda$ for $c_\infty << 1$, we find that the flux $F(t)$ is given by

$$F(t) = \frac{c_\infty\sqrt{\pi}}{2^{\alpha}(4t)^{\alpha/2}\Gamma(\frac{1+\alpha}{2})}\Big(\frac{\lambda+\alpha}{2\lambda\alpha} - \frac{\alpha-\lambda}{\lambda\alpha} \times \frac{1}{2(4t)^{\alpha}} \times \frac{\Gamma(-\alpha)}{\Gamma(\alpha)} \times \frac{\Gamma(1+\alpha/2)}{\Gamma(1-\alpha/2)}\Big)^{-1}. \tag{3.49}$$

We also include the small shift in the time origin, i.e., we take $t \to t + t_0$, as to have $F = \lambda c_\infty$ at $t = 0$ (as in Chapter 2). The time-shift $t_0 = x^{-2/\alpha}/4$, where x is

$$x = \sqrt{\left(\frac{c_\infty\sqrt{\pi}}{2^\alpha\Gamma(\frac{1+\alpha}{2})}\right)^2 + 2\frac{c_\infty^2(\alpha^2-\lambda^2)\Gamma(-\alpha)\Gamma(1+\alpha/2)}{\alpha^2\Gamma(\alpha)\Gamma(1-\alpha/2)}} - \\ - \frac{\alpha\Gamma(\alpha)\Gamma(1-\alpha/2)c_\infty\sqrt{\pi}}{2^{\alpha+1}c_\infty(\alpha-\lambda)\Gamma(-\alpha)\Gamma(1+\alpha/2)\Gamma(\frac{1+\alpha}{2})}. \tag{3.50}$$

The comparison between the numerical experiments with the full non-linear model root nutrient uptake and uptake given by (3.49) is shown on Figure 3.7. We can see that the numerical experiments with the model agree remarkably well at large times with the analytical approximation.

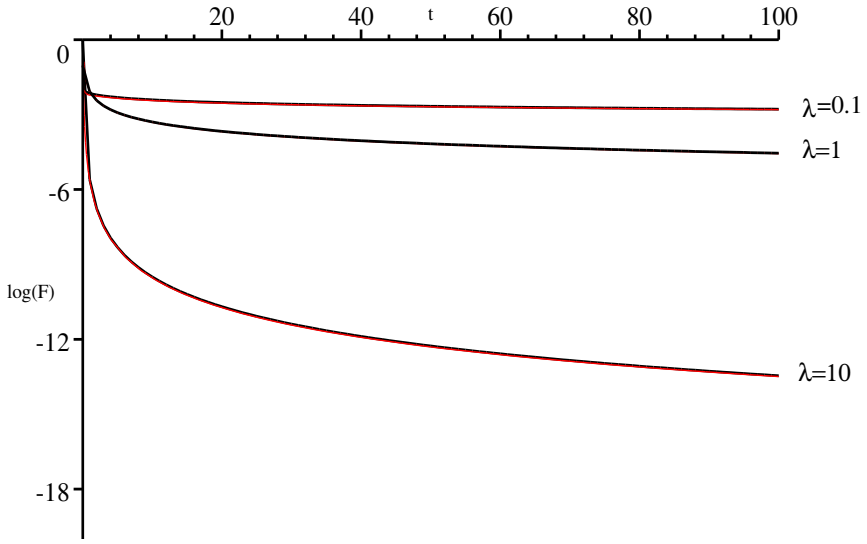

Figure 3.7: Nutrient uptake by the root in the presence of mycorrhizae for $c_\infty = 0.1$ and $\alpha^2 = 2\pi\kappa^2 a_m\lambda = 0.628, 6.28, 62.8$ corresponding to $\lambda = 0.1, 1, 10$. Black lines are the numerical solutions to the model given by the equation (3.37) and red lines are the analytical approximations given by (3.49).

The overall removal of nutrients from the soil by the root and by the mycorrhizae is calculated taking into account the nutrient uptake by the root at the root surface plus the nutrient uptake by the mycorrhizae. Hence the removal of nutrients from the soil $F_{\text{tot}}(t)$ is

$$F_{\text{tot}}(t) = F(t) + \int_1^\infty \frac{\alpha^2 c(r,t)}{r^2}\, dr, \tag{3.51}$$

where $c(r,t)$ is the uniformly valid approximation to the concentration profile. The uniformly valid approximation will be the outer expansion given with the parameters which have been determined from the matching, since at the small r limit the outer

approximation is equal to the inner approximation (see Figure 3.8). Hence, we have

$$c(r,t) = e^{-\frac{r^2}{8t}}[\frac{\Gamma(1+\frac{\alpha}{2})}{2(4t)^{(\alpha-1)/2}\Gamma(\alpha)}(\frac{F(t)}{\lambda}-\frac{F(t)}{\alpha})\frac{W_{-\frac{1}{2},\frac{\alpha}{2}}(\frac{r^2}{4t})}{r}+ \\ +\frac{c_\infty r}{2}\sqrt{\frac{\pi}{4t}}(I_{\frac{\alpha-1}{2}}(\frac{r^2}{8t})+I_{\frac{\alpha+1}{2}}(\frac{r^2}{8t}))], \tag{3.52}$$

where $F(t)$ is given by (3.49).

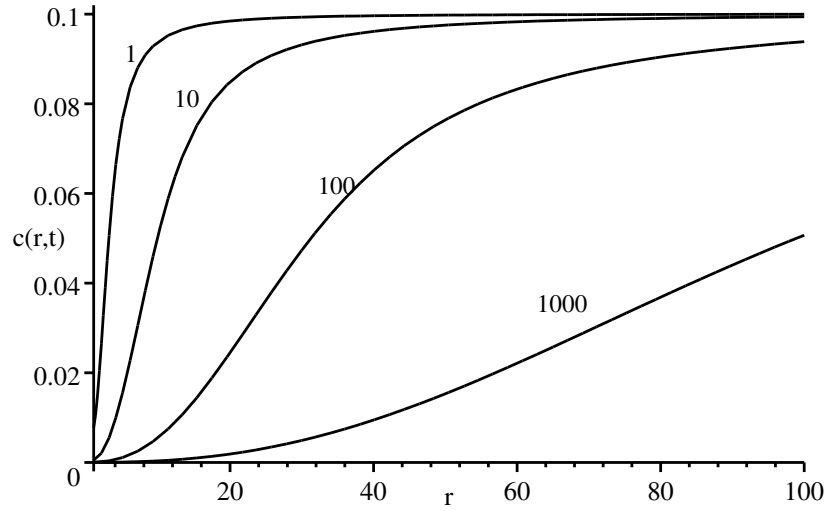

Figure 3.8: Concentration profile around the root given by equation (3.52) for times $t = 1, 10, 100$ and 1000. $c_\infty = 0.1$, $\lambda = 1$, $\alpha^2 = 6.28$.

Our task is now to evaluate the integrals

$$\int_1^\infty \frac{e^{-r^2/8t}}{r^3} W_{-\frac{1}{2},\frac{\alpha}{2}}(\frac{r^2}{4t})\,dr \quad \text{and} \quad \int_1^\infty \frac{e^{-r^2/8t}}{r} I_\beta(\frac{r^2}{8t})\,dr, \tag{3.53}$$

where $\beta = \frac{\alpha-1}{2}$ and $\frac{\alpha+1}{2}$. By change of variables to $\eta = r^2/8t$ these integrals can be transformed to

$$\frac{1}{16t}\int_{1/8t}^\infty \frac{e^{-\eta}}{\eta^2} W_{-\frac{1}{2},\frac{\alpha}{2}}(2\eta)\,d\eta, \quad \text{and} \quad \frac{1}{8t}\int_{1/8t}^\infty \frac{e^{-\eta}}{\eta} I_\beta(\eta)\,d\eta. \tag{3.54}$$

The analytical expression for the Bessel function integral involves the infinite series of Meijel's G function [3]. However, in the view of this study into plant nutrient uptake we will neglect this result because of its relative complexity. Hence we opt for estimating their value numerically. A graph of the root, mycorrhizae and total nutrient uptake is shown on Figure 3.9. As can be seen, most of the nutrient gets

[3] $\int_1^\infty \frac{e^{-r^2/8t}}{r} I_\beta(\frac{r^2}{8t})\,dr = \frac{1}{8t\sqrt{\pi}}\,G_{23}^{21}(1/4t| -1/2, 0; -1, \beta-1, -\beta-1)$ where G_{23}^{21} notes the series of Meijel's G functions.

taken up by the mycorrhizae. This is due to the low nutrient concentration at the root surface. This development of a depletion profile around the root is enhanced by the very high mycorrhizal profile around the root.

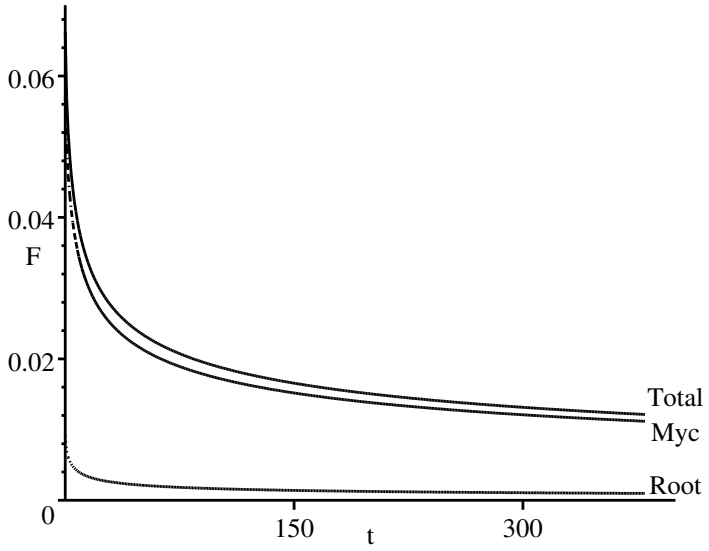

Figure 3.9: Nutrient uptake by root and mycorrhizae for $\lambda = 0.1$, $c_\infty = 1$ and $\alpha^2 = 0.628$.

We could now conduct a similar analysis for the c_∞ large limit. However, we will not do so for the following reasons. Firstly, most mycorrhizal experiments are concerned with phosphorus uptake, but for phosphorus c_∞ is of order 1 or less. Hence the approximation presented above is valid for cases where mycorrhizae uptake had been thought to be important, i.e., phosphorus. Secondly, the mycorrhizal profile obtained from [64] measures the first data point approximately 3 cm from the root surface. For a root with radius of order 10^{-2} cm this is very far away from the root, and the mycorrhizae length density profile κ^2/r^2 might not be valid near the root surface. This in turn implies that the distribution must be more complicated. The simplest alternative to the length density profile κ^2/r^2 is to incorporate space shift into it, i.e., to take the length density given by $\kappa^2/(r-r_0)^2$ where r_0 is a parameter to be determined from experiments. As long as $r_0 << 1$ the solutions presented above are valid at the leading order, but when $1 \lesssim r_0$ the solution procedure breaks down. Hence, in this case one would need to solve the model numerically. The experimental measurements of myrorrhizae length density profiles presented in [64] and on Figure 3.6 can be interpreted as having the space shift equal to $r_0 \approx 3$ cm. The result of numerical experiment with this profile is presented in Figure 3.10. As we can see, the importance of mycorrhizae to overall nutrient removal from the soil is still large, however, the relative importance of root nutrient uptake has increased.

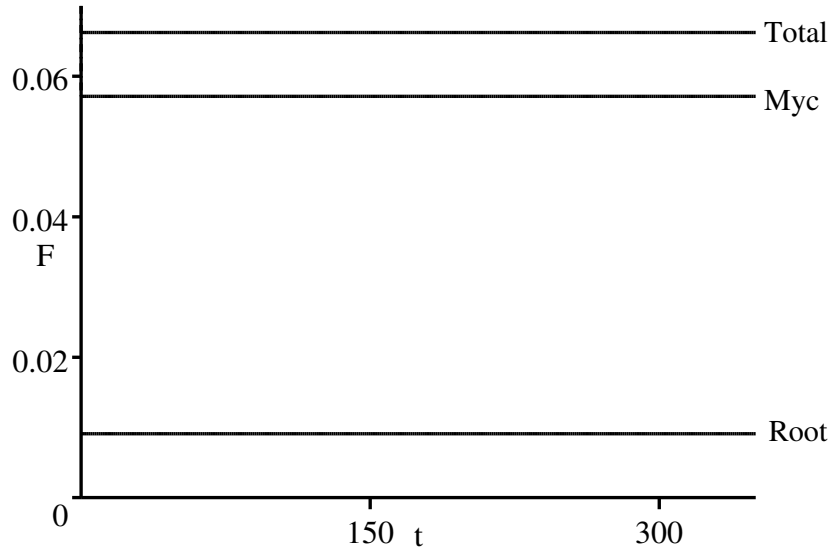

Figure 3.10: Nutrient uptake by root and mycorrhizae for $\lambda = 0.1$, $c_\infty = 1$, $\alpha^2 = 0.628$ (as on Figure 3.7) and the dimensionless mycorrhizae uptake term given by $\frac{\alpha^2}{(r - r_0^*)^2} \frac{c}{1+c}$ where $r_0^* = r_0/a = 3\text{cm}/0.02\text{cm} = 150$.

There are of course many other alternative forms for the mycorrhizal length density, but ultimately the accurate experimental measurements of it are needed.

We have presented above a model for nutrient uptake by roots with mycorrhizae. The results of this model crucially depend on the mycorrhizae length distribution in the soil. Current analysis on the model indicates that even at very low values of mycorrhizae length density the uptake of nutrients by mycorrhizae has potentially a large contribution to the nutrient uptake by the root (see Figure 3.9). When more accurate experimental evidence on mycorrhizae profile and nutrient uptake emerges, we can review our current model.

3.3 Concluding Remarks on Root Hairs and Mycorrhizae

In the previous two sections we have been able to calculate nutrient uptake by mycorrhizae and by root hairs. In order to maintain the nutrient uptake essential for survival, the plant has to invest carbon into upkeep of its tissues. The optimum carbon investment strategy is a matter of current debate. It is generally thought that it is in a plant's interest to invest as little as possible in the upkeep of its non-reproducing organs. Therefore it is thought that since the upkeep of root hairs and mycorrhizae

is relatively "cheap" the plants start creating more root hairs and supporting mycorrhizae in nutrient deficient environments.

The volume of root mass per unit length is given by $V_r = \pi a^2 = 1.2 \times 10^{-3}$ cm^3, volume of root hairs per unit length of root is $V_h = \pi a_h^2 l n = 3 \times 10^{-4}$ cm^3 (a_h is the root hair radius, l is the root hair length, and n is the number of root hairs per unit length of the root), and the total volume of mycorrhizae per unit length of the root is $V_m = 2\pi a \pi a_m^2 \int_a^\infty \frac{\kappa^2}{r^2}\, dr = 2 \times 10^{-2}$ cm^3.

As was shown in section 3.1.3, the volume of root hairs compared to the root volume differs by a factor of up to 4 or 5. Hence, it is natural to expect that it is more beneficial for a plant to produce more root hairs, since the upkeep of the root hair tissue is probably as costly as that of the root tissue (since the root hairs are basically part of the root surface epidermal cells anyway).

In the case of mycorrhizae the answer is not that clear, due to the lack of information on the mycorrhizal profile in the soil. However, it can be expected that the upkeep of mycorrhizae is cheaper for the plant than the upkeep of its own tissue. Hence, therefore it might be more beneficial for a plant to upkeep mycorrhizae than it is to develop new root hairs. However, at the present stage this is pure speculation, since there is no sufficient experimental evidence supporting this hypothesis.

Chapter 4

Root Population Development and Nutrient Uptake

In Chapter 2 we calculated the flux into one cylindrical root. In reality the branched root systems of agriculturally important plants consist of roots with different radii and different lengths. In order to construct a more realistic model of nutrient uptake by plants, one has to consider the root system morphology.

In this chapter we at first consider the nutrient uptake by static root size distributions in order to establish the errors arising from different averaging methods. Then in the later part of this chapter a model describing the root system development, i.e., the branching of roots into sub-branches and their elongation, will be presented. The results of Chapter 2 will then be extended to give an estimate of the nutrient uptake by the developing root system. Before proceeding we recall the calculation of dimensional nutrient uptake by one cylindrical root in terms of non-dimensional flux found in the Chapter 2.

4.1 Calculation of Dimensional Flux into the Root

In Chapter 2 we found an explicit analytical approximation to the nutrient flux into a single cylindrical root at the limit of large time. Using this dimensionless flux $F(t;\lambda,c_\infty)$ formulae (2.120) the dimensional flux is given by

$$F_{\text{dim}}(t_{\text{dim}}) = \frac{F_m}{\lambda} F(t_{\text{dim}};\lambda,c_\infty), \tag{4.1}$$

where $t_{\text{dim}} = [a^2(\phi_l + b)/D\phi_l]t$ is dimensional time in terms of dimensionless time t (see Chapter 2 Section 2.2.1), λ, c_∞ are the dimensionless nutrient uptake and concentration constants, and F_m [μmol cm^{-2}s^{-1}] is the dimensional Michaelis-Menten nutrient uptake coefficient.

The dimensional flux into root with radius a and length l is given by

$$F_{\text{tot}}(t_{\text{dim}}) = 2\pi al \frac{2F_m c_\infty}{1 + c_\infty + L(t_{\text{dim}}) + \sqrt{4c_\infty + (1 - c_\infty + L(t_{\text{dim}}))^2}}, \tag{4.2}$$

where $L(t_{\text{dim}}) = \frac{\lambda}{2} \ln\{4e^{-\gamma} \frac{D\phi_l}{a^2(\phi_l + b)} t_{\text{dim}} + 1\}$, $\lambda = F_m a/(DK_m\phi_l)$, and $c_\infty = c_0/K_m$.

4.2 Fixed Root Population and Averaging

Barber [6] and Nye and Tinker [95], [129] in their calculations of nutrient uptake use the average root radius obtained from experiments to calculate the nutrient uptake by the root system. In this section we illustrate the differences in the estimation of nutrient uptake depending on the averaging method used. For example in [111] and [6] Barber calculates the average root radius from the equation

$$\bar{a} = \sqrt{\frac{Fw_r/\rho}{\pi L_r}}, \tag{4.3}$$

where Fw_r is the fresh weight of the roots [g], ρ is the average root tissue density [g cm^{-3}], and L_r is the overall root length [cm]. The overall root length is obtained from experiments using the line intersect method described in [122]. The average root tissue density varies for different plants, but for the maize plant it is thought to be of order 10^6 g m^{-3}, i.e., roughly the density of water. The formula (4.3) suggests that the easiest way of calculating the average root radius from the experiments would be to average it over the volume of the roots, i.e., volume averaged root radius. Assuming that the calculation of the fresh weight and root tissue density is reasonably accurate, the largest error for those average root radii estimates might come from the estimation of the root length.

The root systems of agricultural plants consist of roots of different length and different radii. Hence, to extend the model of nutrient uptake one would need to consider the root size distribution. One way of doing that would be to take the length distribution of roots l to be dependent on its radius a, i.e., consider $l(a)\,da$ to be sum of lengths of all roots in the root population which are in the radius interval $(a, a + da)$. Averaging this root population with respect to root surface we find the surface area average, $\bar{a}$, given by

$$\bar{a}_s = \frac{\int_0^\infty a l(a)\,da}{\int_0^\infty l(a)\,da}, \tag{4.4}$$

Similarly the volume averaged root radius, $\bar{a}_v$, is calculated as

$$\bar{a}_v = \left(\frac{\int_0^\infty a^2 l(a)\,da}{\int_0^\infty l(a)\,da} \right)^{1/2}. \tag{4.5}$$

The total length of the root population is calculated as

$$l_{\text{tot}} = \int_0^\infty l(a)\, da. \tag{4.6}$$

The nutrient uptake by the root size distribution can be calculated by integrating (4.2) over all possible root radii. Hence the root distribution uptake is given by

$$F_p(t_{\text{dim}}) = \int_0^\infty 2\pi\, a\, l(a) F_{\text{dim}}(a, t_{\text{dim}})\, da, \tag{4.7}$$

where the dimensional time t_{dim} in terms of dimensionless time t is $t_{\text{dim}} = [a^2(\phi_l + b)/D\phi_l]t = a^2 t/s$, with $s = D\phi_l/(\phi_l + b)$. The dimensionless parameter λ is also dependent on the root radius a, i.e., from Chapter 2 Section 2.2.1, we can write $\lambda = \bar{\lambda} a$.

From the point of view of experiments the more important quantity is cumulative uptake which is calculated as

$$F_c(t_{\text{dim}}) = \int_0^{t_{\text{dim}}} F_p(\tau)\, d\tau. \tag{4.8}$$

This is the amount of nutrient removed from the soil by the plant during the time-interval $[0, t_{\text{dim}}]$. We will now proceed to show the differences in the nutrient uptake for two specific root size distributions, i.e., uniform and normal distribution. Uniform distribution is suitable for root systems which have relatively small variations in the root radii and lengths. A normal distribution is more applicable to root systems with a wider range of root radii and more distinct favourable radii. However, in reality the root distribution changes also in time. In this section we will ignore the time changes to find out the difference in flux due to the different root radius averaging methods. This should provide information for deciding which method one should be using for calculating the flux into the fully grown root system. The problem of root distribution development, i.e., branching of roots and sub-branch elongation, will be considered in later sections of this chapter.

4.2.1 Uniform Root Length Distribution

We first consider the root size distribution to be given by the uniform distribution, i.e.,

$$l(a) = l_{\text{tot}}/(\alpha_2 - \alpha_1) \quad \text{for} \quad \alpha_1 \le a \le \alpha_2, \tag{4.9}$$

and $l(a) = 0$ for $0 < a < \alpha_1$ and $a > \alpha_2$.

The average root radius with respect to the length and root surface area is $\bar{a}_s = (\alpha_1 + \alpha_2)/2$. Since the mean of the distribution $l(a)$ is also $(\alpha_1 + \alpha_2)/2$ then $\bar{a}_s$ is also

the average over the total root length. The average radius over the volume becomes $\bar{a}_v = \frac{\sqrt{3}}{3}(\alpha_1^2 + \alpha_1\alpha_2 + \alpha_2^2)^{1/2}$. For example when $\alpha = 0.005$ cm and $\alpha_2 = 0.035$ cm then $\bar{a}_s = 0.02$ and $\bar{a}_v \approx 0.022$. As we see the differences in the averages for this distribution are approximately 10%.

If total length of this root distribution is l_{tot}, then nutrient uptake with average root radii can be calculated according to (4.2) as $F_s(t_{\text{dim}}) = 2\pi\bar{a}_s l_{\text{tot}} F_{\text{dim}}(\bar{a}_s, t_{\text{dim}})$ and $F_v(t_{\text{dim}}) = 2\pi\bar{a}_v l_{\text{tot}} F_{\text{dim}}(\bar{a}_v, t_{\text{dim}})$. These are the Barber fluxes into one cylindrical root with length l_{tot} and average root radius calculated in two different ways, i.e., over surface area and volume.

The comparison between the root size distribution uptake F_p and averaged uptake F_s and F_v is presented in Figure 4.1 for $\alpha_1 = 0.005$ and $\alpha_2 = 0.035$.

As we can see the biggest error comes (up to 10%) from the volume averaging calculations. However, the differences are well within the experimental error.

4.2.2 Normal Distribution with Cutoff Tails

Considering now the normal length distribution in the same radius interval as before, i.e., for $\alpha_1 \le a \le \alpha_2$, and the same total root population length, we take

$$l(a) = \frac{l_{\text{tot}}}{n} \frac{1}{\sigma\sqrt{2\pi}} e^{-(a-\mu)^2/2\sigma^2}, \tag{4.10}$$

where $n = [\text{erf}(\frac{\alpha_2-\mu}{\sqrt{2\sigma^2}}) - \text{erf}(\frac{\alpha_1-\mu}{\sqrt{2\sigma^2}})]/2$. For $a < \alpha_1$ and $a > \alpha_2$ we take $l(a) = 0$. The total length of this root population is $l_{\text{tot}} = \int_0^\infty l(a)\, da$. In this case the surface average is

$$\bar{a}_s = \mu + \sqrt{\frac{2\sigma^2}{\pi}} \times \frac{e^{-(\mu-\alpha_1)^2/2\sigma^2} - e^{-(\mu-\alpha_2)^2/2\sigma^2}}{\text{erf}(\frac{\alpha_2-\mu}{\sqrt{2\sigma^2}}) - \text{erf}(\frac{\alpha_1-\mu}{\sqrt{2\sigma^2}})}, \tag{4.11}$$

and the volume average is

$$\bar{a}_v = \sqrt{\mu^2+\sigma^2} + (\frac{2\sigma^2}{\pi})^{1/4} \sqrt{\frac{\mu[e^{-\frac{(\mu-\alpha_1)^2}{2\sigma^2}} - e^{-\frac{(\mu-\alpha_2)^2}{2\sigma^2}}] + [\alpha_1 e^{-\frac{(\mu-\alpha_1)^2}{2\sigma^2}} - \alpha_2 e^{-\frac{(\mu-\alpha_2)^2}{2\sigma^2}}]}{\text{erf}(\frac{\alpha_2-\mu}{\sqrt{2\sigma^2}}) - \text{erf}(\frac{\alpha_1-\mu}{\sqrt{2\sigma^2}})}}. \tag{4.12}$$

Choosing $\mu = 0.02$, $\sigma = 0.0075$, $\alpha_1 = 0.005$ and $\alpha_2 = 0.035$, the surface average is $\bar{a}_s = 0.02$ and volume average is $\bar{a}_v \approx 0.021$. The nutrient uptake by this normal distribution is shown on Figure 4.2.

In conclusion to this section of nutrient uptake by the fixed root system we note that depending on the method of root radius averaging one would get slightly different estimations to the nutrient uptake. However, as discussed earlier, Barber [6] uses the volume averaging method, and in the case of experiments where the root radius does

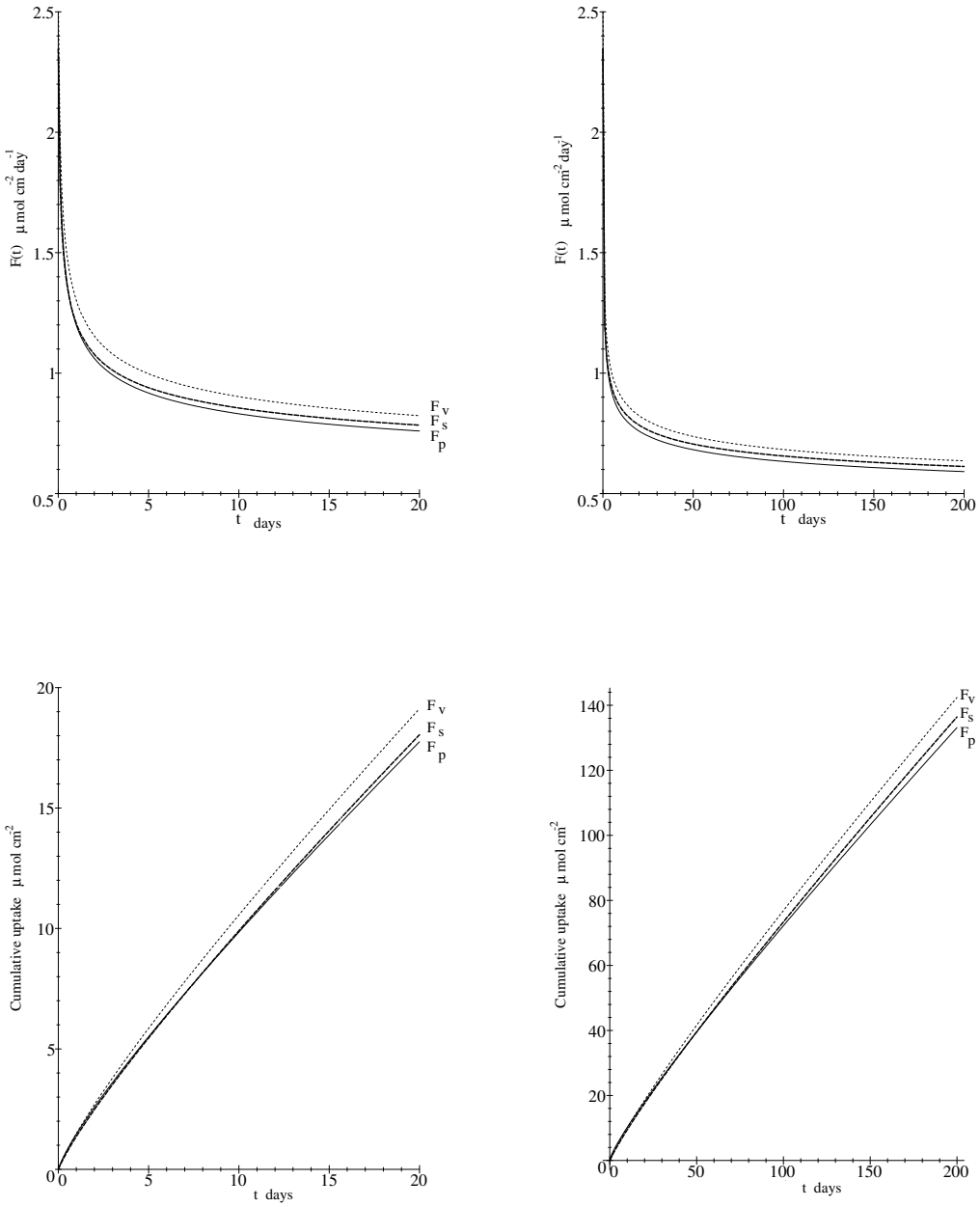

Figure 4.1: Comparison between the phosphate uptake F and the cumulative uptake F_c by the uniform root length distribution F_p (solid line); by the cylindrical root which has the average root radius calculated over the root distribution surface area F_s (fat dashed line); average over the root distribution volume F_v (dashed line). Parameter values are: $\alpha_1 = 0.005$, $\alpha_2 = 0.035$, $\bar{a}_s = 0.02$, and $\bar{a}_v \approx 0.022$. Phosphate uptake parameter values are: $\lambda = 56a$, $t = 3.6 \times 10^{-3} t_{\text{dim}}/a^2$ (where t_{dim} is measured in days), $F_m = 2.8$ μmol cm^{-2} day^{-1}, and $c_\infty = 0.5$.

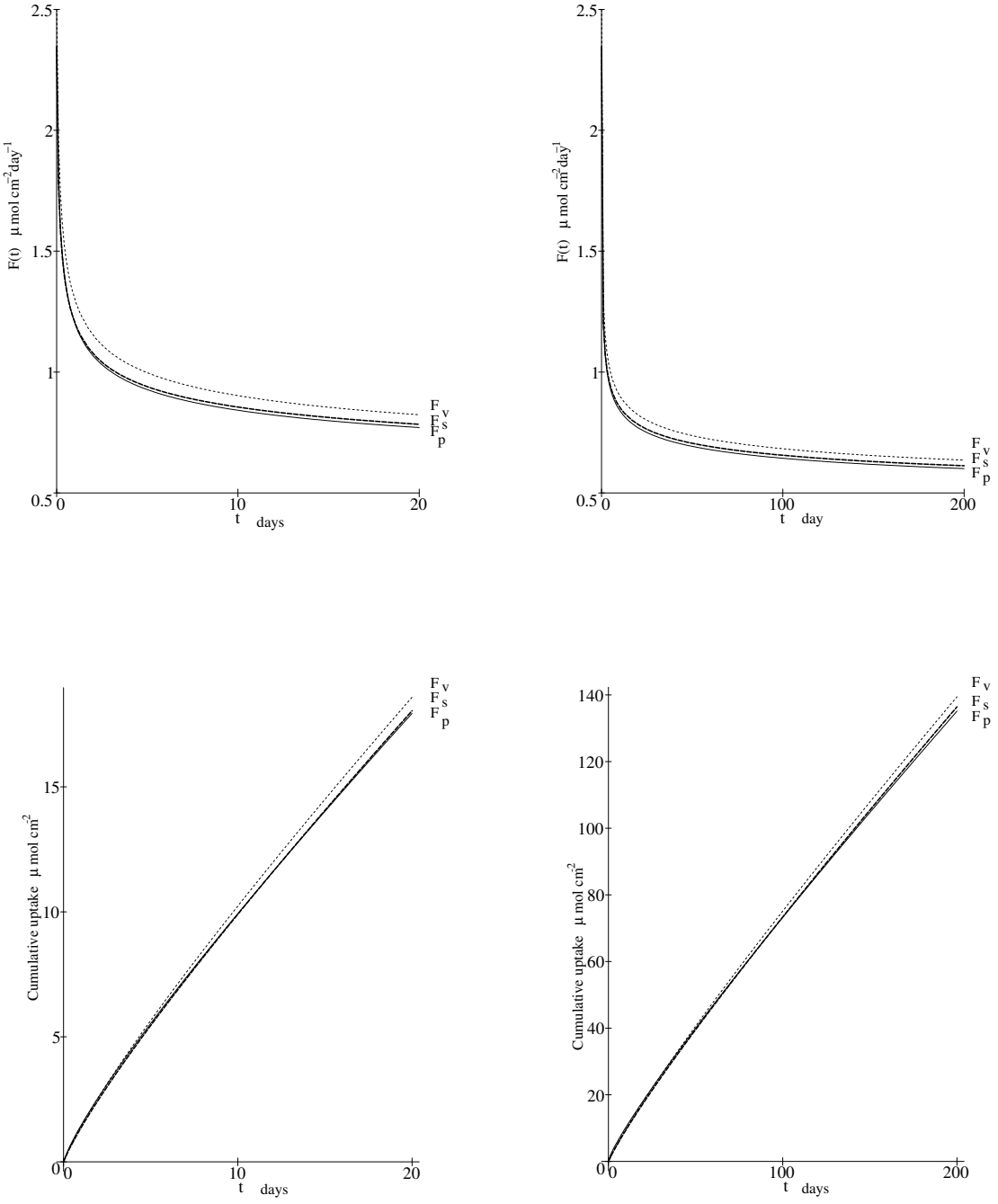

Figure 4.2: Comparison between the rate of phosphate uptake F and the cumulative uptake F_c by the normal root length distribution F_p (solid line); by the cylindrical root which has the average root radius calculated over the root distribution surface area F_s (fat dashed line); and over the root distribution volume F_v (dashed line). Phosphate parameter values are: $\lambda = 56a$,$t = 3.6 \times 10^{-3} t_{\text{dim}}/a^2$ (where t_{dim} is measured in days), $F_m = 2.8$ μmol cm^{-2} day^{-1}, and $c_\infty = 0.5$.

not vary in time this approximation is satisfactory giving the approximate error of 10%. Looking at the experiment error, we notice that it is mostly in the same range [6]. However, sometimes the experimental error is much larger, in which case it has been attributed to inadequate modelling assumptions concerning the neglection of mucilage, bacterial colonies, root hairs, mycorrhizae etc. We will return to this in later sections of this chapter.

4.3 Description of the Root System of Agriculturally Important Plants

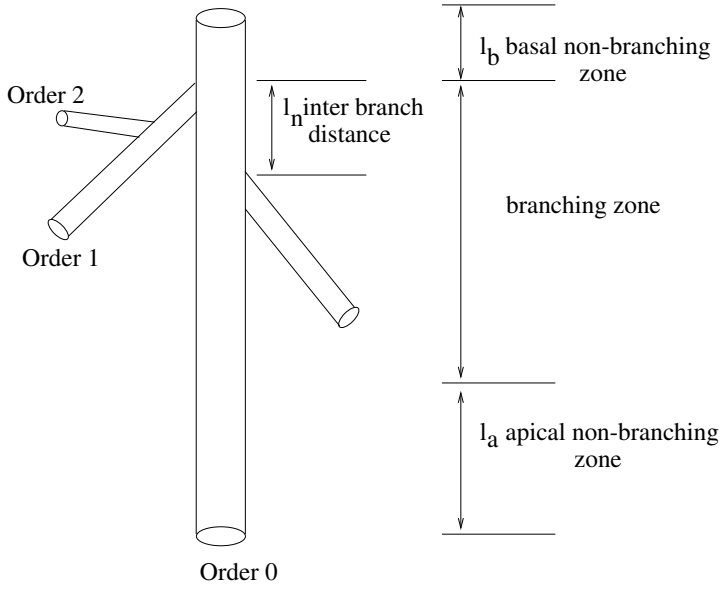

Figure 4.3: Schematic structure of the maize root branching structure after [97].

Roots of cereal plants, like maize, have typically 3 or 4 orders [95], [129]. The branches which emerge from the seed are called zero order branches, and the rest are called higher order branches. A maize root is also considered to emit zero order roots from its shoot. In this chapter we suppose that the initial root distribution consists of all such zero order roots. Thus we will not be concerned with the very early stages of root development, i.e., germination and initial elongation.

Each sub-branch can be divided into three functionally different regions (see Figure 4.3): a basal non-branching zone of length l_b, a branched zone, and an apical non-branching zone of length l_a. The roots can develop branches if the total length l is larger than $l_b + l_a$. New branches are developed at approximately equal distance from each other in the branching region. The distance between branches is called the

inter-nodal distance l_n. Hence, a root of length l has $k_{\max} = [(l - l_b - l_a)/l_n]$ branches ($[x]$ notes the integer part of the real number x).

The lengths l_b, l_a, and l_n depend primarily on the branch order, but they can also be considered to be dependent on the nutrient availability, age, and other environmental variables.

The connection between the radii of the roots of different orders is not very well established. The simplest form of the Leonardo da Vinci branching rule [115] can be used, i.e., we can take

$$a_i = \sigma_{i-1} a_{i-1}, \tag{4.13}$$

where a_i is the radius of the root of order i and σ_i is the proportionality constant. However, where possible, the numerical estimation of root radii from field experiments should be used. The radius will be considered to be a constant for each root order. In reality the radii vary within the order, but probably not very much.

On the other hand, roots grow by elongation and the growth rate of roots is known to slow down with the age of the root and in fact each root has a maximum length which depends on its order [97].

Pagès, Jourdan, and Picard [97] use a model based on simple branching structures, similar to those described above, in order to simulate root system development. The purpose of their research was to compare simulated three-dimensional root architectures to root density profiles and root maps obtained from field experiments. In this chapter their estimation of maize root elongation and branching will be used to calculate the total length of the roots of different orders.

4.4 Root Population Development

We wish to describe the distribution of roots in each order as a function of length l. Therefore we define the root size density function of order i roots to be $\phi_i(l, t)$, where $\phi_i \, dl$ is the number-density of roots of length l in the length interval $(l, l + dl)$.

The length l of a root of order i increases in time, but it is limited by the maximum possible length K_i. We suppose that the elongation rate L_i is given by

$$L_i = r_i(1 - \frac{l}{K_i}), \tag{4.14}$$

where r_i is the elongation rate of new order i roots.

Maize roots also die due to the effects of insects, environmental stresses etc. We assume that root death can be described by the specific mortality rate μ_i, which could depend on root length or other factors. The discussion of the root death rate μ_i will be presented in the later Section 4.8.

In order to derive an equation for ϕ_i, we consider the conservation of the number of roots in an arbitrary, but fixed, length interval (l_1, l_2). The change in the number of roots in this interval is equal to the number of roots dying plus the net influx of roots of lengths $l = l_1$, and $l = l_2$, which is determined by the root growth rate at these points. Hence

$$\frac{\mathrm{d}}{\mathrm{d}t}\int_{l_1}^{l_2} \phi_i(l,t)\, dl = -\int_{l_1}^{l_2} \mu_i \phi_i(l,t)\, dl + [\phi_i(l,t) L_i(l)]_{l_2}^{l_1}, \tag{4.15}$$

which gives

$$\int_{l_1}^{l_2} \left\{ \frac{\partial \phi_i}{\partial t} + \frac{\partial}{\partial l}[L_i(l)\phi_i(l,t)] + \mu_i \phi_i(l,t) \right\} dl = 0. \tag{4.16}$$

Since the fixed interval (l_1, l_2) was arbitrarily chosen, the integrand must vanish, i.e., we obtain the following hyperbolic equation

$$\frac{\partial \phi_i}{\partial t} + r_i(1 - \frac{l}{K_i})\frac{\partial \phi_i}{\partial l} = (-\mu_i + \frac{r_i}{K_i})\phi_i. \tag{4.17}$$

The initial and boundary conditions to this model should be described at $t = 0$ and $l = 0$. The condition at $t = 0$ is the initial condition and the condition at $l = 0$ represents the effect of new root generation.

4.4.1 Initial Condition at $t = 0$

We take the initial condition at $t = 0$ for the zero order roots to be given by $\phi_0(l, 0) = \phi_{00}(l)$, where $\phi_{00}(l)$ is the initial distribution of roots of order zero. For simplicity it can be taken to be the uniform initial distribution. Hence, for $\beta_1 < l < \beta_2$ we take $\phi_{00} = 1$ and elsewhere $\phi_{00} = 0$. This implies that at $t = 0$ we have $\beta_2 - \beta_1$ number of roots in length interval $[\beta_1, \beta_2]$.

We can assume now that our time origin is chosen such that the higher order roots are not present, i.e., the initial condition for order i roots is $\phi_i(l, 0) = 0$, when $i > 0$.

4.4.2 Boundary condition at $l = 0$

The boundary condition at $l = 0$ represents the creation of new roots. For simplicity we assume that zero order roots are not being created at a later time $t > 0$, i.e, $\phi_0(0, t) = 0$. This implies that all zero order roots emitted by the seed and shoot are already present at $t = 0$.

We assume that the higher order roots are created by branching from the lower order roots. As discussed earlier, the branching, i.e., creation of new roots of higher order, is dependent on the length of the lower order root, and that the branching occurs at discrete branching lengths.

The total number of roots of order i in the population changes only due to root death and root birth via branching from lower order roots. Hence, the conservation law can be written as

$$\frac{\mathrm{d}}{\mathrm{d}t}\int_0^\infty \phi_i(l,t)\,dl = -\int_0^\infty \mu_i\phi_i(l,t)\,dl + \int_0^\infty L_{i-1}(l)G_{i-1}(l)\phi_{i-1}(l,t)\,dl, \tag{4.18}$$

where $G_{i-1}(l)$ is the length specific root generation rate, i.e., the number of roots of order i created per unit length of root of order $i-1$. Comparison of (4.15) and (4.18) implies that the birth rate is

$$r_i\phi_i(0,t) = \int_0^\infty L_{i-1}(l)G_{i-1}(l)\phi_{i-1}(l,t)\,dl. \tag{4.19}$$

Assuming that the branching occurs at the discrete branching points given by $l_{\text{branch}} = l_{0,i-1} + kl_{n,i-1}$, where $l_{0,i-1} = l_{b,i-1} + l_{a,i-1}$ is the sum of apical and basal non-branching zones for the order $i-1$, $l_{n,i-1}$ is the inter-branch distance for order $i-1$, and k is the number of the branch, the length specific root generation rate becomes $G_{i-1}(l) = \sum_{k=0}^{\infty}\delta[l-(l_{0,i-1}+kl_{n,i-1})]$, where δ is the Dirac delta function. Hence, the boundary condition at $l=0$ is given by

$$\phi_i(0,t) = B_i(t) = \sum_{k=0}^{\infty}\phi_{i-1}(l_{0,i-1}+kl_{n,i-1},t)\frac{r_{i-1}}{r_i}(1-\frac{l_{0,i-1}+kl_{n,i-1}}{K_{i-1}}), \tag{4.20}$$

where ∞ can be replaced by $k_{\max,i-1}$, which is the maximum number of branches on root of order $i-1$, i.e., $k_{\max,i-1} = [(K_{i-1}-l_{0,i-1})/l_{n,i-1}]$.

4.5 Parameter Estimation

Pagès et al. [97] give the rate of elongation of maize root in terms of the age of the root, rather than the length, i.e, the rate of elongation is given by $\alpha e^{-\beta T}$ cm day^{-1}, where T is the age of the root. Hence, in their case the development of the length of the root will be given by

$$l(t) = \frac{\alpha}{\beta}(1-e^{-\beta(t-t_0)}), \tag{4.21}$$

where t_0 is the time of creation of the root; thus from equation (4.14), this implies $r=\alpha$ and $K=\alpha/\beta$.

Pagès et al. [97] also give an estimation for the lengths of the apical non-branching zone, the branching zone, and the basal non-branching zone. Parameter estimation, based on their data, is presented in Table 4.1. Pagès et al. do not consider the decay in the growth rate of zero order roots. Hence, they do not have a maximum length for roots of order zero. The maximum length of zero order roots will be taken to be

i	K_i(cm)	r_i(cm day^{-1})	$l_{b,i}$(cm)	$l_{a,i}$(cm)	$l_{0,i}$(cm)	$l_{n,i}$(cm)	$k_{\max,i}$
0	51	2.0	0.7	15.0	15.7	0.7	50
1	8	6.4	0.7	2.0	2.7	0.7	7
2	0.1875	1.5	-	-	-	-	-

Table 4.1: Root development parameters after [97] and [95]. K_i is the maximum length of roots of order i, r_i is the elongation rate of roots of order i at birth, $l_{b,i}$ is the length of the basal non-branching zone of roots of order i, $l_{a,i}$ is the length of the apical non-branching zone of roots of order i, $l_{n,i}$ is the inter-nodal distance of roots of order i, and $k_{\max,i}$ is the maximum number of branches on roots of order i.

51 cm, based on the reports by Varney and Canny [131] that the zero order maize roots varied from 50 to 100 cm.

4.6 Solution for Root Population Model

Solution to this hyperbolic partial differential equation (4.17) can be found using the method of characteristics. The characteristics of this equation for order i roots are (see Figure 4.4) given by

$$\frac{\mathrm{d}l}{\mathrm{d}t} = r_i(1 - \frac{l}{K_i}), \tag{4.22}$$

For the first order roots the equation (4.17) will be solved with initial conditions $\phi_0(l,0) = \phi_{00}(l)$ and $\phi_0(0,t) = 0$. Hence, the solution for $0 < l < K_0(1 - e^{-r_0 t/K_0})$ and $l > K_0$ is $\phi_0(l,t) = 0$, but for $K_0(1 - e^{-r_0 t/K_0}) < l < K_0$ the solution becomes

$$\phi_0(l,t) = \phi_{00}[K_0 + (l - K_0)e^{r_0 t/K_0}]e^{(\frac{r_0}{K_0} - \mu_0)t}. \tag{4.23}$$

The total length of the root system of order i is given by

$$l_i(t) = \int_0^{K_i} l\phi_i(l,t)dl. \tag{4.24}$$

Suppose now that there are approximately five zero order roots per unit volume of soil at time $t = 0$ in the length interval $[5\text{cm}, 10\text{cm}]$. One possible way of describing this situation at the initial time $t = 0$ would be to use the uniform distribution, i.e., take the initial condition to be given by $\phi_{00}(l) = 1$ for $5 < l < 10$ and $\phi_{00}(l) = 0$ for $l < 5$ and $l > 10$. The development of total length for this zero order root population is shown on Figure 4.5.

For the roots of order 1 and higher, the system (4.17) needs to be solved with initial conditions $\phi_i(l,0) = 0$ and $\phi_i(0,t) = B_i(t)$, where $B_i(t)$ is given by the equation (4.20) (see also Figure 4.6). In this case, using the method of characteristics, we find that

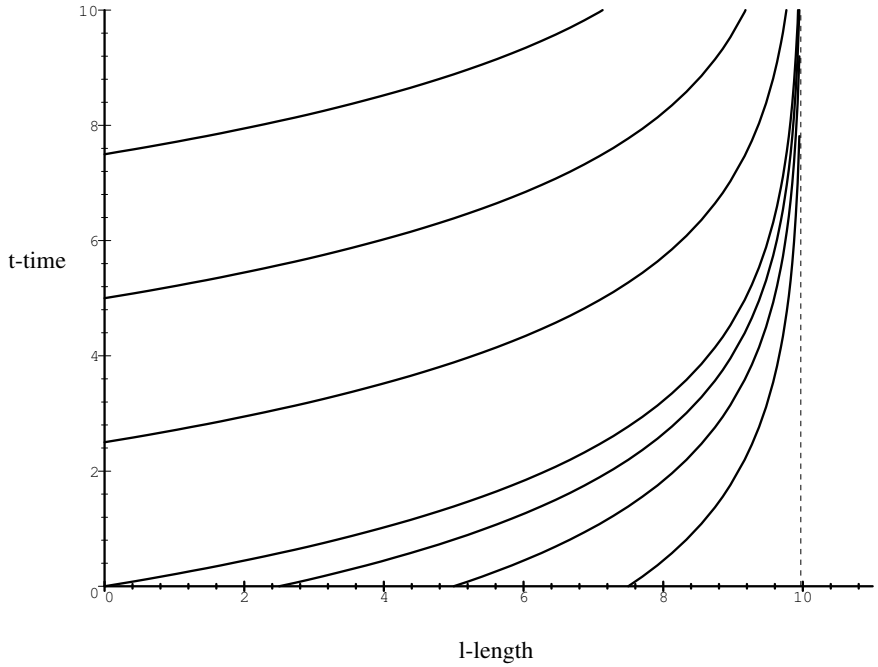

Figure 4.4: Characteristic diagram ($K_0 = 10$ and $r_0 = 5$) for equation (4.17). [Characteristic curves show the development of the length of one root as a function of time. Characteristics originating from the l-axis show the development of the length of roots which are present initially at time $t = 0$. Characteristics originating from the t-axis describe the development of length of roots which are created with zero length at later time.]

$\phi_i(l,t) = 0$ for $l > K_i(1 - e^{-r_i t/K_i})$, and for $0 < l < K_i(1 - e^{-r_i t/K_i})$ the solution becomes

$$\phi_i(l,t) = B_i(s)(1 - \frac{l}{K_i})^{\frac{\mu_i K_i}{r_i} - 1}, \tag{4.25}$$

where $s = t + \dfrac{K_i}{r_i} \ln(1 - \dfrac{l}{K_i})$, and B_i is defined by equation (4.20). The results for the order 1 and 2 roots are also shown on Figure 4.5.

The solutions shown on Figure 4.5 are exact solutions calculated and drawn using the *xMaple* symbolic calculation package. Solutions have discontinuities due to the discrete set of branching points and the uniform distribution initial condition.

We notice on Figure 4.5 that the overall length of first order roots is much larger than that of the zero order and second order. Therefore we expect them to give the largest contribution to the overall nutrient uptake by the plant.

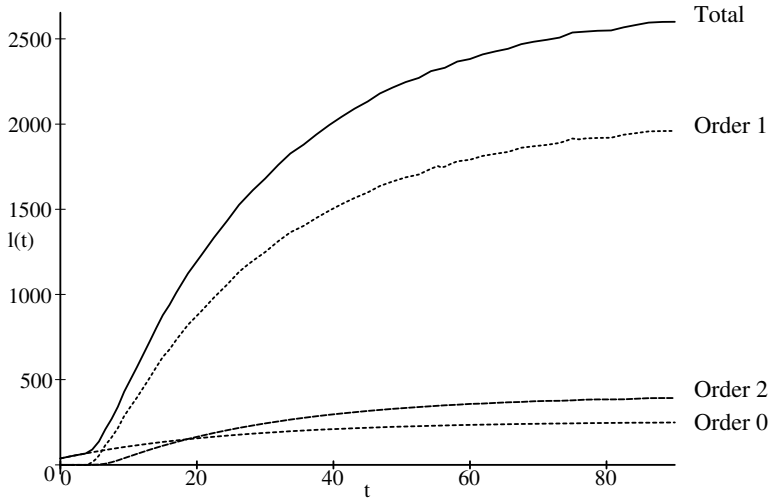

Figure 4.5: Total length [cm] of root population with the initial conditions $\phi_0(l,0) = 1$ for $5 < l < 10$ and $\phi_0(l,0) = 0$ for $l < 5$ and $l > 10$. Other coefficients are shown in Table 4.1. Time t in days.

4.7 Nutrient Uptake by the Growing Root System

In Chapter 2 we dealt with the calculation of nutrient uptake by one cylindrical root. The approximation to the flux at the limits when non-dimensional nutrient uptake coefficient λ was large, small, and order one was found. Hence, we can calculate the flux of nutrients into the growing root system assuming that all branches in that root system are not competing between each other for the nutrients. This assumption is applicable for the coarsely branched root structures and in the case when the nutrient in the soil is relatively immobile, i.e., phosphate for example[1]. It is also reasonable to assume that for short times the competition effect between the neighbouring sub-branches can be neglected. However, in the case when the nutrient is very mobile in the soil, nitrate for example, the diffusion profiles around sub-branches start overlapping considerably and the assumption of no competition becomes invalid. Nevertheless, for controlled Barber experiments the flux in the absence of competition between sub-branches can provide valuable information on the accuracy of root radii averaging methods. This calculation would also give the estimation on the upper bound of nutrient uptake.

[1]We will discuss the diffusional length scales of different nutrients in the soil in the next Chapters 5 and 6, when we consider the inter-root competition in the soil.

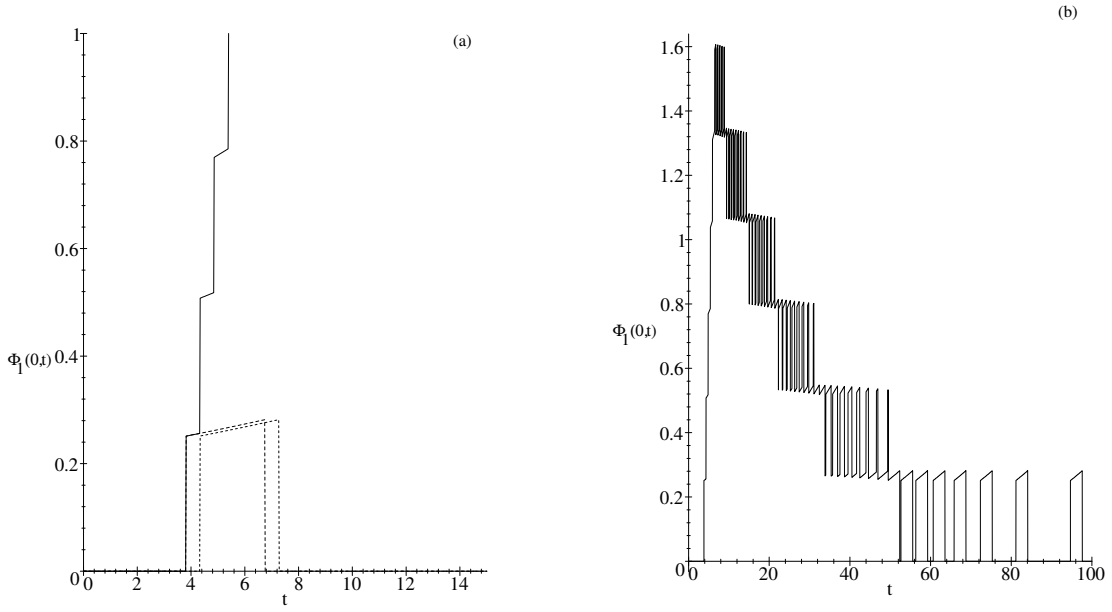

Figure 4.6: Creation of first order roots with length zero per unit time. (a) shows the mechanism of formation of creation of roots with length zero. Dotted lines are the first and second branch formation and the solid line is the full branch formation as a function of time t. (b) is the initial condition at $l = 0$ for ϕ_1. In total there will be 50 first order branches developed for each zero order branch. In time the creation of new sub-branches will become zero, since eventually zero order roots achieve their maximum possible length K_0 and by then would have passed through all the branching lengths.

Dimensional flux of nutrient into the root branching structure is given in terms of dimensionless flux (see Chapter 2) by

$$F_{\text{dim}}(t_{\text{dim}}) = \frac{F_m}{\lambda} F(t_{\text{dim}}; \lambda, c_\infty), \tag{4.26}$$

with dimensional time $t_{\text{dim}} = [a^2(\phi_l + b)/D\phi_l]t$ and $\lambda = \bar{\lambda}a$.

In the previous sections of the present chapter the evolution of the total length of roots of different order has been established. Hence the nutrient flux into the root system, assuming that there is no competition for nutrients between different roots, can be calculated using the fluxes into the single root, i.e.,

$$F_{\text{sys}}(t_{\text{dim}}) = \sum_{i=0}^{i_{\max}} 2\pi a_i l_i(t_{\text{dim}}) F_{\text{dim}}(a_i, t_{\text{dim}} - t_i), \tag{4.27}$$

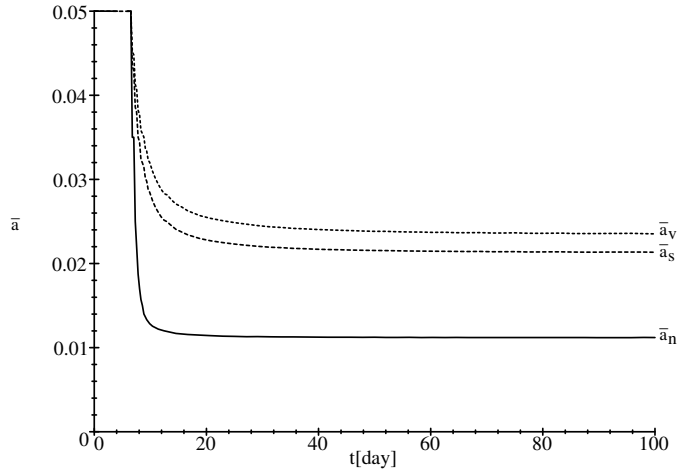

Figure 4.7: Average root radius for maize. $\bar{a}_n$ is the average over the number of roots, $\bar{a}_s$ is the average over root surface area, and $\bar{a}_v$ is the average over the volume of the roots.

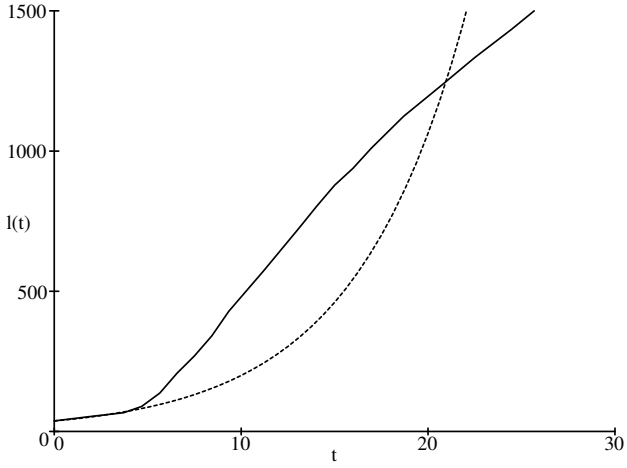

Figure 4.8: Comparison between the overall root length calculated from the root system development model (solid line) and the length calculated according to the Barber [6] experiment exponential elongation (dashed line). For population the initial conditions $\phi_0(l,0) = 1$ for $5 < l < 10$, $\phi_0(l,0) = 0$ for $l < 5$ and $l > 10$, and also $\phi_0(0,t) = 0$. All root growth coefficients are shown on Table 4.1. The exponential elongation given by $l(t) = l_0 e^{kt}$, where $l_0 = \int_0^\infty l\phi_{00}(l)\,dl = (\beta_2^2 - \beta_1^2)/2 = 37.5$, and $k = \{\ln[l_{\text{tot}}(21)] - \ln[l_0]\}/21$.

where a_i is the radius of order i roots; $l_i(t)$ is the length of order i roots given by equation (4.24); $F_{\dim}(a_i, t_{\dim})$ is the flux per unit surface area into the root with radius a_i; $i_{\max}$ is the maximum number of root orders, and t_i is the time of creation of first ith order root, i.e., $t_0 = 0$, $t_1 = -(K_0/r_0)\ln[(l_{0,0} - K_0)/(\beta_2 - K_0)]$ and $t_i = t_{i-1} - (K_{i-1}/r_{i-1})\ln(1 - l_{0,i-1}/K_{i-1})$ for $i > 1$. The results of nutrient uptake by the root system are presented in Figure 4.9. The development of average root radius and the length of total root population compared to Barber's exponential elongation [6] is also presented in Figures 4.7 and 4.8.

Suppose now, that we measure the total length and the average root radius of the root system at day 21 just as in the Barber experiments. The root branching model gives for the total length of the roots $l_{\text{tot}} = 1178$ cm, for the number average $\bar{a}_n = 0.0114$ cm, surface average $\bar{a}_s = 0.0227$ cm, and volume average $\hat{a}_v = 0.0254$ cm. The relative exponential root elongation rate k is calculated in the case of Barber experiments as $k = \{\ln[l_{\text{tot}}(t_2)] - \ln[l_{\text{tot}}(t_1)]\}/(t_2 - t_1) = [\ln(1178) - \ln(37.5)]/(21 - 0) = 0.16$. Using these parameters we can now calculate the flux into the cylindrical root.We can see from Figure 4.10 that the differences in the nutrient uptake are large. This is due to the averaging of the root radius and the elongation rate of the roots. We also note that it is not reasonable to assume that during the Barber 21 day experiment the average root radius stays constant. We can see from Figure 4.7 the average root radius changes relatively rapidly during that time and this suggests that the radius averaging in this time region is not at all acceptable.

4.8 Death Rate μ_i of Order i Roots

The death rate μ_i describes the proportion of roots of order i dying per unit time. If the lower order root dies, then all the roots branching out from it also die. Hence, the death rate of roots of order i depends on the death rates of the roots with a lower order.

Considering the rate of survival of ith order roots, i.e., the proportion of roots surviving a unit time, to be $\sigma_i = 1 - \mu_i$. If $\hat{\sigma}_i$ is the survival of ith order roots in the absence of an influence from other order roots, then in the presence of the higher order roots (after [58]) it becomes

$$\sigma_i = \Pi_{k=0}^{i}\hat{\sigma}_i = \Pi_{k=0}^{i}(1 - \hat{\mu}_i). \tag{4.28}$$

If the death rate of all roots in the absence of others is μ, i.e., $\hat{\mu}_i = \mu$ then it follows from $\mu_i = 1 - \sigma_i$ that

$$\mu_i = 1 - (1 - \mu)^{i+1}, \tag{4.29}$$

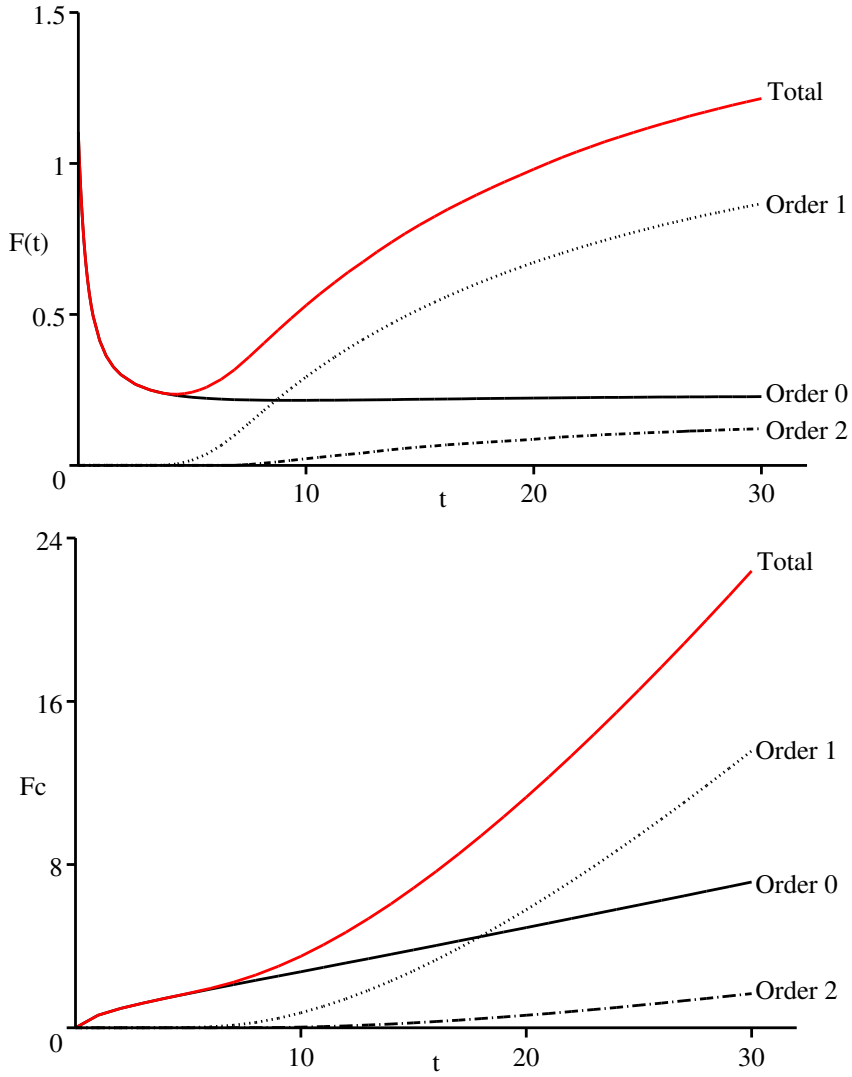

Figure 4.9: Nutrient uptake [μmol day^{-1}] (on top graph) and cumulative uptake [μmol] (on bottom graph) by a root population which has three orders. Solid red line is the uptake by the total root population and dashed lines are uptakes by the different orders. The initial conditions $\phi_0(l,0) = 1$ for $5 < l < 10$, $\phi_0(l,0) = 0$ for $l < 5$ and $l > 10$, and also $\phi_0(0,t) = 0$. Root system development coefficients are shown on Table 4.1 and the phosphorus uptake coefficients are for different orders as follows: $\lambda_0 = 30.8$, $\lambda_1 = 12.32$, $\lambda_2 = 6.16$ and $c_\infty = 0.5$ (dimensionless) and $F_m = 0.28$ [μmol cm^{-2} day^{-1}].

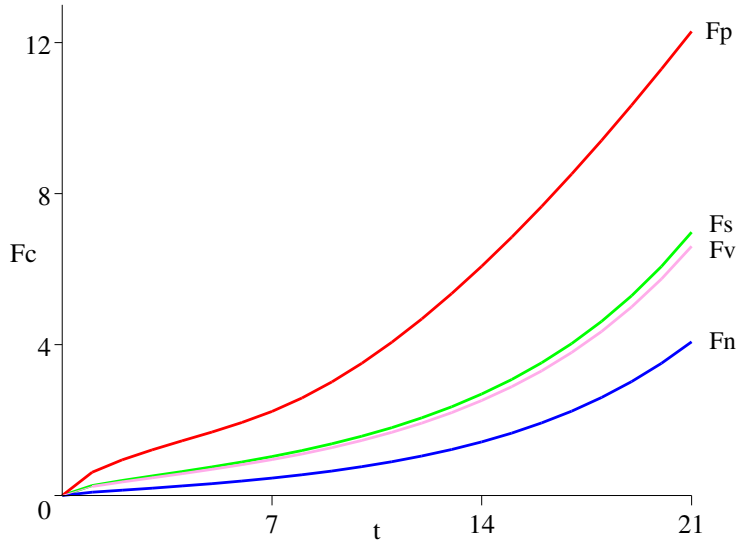

Figure 4.10: Comparison between the developing root system nutrient uptake F_p (solid line) and nutrient uptake by averaged roots (dashed lines). $F_n(t)$ is the uptake calculated using the average root radius calculated over the number of roots. $F_s(t)$ corresponds to the average over root surface area, and $F_v(t)$ the average over the volume of the roots. $F_v(t)$ is so called Barber flux [6].

i.e., in the present case $\mu_0 = \mu$, $\mu_1 = 2\mu - \mu^2$, and $\mu_2 = \mu^3 - 3\mu^2 + 3\mu$. It must be noted, that it is extremely difficult to obtain data about the root death rate and therefore we have ignored it in the previous calculations of the nutrient uptake. However, we note that if this data becomes available then we can include it in our solution very easily.

4.9 Conclusions

In this chapter the nutrient uptake by root systems in the absence of competition between the root branches was considered. Based on the analysis, we can conclude that the most critical, i.e., nutrient deficient, time for plant development occurs just before the emergence of the first sub-branches (Figure 4.9). After the emergence of the first sub-branches, the nutrient uptake by the root system increases considerably due to the uptake by them. Hence, sub-branches play a crucial role in the nutrient supply to the plant. First order sub-branches have a smaller radius than the lower order branches, but their overall number and hence the total length and therefore also surface area is considerably larger than that of zero order roots.

Current experiments measure nutrient uptake from the 6th day after germination up to 20 days of growth (see Barber experiment description [21]). Before conducting the experiments Barber [21] also trimmed the roots so as to “enhance branching”. At

the end of the experiments the average root radius is calculated based on morphological properties of the root system at that time. However, this trimming possibly serves the purpose of forcing the average root radius to be more or less constant throughout the experiment since the trimmed roots would almost immediately start producing sub-branches and hence become more dominant. As we have shown above, for un-trimmed plants the average root radius goes through quite noticeable changes during this period of plant development (see Figure 4.7). In the reality, the roots are not being trimmed in the process of agricultural production and hence the estimation of nutrient uptake based on the measurement of average root radius is not accurate enough.

The results of the current chapter also stress the implication of root radius and elongation averaging. We showed that the methods used by Barber and others can result in 30% error in the calculation of nutrient uptake by developing root branching structure.

Chapter 5

Root Competition in Static Root Systems

In Chapter 4 we developed and discussed a root branching model. This model enabled us to calculate the nutrient uptake by root branching structure, but assumed that the sub-branches are not competing with each other for nutrients. However, in general, there will be competition for the usually limited amount of nutrients present in the soil. In this chapter we aim to develop a strategy for modelling the inter-root competition for the nutrients. We begin by considering a time-independent spatial root distribution. In Chapter 6 the model for nutrient uptake by a root distribution that changes in time and space will be presented.

5.1 Static Root Distribution

As discussed in Chapters 1 and 4, root systems are complicated branching structures (see Figure 4.3). This makes it almost impossible to calculate the nutrient uptake with full root positional information. Therefore, a simplified strategy accounting for the root branching structure and nutrient uptake needs to be developed. One way of doing so would be to consider the root system to be a spatially averaged root size distribution. Thus, we will base the modelling in this chapter on experimentally measured root length density distributions [cm of roots per cm^3 of soil] in the soil.

As discussed in Chapter 4, the average distance between the sub-branches is 0.7 cm (in the case of maize), i.e., order 1 cm [97]. The same group of authors have also found that the distance between the sub-branches can vary along the zero order root [100], [98], [101], [123], [132], but in general the diameter of sub-branches is at least an order of magnitude smaller than the distance between them. Experimental measurements of distance between different maize roots in field conditions were conducted by Tardieu [119] and Varney et al. [132]. These measurements indicate that the distance between

roots is in the range 0.1-5 cm, or even greater in soil that has been compacted by heavy agricultural machinery. As the root radius of current interest is of order 10^{-2} cm or less, the inter-branch distance on average is at least an order of magnitude larger than the root radius. A typical time scale $[t]$ for pot-plant experiments is 20 days $\approx 1.7 \times 10^6$ seconds. For an agricultural plant growing in the field, the time-scale of interest is 4 months $\approx 10^7$ seconds. The effective diffusion coefficient D_{eff} for different nutrients typically ranges from 10^{-6} cm^2 s^{-1} for nitrate to 10^{-8} cm^2 s^{-1} for phosphorus. Thus, the typical diffusional length scale given by $\sqrt{D_{\text{eff}}[t]}$ ranges from 0.1 cm to 3 cm for $[t] = 4$ months. Therefore, for most cases the diffusional length scale is smaller than the inter root branch distance. Hence, we can consider the root system to be a space-averaged distribution which will enable us to build a model of nutrient uptake by plant roots using the formula derived for plant nutrient uptake with a prescribed nutrient concentration far away from the root (Chapter 2). When the branch separation becomes comparable to the diffusional time-scale or to the root radius then the assumption of weak competition is not appropriate because of the strong interactions between the roots, i.e., nitrate uptake for period of 4 months. We will discuss the strong competition in the end of Chapter 6.

These calculations are in agreement with the observations presented in Baldwin et al. [5] concerning numerical calculations of competition between parallel cylindrical roots. They conducted a series of numerical simulations of flux into two parallel cylindrical roots for different inter-root distances and different diffusional length scales. When the inter-root distance is orders of magnitude larger than root radii, the reduction in nutrient uptake by the roots compared to the uptake in absence of competition was found to be of order 10% or much less on root vegetative times scales. This is in agreement with our results. We will refer to the case when the diffusion length-scale on a vegetational time-scale is less than inter-root distance, as that of weak competition between roots.

Our ideas are also supported by the numerical experiments conducted by Leadley [74]. He calculated the diffusion profiles around parallel cylindrical roots for different spatial arrangements and concluded that the neighbouring roots start interacting strongly with each other in case of nitrate after a time-scale of 1 month and in case of phosphate after 4 months.

The root density profiles are measured experimentally and many of these have already been reported in the literature. Usually these are measurements of root length density (cm of root per cm^3 of soil), or root number density (number of roots per cm^3 of soil), or fresh weight density (gramme of fresh weight per cm^3 of soil). These measurements report many different forms for the root distributions, however commonly the root length density monotonically decreases with depth [118], [79], [80],

[95]. The measurements also show the possibility of more complicated distributions, for example with two local maxima at finite distance from the top of the soil [108] corresponding to simultaneous measurement of at least two coexisting species with two different rooting depths. Pagès et al. have also done 3 dimensional maize root branching simulations and extracted the root length density profiles from those simulations [49], [97]. Their simulations show one single maximum of root length distribution at about 10 cm depth in the soil (see Figure 5.1).

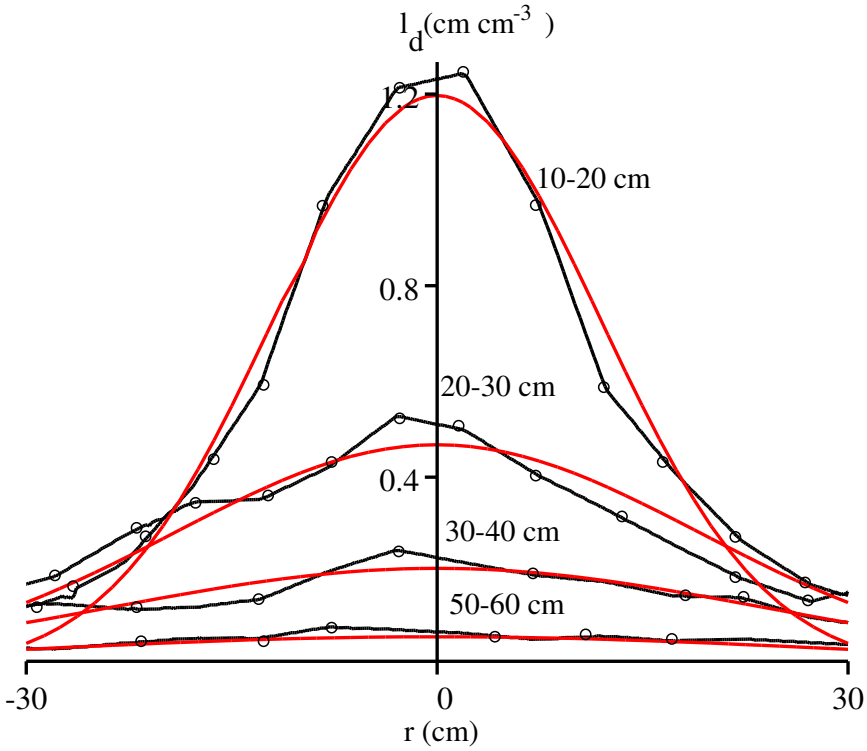

Figure 5.1: Length density l_d [cm of roots per cm^3 of soil] as a function of horizontal distance from the axis of the seed at different depths in soil as shown in [49]. Points fitted with normal distribution curves.

We begin by considering the root system to have a normal distribution in space. This is suggested in the article by Grabarnik et al. [49] whose results can be interpreted so that the root density distribution is hemispherically symmetric with respect to the location of the seed. This distribution can then be approximated by a normal distribution as a distance from the seed. Their data fitted to a normal distribution using least square fit is shown on Figure 5.1. Hence, assuming that the length density, $l_d(r)$ [cm of roots per cm^3 of soil] of the root system is given, we can calculate the volume density of roots using the average root radius a_r [cm]. Thus the volume density of roots [cm^3 of root tissue per cm^3 of soil] is given by $\phi_r(r) = \pi a_r^2 l_d(r)$. In the

case of the field crop the plants are relatively close together. Therefore the horizontal variations in root density are very small and root length density profile depends mainly on depth. In the following sections we will discuss the nutrient uptake by a hemispherically symmetric root system, corresponding to an isolated plant in an infinite extent of the soil, and vertically varying root distribution, corresponding to a field crop condition, with the soil surface having been fertilised.

5.1.1 Model equations

We begin the modelling by considering the soil with the root fraction only, neglecting root hairs and mycorrhiza. Hence we consider the volume fraction of roots per unit volume of soil to be ϕ_r, the volume fraction of solid particles per unit volume of soil to be ϕ_s, and the volume fraction of liquid per unit volume of soil to be ϕ_l. We will take $\phi_r = \phi_r(\mathbf{r})$, since the volume fraction of roots depends on the spatial position. However, we consider ϕ_s and ϕ_l to be constant in space and $\phi_l \approx \phi$ where ϕ is the porosity of the soil. Thus, we are assuming that the soil is fully saturated. This assumption also implies that the root mass in the soil does not influence the porosity of the soil. We notice that $\phi_r = \pi a^2 l_d << \phi$ for $l_d \lesssim O(1)$, and the average root radius $a \sim O(10^{-2})$. Hence, we have

$$\phi_s + \phi_l \approx 1 \quad \text{for} \quad \text{all} \quad \mathbf{r}. \tag{5.1}$$

Taking into account all the buffer power arguments presented in Chapter 2, equations (2.6), (2.7), (2.8) and including the nutrient removal from the liquid phase of the soil only, we arrive at the following equation for the nutrient concentration in the soil pore water

$$\frac{\partial}{\partial t}[(b + \phi_l)c_l] + \nabla \cdot (c_l \mathbf{u}) = \nabla \cdot (\phi_l D \nabla c_l) - F_r, \tag{5.2}$$

where b is the buffer power of the soil, F_r is the nutrient uptake by the roots per unit volume of soil.

5.1.1.1 Nutrient uptake by the roots F_r

We now face the task of estimating the nutrient uptake by the root system. We consider the spatially averaged root distribution and use the formulae (2.120) for flux per unit root surface area with the far-field concentration c_∞ given by the local concentration between the two branches, i.e., so called "local far-field" concentration. The area of the roots per unit volume of soil is given by $S = 2\pi a l_d(\mathbf{r})$, where a is the

radius of the roots [cm] and $l_d(\mathbf{r})$ is the length of the roots per unit volume of soil [cm cm^{-3}]. Hence we suppose that the nutrient uptake is given by

$$F_r = 2\pi a l_d(\mathbf{r}) \frac{2F_m c_l/K_m}{1 + c_l/K_m + L + \sqrt{4c_l/K_m + (1 - c_l/K_m + L)^2}}, \tag{5.3}$$

where F_m is the maximum flux of nutrient into the root [μmol cm^{-2}s^{-1}], K_m is the Michaelis-Menten coefficient [μmol cm^{-3}], $\lambda = F_m a/(DK_m\phi_l)$, and

$$L = \frac{\lambda}{2} \ln \Big[4e^{-\gamma} \frac{D\phi_l}{a^2(\phi_l + b)} (t - t_0(\mathbf{r})) + 1 \Big], \tag{5.4}$$

where D is the nutrient ion diffusion coefficient in the soil [cm^{2}s^{-1}], b is the buffer power of the soil [non-dimensional] , and a is the average root radius [cm]. The time-delay term $t_0(\mathbf{r})$ describes the time it takes for the first roots to reach the spatial position $\mathbf{r}$. As a first approximation we are considering the root distribution to be independent of time and hence we will take $t_0(\mathbf{r}) = 0$. However, we will return to this in the following Chapter 6 when we consider developing root distribution.

5.1.2 Non-dimensionalisation

To non-dimensionalise the system we choose a typical length scale to be l_0, which describes, for example, the length of the longest root in the system or the maximum rooting depth. The time-scale $[t]$ can be chosen to be equal to the duration of an average experiment, i.e., ≈ 1 month. Hence by taking

$$\mathbf{r} = l_0 \mathbf{r}^*, \quad t = [t]t^*, \quad c_l = K_m c^*, \tag{5.5}$$

we arrive at the following dimensionless equation (after dropping *s)

$$\frac{\partial c}{\partial t} + \epsilon Pe \nabla \cdot (\mathbf{u}c) = \epsilon \nabla^2 c - S\, l(\mathbf{r}) \frac{2c}{1 + c + L(t) + \sqrt{4c + (1 - c + L(t))^2}}, \tag{5.6}$$

where

$$\epsilon = \frac{\phi_l D[t]}{l_0^2(\phi_l + b)}, \quad S = \frac{2\pi a l_{d,\max} F_m[t]}{K_m(\phi_l + b)}, \tag{5.7}$$

and $l(\mathbf{r}) = l_d(\mathbf{r})/l_{d,\max}$ is the normalised root length density distribution. The time-dependent term $L(t)$ becomes

$$L(t) = \frac{\lambda}{2} \ln(\alpha t + 1) \quad \text{with} \quad \alpha = 4e^{-\gamma} \frac{D\phi_l[t]}{a^2(\phi_l + b)} \tag{5.8}$$

and $Pe = Ul_0/D$ is the Péclet number. U is the scale for the Darcy flux of water in the soil.

5.1.3 Péclet Number and Parameter Estimation

Péclet Number

The Péclet number is a dimensionless number which describes the balance between the water flux, length scale and diffusion, i.e., $Pe = Ul_0/D\phi_l$, where U is the Darcy flux, l_0 is the length scale, and D is the diffusion coefficient. In this expression for the Péclet number we know the diffusion coefficient for different nutrients and the length scale of the root system. However, the speed of water flow in the rooting region of the soil is not given explicitly by experiments. For fully saturated soil we can estimate that per unit volume of soil, the roots take up water proportional to their root surface area $S = 2\pi a l_d$, where a [cm] is the root radius and l_d [cm cm^{-3}] is the length density of roots per unit volume of soil. Hence, the water uptake per unit volume of soil is $q^* = SV = 2\pi a l_d V$, where V is the Darcy flux of water into one root. However, total amount of water in the soil-system must be conserved. Hence we require

$$\nabla \cdot \mathbf{u} + q^* = 0. \tag{5.9}$$

From there the water flow speed scale is proportional to length-scale times water uptake, i.e., $U \sim q^* l_0 = 2\pi a l_d V l_0$. The Péclet number now becomes

$$Pe = \frac{l_0^2 2\pi a l_d V}{D\phi_l} = 2\pi l_0^2 l_d Pe_r, \tag{5.10}$$

where $Pe_r = aV/(D\phi_l)$ is the Péclet number for a single root. The single root Péclet number, Pe_r, was found in Chapter 2 Section 2.2.2 to be of order 10^{-3} to 10^{-7} for agriculturally important plants, and typical values for other parameters are $l_0 \sim 50$ cm, $l_d \lesssim 1$ cm cm^{-3}. Thus, we find that

$$Pe \sim O(10) - O(10^{-5}). \tag{5.11}$$

For the single root Péclet number $Pe_r = 2 \times 10^{-3}$ corresponding to the root radius $a = 0.02$ cm, the length l_0 of the root system when $Pe \sim O(1)$ is approximately $l_0 \sim 10$ cm, i.e., for relatively short root systems the Péclet number is small.

We note that in this calculation we have assumed that throughout the root system $l_d \sim 1$ uniformly. However, this is clearly not the case (see Figure 5.1) since the root density decreases the further away one is from the seed or so called "centre" of the root system. Hence the Péclet number is likely to be smaller because of this decrease of root density. Thus, for $Pe << 1$, we will neglect the water movement in this chapter. However, we will return to this problem in Chapters 7-9 when we consider the water movement and uptake together with resulting nutrient movement in the soil.

Nutrient	α	ϵ	S	λ	c_∞	$\ln(\alpha+1)$
N	10^4	7.15×10^{-4}	100	8.8	200	9.2
K	333	2.4×10^{-5}	16	47	3.28	5.8
S	5.7×10^3	4×10^{-4}	4.2	0.66	10	8.6
P	54.7	3.9×10^{-6}	0.75	12.32	0.5	4.02
Mg	8.7×10^3	6.2×10^{-4}	5.87	0.55	6.7×10^{-3}	9.07
Ca	83.8	5.9×10^{-6}	0.012	5.5×10^{-3}	2×10^{-4}	4.44

Table 5.1: Values of dimensionless parameters for different nutrients for time-scale $[t] = 1$ month$= 2.6 \times 10^6$ seconds, $\phi_l = 0.3$, $D = D_f f$ with $D_f = 10^{-5}$ cm^2 s^{-1} and $f = 0.3$.

Non-dimensional Parameter Estimation

Just as the Péclet number indicates the relative importance of diffusion compared to convection, ϵ shows the relative importance of both of those terms compared to the non-linear nutrient uptake term. The diffusion coefficient in the soil is $D = fD_f$, where f is the impedance factor, and D_f is the diffusion coefficient in the free water approximately 10^{-5} cm^2 s^{-1}. The parameter estimation based on this value for time-scale $[t] = 1$ month is shown in Table 5.1.

We note that the nutrient uptake parameter S is very small or order 1 for phosphate, sulphate, magnesium and calcium. Since the diffusion coefficients ϵ for different nutrients are all very small, we can expect no considerable diffusion gradient on the root system length scale. All the nutrient gradients in the soil are expected to be mainly due to the non-uniform nutrient uptake by non-uniform root distribution in the soil.

Summary of The Equation

The equation we need to solve is

$$\begin{aligned} \frac{\partial c}{\partial t} + \epsilon Pe \nabla \cdot (\mathbf{u}c) &= \epsilon \nabla^2 c - S\, l(\mathbf{r}) \frac{2c}{1 + c + L(t) + \sqrt{4c + (1 - c + L(t))^2}}, \\ \text{with} \quad L(t) &= \frac{\lambda}{2} \ln(\alpha t + 1), \end{aligned} \tag{5.12}$$

where ϵ is small, but α is large. S can be either large or small or order 1. In this chapter we will limit our interest only to the $Pe << 1$ case, because when Pe becomes large there are likely to be large moisture gradients present in the soil and the assumption that the moisture conditions are constant throughout the soil does not hold. Hence in this case one would need to model the water movement in the soil. This together with the nutrient uptake model will be presented in Chapters 7-9.

5.1.4 Boundary Conditions

In prescribing the boundary conditions for this model we are faced with at least two possibilities. First we consider a root system of a single plant in infinite soil. In this case the root system of one plant is not competing with the root system of the neighbouring plants.

The second case would be to consider a field of agriculturally produced plants which have a root density distribution that is fairly uniform horizontally, but changes with the depth of the the soil zone [118], [119]. In this case we will impose a constant nutrient flux boundary condition at the soil surface corresponding to a prescribed fertiliser input. We will take the nutrient concentration to be constant at a fixed depth corresponding to the concentration of nutrient in the ground water.

5.1.5 Single Root System Boundary Condition

For the single root system in an infinite soil we will first consider the specific root length density distribution $l(\mathbf{r})$ which is zero infinitely far away from the origin of the root system. This implies that we can take the boundary condition at infinity to be

$$c \to c_\infty \quad \text{as} \quad r \to \infty. \tag{5.13}$$

Considering the root system distribution to be spherically symmetric, i.e., $l(r)$ with $r = \sqrt{x^2 + y^2 + z^2}$, then after neglecting $\epsilon Pe << \epsilon << 1$ terms since $\epsilon << S$, the equation (5.12) becomes

$$\frac{\partial c}{\partial t} = -S\, l(r) \frac{2c}{1 + c + L(t) + \sqrt{4c + (1 - c + L(t))^2}}. \tag{5.14}$$

In general, this equation needs to be solved numerically. However, for phosphorus, magnesium and calcium $c_\infty << \lambda$ and $c_\infty << 1$. This enables us to simplify the uptake equation further (see also Chapter 2 section 2.6.2).

5.1.6 $c_\infty << 1$ Limit

For phosphorus, magnesium, and calcium we found in Chapter 2 that the equation (5.14) for nutrient uptake simplifies at the leading order to

$$\frac{\partial c}{\partial t} \approx -\frac{S\, l(r) c}{1 + \frac{\lambda}{2} \ln(\alpha t + 1)}. \tag{5.15}$$

The solution that satisfies initial condition $c = c_\infty$ at $t = 0$ is given by

$$c(t) \approx c_\infty \exp\Big\{ -\frac{2S\, l(r)}{\alpha\lambda} e^{-2/\lambda} [Ei(\ln(\alpha t + 1) + \frac{2}{\lambda}) - Ei(\frac{2}{\lambda})] \Big\}, \tag{5.16}$$

where $Ei(x) = -\int_{-x}^{\infty} \frac{e^{-y}}{y} dy$ is the exponential integral. The comparison between the numerical solution to (5.14) and analytical approximation given by (5.16) is shown on Figure 5.2 for $l(r) = 1$.

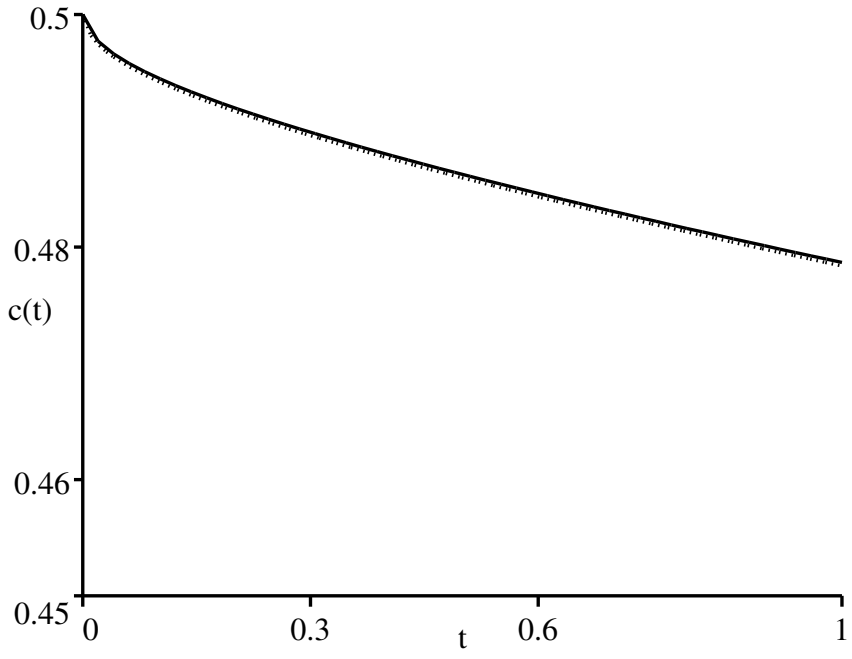

Figure 5.2: Comparison between numerical solution using Runge-Kutta method (solid line) and analytical solution (dotted line) given by (5.16) for phosphorus. $t = 1$ corresponds to 1 month.

5.1.7 $\lambda << c_\infty$ Limit

In the case of nitrate and sulphur the nutrient uptake coefficient λ is small compared to the initial nutrient concentration. More specifically, for the duration of 1 month the time dependent term $L(t) = (\lambda/2)\ln(\alpha t + 1) << c_\infty$ (see table 5.1). Hence, we can use this to simplify the model.

$L(t) << c_\infty$ Limit

For $L(t) = (\lambda/2)\ln(\alpha t + 1) << c_\infty$ the equation simplifies to

$$\frac{\partial c}{\partial t} = -\frac{S\, l(r) c}{1 + c}. \tag{5.17}$$

This equation has a solution in the form of Lambert W functions[1], i.e., the solution is given by the following transcendental equation for c

$$c(t)e^{c(t)} = c_\infty e^{c_\infty - S\,l(r)t}, \quad \text{i.e.,} \quad c(t) = W_L(c_\infty e^{c_\infty - S\,l(r)t}). \tag{5.18}$$

Expanding the Lambert W function for large times we find that c is given by

$$c(t) \sim c_\infty e^{c_\infty - S\,l(r)t} - c_\infty^2 e^{2c_\infty - 2S\,l(r)t} + O(e^{-3S\,l(r)t}). \tag{5.19}$$

We see that for the nitrate the solution given by (5.18) is accurate for times up to 1.5 months (see Figure 5.3). After approximately 2 months the concentration has fallen to exponentially small level and hence the c term becomes comparable in size to the $L(t)$ term.

For small times we found in Chapter 2, that relative nutrient uptake of nitrate was small, i.e., $\lambda/c_\infty << 1$ for $c_\infty >> 1$, and therefore the nutrient diffusion profile around the single root was found to be relatively flat. After 1 month $c_\infty << \lambda$ and the uptake is nolonger small compared to the local far-field concentration. However, by that time the diffusion profile has spread over a distance comparable to the inter-root distance and thus due to the strong competition between the sub-branches the concentration profile between the branches will remain flat. Therefore, we can use the equation (5.17), and hence also the Lambert function solution (5.18) to it, throughout the growth period of 4 months.

$c << L(t)$ Limit

In general, when c becomes small we can no-longer neglect $L(t)$ in comparison to it in the equation (5.14), assuming of course that the distribution model is still valid. In this case we approximate the equation (5.14) by

$$\frac{\partial c}{\partial t} = -\frac{S\,l(r)c}{1 + \frac{\lambda}{2}\ln(\alpha t + 1)}, \tag{5.20}$$

which will have the solution in the form

$$c(t) = A\exp[-\int^t \frac{S\,l(r)d\tau}{1 + \frac{\lambda}{2}\ln(\alpha\tau + 1)}]. \tag{5.21}$$

In terms of the exponential integral $Ei(x) = -\int_{-x}^{\infty}(e^{-y}/y)\,dy$ this can be written

$$c(t) = A\exp[-\frac{2S\,l(r)}{\alpha\lambda}e^{-2/\lambda}Ei[\ln(\alpha t + 1) + 2/\lambda]]. \tag{5.22}$$

[1]Lambert W function $W_L(x)$, or for some authors ω function, is defined to be the solution of the transcendental equation $W_L(x)e^{W_L(x)} = x$.

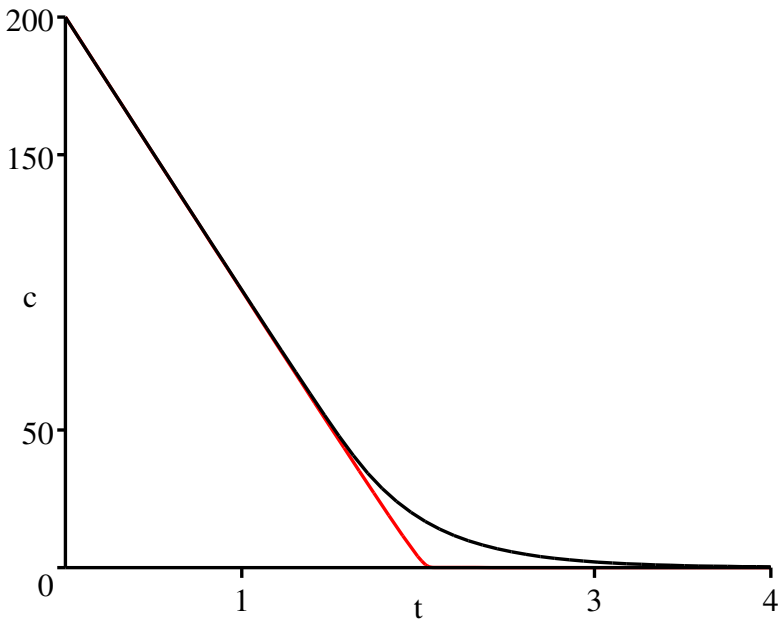

Figure 5.3: Comparison of numerical solution using Gear's method (solid line) and analytical solution (red line) given by (5.18) for nitrate. $t = 1$ corresponds to 1 month.

where A is the coefficient to be determined from matching $L(t) << c$ solution to $c << L(t)$ solution. At small times the leading order approximation of (5.22) is given by

$$c \sim A \exp[-\frac{2S\,l(r)}{\alpha\lambda} e^{-2/\lambda} Ei[2/\lambda] - S\,l(r)t]. \tag{5.23}$$

Matching

To match the two limits together in order to determine the unknown parameter A we need to have the intermediate region where both solutions are valid. This overlap region exists if $L(t) << 1$ while $c << 1$, i.e., when $S\,l(r) >> c_\infty$ in (5.19). Provided such an overlap region exists for our parameter régime, we can proceed with matching. To match the $L(t) << c$ solution and $c << L(t)$ solution we first have expanded (5.22) for small time (equation (5.23)), and (5.18) for large time (equation (5.19)). Equating the coefficients of $e^{-S\,l(r)t}$, we find that A is given by

$$A e^{-\frac{2S\,l(r)}{\alpha\lambda} e^{-2/\lambda} Ei[2/\lambda]} = c_\infty e^{c_\infty}. \tag{5.24}$$

We form the uniformly valid composite approximation using the van Dykes matching rule. Van Dykes matching rule states that the composite approximation is equal to small time approximation plus large time approximation minus the common part.

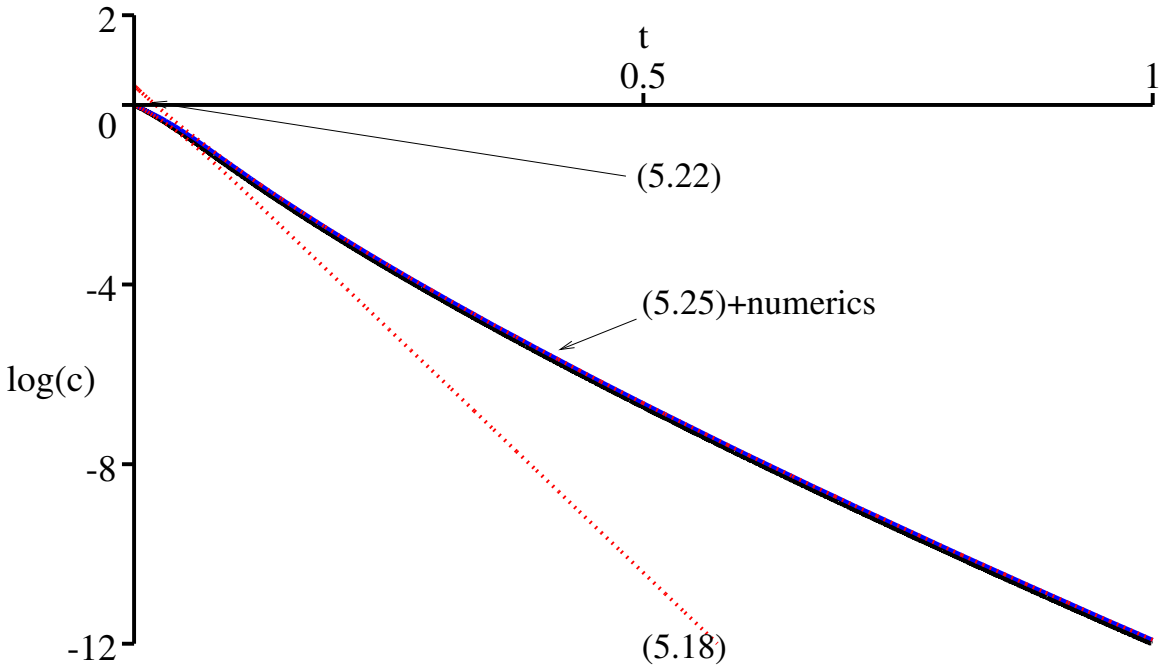

Figure 5.4: Comparison between numerical solution (black line); analytical solutions (5.18) and (5.22) (both red lines); and composite approximation (5.25) (blue line) for $\alpha = 10$, $S = 50$, $\lambda = 1$, and $c_\infty = 1$.

Hence we will have

$$c(r,\tau) \sim W_L(c_\infty e^{c_\infty - S\,l(r)t}) + c_\infty e^{c_\infty + \frac{2S\,l(r)}{\alpha\lambda} e^{-2/\lambda}(Ei[2/\lambda] - Ei[\ln(\alpha t+1)+2/\lambda])} - c_\infty e^{c_\infty - S\,l(r)t}, \tag{5.25}$$

where W_L is the Lambert W function. The comparison between the numerical solution and short time, long time and composite approximation is shown on Figure 5.4 for $c_\infty = 1$, $\lambda = 1$, $\alpha = 10$ and $S = 50$, i.e., $S > \lambda$.

Full Root System Uptake

In equation (5.25) and in other apporoximate solutions of equation (5.14) the root length density $l(\mathbf{r})$, is spatially dependent and hence to obtain the full root system nutrient uptake one would need to integrate over all of the root system R, i.e.,

$$F_{\text{sys}}(t) = \int_R \frac{S\,l(\mathbf{r})2c}{1 + c + L(t) + \sqrt{4c + (1 - c + L(t))^2}}\, dV(\mathbf{r}), \tag{5.26}$$

where c is given by the solution to (5.14). In general this integration should be carried out numerically.

As discussed earlier, we take the root volume distribution to be given by a spherically symmetric normal distribution. This implies that $l(r) = e^{-r^2/\kappa}$, where κ is a

dimensionless density distribution parameter and $r = \sqrt{x^2 + y^2 + z^2}$. There are of course many more possible root density distributions which will depend on the species and environment of the plant. However, in this chapter we will limit our attention to only one of those in order to illustrate the calculation of the nutrient uptake by single plant root system.

For simplicity we will only calculate the nutrient uptake by the root system that is a hemisphere (see Figure 5.1) and integrate from $r = 0$ to 1 only since $l(r) \approx 0$ when $r > 1$, i.e.,

$$F_{\text{sys}} = 4\pi^2 S \int_0^1 \frac{l(r)c}{1 + c + L(t) + \sqrt{4c + (1 - c + L(t))^2}}\, dr. \tag{5.27}$$

The results of numerical integration for phosphorus[2] are shown on Figure 5.5.

5.1.8 Field Crop Boundary Condition

In the case of the field crop we look for vertical variation in the root length density only. This implies that plants are sufficiently near to each other so that horizontal variations in root density are small. However, we will consider it to be changing with the depth of the soil, i.e., $l = l(z)$ [118], [119], [97]. We consider the soil layer in the z direction, with the surface of the soil at $z = 0$ to the ground water level at $z = z_w$. Use of non-dimensional scaling

$$z = z_w z^*, \quad t = [t]t^*, \quad c_l = K_m c^*, \tag{5.28}$$

where $[t]$ is the typical timescale, gives the following dimensionless equation (after dropping $*$s)

$$\frac{\partial c}{\partial t} = \epsilon \frac{\partial^2 c}{\partial z^2} - S\, l(z) F(c, t), \tag{5.29}$$

with

$$F = \frac{2c}{1 + c + L + \sqrt{4c + (1 - c + L)^2}} \quad \text{and} \quad L(t) = \frac{\lambda}{2} \ln(\alpha t + 1), \tag{5.30}$$

and $\epsilon = D\phi_l[t]/[(b + \phi_l)z_w^2]$. The boundary condition at the ground water level will be taken to be

$$c = c_\infty \quad \text{at} \quad z = 1. \tag{5.31}$$

At the surface of the soil $z = 0$ the boundary condition will be taken to be one of constant flux. This implies that there is a nutrient source at the surface of the soil due to fertiliser, organic matter decomposition etc., thus we take

$$-\frac{\partial c}{\partial z} = \varrho \quad \text{on} \quad z = 0, \tag{5.32}$$

[2]The dimensional root system nutrient uptake $F_{\text{sys,dim}}$ is calculated as $F_{\text{sys,dim}} = \frac{K_m(\phi_l + b)}{[t]} F_{\text{sys}}$.

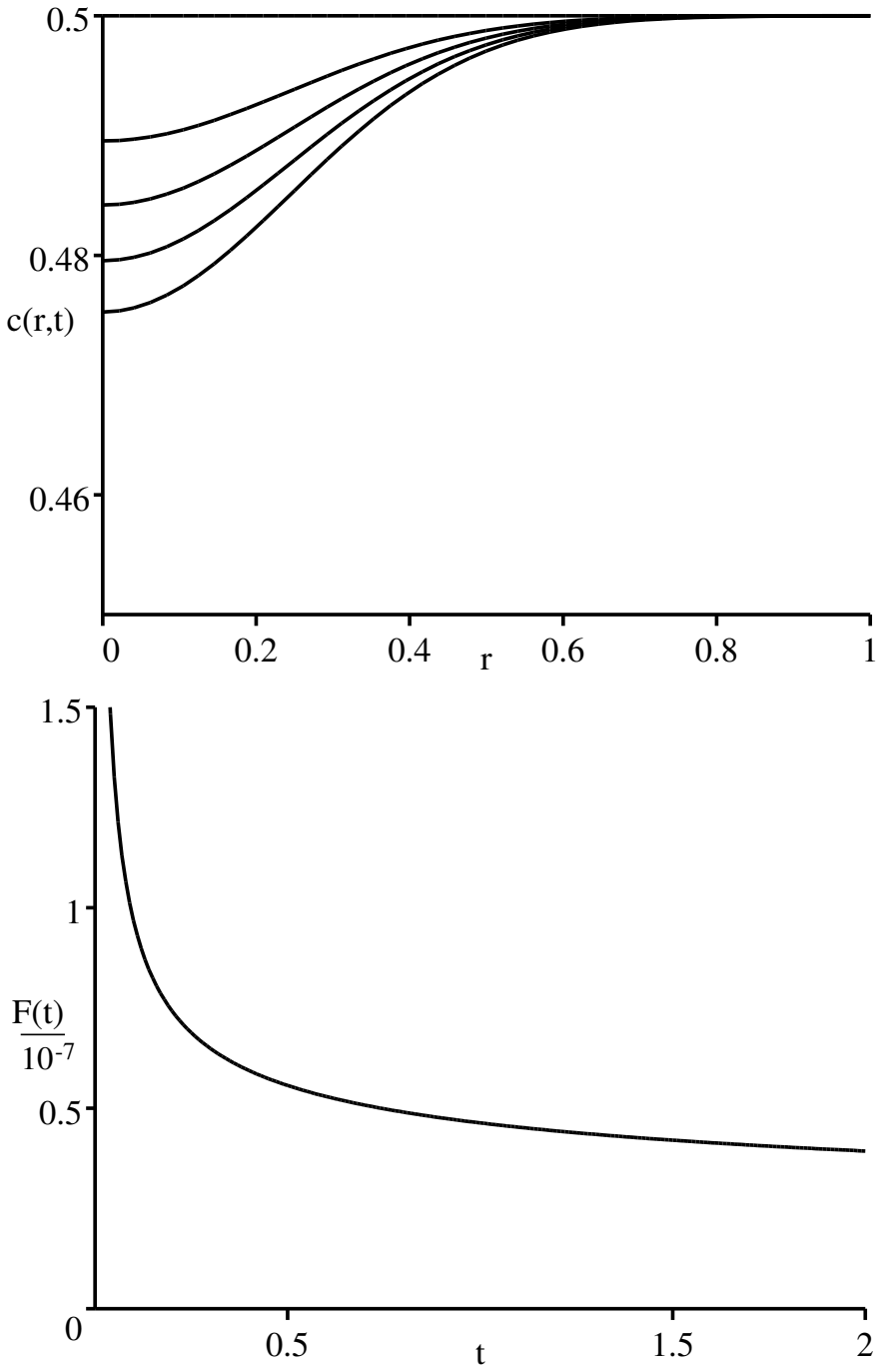

Figure 5.5: The top graph shows the dimensionless concentration of phosphorus per unit volume of soil (also known as average local far-field concentration) as a function of space for dimensionless time $t = 0, 0.25, 0.5, 0.75$ and 1. Dimensionless time $t = 1$ corresponds to dimensional time 1 month. Root volume density is given by $l(r) = e^{-8.6r^2}$. The bottom graph shows the dimensional rate of phosphate uptake [μmol s^{-1}] by the root system as a function of time [months].

where $\varrho = \varrho_{\text{dim}} z_w/(DK_m\phi_l)$, with ϱ_{dim} being the rate of nutrient application per unit surface of the soil in unit time [μmol cm^{-2} s^{-1}].

Rate of Fertiliser Application

The rate of nutrient application will be determined from experiments or from agricultural statistics. For instance, according to [27], the typical nitrate (NO_3^-) nitrogen application in England in 1998 was of order 120 kg ha^{-1} per year. Assuming that this is applied uniformly over a 6 month period starting from March and finishing in August, we find that in our units it corresponds to approximately 10^{-6} μmol cm^{-2}s^{-1}. In the case of phosphate (P_2O_5) the corresponding numbers are 30 kg ha^{-1} per year corresponding to approximately 10^{-7} μmol cm^{-2}s^{-1}. The dimensionless fertiliser application rate ϱ for nitrate and phosphorus is 48720 and 5172 respectively.

In reality the fertiliser application depends on the time of a year. Usually farmers apply fertiliser to the crop in the beginning of vegetative period, i.e., in spring. Smaller amounts of fertiliser are applied in later stages. According to [27] almost 50% of yearly fertiliser is applied during March and April (nitrate fertiliser $\approx 30 - 35$ kg ha^{-1}). However, the application rate in May is approximately half of that in April, i.e., 15 kg ha^{-1} of nitrate fertiliser.

In this chapter we will investigate the effect of constant fertiliser application rate as to find out the possible mechanisms working in this simple case. At this stage we also assume constant moisture conditions, and hence the only mechanism for transporting the nutrient to the roots will be diffusion.

We expect the solution to this model to reach a steady state in space. However, since it is a highly non-linear system one has to solve it numerically. The numerical solutions for phosphorus and nitrogen with uniform initial condition is shown on Figure 5.7 for the root distribution shown on Figure 5.6.

5.1.9 Interpretation of Numerical Results

We can "split" the solutions up to three distinctive stages in time. The first one is characterised by an initial reduction in the concentration due to the presence of roots, but the concentration near $z = 1$ is still approximately c_∞. That is, the diffusion has not started to influence the nutrient concentration away from the main root section, i.e., away from $z = 0$.

The second stage may be called a "pseudo-steady state". This is when the concentration profile changes very slowly in time due to diffusion and because $\ln(\alpha t + 1)$ changes very slowly in time for $t >> 1$ and $\alpha >> 1$. That makes it possible for diffusion to "kick in" and develop a profile that changes very slowly in time.

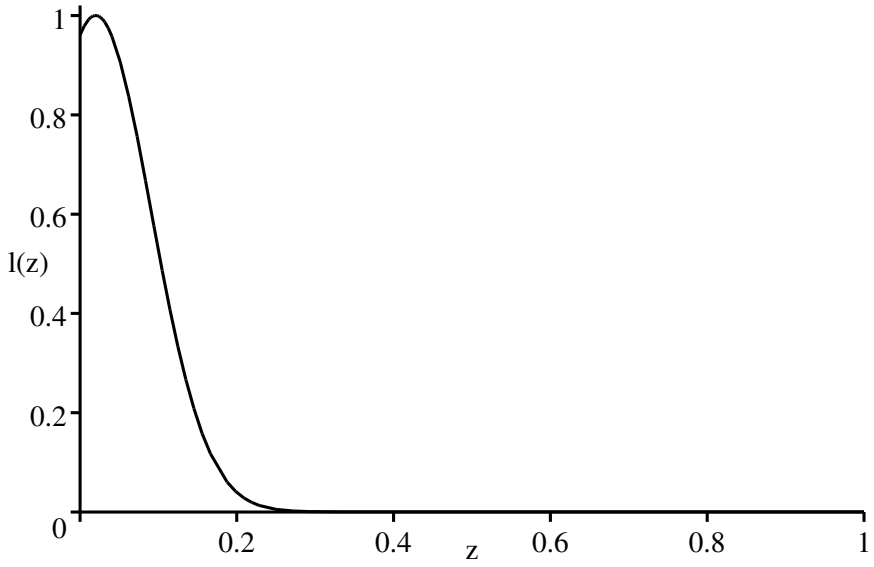

Figure 5.6: Normalised root length density distribution given by $l(z) = e^{-(z-0.02)^2/0.01}$.

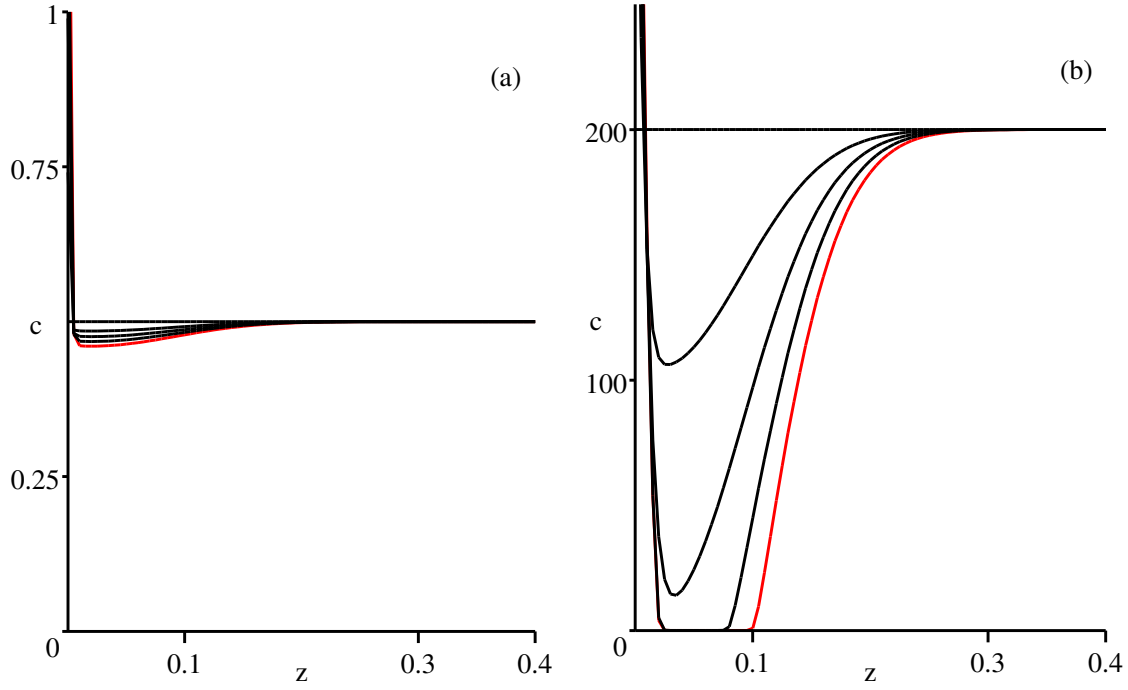

Figure 5.7: Concentration of phosphorus and nitrate for times up to 4 months (red line). (a) shows the concentration of phosphorus in the soil for $c_\infty = 0.5$, $S = 1$, $\lambda = 24$, $\varrho = 5172$, $\alpha = 54.7$, and $\epsilon = 2.4 \times 10^{-7}$ and $t = 0, 1, 2, 3, 4$ months. (b) shows the concentration of nitrate in the soil for $c_\infty = 200$, $S = 100$, $\lambda = 8.8$, $\varrho = 48720$, $\alpha = 10^4$, and $\epsilon = 4.4 \times 10^{-5}$ $t = 0, 5$ days and $1, 2, 3, 4$ months. See also Figure 5.6 for root length density profile used.

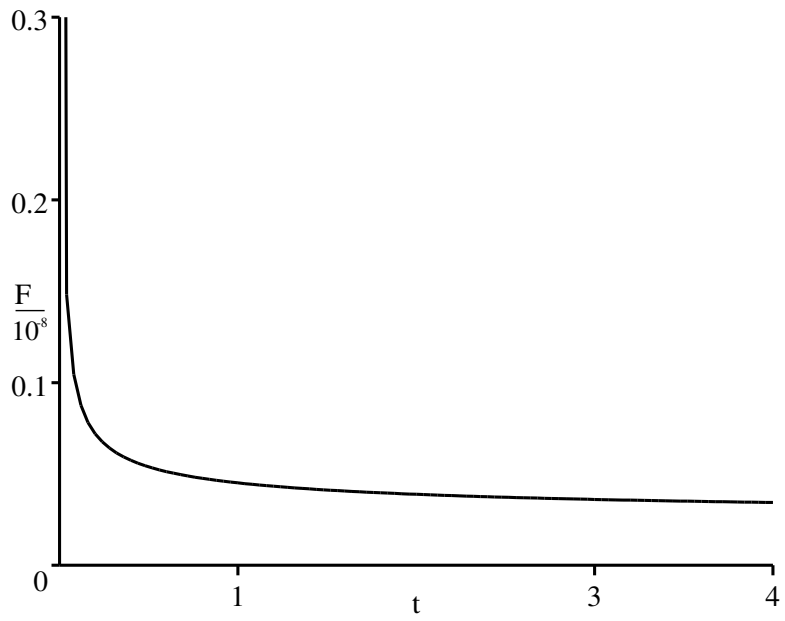

Figure 5.8: Uptake rate of phosphorus [μmol s^{-1}] by the full root system per unit soil surface area [cm^2].

The third stage is activated when $L(t) >> 1$, in which case as $t \to \infty$ the sink term in the equation approaches zero and the solution approaches the final steady state given by $c = c_\infty + \varrho(1 - z)$.

We interpret the numerical results using a simplified root length density distribution $l(z)$, i.e., we take

$$l(z) = 1 \quad \text{for} \quad 0 < z < z_0 \quad \text{and} \quad l(z) = 0 \quad \text{for} \quad z_0 < z < 1. \tag{5.33}$$

Initial Reduction

Initially in this system, due to very limited diffusion $\epsilon << 1$, the concentration starts decreasing locally due to the presence of roots in the system, i.e.,

$$\frac{\partial c}{\partial t} = -\frac{2Sc}{1 + c + L + \sqrt{4c + (1 - c + L)^2}}, \tag{5.34}$$

where $L = (\lambda/2)\ln(\alpha t + 1)$ with $\alpha >> 1$. For $L(t) << c_\infty$ (see also Section 5.1.7) this equation simplifies to

$$\frac{\partial c}{\partial t} = -\frac{Sc}{1 + c}. \tag{5.35}$$

The solution to this was found in Section 5.1.7 to be given by the Lambert function, i.e.,

$$c(t) = W_L(c_\infty e^{c_\infty - St}). \tag{5.36}$$

At the timescale proportional to $t \sim c_\infty/S$ the concentration c becomes exponentially small. However, during the transient time $St << 1$ we can approximate the solution in the main rooting region by expanding the Lambert function solution in powers of St (see Figure 5.3), i.e.,

$$\begin{aligned} c(t) &\approx c_\infty - \frac{c_\infty}{1+c_\infty} St + O((St)^2), \\ &\approx c_\infty - St + O((St)^2) \quad \text{for} \quad c_\infty >> 1. \end{aligned} \tag{5.37}$$

Due to the large nutrient application rate ϱ and small diffusion term ϵ there will be a boundary layer near $z = 0$ where the concentration of nutrient has not dropped to an exponentially small level. Changing into the boundary layer stretched variable $z = \sqrt{\epsilon}\xi$ we arrive at the boundary layer equation

$$\frac{\partial c}{\partial t} = \frac{\partial^2 c}{\partial \xi^2} - \frac{Sc}{1+c}, \tag{5.38}$$

with boundary condition

$$-\frac{\partial c}{\partial \xi} = \sqrt{\epsilon}\varrho \quad \text{at} \quad \xi = 0, \tag{5.39}$$

where for nitrate $\sqrt{\epsilon}\varrho \approx 323 >> 1$. Rescaling $c = \hat{\varrho}C$, with $\hat{\varrho} = \sqrt{\epsilon}\varrho$ we get

$$\begin{aligned} \frac{\partial C}{\partial t} &= \frac{\partial^2 C}{\partial \xi^2} - \frac{SC}{1+\hat{\varrho}C}, \\ &= \frac{\partial^2 C}{\partial \xi^2} - \frac{S}{\hat{\varrho}}, \qquad \hat{\varrho} >> 1. \end{aligned} \tag{5.40}$$

We solve this boundary layer equation subject to the following boundary conditions

$$-\frac{\partial C}{\partial \xi} = 1 \quad \text{at} \quad \xi = 0, \tag{5.41}$$

and as $\xi \to \infty$ we want it to be matched to the leading order outer solution in the main rooting region, i.e., from equation (5.37)

$$C \to \frac{c_\infty - St}{\hat{\varrho}} \quad \text{as} \quad \xi \to \infty. \tag{5.42}$$

The boundary layer solution at the leading order is given by (rescaling back to variable z, i.e., $\xi = z/\sqrt{\epsilon}$ and to $c = \hat{\varrho}C$)

$$c = c_\infty - St + \varrho\sqrt{\frac{\epsilon}{\pi t}} e^{-z^2/(4\epsilon t)}. \tag{5.43}$$

There is also another boundary layer near $z = z_0$ which will result in the same boundary layer equation to (5.38) with the boundary layer variable η defined as

$z = z_0 - \sqrt{\epsilon}\eta$. The boundary layer in fact exists on both sides of z_0. To the left of z_0 the boundary layer equation for $c_\infty >> 1$ is

$$\frac{\partial c}{\partial t} = \frac{\partial^2 c}{\partial \eta^2} - S, \tag{5.44}$$

with far-field boundary condition

$$c \to c_\infty - St \quad \text{as} \quad \eta \to \infty. \tag{5.45}$$

The boundary layer equation to the right from z_0 is

$$\frac{\partial c}{\partial t} = \frac{\partial^2 c}{\partial \eta^2}, \tag{5.46}$$

with boundary condition

$$c \to c_\infty \quad \text{as} \quad \eta \to -\infty. \tag{5.47}$$

At z_0, i.e., at $\eta = 0$ the solutions to the right and left have to satisfy the continuity conditions, i.e., the values of c and $\frac{\partial c}{\partial z}$ have to be equal.

The solution to this double boundary layer problem with continuity conditions at $\eta = 0$ can be found using the Laplace transform and it is given by

$$c = \begin{cases} c_\infty - St + \frac{S}{2}\Big[(t + \frac{(z_0-z)^2}{2\epsilon})\text{erfc}(\frac{z_0-z}{2\sqrt{\epsilon t}}) - (z_0 - z)\sqrt{\frac{t}{\pi\epsilon}}e^{-\frac{(z_0-z)^2}{4\epsilon t}}\Big] & \text{for } 0 < z < z_0, \\ c_\infty - \frac{S}{2}\Big[(t + \frac{(z-z_0)^2}{2\epsilon})\text{erfc}(\frac{z-z_0}{2\sqrt{\epsilon t}}) - (z - z_0)\sqrt{\frac{t}{\pi\epsilon}}e^{-\frac{(z-z_0)^2}{4\epsilon t}}\Big] & \text{for } z_0 < z < 1. \end{cases} \tag{5.48}$$

The uniform approximation in region $0 < z < z_0$ can be formed by adding up the boundary layer approximations near $z = 0$ and $z = z_0$ with the main rooting region solution given by Lambert function (equation (5.36)) and subtracting the common part, i.e., subtracting the leading order approximation $c_\infty - St$ twice since there are two boundary layers in the region. Thus, the uniform approximation becomes

$$\begin{aligned} c &= W_L(c_\infty e^{c_\infty - St}) + \varrho\sqrt{\frac{\epsilon}{\pi t}}e^{-z^2/(4\epsilon t)} \\ &+ \frac{S}{2}\Big[(t + \frac{(z_0 - z)^2}{2\epsilon})\text{erfc}(\frac{z_0 - z}{2\sqrt{\epsilon t}}) - (z_0 - z)\sqrt{\frac{t}{\pi\epsilon}}e^{-(z_0-z)^2/(4\epsilon t)}\Big]. \end{aligned} \tag{5.49}$$

The comparison between numerical solution and analytical approximation is shown in Figure 5.9.

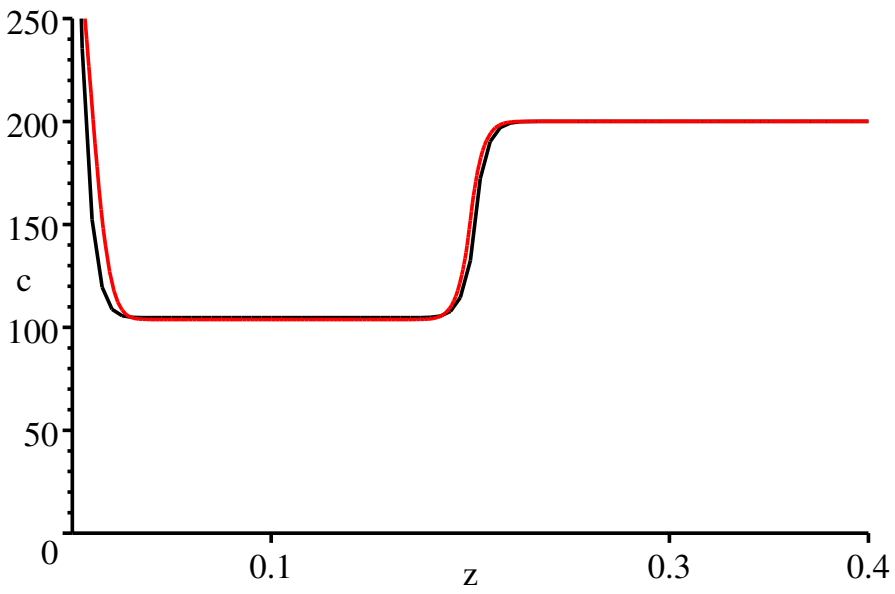

Figure 5.9: Concentration of nitrogen during initial reduction period at time $t = 1$ month. Simplified root length distribution given by $l = 1$ when $0 < z < z_0$, $z_0 = 0.2$ and zero elsewhere. Red line is a approximate solution (5.49), black line is a numerical solution.

Diffusion and "Pseudo-Steady State"

Diffusion will become important once the concentration of nutrients in the main rooting region has dropped to low level such that the uptake term $SF(c,t)$ becomes comparable to the diffusion term. Since the diffusion is slow and the time-dependent term in $F(c,t)$ is also slowly varying in time, i.e., $L(t) = (\lambda/2)\ln(\alpha t + 1)$ gives $\frac{\mathrm{d}L}{\mathrm{d}t} = \frac{\lambda}{2}\frac{\alpha}{\alpha t+1} << 1$ for $t >> \lambda/2$, the rooting region will move into the so called "pseudo-steady state", i.e., to the state that is changing very slowly in time. Hence for the rooting region the concentration has fallen to exponentially low level (Lambert function solution) and therefore the "pseudo-steady state" equation is given for $c << L << 1$

$$0 = \epsilon\frac{\partial^2 c}{\partial z^2} - \frac{Sc}{1+L}, \tag{5.50}$$

where we will treat $L = (\lambda/2)\ln(\alpha t + 1)$ as a constant since it is slowly varying function. This also has a boundary layer behaviour near $z = 0$ and hence changing to $z = \sqrt{\epsilon}\xi$ and $c = \sqrt{\epsilon}C$ we find that the boundary layer equation becomes

$$\frac{\partial^2 C}{\partial \xi^2} = \frac{SC}{1+L} \tag{5.51}$$

with

$$-\frac{\partial C}{\partial \xi} = \varrho \quad \text{at} \quad \xi = 0, \tag{5.52}$$

and

$$C \to 0 \quad \text{as} \quad \xi \to \infty. \tag{5.53}$$

The boundary layer solution is now given by

$$C = \varrho\sqrt{\frac{1+L}{S}}\exp[-\sqrt{\frac{S}{1+L}}\xi]. \tag{5.54}$$

However, for example in the case of nitrate we took $L = 0$ for all times since the diffusional length scale was so large that the local nitrate gradient changes in time were negligible (see Section 5.1.7). Therefore, we approximate the solution by

$$c = \frac{\varrho}{\sqrt{S}}\exp[-\sqrt{S}\xi]. \tag{5.55}$$

Similarly to initial reductions stage, discussed earlier in this section, there is also another boundary layer near $z = z_0$. With boundary layer variable $z = z_0 - \sqrt{\epsilon}\eta$ we get the following solution for $L << 1$

$$c = A\exp[-\sqrt{S}\eta], \tag{5.56}$$

where parameter A needs to be found from patching $z < z_0$ solution to $z > z_0$ solution. However, at large times the diffusion will start influencing the concentration of nutrient in the $z_0 < z < 1$ region. Near $z = z_0$ we write the diffusion equation in terms of η and assume that the diffusion gradient is changing very slowly in time since $\epsilon << 1$. Hence, we need to solve

$$\frac{\partial c}{\partial t} = \frac{\partial^2 c}{\partial \eta^2}, \tag{5.57}$$

subject to continuity conditions across $z = z_0$, i.e., $\eta = 0$ and for $\eta \to -\infty$ $c \to c_\infty$. Similarity solution satisfying the far-field condition is

$$c = c_\infty - B\text{erfc}(-\frac{\eta}{2\sqrt{t}}). \tag{5.58}$$

Parameters A and B are now to be found from continuity conditions at $z = z_0$ and they give that

$$A = \frac{c_\infty}{\sqrt{\pi S t}+1}, \tag{5.59}$$

and

$$B = \frac{c_\infty\sqrt{\pi S t}}{\sqrt{\pi S t}+1}. \tag{5.60}$$

Hence, the solution is now given by

$$c = \varrho\sqrt{\frac{\epsilon}{S}}\exp[-\sqrt{\frac{S}{\epsilon}}z] + \frac{c_\infty}{\sqrt{\pi S t}+1}\exp[-\sqrt{\frac{S}{\epsilon}}(z_0 - z)] \quad \text{for} \quad 0 < z < z_0, \tag{5.61}$$

and

$$c = c_\infty - \frac{c_\infty\sqrt{\pi S t}}{\sqrt{\pi S t}+1}\text{erfc}(\frac{z - z_0}{2\sqrt{\epsilon t}}) \quad \text{for} \quad z_0 < z < 1. \tag{5.62}$$

Steady State

When the time-dependent term $L(t)$ gets much larger than Sc_∞, i.e., $(\lambda/2)\ln(\alpha t + 1) >> Sc_\infty$ the nutrient uptake term approaches zero and the final steady state of this equation is a steady state of the equation

$$\frac{\partial c}{\partial t} = \epsilon \frac{\partial^2 c}{\partial z^2}, \tag{5.63}$$

with

$$c = c_\infty \quad \text{at} \quad z = 1, \quad \text{and} \quad -\frac{\partial c}{\partial z} = \varrho \quad \text{at} \quad z = 0. \tag{5.64}$$

Hence, the steady state is given by

$$c = c_\infty + \varrho(1 - z). \tag{5.65}$$

However, we note that for the current parametrisation, this steady state can only start to develop during the vegetative period of 4 months for calcium, since for calcium $S = 0.012$, $\lambda = 5.5 \times 10^{-3}$, $c_\infty = 2 \times 10^{-4}$ and $\alpha = 83.8$ and therefore $Sc_\infty << \frac{\lambda}{2}\ln(\alpha t + 1)$ for times $t >> 0.01$ months, i.e., $t >> 9$ hours (see Figure 5.10). However, as we see, because of the small diffusion term, it does not have time to develop fully.

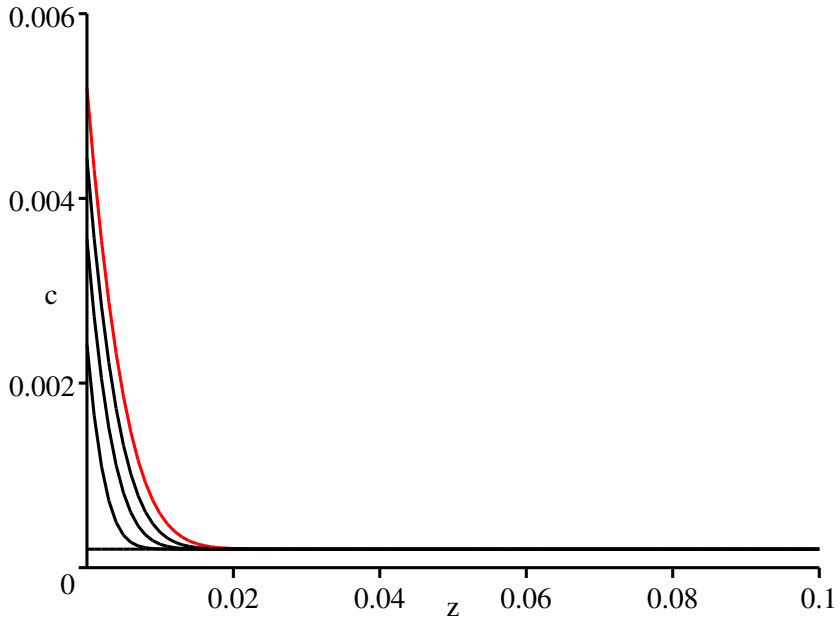

Figure 5.10: Calcium concentration for times equal to $t = 0, 1, 2, 3$ and 4 months for $\varrho = 1$, $c_\infty = 2 \times 10^{-4}$, $\lambda = 5.5 \times 10^{-3}$, $\epsilon = 5.9 \times 10^{-6}$, $\alpha = 83.8$, and $S = 0.012$.

5.2 Time-dependent Fertiliser Application

According to statistics presented in [27] most of the fertiliser is applied in March-April. We can use the data presented in [27] by fitting it to a normal distribution. Dimensionless nitrate application rate that was found in such a way is presented on Figure 5.11.

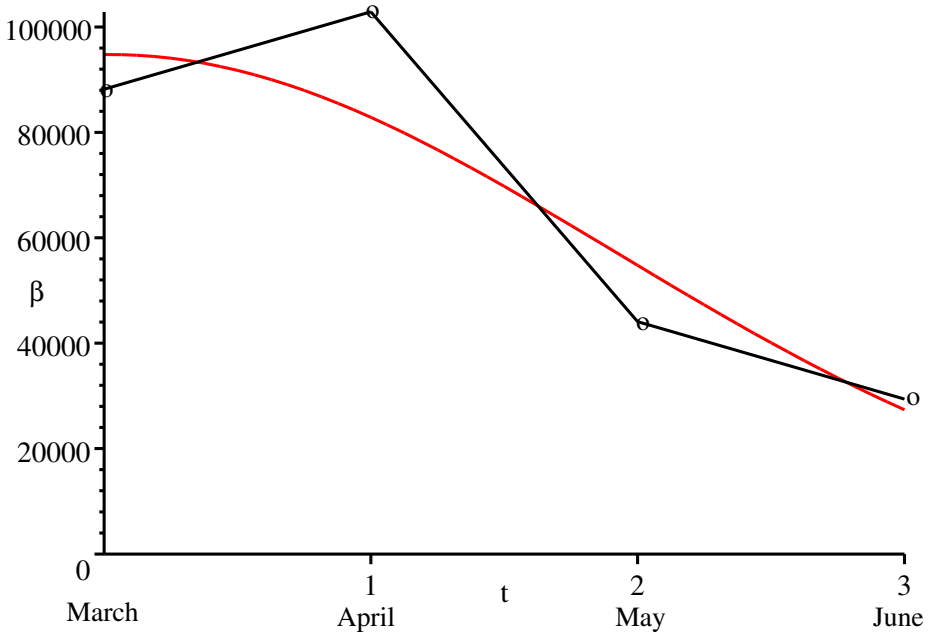

Figure 5.11: Dimensionless time dependent fertiliser application rate ϱ. Black line is data after [27] fitted with normal distribution curve (red line) $\varrho = e^{-.14t^2+0.005t+11}$ using *xMaple* curve-fitting routines.

Numerical experiments conducted with the model together with time-dependent fertiliser application $\varrho = \varrho(t)$ (see Figure 5.12) indicate that the accumulation of the fertiliser at the soil surface has decreased. There is no longer a region near the soil surface where the concentration of nitrate is much larger than in the rest of the soil. This is due to the time-dependent fertiliser application. By having most of the nutrient applied at the beginning of the growth season and decreasing it towards the end, the fertiliser has more time to diffuse into the main rooting region where it gets taken up by the plant. Hence, by adopting time-dependent fertiliser application we can maximise the fertiliser taken up by the root system, therefore decreasing the risk of fertiliser runoff and pollution.

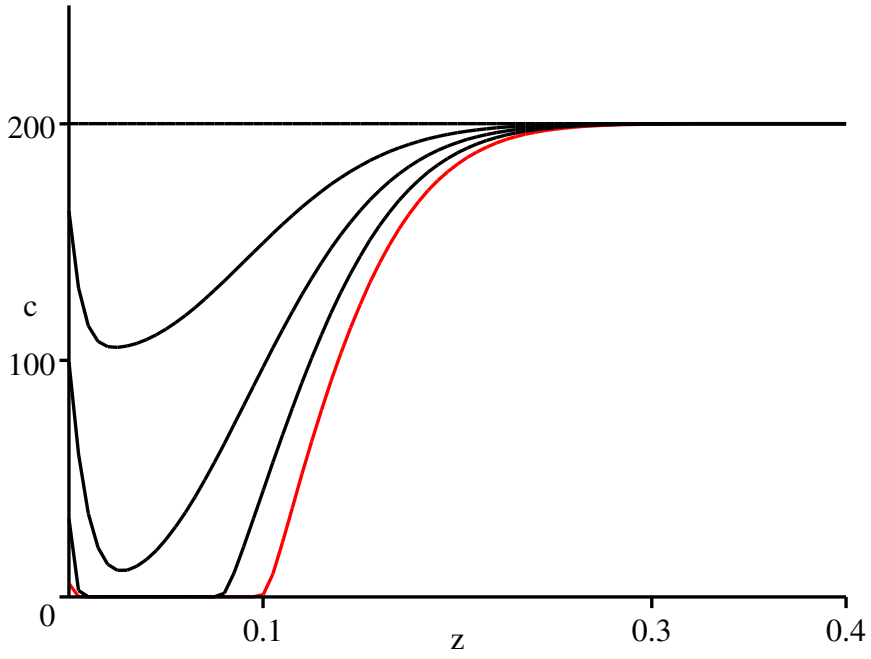

Figure 5.12: Concentration profile of nitrate in the soil calculated using time dependent fertiliser application (see Figure 5.11). Time $t = 0, 1, 2, 3$ and 4 months. Red line presenting $t = 4$ months.

5.3 Concluding Remarks

In this chapter we have demonstrated how to calculate the nutrient uptake by a root system that can be considered as a space averaged distribution. We found that in most cases the diffusion of nutrient ions within the soil was very small compared to the uptake. However, the uptake term strongly depends on the buffer power of the soil. We can conclude that the uptake of nutrient ions is limited by their release from the solid particles, i.e., buffer power.

In the case of phosphorus the uptake is limited by both its buffer power being large and by its low levels in the soil. It was found that the concentration of phosphorus does not change very much in the soil due to uptake by plants. One way of raising the uptake is to fertilise with the hope of raising the overall level of phosphorus in the soil. However, as it can be seen on Figures 5.5 and 5.7, due to limited diffusion and in the absence of water flow from the top of the soil to the bottom, the phosphorus fertiliser accumulates in a very thin region on the top of the soil. Hence, diffusion is not sufficient to carry the fertiliser to the roots. Water flow is needed to effectively move the fertiliser from the top layer to lower layers of the soil. This is probably why it is advantageous to fertilise crops in March and April which are before the main growing season. Other possible way of increasing the capture of nutrient, for example

phosphate, by plant roots is to place the fertiliser during the ploughing to the deeper layers in the soil [129].

In the case of nitrate it was found that its uptake is limited by the large requirements. The nitrate in the rooting zone was depleted to very low levels from its initial value very rapidly (see Figure 5.7). Again, one way of dealing with this would be to add fertiliser, however, the vertical water movement is again needed for effective transport of fertiliser to the rooting zone. An alternative strategy would be to include crop cycling, so that for roots with varying rooting depths, the regions that were previously heavily depleted can recover while the other regions are being depleted.

Overall, the results presented in this chapter strongly indicate that water movement plays an important part in the transport of fertiliser from the top of the soil to the roots. Diffusion is not sufficient to do that since due to a slow diffusion the fertiliser will start accumulating in the top layers of the soil. This is why farmers apply almost half of the yearly fertiliser during March and April [27]. During this period the rainfall is quite high, hence providing the effective transport of nutrients into the rooting region.

A model including water movement together with nutrient uptake will be presented in the Chapter 7-9.

Chapter 6

Root Competition in Developing Root Systems

In the previous chapter we demonstrated how to calculate the nutrient uptake by time-independent root distributions. This corresponds to the case when the roots have grown to their maximum extent or are growing extremely slowly, i.e., trees and perennial plants. However, as discussed in Chapter 4, roots of agriculturally important plants, such as maize and beans, grow reasonably fast during the whole vegetative period. This motivates us to develop a model that takes account of spatial root distribution development and nutrient uptake.

6.1 Developing Root Distribution

Several authors have tried to tackle the modelling of developing root system by considering the root system to be a length density of roots diffusing through the soil. Acock and Pachepsky [2] developed such a model for the development of the root system in the soil by considering two sub-populations, young and old roots. They considered the mass of young roots to be diffusing radially outwards and at the same time changing from young roots to old roots. Old roots were considered to be stationary, i.e., not diffusing outwards. The aim was to compare the experimental measurements of chrysanthemum plant root density profiles to calculated root density profiles. This was achieved with a reasonable degree of accuracy. The same group of authors has also developed more general soil simulator programs for use in agriculture. However, all this work relies heavily on large scale numerical computations making it less transparent for spotting the mechanisms controlling the behaviour of the system.

Pagès et al. have conducted three dimensional simulations of root development for maize [49], [97], [98], [100], [101]. For example in [49] they calculate root length density profiles using a 3 dimensional branching model. It can be concluded from

their work that a discrete branching structure can be modelled by a continuous space distribution.

In this chapter we will first develop a framework for the spatial root density distribution development based on a simple set of basic branching rules first discussed in Chapter 4. We then extend this theory to include the nutrient uptake by the developing branching structure assuming that along each individual root the uptake parameters, F_m and K_m, are the same. However, as will be seen later, even under these simple assumptions variations in the nutrient uptake along each root can occur.

6.2 Spatial Root Density Development

In Chapter 4 we discussed the root size density function describing the number of roots of a given length at a given time. In that chapter we neglected the spatial distribution of the roots. In this section we aim to derive the time-dependent spatial distribution development using the same parametrisation (see Figure 4.3 and Table 4.1).

6.2.1 Zero Order Root Distribution

In Chapter 4 we considered the rate of elongation $\frac{dl_i}{dt}$ [cm s^{-1}] of i-th order roots to be given by

$$\frac{dl_i}{dt} = r_i e^{-r_i t/K_i} \quad \text{or} \quad \text{alternatively} \quad \frac{dl_i}{dt} = r_i(1 - \frac{l_i}{K_i}), \tag{6.1}$$

where t is the time measured from the creation of the root. Hence, the length, l_0, of the zero order root created at time $t = 0$ is given by

$$l_0(t) = K_0(1 - e^{-r_0 t/K_0}). \tag{6.2}$$

If we suppose that there are n_0 zero order roots emerging at the same time from the seed and growing radially into the soil, then in each hemispherical shell $(r, r + dr)$ the length of zero order roots is proportional to $n_0 dr$, and hence the length density distribution (cm of root per cm^3 of soil) is given by

$$l_{d,0}(r) = \frac{n_0 dr}{dV} = \frac{n_0 dr}{2\pi r^2 dr} = \frac{n_0}{2\pi r^2} \quad \text{for} \quad r \leq K_0(1 - e^{-r_0 t/K_0}). \tag{6.3}$$

Similarly, the volume, $\phi_0(r, t)$, and surface area, $S_0(r, t)$, of zero order roots per unit volume of soil, as a function of radial coordinate r are given by

$$\phi_0 = \frac{n_0 a_0^2}{2r^2}, \quad S_0 = \frac{n_0 a_0}{r^2} \quad \text{for} \quad r \leq K_0(1 - e^{-r_0 t/K_0}), \tag{6.4}$$

where a_0 is the radius of the zero order root.

6.2.2 First Order Root Distribution

In Chapter 4 the first order roots were considered to be branching out from a discrete set of branching points along the zero order roots. These first order roots grow at an angle β in relation to the zero order roots. Thus, the overall length of each first order root in hemispherical shell $(r, r + dr)$ is proportional to $dr/\cos\beta$.

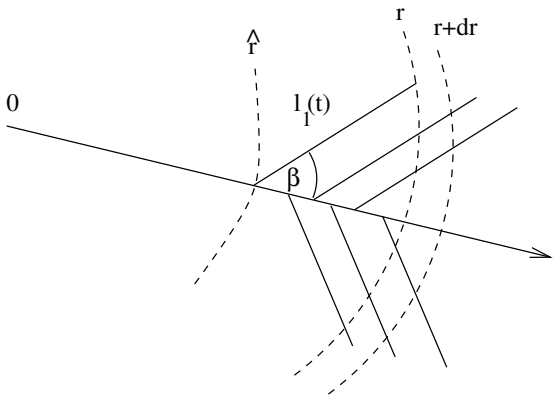

Figure 6.1: Branching of first order roots. Interval $(\hat{r}, r)$ from where roots reach the shell at r.

The first order root created at a radial position r' has a length

$$l_1(r', t) = K_1(1 - e^{-r_1(t-\tau(r'))/K_1}), \tag{6.5}$$

where τ is the time of its creation at the branch-point $r = r'$. The time-delay τ can be calculated from the equation (6.2), since a zero order root will develop a branch at r' if its length is larger than r' by the amount equal to the apical non-branching zone $l_{a,0}$, i.e., $l_0 = r' + l_{a,0}$. Hence, from equation (6.2) we deduce that

$$\tau(r') = -\frac{K_0}{r_0}\ln(1 - \frac{r' + l_{a,0}}{K_0}), \tag{6.6}$$

and thus the length of a first order root branching out from r' will be given by

$$l_1(r', t) = \begin{cases} K_1(1 - e^{-r_1 t/K_1}(1 - \frac{r'+l_{a,0}}{K_0})^{-\frac{r_1 K_0}{r_0 K_1}}) & \text{for} \quad t \geq \tau(r'), \\ 0 & \text{for} \quad t < \tau(r'). \end{cases} \tag{6.7}$$

Using basic geometry we find that the tip of the root created at r' is at a distance $r' + l_1(r', t)\cos\beta$ from the origin, i.e., from the seed. If the position of the root tip is known, then we can also calculate the inverse problem, i.e., from which given branching distance $\hat{r}$ do roots reach r (see Figure 6.1). That implies that $\hat{r}$ is defined as the solution of

$$r = \hat{r} + \cos\beta K_1(1 - e^{-r_1 t/K_1}(1 - \frac{\hat{r} + l_{a,0}}{K_0})^{-\frac{r_1 K_0}{r_0 K_1}}) \quad \text{for} \quad t \geq \tau(\hat{r}). \tag{6.8}$$

Hence, the overall number of first order roots in the shell $(r, r+dr)$ is proportional to

$$n_1(r,t) = n_0 \int_{\hat{r}}^{r} \psi_1(r')\, dr', \tag{6.9}$$

where $\psi_1(r)$ is the distribution of the first order root branching points on one zero order root (number of branches per unit length) and n_0 is the number of zero order roots.

We can take the distribution of branching points to be either discrete or continuous. For the discrete set of branching points $\psi_1(r) = \sum_i \delta(r - r_i)$, with $r_i = l_{b,0} + i l_{n,0}$, where $l_{b,0}$ is the length of zero order root basal non-branching zone, and $l_{n,0}$ is the inter-branch distance[1]. Some of the measurements of root branching density indicate that there are more sub-branches per cm of root length near the base of the root than near the tip [100], [98], [101]. However, for simplicity we will use in this chapter a piecewise continuous distribution as used by Pagés et al. [97] and take the branching points to be distributed uniformly in the branching zone, i.e., we take $\psi_1(r) = 1/l_{n,0}$ for $l_{b,0} < r < l_0(t) - l_{a,0}$, and $\psi_1(r) = 0$ for $0 < r < l_{b,0}$ and $r > l_0(t) - l_{a,0}$, where $l_0(t)$ is the length of zero order root at time t given by equation (6.2) and $l_{n,0}$ is the inter-branch distance. Thus the length density of first order roots is given by

$$l_{d,1}(r,t) = \frac{n_1(r,t)dr/\cos\beta}{dV} = \frac{n_1(r,t)}{2\pi r^2 \cos\beta} = \frac{n_0 \int_{\hat{r}}^{r} \psi_1(r')\, dr'}{2\pi r^2 \cos\beta}, \tag{6.10}$$

where $dV = 2\pi r^2 dr$ is the hemispherical volume element at position r and n_0 is the number of zero order roots. The comparison between the discrete and piece-wise continuous distribution is shown in Figure 6.2 for the branching angle[2] $\beta = \pi/3$.

Second Order Branches

The structure of the length density distribution of the second order branches is clearly far more complex than that of the first order branches. However, we notice from the nutrient uptake calculations presented in Chapter 4 that in the absence of competition between the roots (see Figure 4.9) the uptake by the second order branches was very small. Competition is expected to cause the uptake to decrease even further.

The reason why the contribution from second order branches is so small is that their radius and length is very small and they are very far apart from each other. The typical length of a second order root is ≈ 0.2 cm, i.e., 2 mm, and radius $\approx 10^{-2}$

[1] δ is the Dirac's delta function.

[2] Here on Figure 6.2 we have approximated $\hat{r}$ using a binomial expansion since $(\hat{r} + l_{a,0})/K_0 < 1$. Hence we find that the first-order approximation to $\hat{r}$ is given by $\hat{r} = r - \frac{K_1 \cos\beta[1 - e^{-r_1 t/K_1}(1 + \frac{r_1(r+l_{a,0})}{r_0 K_1})]}{1 - \cos\beta e^{-r_1 t/K_1} \frac{r_1}{r_0}}$ for $t \geq t_0 = -\frac{K_0}{r_0} \ln(1 - \frac{\hat{r} + l_{a,0}}{K_0})$.

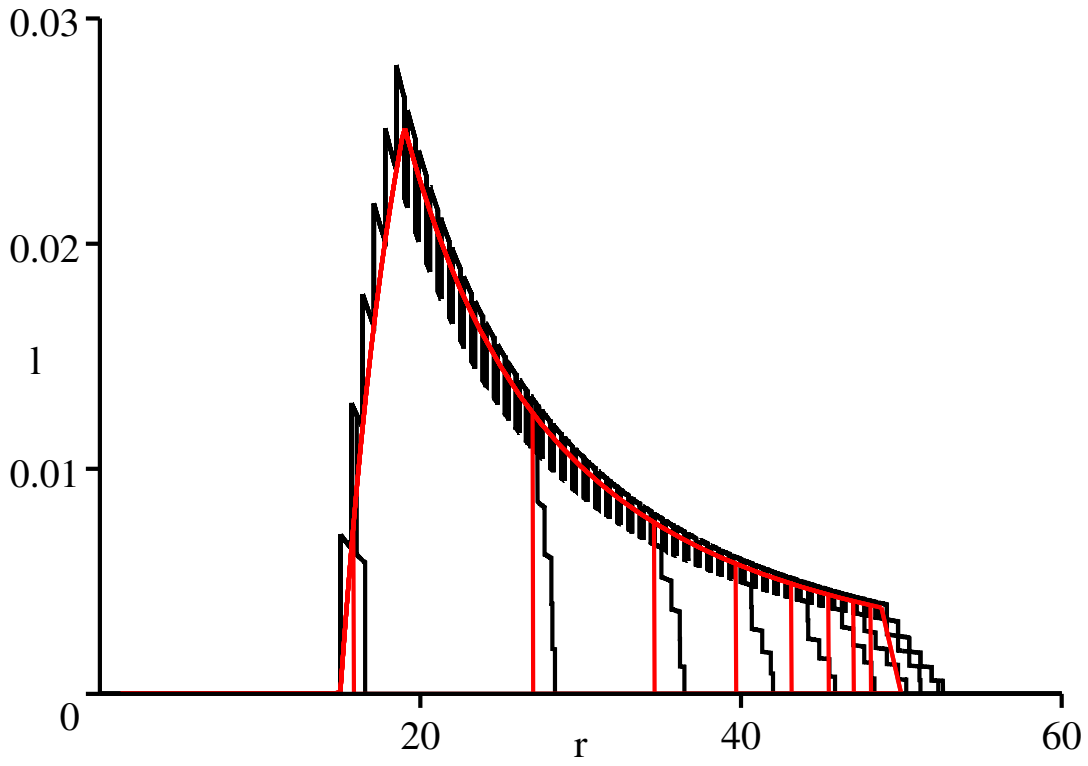

Figure 6.2: Length density distribution (cm of roots per cm^3 of the soil) of first order roots with branching angle $\beta = \pi/3$ for times t = 10, 20, 30, 40, 50, 60, 70, 80, 90 and 100 days. Red lines are the piecewise continuous distribution of branching points and black lines are from a fully discrete set of branching points. Growth coefficients are the same as presented in Chapter 4 Table 4.1 except we have taken the width of apical and basal non-branching zones equal to 15 cm for the purposes of clarity of this Figure.

cm. The average length of the root hairs is of order 1 mm, radius is 10^{-3} cm, and distance 10^{-2} cm. The average root hair radius is 10^{-2} cm, length 1 mm and density 500-2000 root hairs per cm of root length, i.e., the average distance between them is of order 10^{-2} cm. Hence, second order roots are very similar to root hairs except that their radius is larger and their density is lower. However, the relative distances, i.e., distance compared to radius, between the root hairs and between second order roots is approximately same, i.e., order 10.

Second Order Roots in Comparison to Root Hairs

The similarity of root hairs and second order roots causes us to ask the question: why do plants have second order roots? One explanation would be that they provide more efficient nutrient transportation within themselves since, as opposed to unicellular root hairs, 2nd order roots contain xylem and phloem, thus providing a better

transport for nutrients inside the root system. Another explanation would be that 2nd order roots produce mucilage. Mucilage is a gelatinous material that is thought to be excreted mostly by the growing root tip which might have a positive effect on nutrient uptake and provide the environment for plant friendly bacteria to grow in. It can also protect the root apical zones from desiccation [80] which is important for the roots to be long lasting.

A third explanation would be to do with the fact that root hairs are usually very short lived, with average age being approximately 1 week [57]. It is also found that old epidermial cells do not develop root hairs. Hence, second order roots may gain importance over root hairs because of their relatively longer lifetime.

As discussed earlier, there are approximately 1000 root hairs per cm of second order root length. Each root hair is 1 mm long with radius 10^{-3} cm and the lifetime of each root hair is 1 week. During a 4 week period the plant has to allocate resources (mainly carbon) for creation of 1.26×10^{-3} cm^3 of root tissue per cm of first order root length towards root hairs. However, for second order roots with radius 10^{-2} cm, length 0.2 cm and inter-nodal distance 0.7 cm, the plant has to create during the same period only 8.4×10^{-5} cm^3 of root tissue. Hence, in comparison to root hairs, second order roots are relatively cheap to produce. However, they take up much less nutrients than root hairs, since their density is lower.

Using the simplistic calculation we find that root hairs extend the root surface area by approximately 600%, while second order roots extend the surface area of first order roots approximately by 5%. In Chapter 3 we found that reasonably good approximation to the nutrient uptake by roots with root hairs was given by the use of so called "effective root radius". We discuss this concept in more detail.

Effective root radius is the radius that corresponds to the radius of the cylinder which has the same surface area as a root with root hairs, i.e., $\bar{a}_{\text{hair}} = a + a_h nl$ where $a = 0.02$ cm is a root radius, $a_h = 10^{-3}$ cm is root hair radius, $l = 0.1$ cm is a root hair length, and $n = 1000$ is the number of root hairs per cm of root length. Hence, the effective root radius is $\bar{a}_{\text{hair}} = 0.12$ cm. The increase in root surface area is 6 times, but the root volume increases only 1.25 times.

The effective first order root radius is $\bar{a}_1 = a_1 + a_2 K_2 / l_{n,1}$, where a_1 is the radius of first order root, a_2 is the radius of the second order root, K_2 is the maximum length of the second order branch[3], and $l_{n,1}$ is the inter-nodal distance. For the second order root with maximum length $K_2 = 0.2$ cm, radius $a_2 = 0.01$ cm and internodal distance $l_{n,1} = 0.7$ cm we find that the effective first order root radius is $\bar{a}_1 \approx 0.021$. Thus the root surface area increases 1.05 times and volume increases 1.07 times.

[3]Second order roots are thought to achieve their maximum length in less than one day.

We can now construct the cost function which measures the benefits, i.e., increase in the nutrient flux proportional to root surface area increase, over 1 month period against the resources allocated over the same period, i.e., we take the cost function M to be given by

$$M = \frac{N}{C}, \tag{6.11}$$

where N is the increase in nutrient uptake, and C is the corresponding resource investment. For root hairs we have taken the nutrient uptake to be proportional to the effective root surface area, i.e., $N = 2\pi\bar{a}_{\text{hair}} = 0.75$ cm^2, and the resource an investment to be equal to the volume of root hairs created over 1 month plus the volume of the root, i.e., $C = \pi a^2 + g\pi a_h^2 ln = 2.5 \times 10^{-3}$ cm^3, where $g = 4$ shows the number of root hair generations being generated during one month, i.e., $g = 4$ corresponds to the root hair lifetime of approximately 1 week. Hence the root hair cost function M becomes $M = 300$. By the same calculation, second order lateral cost function is $M = 100$ with $N = 0.13$ cm^2 and $C = 1.3 \times 10^{-3}$ cm^3. Thus, according to our analysis, the root hairs are approximately 3 times more beneficial to the plant than second order lateral roots.

This analysis is conducted using the assumption that the mechanism of nutrient uptake by second order lateral roots and root hairs is the same. However, this assumption might not hold since root hairs are unicellular root surface cell extensions, but the second order lateral roots are more complicated multicellular formations. Therefore the second order laterals might be more effective in taking up nutrients than root hairs. The root hair length density is thought to vary depending on the nutritional status of a plant. Hofer [57] reports that the density can vary from 500 to 2000 root hairs per centimetre of root length depending on the phosphorus concentration in the soil (less phosphorus more root hairs and *vice versa*). The number of root hair generations g_c in one month that makes the root hair cost function equal to the second order lateral root cost function is given by

$$g_c = \frac{1}{a_h^2 ln}\Big(\frac{(2a_1 + 2a_h ln)(a_1^2 + a_2^2 K_2/l_{n,1})}{a_1 + a_2 K_2 1/l_{n,1}}\Big). \tag{6.12}$$

Hence for the parametrisation presented earlier the number of root hair generations during one month has to be larger or equal to 19 for the cost of root hairs to be larger or equal to second order lateral roots. $g = 19$ implies that the lifetime of one root hair generation is approximately 1.6 days. According to [57] this situation is possible. Therefore more research into the root hair lifetime correlation with its density needs to be conducted for further analysis of root hair importance. More experimental investigation on the rates of nutrient uptake by root hairs and roots of similar morphological properties is also needed.

6.2.3 Model for Nutrient Uptake by Spatial and Time Dependent Root Distribution

The model for nutrient uptake by a developing root system including roots of different orders, radii and lengths is essentially the same as the one given for the static root distribution in Chapter 5 by the equation (5.2). However, the nutrient uptake term is modified to include the roots of different order, i.e., the model is given by

$$(b+\phi_l)\frac{\partial c_l}{\partial t} + \nabla\cdot(c_l\mathbf{u}) = \nabla\cdot(D\phi_l\nabla c_l) - \sum_i F_i \quad \text{inside} \quad \partial R \tag{6.13}$$

where ∂R is the boundary of the domain of the soil with roots, and F_i is the nutrient uptake by i-th order roots per unit volume of soil.

6.2.3.1 Nutrient Uptake by Different Orders

Nutrient Uptake by Zero Order Roots

In Chapter 2 we found the expression for nutrient uptake per unit root surface area [μmol cm^{-2} s^{-1}] by a cylindrical root as a function of time, where time was measured from the start of the nutrient uptake. Zero order roots reach the radial position r at time t_0 given by

$$t_0 = -\frac{K_0}{r_0}\ln(1-\frac{r}{K_0}), \tag{6.14}$$

i.e., zero order roots take up nutrients from radial position r after time t_0.

We have shown that the surface area of zero order roots [cm^{2}cm^{-3}] is given by

$$S_0 = 2\pi a_0 l_{d,0}(r) = \frac{2\pi a_0 dr}{dV} = \frac{a_0 n_0}{r^2}, \tag{6.15}$$

where a_0 is the radius of zero order roots, and $l_{d,0}$ the length of zero order roots per unit volume of soil given by equation (6.3). Therefore we take the nutrient uptake by zero order roots per unit volume of soil [μmol cm^{-3}s^{-1}] to be given by

$$F_0 = \frac{a_0 n_0}{r^2}\times\frac{2F_m c_l/K_m}{1+c_l/K_m+L_0(t-t_0)+\sqrt{4c_l/K_m+(1-c_l/K_m+L_0(t-t_0))^2}}, \tag{6.16}$$

where $L_0 = (\lambda_0/2)\ln[\alpha_0(t-t_0)+1]$ with $\alpha_0 = 4e^{-\gamma}D\phi_l/[a_0^2(\phi_l+b)]$, and the spatial time-delay $t_0 = t_0(r)$ is given by equation (6.14). By including the time-delay t_0 in the nutrient uptake term above, we have introduced the non-uniform uptake of nutrients along the root. For the initial uniform soil nutrient concentration the growing root tip is always taking up more nutrient than the base, because the tip is continuously growing into the relatively undepleted soil.

Nutrient Uptake by First Order Roots

As in the case of zero order roots, the first order roots reach position r at time t_1. However, t_1 will be different for first order roots which branch from the zero order roots at different branching points r', i.e., $t_1 = t_1(r, r')$. The total time t_1 when the first order root branching out from r' at an angle β reaches position r is given by

$$t_1(r, r') = -\frac{K_0}{r_0}\ln(1 - \frac{r' + l_{a,0}}{K_0}) - \frac{K_1}{r_1}\ln(1 - \frac{r - r'}{K_1\cos\beta}). \tag{6.17}$$

Following the same reasoning as for the zero order roots, we find that for a root at radial position r the nutrient uptake f_1 per unit root surface area is given by

$$f_1 = \frac{2F_m c_l/K_m}{1 + c_l/K_m + L_1(t - t_1) + \sqrt{4c_l/K_m + (1 - c_l/K_m + L_1(t - t_1))^2}}, \tag{6.18}$$

where $L_1(t - t_1) = (\lambda_1/2)\ln[\alpha_1(t - t_1) + 1]$ and $\alpha_1 = 4e^{-\gamma}D\phi_l/[a_1^2(\phi_l + b)]$.

As found in Section 6.2, the roots grow into an interval $(r, r + dr)$ only from the branch-point interval $(\hat{r}, r)$, where $\hat{r}$ is given by equation (6.8) (see also Figure 6.1). Hence for each zero order root that develops branches, the cumulative uptake by all of those branches in the shell $(r, r + dr)$ is

$$2\pi a_1 \frac{dr}{\cos\beta}\int_{\hat{r}}^{r} f_1(r, t; r')\psi_1(r')\,dr', \tag{6.19}$$

where ψ_1 is the distribution of first order root branch points on zero order roots, i.e., $\psi_1(r)dr$ is the number of branching points in the interval $(r, r + dr)$. The total number of first order branch points is $\int_0^\infty \psi_1(r)\,dr$. Hence, the nutrient uptake by all first order roots per unit volume of soil at radius r is

$$F_1 = n_0\frac{2\pi a_1\frac{dr}{\cos\beta}\int_{\hat{r}}^{r} f_1(r, t; r')\psi_1(r')\,dr'}{dV} = n_0\frac{a_1\int_{\hat{r}}^{r} f_1(r, t; r')\psi_1(r')\,dr'}{r^2\cos\beta}, \tag{6.20}$$

where $dV = 2\pi r^2 dr$ defines the hemispherical volume element at r and n_0 is the number of zero order roots.

Non-dimensionalisation

We choose the same non-dimensional scaling as given by (5.5) in Chapter 5, i.e., we take

$$\mathbf{r} = K_0\mathbf{r}^*, \quad t = [t]t^*, \quad c_l = K_m c^*, \tag{6.21}$$

where K_0 is the maximum length of the zero order root[4], and $[t]$ is the time-scale, typically 1 month$\approx 2.5 \times 10^6$ seconds. Hence, we get the following dimensionless

[4]The zero order root is the longest root in the system.

equation

$$\frac{\partial c}{\partial t} + \epsilon Pe \nabla \cdot (\mathbf{u}c) = \epsilon \nabla^2 c - \sum_i S_i F_i(r,t;c), \tag{6.22}$$

where

$$\epsilon = \frac{\phi_l D[t]}{K_0^2(b+\phi_l)}. \tag{6.23}$$

S_iF_i is the dimensionless uptake of nutrient by i-th order roots per unit volume of soil. The dimensionless nutrient uptake by zero order roots is given by

$$F_0(r,t;c) = \frac{1}{r^2} \cdot \frac{2c}{1+c+L_0(r,t)+\sqrt{4c+(1-c+L_0(r,t))^2}}, \tag{6.24}$$

where

$$L_0(r,t) = \frac{\lambda_0}{2} \ln\Big[\alpha_0 t + 1 + \alpha_{00}\ln(1-r)\Big]. \tag{6.25}$$

The dimensionless coefficients S_0, α_0 and α_{00} are given by

$$S_0 = \frac{a_0 n_0 F_m[t]}{K_0^2 K_m(b+\phi_l)}, \quad \alpha_0 = 4e^{-\gamma}\frac{D\phi_l[t]}{a_0^2(\phi_l+b)}, \quad \alpha_{00} = 4e^{-\gamma}\frac{D\phi_l}{a_0^2(\phi_l+b)}\frac{K_0}{r_0}, \tag{6.26}$$

where a_0 is the radius of the zero order root, n_0 is the total number of zero order roots, K_0 is the maximum length of the zero order root, and r_0 is the rate of growth of zero order root, other coefficients D, ϕ_l etc. as before in previous chapters.

The dimensionless first order nutrient uptake is given by

$$F_1 = \frac{1}{r^2}\int_{\hat{r}}^{r} \frac{2c\psi_1(r')\,dr'}{1+c+L_1(r,t;r')+\sqrt{4c+(1-c+L_1(r,t;r'))^2}}, \tag{6.27}$$

with $L_1(r,t;r')$ defined by

$$L_1(r,t;r') = \frac{\lambda_1}{2}\ln\Big[\alpha_1 t + 1 + \alpha_{11}\ln(1-r'-l_{a,0}) + \alpha_{111}\ln(1-\frac{(r-r')}{K_1\cos\beta})\Big]. \tag{6.28}$$

The parameters S_1, α_1, α_{11}, and α_{111} are given by

$$\begin{aligned} S_1 &= \frac{n_0 a_1 F_m[t]}{l_{n,0}K_0\cos\beta(b+\phi_l)K_m}, \quad \alpha_1 = \frac{4e^{-\gamma}D\phi_l[t]}{a_1^2(\phi_l+b)}, \\ \alpha_{11} &= \frac{4e^{-\gamma}D\phi_l}{a_1^2(\phi_l+b)}\frac{K_0}{r_0}, \quad \alpha_{111} = \frac{4e^{-\gamma}D\phi_l}{a_1^2(\phi_l+b)}\frac{K_1}{r_1}. \end{aligned} \tag{6.29}$$

The dimensionless first order root branch point distribution ψ_1 is given by[5]

$$\psi_1 = 1 \quad \text{for} \quad l_{b,0} < r' < l_0(t) - l_{a,0}, \quad \text{and} \quad \psi_1 = 0 \quad \text{elsewhere.} \tag{6.30}$$

[5]Notice that we have absorbed the distribution parameter $l_{n,0}$, distance between branches, into the coefficient S_1.

$Pe = K_0[u]/D$ is the Péclet number. It is approximately the same as found in Section 5.1.3 for the static root distribution and it can range from $O(10)$ to $O(10^{-5})$ depending on the root density. However, this value is calculated using the maximum possible length of the root system K_0, i.e., the maximum length of the zero order roots. We know that in the developing root system the length of the longest root is always less than or equal to K_0. Hence, the Péclet number calculated based on length scale K_0 is an upper bound. In this chapter, as in the previous one, we will only deal with the case when $Pe << 1$ since when the Péclet number is large we are likely to have large moisture gradients in the soil. Models considering water movement and uptake are presented in the following Chapters 7-8. The model for simultaneous water movement and nutrient uptake is presented in Chapter 9.

For a hemispherical root system the root system boundary ∂R is at $r = 1 - e^{-\nu t}$, where $\nu = r_0[t]/K_0$. The parameter r_0 is the maximum growth rate of zero order root and K_0 is the maximum length of the zero order root[6]. The dimensionless diffusion equation, i.e., neglecting $Pe << 1$ terms, in spherical symmetry becomes

$$\frac{\partial c}{\partial t} = \epsilon \frac{1}{r^2}\frac{\partial}{\partial r}(r^2 \frac{\partial c}{\partial r}) - \sum_i S_i F_i(r, t; c) \quad \text{for} \quad r \leq r_B = 1 - e^{-\nu t}, \tag{6.31}$$

and

$$\frac{\partial c}{\partial t} = \epsilon \frac{1}{r^2}\frac{\partial}{\partial r}(r^2 \frac{\partial c}{\partial r}) \quad \text{for} \quad r > r_B = 1 - e^{-\nu t}. \tag{6.32}$$

For the boundary conditions, we prescribe a constant nutrient concentration far away from the root system, i.e.,

$$c \to c_\infty \quad \text{as} \quad r \to \infty. \tag{6.33}$$

We need the concentration to be continuous at the root system boundary $r_B = 1 - e^{-\nu t}$, i.e.,

$$\Big[c\Big]_-^+ = 0 \quad \text{at} \quad r = r_B = 1 - e^{-\nu t}. \tag{6.34}$$

At the inner boundary of the root system, i.e., near the seed of the plant the flux of nutrients is zero which implies that the seed is not taking up nutrients. Hence we take

$$r^2 \frac{\partial c}{\partial r} \to 0 \quad \text{as} \quad r \to 0. \tag{6.35}$$

[6]The total dimensional growth rate of zero order root is given by $dl_0/dt = r_0(1 - l/K_0)$, where r_0 is the maximum growth rate, l_0 is the length of zero order and K_0 is the maximum length of the zero order.

Parameter Estimation

The values of dimensionless parameters for the different orders of roots are presented in Table 6.1. Values of ϵ for different nutrients are the same as presented in Table 5.1, the time-delay parameters α_i, α_{ii} and α_{iii} are shown in Table 6.2. Other dimensionless parameters are the same for all nutrients, i.e., the zero order root elongation parameter is $\nu = r_0[t]/K_0 \approx 1.2$ for $[t] = 30$ days, the length of apical non-branching zone of zero order root is $l_{a,0} \approx 0.3$, first order time-delay parameter is $1/(K_1 \cos\beta) \approx 7.21$, and the length of basal non-branching zone is $l_{b,0}/K_0 \approx 0.014$.

Parameter	ϵ	c_∞	λ_0	λ_1	S_0	S_1
N	7.15×10^{-4}	200	22	8.8	0.08	4.56
K	2.4×10^{-5}	3.28	117.5	47	0.014	0.81
S	4×10^{-4}	10	1.65	0.66	0.0034	0.19
P	3.9×10^{-6}	0.5	30.8	12.32	6.1×10^{-4}	0.035
Mg	6.2×10^{-4}	6.7×10^{-3}	1.375	0.55	4.6×10^{-3}	0.253
Ca	5.9×10^{-6}	2×10^{-4}	0.014	5.5×10^{-3}	4.16×10^{-7}	2.37×10^{-5}

Table 6.1: Values of dimensionless parameters for root radii $a_0 = 0.05$ cm and $a_1 = 0.02$ cm. Subindex i describes the order of the roots this parameter belongs to. The branching angle is taken to be $\beta = \pi/3$, number of first order roots is $n_0 = 5$ and time-scale $[t] = 30$ days.

Nutrient	α_0	α_{00}	α_1	α_{11}	α_{111}
N	1612	1343	10075	8395	420
K	53.2	44.43	333	277	13.89
S	911	759	5694	4745	237.2
P	8.757	7.297	54.73	45.6	2.28
Mg	1397	1164	8731	7276	363.82
Ca	13.4	11.173	83.8	69.83	3.49

Table 6.2: Parameters for time-delay $t_i(r)$. Subindex i describes the order of the roots this parameter belongs to in equations (6.25) and (6.28).

6.2.4 Numerical Solution

To solve those equations numerically we have used a fully implicit finite difference scheme, similar to the one used in previous chapters, taking into account the spherical symmetry and mass conservation [87]. The resulting system of algebraic equations was solved using the Thomas algorithm [87]. The non-linearity of the uptake terms F_i was dealt with by having a separate iteration loop inside the main finite difference loop.

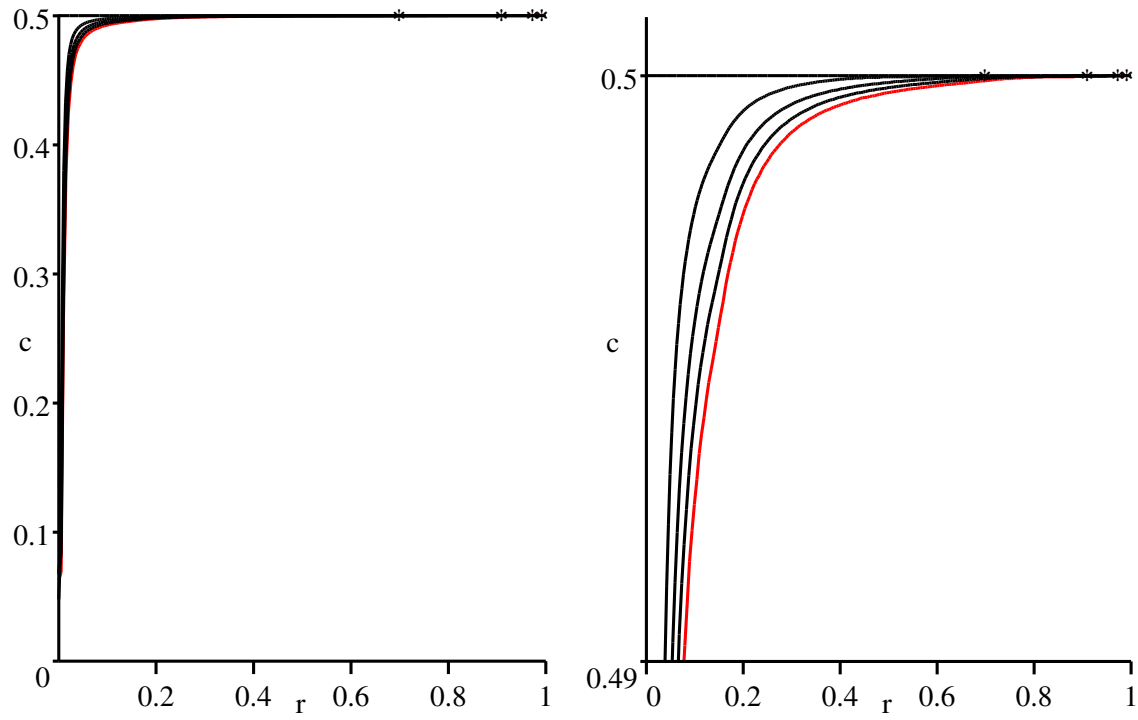

Figure 6.3: Phosphorus concentration for times $t = 0, 1, 2, 3, 4$ months. $*$ shows the position of the zero order root tip.

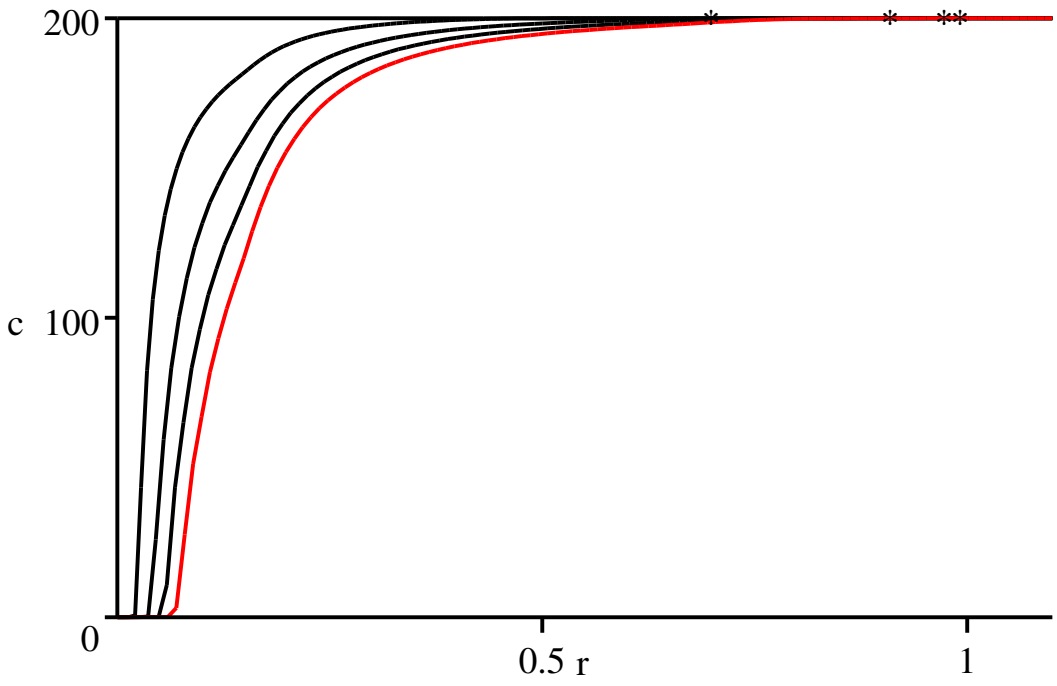

Figure 6.4: Nitrogen concentration for times $t = 0, 1, 2, 3, 4$ months. $*$ shows the position of the zero order root tip.

As can be seen on Figures 6.3 and 6.4 the nutrient uptake by growing plant roots has a much less severe effect on the nutrient concentration profile in the soil than was found in the case of a fixed root system in the previous chapter. In comparison to the phosphate uptake by a non-competing root system, presented in Chapter 4 Figure 4.9, we note that the dominance of first order roots over zero order roots in the overall nutrient uptake has decreased when we have included inter-root competition (see Figure 6.5). This is mainly due to two factors: firstly, the tip of the zero order root is always in soil with higher concentration and hence the inclusion of the time-delay term ensures that the maximum rate of uptake per unit root surface area is also at the tip of the zero order root. Secondly, early first order branches emerge from the branch points near the base of the zero order roots and hence grow into the soil already depleted by zero order roots. Therefore, for short times, the overall importance of the zero order roots increases. However, after about 1 week the number of first order branches has grown so large that the rate of nutrient uptake by the root system is again dominated by them. This is due to their large number and hence also large surface area.

The rate of nutrient uptake by the full developing root system is presented on Figure 6.5.

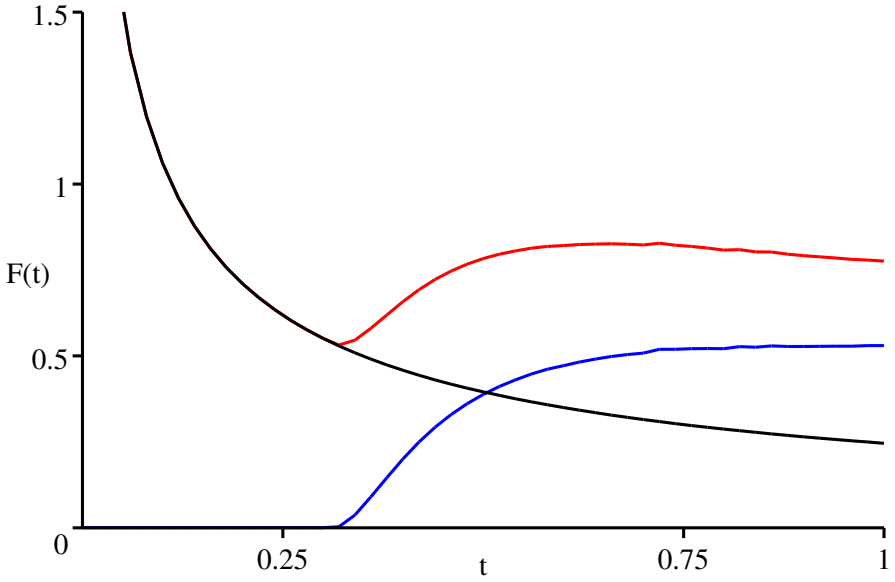

Figure 6.5: Rate of phosphate uptake $F(t)$ by the full root system [μmol day^{-1}] as a function of time [months]. Red line shows the total uptake of nutrients by the root system, blue line shows the uptake by first order roots and black line shows the uptake by zero order roots.

6.3 Field Crop Model

Similarly to Chapter 5, we will now modify the model presented in the previous section to address a field crop situation. We will assume that the zero order roots are parallel to each other and that the distance between them is such that the first order roots emerging from one zero order root are not overlapping with the first order roots emerging from the neighbouring zero order root. That implies that we assume the half-distance d between the zero order roots to be given by $\tilde{a} = a_0 + K_1 \cos\beta$ (see Figure 6.6).

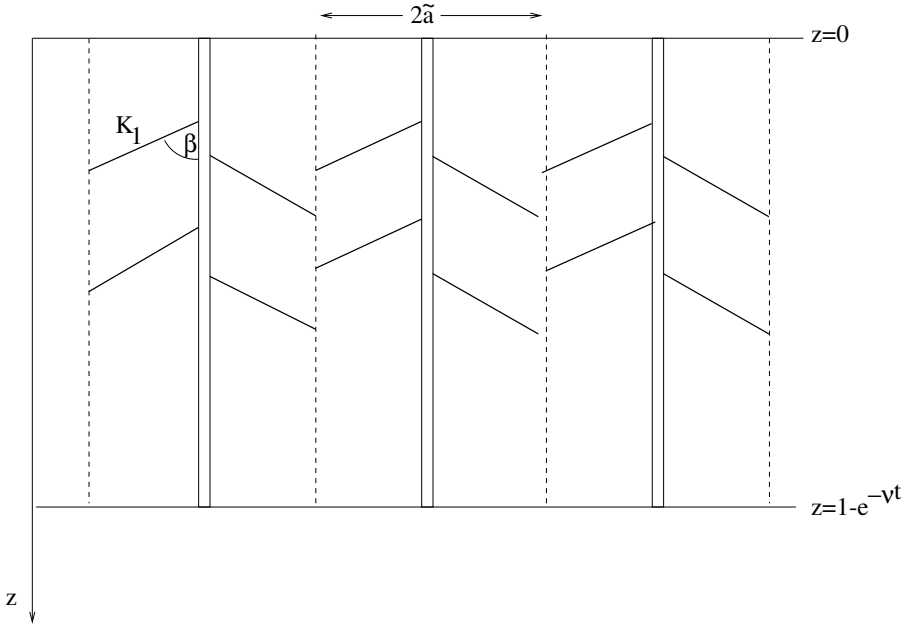

Figure 6.6: Vertical root distribution.

The equation for nutrient concentration in the soil stays the same as shown in Section 6.2.3 and is

$$(b + \phi_l)\frac{\partial c_l}{\partial t} + \nabla \cdot (c_l \mathbf{u}) = \nabla \cdot (\phi_l D \nabla c_l) - \sum_i F_i \quad \text{inside} \quad \partial R. \tag{6.36}$$

To calculate the nutrient uptake terms F_i we use the cylindrical volume element given by $dV = \pi\tilde{a}^2 dz = \pi(a_0 + K_1 \cos\beta)^2 dz$ in equations (6.15) and (6.20) instead of hemispherical volume elements. Hence, with the same non-dimensionalisation as before given by (6.21), and assuming $Pe << 1$, we arrive at the dimensionless equation

$$\frac{\partial c}{\partial t} = \epsilon \frac{\partial^2 c}{\partial z^2} - \sum_i S_i F_i(r, t; c) \quad \text{for} \quad z < 1 - e^{-\nu t}, \tag{6.37}$$

where the F_i are given by

$$F_0 = \frac{2c}{1 + c + L_0(z,t) + \sqrt{4c + (1 - c + L_0(z,t))^2}}, \tag{6.38}$$

and

$$F_1 = \int_{\hat{z}}^{z} \frac{2c\psi_1(z')\,dz'}{1 + c + L_1(z,t;z') + \sqrt{4c + (1 - c + L_1(z,t;z'))^2}}, \tag{6.39}$$

with the time-dependent parameters L_i given by

$$L_0(z,t) = \frac{\lambda_0}{2} \ln\Big[\alpha_0 t + 1 + \alpha_{00} \ln(1 - z)\Big], \tag{6.40}$$

and

$$L_1(z,t;z') = \frac{\lambda_1}{2} \ln\Big[\alpha_1 t + 1 + \alpha_{11} \ln(1 - z' - l_{a,0}) + \alpha_{111} \ln(1 - \frac{(z - z')}{K_1 \cos\beta})\Big]. \tag{6.41}$$

The branch-point region $(\hat{z}, z)$ for each z is defined as before by $\hat{z}$ as the solution to

$$z = \hat{z} + \cos\beta K_1 (1 - e^{-\nu_1 t}(1 - \hat{z} - l_{a,0})^{-\frac{r_1 K_0}{r_0 K_1}}) \quad \text{for} \quad t \geq -\frac{1}{\nu} \ln(1 - \hat{z} - l_{a,0}). \tag{6.42}$$

Dimensionless coefficients S_i are given by

$$S_0 = \frac{2a_0 F_m[t]}{(a_0 + K_1 \cos\beta)^2 (\phi_l + b) K_m}, \quad S_1 = \frac{2a_1 F_m K_0[t]}{(a_0 + K_0 \cos\beta)^2 \cos\beta (\phi_l + b) K_m l_{n,0}}. \tag{6.43}$$

The values of ϵ, α_i, α_{ii} and α_{iii} are the same as shown in Table 6.2. Values of S_i are shown in Table 6.3.

Nutrient	S_0	S_1
N	4.86	278
K	0.86	49.2
S	0.206	11.8
P	3.71×10^{-2}	2.12
Mg	0.28	16.05
Ca	2.5×10^{-6}	1.44×10^{-3}

Table 6.3: Values of dimensionless nutrient uptake parameters S_i.

6.3.1 Boundary Conditions

As in Chapter 5 we take the boundary condition at the soil surface to be a constant flux corresponding to a constant rate of fertilisation, i.e., we take

$$-\frac{\partial c}{\partial z} = \varrho \quad \text{at} \quad z = 0. \tag{6.44}$$

At the ground water level we will apply a constant nutrient concentration boundary condition, i.e.,

$$c = c_\infty \quad \text{at} \quad z = z_w. \tag{6.45}$$

6.3.2 Numerical Solution

As can be seen from the Figure 6.7, the fertiliser application rate suggested by [27] is relatively large so that the fertiliser, in the absence of rainfall and water movement, accumulates on the surface of the soil. Thus, the increase in nutrient uptake by the root system due fertiliser applied to the surface of the soil is negligible.

Accumulation of fertiliser on the surface of the soil is not desirable since it can cause extensive pollution of rivers and lakes via surface runoff. However, since in this chapter we have ignored the effect of rainfall and water movement in the soil, we have probably overestimated the amount of nutrient accumulation on the soil surface.

6.4 The Importance of Root Growth to Nutrient Uptake

It can be seen from the numerical simulations (Figures 6.3-6.5 and 6.7), that root growth plays an important part in nutrient uptake. Firstly, we notice that the uptake is proportional to the length density. In a case of the nutrient uptake by a growing root system, the length density is clearly less than that of a fully grown root system and hence its effect on the nutrient profile in the soil is less severe. Secondly, the time-delay terms $L_i(t-t_i)$ in the nutrient uptake terms are progressively increasing in time and hence F_i decreases in time. Writing L_i in terms of the rescaled variable $R = r/(1-e^{-\nu t})$ we get

$$L_0 = \frac{\lambda_0}{2} \ln \Big[\alpha_0 t + 1 + \alpha_{00} \ln[1-(1-e^{-\nu t})R] \Big], \tag{6.46}$$

and

$$L_1 = \frac{\lambda_1}{2} \ln \Big[\alpha_1 t + 1 + \alpha_{11} \ln[1-(1-e^{-\nu t})R' - l_{a,0}] + \alpha_{111} \ln[1 - \frac{(1-e^{-\nu t})}{K_1 \cos\beta}(R-R')] \Big]. \tag{6.47}$$

The time-delay term $\alpha_{00} \ln[1-(1-e^{-\nu t})R]$ becomes negligible when $\alpha_0 t + 1 >> \alpha_{00} \ln[1-(1-e^{-\nu t})R]$. In this case $L_0 \approx \frac{\lambda_0}{2} \ln(\alpha_0 t + 1)$ (exactly the same expression we used in Chapter 5).

These simulations may explain the reason why in some experimental measurements the nutrient concentration profiles in the soil were found to be decaying with depth [95]. Even when there is relatively small nutrient input at $z = 0$ there is likely to be a quite noticeable concentration gradient which is mainly due to the slow diffusion of nutrient ions in the soil and relatively low uptake near the soil surface. The effect of vertical water movement on fertiliser transport into the deeper layers in the soil will be discussed in Chapter 9.

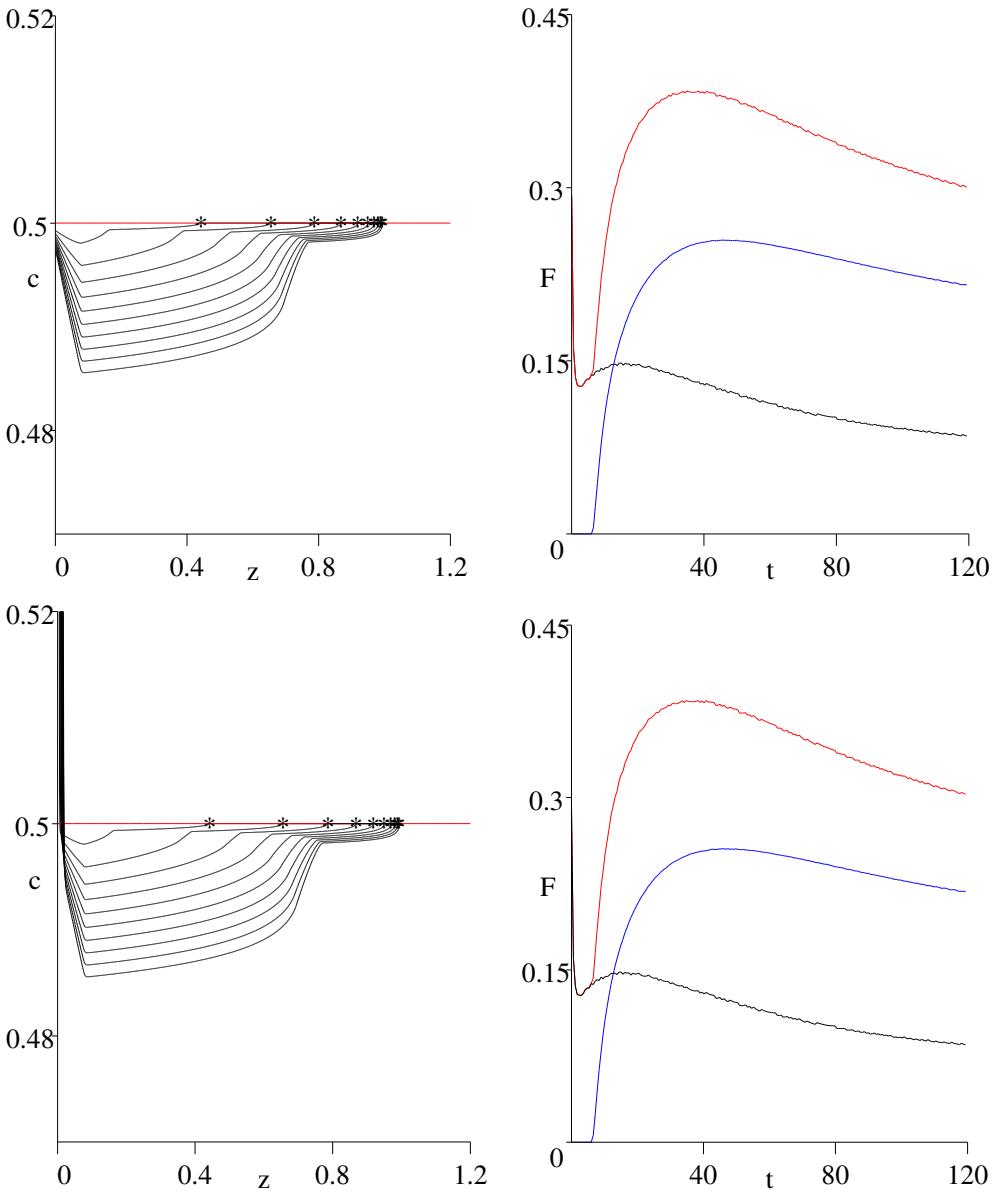

Figure 6.7: Left hand column is dimensionless phosphorus concentration for times $t = 0$ to 4 months after equal time intervals of 12 days (red line corresponding to the initial condition). Right hand column is the corresponding dimensional rate of phosphorus uptake F [μmol day^{-1}] per one zero order root with first order branches as a function of dimensional time t in days. Black line shows the uptake by zero order root, blue line shows the uptake by first order lateral branches and red line shows the total uptake. Top row is the result with zero flux at the soil surface, i.e., $\varrho = 0$, and bottom row is the result with non-zero flux at the soil surface, i.e., $\varrho = 5172$. $*$ shows the position of the tip of a zero order root.

6.5 Inter-root Competition on the Long Timescale

As discussed earlier, the root distribution model is valid up to the time when the diffusional length scale becomes comparable to the inter-root distance. One can now

Nutrient	N	K	S	P	Mg	Ca
$[t]$ (days)	4	126	7.5	769	5	502

Table 6.4: Diffusional timescale corresponding to the length scale $[r] = 0.5$ cm.

ask the question of how should we alter the model to calculate the nutrient uptake after this time. In Table 6.4 we present the values of diffusional time corresponding to diffusional length-scale 0.5 cm. As we see, in the cases of potassium, phosphate and calcium the competition will never become strong over the period of maize vegetational timescale which is maximum of 4 months. However, for nitrate, sulphate and magnesium the diffusion profiles start overlapping reasonably fast. We notice that the dimensionless nutrient uptake parameter λ for nitrate and sulphate is small compared to the initial local far-field concentration c_∞, i.e., $\lambda << c_\infty$. As it was found in Chapter 2 when $\lambda << c_\infty$ the nutrient concentration profile around the single root is relatively undisturbed by root nutrient uptake, i.e., the profile is nearly flat. This implies that in the case of two competing roots the nutrient concentration profile between them is also relatively flat. Hence, as discussed also in Chapter 5, the nutrient uptake in this case is given approximately by

$$F(t) = \frac{\lambda c}{1+c}. \tag{6.48}$$

We also visualise the strong competition between roots as creating a flat nutrient concentration profile around them. Therefore, the uptake on a long timescale, i.e., time much larger than diffusional timescale corresponding to the inter-root distance length-scale, is also given by the Michaelis-Menten uptake law. Thus, for nitrate and sulphate we take the uptake of nutrients at all times to be given by equation (6.48). See Figure 6.8 for results for nitrate uptake using this sink term.

The other nutrient that has a very short diffusional timescale, and thus strong competition between sub-branches, is magnesium. In the case of magnesium the situation is a bit more complicated than in the case of nitrate and sulphate since for magnesium $\lambda = 0.55 \sim O(1)$ with $c_\infty = 6.7 \times 10^{-3} << 1$. Thus the nutrient concentration profile around the roots is not necessarily flat by the time the competition between sub-branches becomes strong. Therefore, the nutrient uptake term for the root distribution model should be calculated from the following leading order[7]dimensionless model[8]

$$\frac{\partial c}{\partial t} = \frac{1}{r}\frac{\partial}{\partial r}(r\frac{\partial c}{\partial r}), \tag{6.49}$$

$$\frac{\partial c}{\partial r} = \lambda c \quad \text{at} \quad r = 1 \quad \text{and} \quad \frac{\partial c}{\partial r} = 0 \quad \text{at} \quad r = r_{\text{int}}, \tag{6.50}$$

[7]For $c << 1$ the flux $\lambda c/(1+c) \approx \lambda c$.

[8]Same non-dimensional scaling as in Chapter 2.

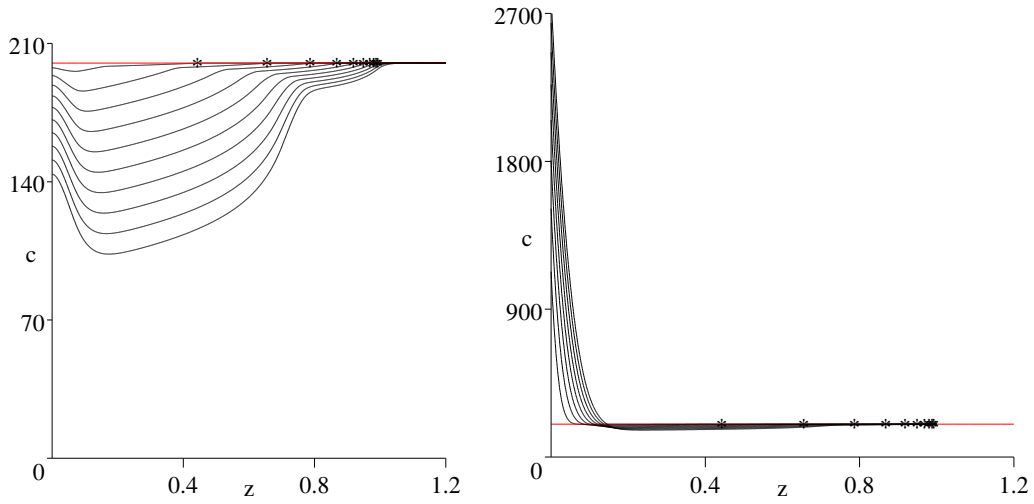

Figure 6.8: Nitrate concentration plotted every 12 days up to 4 months. Left hand graph is for zero fertiliser flux at the surface of the soil and right hand graph is for the dimensionless rate of fertilisation $\varrho = 48720$. Red line corresponding to the initial condition $c_\infty = 200$. The nitrate uptake per unit of root surface area is given by equation (6.48). $*$s show the position of the zero order root tip.

where r_{int} is the half-distance between the roots. The initial condition to this model can still be taken to be that of uniform concentration, i.e.,

$$c = c_\infty \quad \text{at} \quad t = 0 \quad \text{for} \quad 1 < r < r_{\text{int}}. \tag{6.51}$$

The solution to this problem can be found by using Laplace transforms, and it is given by (after [19])

$$\begin{aligned} c &= \lambda c_\infty \pi \sum_{k_n} e^{-k_n^2 t} \frac{J_1^2(r_{\text{int}} k_n)}{(k_n^2 + \lambda^2) J_1^2(r_{\text{int}} k_n) - [k_n J_1(k_n) + \lambda J_0(k_n)]^2} \times \\ &\times \left[J_0(r k_n)[k_n Y_1(k_n) + \lambda Y_0(k_n)] - Y_0(r k_n)[k_n J_1(k_n) + \lambda J_0(k_n)] \right] \end{aligned} \tag{6.52}$$

where k_n is defined as nth root of

$$[k J_1(k) + \lambda J_0(k)] Y_1(r_{\text{int}} k) - [k Y_1(k) + \lambda Y_0(k)] J_1(r_{\text{int}} k) = 0. \tag{6.53}$$

The slowest time decaying mode in this infinite series corresponds to the smallest k, i.e., $k_0 \approx 0.076$ for $\lambda = 0.55$ and $r_{\text{int}} = 10$, and therefore, the solution for long times at the leading order can be taken as the first term in this series.

Phosphate and potassium will have a boundary layer at the root surface, i.e., over very short time the concentration at the root surface will drop to zero (as discussed in detail in Chapter 2). In the case of strong competition between sub-branches, the zero sink model with the reflection boundary condition is applicable, i.e.,

$$\frac{\partial c}{\partial t} = \frac{1}{r} \frac{\partial}{\partial r} \left(r \frac{\partial c}{\partial r} \right), \tag{6.54}$$

$$c = 0 \quad \text{at} \quad r = 1 \quad \text{and} \quad \frac{\partial c}{\partial r} = 0 \quad \text{at} \quad r = r_{\text{int}}, \tag{6.55}$$

The solution can again be found using Laplace transform techniques [19] and it is given by

$$c(r,t) = \pi c_\infty \sum_{k_n} e^{-k_n^2 t} \frac{J_1^2(r_{\text{int}}k_n)[J_0(k_n r)Y_0(k_n) - Y_0(k_n r)J_0(k_n)]}{J_1^2(r_{\text{int}}k_n) - J_0^2(k_n)}, \tag{6.56}$$

where k_n eigenvalues are non-zero roots of

$$J_0(k_n)Y_1(r_{\text{int}}k_n) - Y_0(k_n)J_1(r_{\text{int}}k_n) = 0, \tag{6.57}$$

where J_0, Y_0, J_1 and Y_1 are the Bessel functions of first and second kind.

Hence, the flux of nutrient into the root is $F(t) = \partial c/\partial r|_{r=1}$ and it is given by

$$F(t) = 2c_\infty \sum_{k_n} e^{-k_n^2 t} \frac{J_1^2(r_{\text{int}}k_n)}{J_0^2(k_n) - J_1^2(r_{\text{int}}k_n)}. \tag{6.58}$$

The slowest time decaying mode k_0 corresponds to the smallest positive root of equation (6.57) which for $r_{\text{int}} = 10$ is $k_0 = 0.11$. Hence at large times we take the flux to be given only by this one term in the series.

The sink terms for strong competition mentioned above apply for the situation, when r_{int} is of similar order of magnitude to the diffusional length scale of the nutrient. For phosphate and potassium this means that the length density of roots has to be very high indeed. However, at high root length densities we cannot neglect the water uptake by the root system and therefore there might also be large convective flux of nutrient into the root system. Hence, in the next two chapters the problem of water uptake by the plant roots and root systems will be presented. However, before proceeding, we will illustrate the additional ways of analysing the model presented in this chapter in order to synthesise information on the development of root branching structures.

6.6 Root Structure in Relation to Nutrient Uptake

Many authors have measured the structural response of root systems to the levels of nutrient that is available to them [15], [35],[114], [106]. The majority find that an increase in phosphate level leads to the first order root branch density increasing in order to exploit the soil more effectively, but the root length is generally thought to be less affected by the nutrient level in the soil [15]. However, some studies [35], [114] have found that the length is also affected.

In this section we illustrate techniques to find the most "suitable" first order root length and density in order to maximise the overall nutrient uptake by the plant. For the purposes of comparability, we will assume that the final volume of first order roots is unchanged, thus when the density of roots increases the length decreases and *vice versa*. The density of first order laterals is given by $\psi_1 = 1/l_{n,0}$ [number cm^{-1}], where $l_{n,0}$ is the average inter-root distance. Thus, to have the same final volume of first order lateral roots we need $K_1/l_{n,0} =$ constant. Running the numerical simulations for phosphate for higher and lower first order branch densities, i.e., corresponding to shorter and longer roots, we find that the overall rate of nutrient uptake during the first stages of branching is much higher in the case of higher branch density (see Figure 6.9). However, after about 1 month (30 days) the differences in potential benefits due to root structural changes are negligible.

This simple calculation supports the argument that for the purposes of better phosphate uptake plants should develop more lateral roots per unit length of the zero order root. However, this might not be the case for overall nutrient uptake by the plant, since for example nitrate uptake might be more effective with longer and less denser first order roots, since the competition for nitrate in the soil is very strong because its diffusional length scale is very large. The root architecture development is not in response to only one nutrient, but many. Therefore, more detailed study of simultaneous macronutrient uptake optimisation should be carried out. We will not do this study, since the real test of this approach should be carried out in the framework of a strong experimental and theoretical collaboration. However, in this section we have shown the possibility of doing so using the model presented. We also note that three dimensional computational models with exact branching structures do not yet allow us to conduct such an analysis due to their extensive requirements for computational power.

6.7 Conclusions

In comparison with nutrient uptake by the fixed root system presented in Chapter 5, we have shown in this chapter, by modelling root growth and development, that root growth plays an important role in the nutrient concentration in the soil. As in Chapter 5 for the fixed root system, we found that fertiliser accumulates at the soil surface when vertical water movement is neglected. However, the region of high concentration is much wider in the case of developing root systems than in the case of fixed root systems due to the smaller uptake of nutrients by a growing root system. This enables the influence of slow diffusion to be more noticeable.

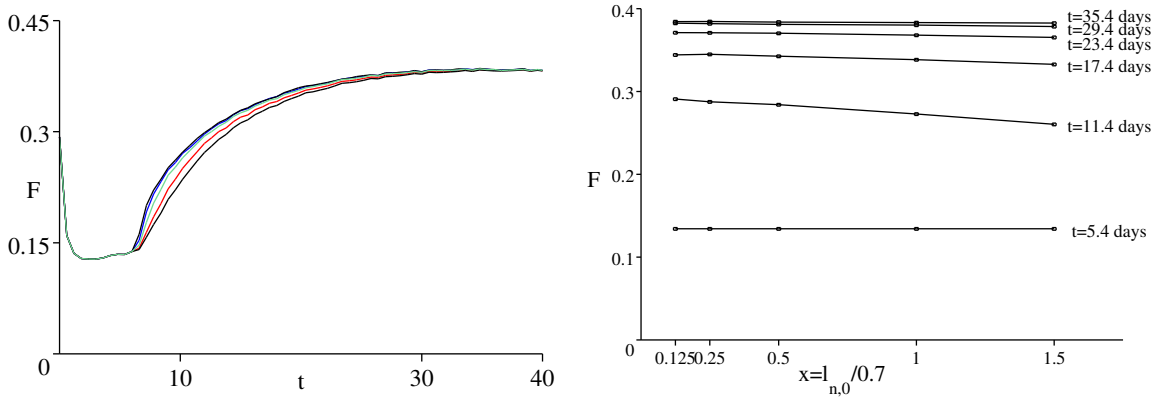

Figure 6.9: Phosphate optimisation graphs. The left hand side graph shows the rate of phosphate uptake [μmol day^{-1}] as a function of time [days] for different first root inter-branch distances $l_{n,0} = 0.7x$ for $x = 0.125$, 0.25, 0.5, 1, 1.5 (black, blue, green, red, black lines respectively) with $K_1/l_{n,0}$ =constant. The graph on the right shows the same calculation as a function of relative inter-branch distance $x = l_{n,0}/0.7$ at different times. First sub-branches are created at $t \approx 7$ days.

These conclusions are also in agreement with other soil and plant nutrient numerical simulations [126], where it is reported that after fertilisation not much depletion by roots can be seen, but instead decreasing "exponential" profiles develop. These general simulators presented in [126] and elsewhere have a very high level of complexity and modularity which makes it difficult to determine why they behave in this way. The model presented in this chapter however, clearly indicates that this behaviour can be due to the fine balance between the root growth, nutrient uptake and slow diffusion.

We also point out that the root system starts having a considerable effect on nutrient concentration in the soil only after a relatively long time. This suggests that reasonable "fine tuning" of the fertiliser application, in order to minimise the losses and maximise the plant nutrient uptake, should be possible. However fertiliser movement in the soil is strongly influenced by the water movement and hence we will deal with it in next three chapters.

Finally, the model presented above can be applied to large scale models of plant coexistence. Ecologists have long been interested in the plant ecosystem diversity and stability. More importantly it is thought that the rates of nutrient uptake by different species in the ecosystem influence the speed at which this system returns to its equilibrium following a perturbation [76], for example an extreme climatic event. This implies that the distinguishing factor for different species in the soil is the rate of nutrient uptake. However, based on the model above, we would speculate that the root branching structure and the speed of its development might be more important.

It has also been found that the reduction in grassland plant richness increases the ecosystem vulnerability to invasions by other species and spread of diseases [69]. Based on the simulations in this chapter and in previous chapter, we can conclude, that many species with similar nutrient uptake characteristics may coexist very successfully in the long term provided that their rooting depths are different.

Chapter 7

Water Movement in the Soil and Uptake by the Root

In the previous two chapters a model for root competition was developed. We found that diffusion does not provide an effective nutrient transport for fertiliser from the top of the soil to the rooting zone. In this chapter we aim to develop a model for water movement and uptake by plant roots and then incorporate this into the nutrient uptake model. Using a similar methodology to that applied to the nutrient uptake we begin the modelling by considering the water uptake by a single cylindrical root in an infinite extent of soil.

7.1 Mechanisms of Water Uptake by Plants

The structure of plant roots was discussed in Chapter 1. In this chapter we will point out the features classically considered important for the transport of water. More detailed description of water transport inside the root branching network is presented in Chapter 8.

Water is taken up by the plant roots and transported to the stems and leaves along the xylem tubes of the root [38]. Xylem tubes are located in the central part of root (see Figure 1.3) inside the Caspian strip[1]. It consists of several different types of cells, the most important ones being the so called tracheary elements and fibers. Tracheary elements are non-living cells [38] and are mainly involved in water transport. As a secondary function they may also provide mechanical strength. Fibers are the primary source of mechanical strength.

For water to be transported from soil to the plant leaves, it first has to move from the soil to the xylem, i.e., it has to pass through the cortex and endodermis of the

[1]In the same region we can also find the phloem, which is responsible for transporting products of photosynthesis from the leaves and stems to the plant roots.

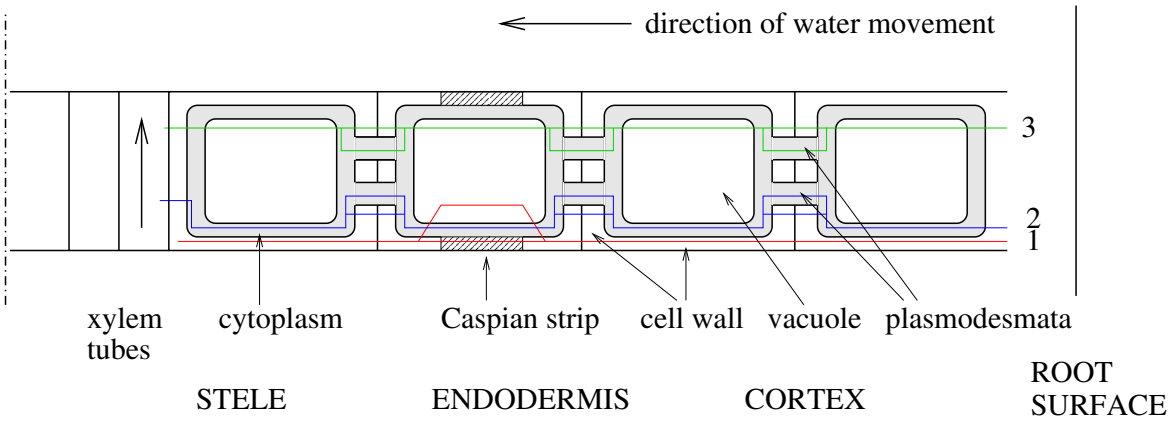

Figure 7.1: Radial water movement pathways after [96] and [84]. Red line describes the two possible apoplastic pathways (1); green line describes two possible cytoplasmic pathways (2); and blue line describes two possible transcellular, i.e., vacuole pathways (3).

root (see Figures 1.3 and 7.1). The pathways along which it does so are still a matter of debate, but according to Oertli [96] and Steudle and Peterson [117] there are at least 3 main pathways (see Figure 7.1):

1. Water flows in the pore system of the cell walls, i.e., in the apoplast (red line on Figure 7.1). Near the Caspian strip[2] this pathway is blocked and hence the water must pass through the vacuole due to the resistivity of the Caspian strip to water flow.

2. Water flows inside the cells in the symplast and transfer from cell to cell occurs either through apoplast[3] or plasmodesmata (blue line on Figure 7.1).

3. Water transport inside the cell occurs across the cytoplasm and then through the vacuole (green line on Figure 7.1).

Whichever pathway dominates is probably strongly dependent on the environmental conditions the plant is growing in. For simplicity we will consider the root endodermis to be a porous material where all possible pathways are absorbed into one radial endodermal water conductivity parameter.

[2]The Caspian strip is a band of corky tissue that is found on the side and walls of the endodermis of roots. The strip is thought to play an important part in maintaining the root internal pressure [3].

[3]i.e., cell wall.

7.2 Overview of Models for Water Uptake by Plants

Plant water uptake models can in general be divided into two classes. The first class deals with the radial movement of water into the xylem through the root cortex and endodermis and uses a simplified water flow within the soil. The second class of models deals with root system water uptake and relies heavily on different approximations of the water uptake by single roots and on measurements of root length density. However, these models do not take account of water flow within roots. Good overviews of both types of models are presented for example in [96], [84], [61], and [99].

7.2.1 Models of Water Flow into and in the Xylem

One of the most extensive overviews of water flow into xylem is presented by Oertli [96]. He bases his theory of water uptake on the theory of semi-permeable membranes. The root surface membrane represents the water movement path across the cortex to the xylem. Hence, the thickness of the root surface membrane is taken to be equal to the thickness of the cortex.

Within this theory the rate of water uptake by plant roots per unit surface area J_w [$\mathrm{cm^3 cm^{-2} s^{-1}}$] is given by

$$J_w = k_r(\Delta P - \sigma \Delta \Pi), \tag{7.1}$$

where k_r is the speed of water flow through the root surface membrane per unit difference in water pressure on either side of the membrane[4], ΔP is the hydraulic water pressure difference across the membrane, [MPa], $\Delta\Pi$ is the osmotic pressure difference across the membrane, [MPa], and σ is the reflection or weighting constant, $-1 \leq \sigma \leq 1$, indicating the efficiency of osmotic pressure in relation to hydrostatic pressure[5].

Molz [84] noted that equation (7.1) is applicable to the case when the pressure distribution across the membrane is in a "pseudo-steady state", i.e., the pressure profile across the membrane is approximately linear and all the uptake is therefore determined by the pressure difference on either side of the membrane. According to his simulations this will normally develop within 30 minutes [84], [85]. He also points out that some authors have modified this equation to include the relative soil moisture condition in it, i.e.,

$$J_w = K_r \frac{\phi_l}{\phi_{l,s}}(\Delta P - \sigma \Delta \Pi), \tag{7.2}$$

[4]This is also known in the soil science as the hydraulic conductivity of root surface membrane.
[5]normally $\sigma \geq 0$

where ϕ_l is the volume of water per unit volume of soil, and $\phi_{l,s}$ is the volume of water in a unit volume of fully saturated soil. This modification is motivated by wanting to include the root-soil contact resistance and root-shrinking effects in the water uptake expression. A more detailed model for root shrinking is presented by Nye in [94]. He considers root shrinking in a situation where the root retains partial soil water contact during this process, and finds that the limiting factor in water inflow into the root is the root tissue conductivity.

The parameter σ in equations (7.2) and (7.1) is usually taken to be equal to zero, i.e., the osmotic pressure differences are neglected [33]. Noticeable osmotic pressure effects can occur when there is, for example, accumulation of calcium at the surface of the root, which results in the root bleeding out water. However, we are not interested in nutrient accumulation and root bleeding problems in this thesis and hence we will also neglect the osmotic pressure effects. We note that more recent models on water uptake by plant root systems also neglect this effect [33], [23].

The water flow inside the xylem has generally been modelled by considering the xylem to be a cylindrical tube and therefore the water flow in it is calculated according to Poiseuille law [96], which assumes that the density and viscosity of water are constant in a time-independent Navier-Stokes' equation.

Various authors have used equations (7.1) or (7.2) as boundary conditions for the Richards' equation describing water flow within roots or soil. For example Taylor et al. [121] use it to calculate the steady state solution for the water flow in the soil when the inter-root boundary is kept at a constant water saturation. Myer and Ritchie [89] and Fiscus et al. [40] use it to calculate the water movement inside the plant.

The main difficulty with these membrane models is the availability of root conductivity data, because of the small size of roots. North and Nobel [92] present a novel experimental measurement technique for measuring the hydraulic conductivity of cactus roots in different directions, i.e., radial, longitudinal and overall root conductivity. Jackson et al. [62] present the measurement of total root hydraulic conductivities of tomato plants at different external pressures in a flooded soil. An extensive overview of various earlier measurements of different root parameters is presented by Iwata et al. [61]. The most used parameters for our model maize plant have been presented by Freunsch and Steudle [43].

7.2.2 Models of Water Uptake by Root Systems

The modelling of root system water uptake started in the late sixties and early seventies, and was primarily concerned with describing water movement in the soil with

the water uptake by the root included as a volume sink [128], [90], [84], [85], [96], [107]. The Darcy-Richards'[6] equation with a volume sink is

$$\frac{\partial \phi_l}{\partial t} = -\nabla \cdot \mathbf{u} - F_w, \tag{7.3}$$

where ϕ_l is the volume of water per unit volume of soil, $\mathbf{u}$ is the flux of water, also known as Darcy's flux, and F_w is the water uptake by roots per unit volume of soil. This volume sink F_w is generally considered to be proportional to the root length density [121], [91], [107]. However, the expression describing the uptake of water per unit length of root has varied considerably. An extensive overview of various possible sink terms is presented in [84] and [85].

For example Rowse et al. [107] use the single cylindrical root/root-membrane model and solve it for a steady state assuming a constant water potential boundary condition at the half-distance between the neighbouring roots. They then include this solution as the sink term and find that the results of their numerical simulations agree remarkably well with the experimental data.

More recently modelling has primarily been concerned with applying the Darcy-Richards equation to 3 dimensional root architecture models [23], [33]. These can be divided into two types: (a) the ones that assume constant soil water pressure conditions and calculate the pressure variations inside the root system [33]; and (b) the ones that assume constant water potential inside the root and calculate the water potential variations in the soil [23]. No reports on models including both of those cases have been published, however, Doussan et al. [33] comment that they are currently trying to achieve this. However even now when computing power has dramatically increased enabling the large 3 dimensional simulations to be carried out, the volume sink models that were introduced in the sixties and seventies remain very popular [20], [103].

Alternative models are 2 dimensional. For example Lafolie, Tardieu et al. [71], [72], [120] calculate the water uptake by an array of parallel cylindrical roots. They conclude that the spatial arrangement can make a huge difference on how much water the plant takes up. However, what they neglect to mention is the critical inter-root distance at which the root density starts noticeably influencing the total plant water uptake.

There is also a wide range of global scale plant water extraction models [126], [125], but they all rely heavily on different approximations and assumptions for relating the small scale behaviour, i.e., one root uptake, to large scale behaviour, i.e., water uptake by a forest.

[6]We will present the detailed derivation of the Darcy-Richards equation in the next section.

7.3 Model for Water Flow in the Soil

Research into water movement in the soil was started actively by the experiments conducted by Henry Darcy in 1856. In a series of experiments Darcy measured the specific discharge (nowadays known more commonly as Darcy flux) of water from a soil column as a function of the gradient of hydraulic head. Since these early experiments, there has been a great deal of work on liquid flow in porous media which has been connected with petroleum engineering, ground water contamination and also plant water uptake.

We begin the modelling of water movement in the soil by describing the law of mass conservation of water in the soil.

7.3.1 Conservation of Water in the Soil and Darcy's Law

The equation for the conservation of water ϕ_l in the soil, assuming that water is incompressible, is given by

$$\frac{\partial \phi_l}{\partial t} + \nabla \cdot \mathbf{u} = -F_w, \tag{7.4}$$

where ϕ_l is the volume of water per unit volume of soil, $\mathbf{u}$ is the volume flux of water and F_w is the volume uptake of water by plant roots per unit volume of soil.

The flux of water $\mathbf{u}$ in the soil is generally given by Darcy's Law [41], [42]. Darcy's Law states that the specific discharge, also known nowadays as Darcy flux, or simply water flux in the soil, $\mathbf{u}$ is given by

$$\mathbf{u} = -\frac{k}{\mu}[\nabla p - \rho g \widehat{\mathbf{k}}], \tag{7.5}$$

where k is the soil permeability, μ is the viscosity of water, and p is the water pressure in the soil, and $\rho g \widehat{\mathbf{k}}$ represents the gravitational effects (see [41], [42]). $\widehat{\mathbf{k}}$ is the unit vector pointing downwards from the soil surface.

Darcy's Law is not valid if, according to [42], (a) the flow is at very low pressure gradients through low-permeability sediments; or (b) large flows through high permeability gradients. However, for most agricultural soils Darcy's Law is valid. Therefore we will limit our interest to this case only.

7.3.2 Soil Permeability and Hydraulic Conductivity

Before we proceed to specify soil permeability k we will discuss the concept of soil hydraulic conductivity. In plant and soil sciences the term soil hydraulic conductivity

is more commonly used than the term soil permeability. The two differ only by a scaling factor, i.e., hydraulic conductivity K is defined as

$$K = \frac{k\rho g}{\mu}, \tag{7.6}$$

where ρg present the density of water and gravity. This expression arises from Darcy's law written not in terms of pressure but in terms of pressure head $h = p/(\rho g)$, i.e., $\mathbf{u} = -K\nabla(h - z)$. We assume that the water pressure p in the soil is measured against the atmospheric air pressure, and hence $p < 0$ assuming that the air pressure in the soil is atmospheric.

The soil permeability k is related to the square of the mean grain size d, i.e., $k = d^2C$, where the parameter C depends on pore configuration [41], [42]. One can derive expressions for C for various different particles shapes, i.e., spherical, tubular etc. (see for example Fowler [41]). However, in practice the conductivity of unsaturated soil is determined from experiments in terms of effective water saturation. Effective water saturation S is defined as

$$S = \frac{\phi_l - \phi_{l,r}}{\phi_{l,s} - \phi_{l,r}}, \tag{7.7}$$

where ϕ_l is the moisture content of the soil, $\phi_{l,r}$ is the residual (minimum) moisture content of the soil, and $\phi_{l,s}$ is the saturated moisture content of the soil, i.e., the soil porosity.

In the article by van Genuchten [130] a formula for the soil hydraulic conductivity as a function of soil moisture content and porosity is presented. He finds that the hydraulic conductivity K is given by

$$K = K_s S^{1/2}[1 - (1 - S^{1/m})^m]^2 \quad \text{for} \quad 0 < m < 1, \tag{7.8}$$

where K_s is the hydraulic conductivity of fully saturated soil. He also presents the values of K_s for various different soil types (see Table 7.1).

7.3.3 Soil Water Suction Characteristic

By *soil water suction characteristic* soil scientists usually mean the relationship between the suction of water into the soil as a function of the relative soil water saturation. It is usually measured experimentally. Hence, we need to link the suction $-p$, where p is the water pressure in the soil measured with respect to atmospheric air pressure, to the relative liquid saturation of the soil S. There are various different analytical expressions that have been fitted to suction characteristic data, one of the most successful and most used being by van Genuchten [130]. In addition to deriving the soil hydraulic conductivity formula (7.8), he also presents a formula for the

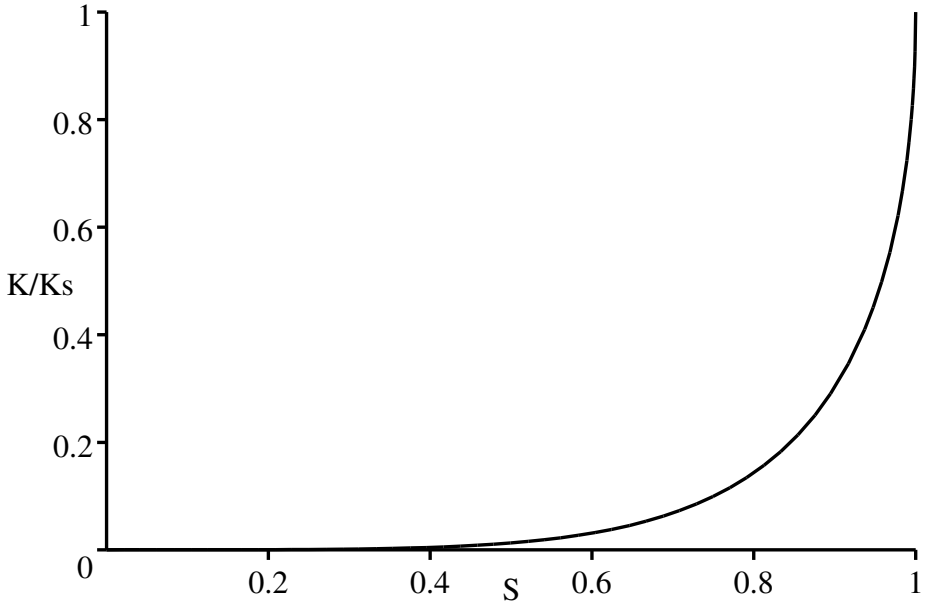

Figure 7.2: Hydraulic conductivity K/K_s after equation (7.8) for $m = 0.5$ which is typical for loam soils (see Table 7.1).

suction characteristic. He uses the pressure head h, however suction $-p > 0$ can be written in terms of pressure head, i.e., $-p = -\rho g h$. Hence from [130] we have

$$S = \Big[\frac{1}{1+(\alpha|h|)^n}\Big]^m = \Big[\frac{1}{1+[\frac{\alpha}{\rho g}(-p)]^n}\Big]^m, \quad m = 1-\frac{1}{n}, \quad 0 < m < 1, \tag{7.9}$$

where α is a fitting parameter that can be inversely linked to the bubbling pressure[7] [130], but in general is estimated directly from experimental suction characteristic data.

Typical values of parameters for van Genuchten's formulae (7.8)-(7.9) are shown in Table 7.1. The typical suction characteristic is shown on Figure 7.3.

Parameter	$\phi_{l,s}$	$\phi_{l,r}$	$K_s = \frac{k_s \rho g}{\mu}$	α	n
Units	$\mathrm{cm}^3\mathrm{cm}^{-3}$	$\mathrm{cm}^3\mathrm{cm}^{-3}$	cm day^{-1}	cm^{-1}	-
Hygiene Sandstone	0.250	0.153	108.0	0.0079	10.5
Touchet Silt Loam G.E.3	0.469	0.190	303.0	0.0050	7.09
Silt Loam G.E.3	0.396	0.131	4.96	0.00423	2.06
Guelph Loam (drying)	0.520	0.218	31.6	0.0115	2.03
Guelph Loam (wetting)	0.434	0.218	-	0.020	2.76
Beit Netofa Clay	0.446	0.0	0.082	0.00152	1.17

Table 7.1: Values for van Genuchten coefficients after [130].

[7] i.e., the "point" on suction characteristic (S, h) where the water starts to drain from the soil.

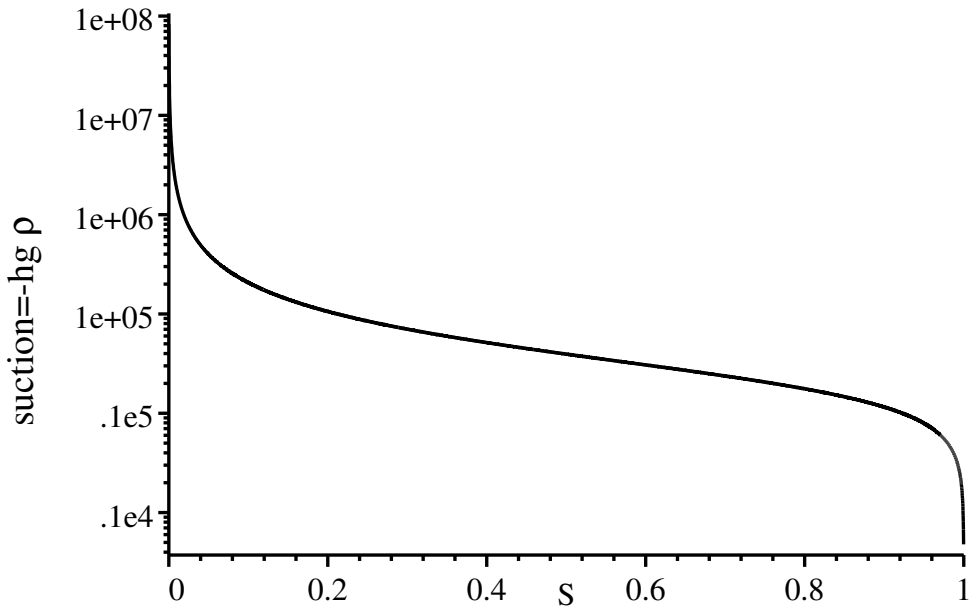

Figure 7.3: $(S, -h\rho g)$ graph showing the suction characteristic for Silt Loam G.E.3 (see Table 7.1). Suction is defined as $-p$ where p is water pressure measured relative to air pressure, $-p > 0$.

7.3.4 Modifications of the van Genuchten Formulae

Many authors have modified the van Genuchten formulas (7.8) and (7.9). For example Clausnitzer, Hopmans et al. [23], [24] have used at least two different versions of it. In [23] they use the formulae presented above, but in [24] they use

$$S = \Big[\frac{1}{1+(-\alpha h)^n}\Big]^m \quad \text{for} \quad h < 0, \quad \text{and} \quad S = 1 \quad \text{for} \quad h \geq 0, \quad m = 1 - \frac{1}{n}, \tag{7.10}$$

$$K = K_s S^l [1 - (1 - S^{1/m})^m]^2, \tag{7.11}$$

where α, n, and l are fitting parameters.

Van Genuchten himself points out in his article [130] that at large values of pressure head h the soil water retention expression (7.9) reduces to

$$S = (\alpha h)^{-mn}, \tag{7.12}$$

and the hydraulic conductivity becomes

$$K = K_s S^{3+2/(n-2)}, \tag{7.13}$$

i.e., at large values of hydraulic pressure head the soil water retention expression (7.9) and hydraulic conductivity (7.8) reduce to simple power laws in the relative moisture content $S = (\phi_l - \phi_{l,r})/(\phi_{l,s} - \phi_{l,r})$ of the soil. Large pressure head implies small

relative water content in the soil, i.e., in the case of Silt Loam G.E.3 the power law is applicable approximately for $S << 0.1$. However, plants require high levels of water for their functioning and hence these power-law approximations might not be useful in modelling realistic situations of water uptake by agricultural plants.

However power laws have been very popular ([20], [41] and others), for they provide a simplification to the full Richards-van Genuchten model. For example [20] uses a cubic power law to calculate the water uptake by chrysanthemum plants.

There is also a wide range of available analytical infiltration models which are derived from fitting experimental data, considering physical arguments etc. and an overview of parameter uncertainty in the most commonly used ones is presented by Clausnitzer et al. in [24].

7.4 Water Uptake Model for a Cylindrical Root with Finite Length in Infinite Soil

We recall that the conservation of water in the soil with no water sink ($F_w = 0$) is given by

$$\frac{\partial \phi_l}{\partial t} + \nabla \cdot \mathbf{u} = 0, \tag{7.14}$$

where $\mathbf{u}$ is given by (we take the z direction pointing downwards into the soil)

$$\mathbf{u} = -\frac{k}{\mu}[\nabla p - \rho g \widehat{\mathbf{k}}], \tag{7.15}$$

with k given by the van Genuchten formulas

$$k = k_s S^{1/2}[1 - (1 - S^{1/m})^m]^2 \quad \text{for} \quad m = 1 - \frac{1}{n}, \quad 0 < m < 1, \tag{7.16}$$

and

$$S = \frac{\phi_l - \phi_{l,r}}{\phi_{l,s} - \phi_{l,r}} = \Big[\frac{1}{1 + (-\frac{\alpha}{\rho g} p)^n}\Big]^m. \tag{7.17}$$

Writing the model in terms of relative moisture content S using the full van Genuchten formulas we get the following nonlinear diffusion-convection equation

$$(\phi_{l,s} - \phi_{l,r})\frac{\partial S}{\partial t} = \nabla \cdot (D(S)\nabla S) - \frac{\rho g}{\mu}\frac{dk}{dS}\frac{\partial S}{\partial z}, \tag{7.18}$$

where $D(S)$ is called the soil water diffusivity and it is defined as

$$D(S) = \frac{k(S)}{\mu}\Big|\frac{\partial p}{\partial S}\Big| = \frac{k_s \rho g}{\mu} \times \frac{(1-m)}{\alpha m} S^{1/2-1/m}[(1-S^{1/m})^{-m} + (1-S^{1/m})^m - 2], \tag{7.19}$$

and

$$\frac{dk(S)}{dS} = k_s\Big[\frac{1}{2}S^{-1/2}[1 - (1 - S^{1/m})^m]^2 + 2S^{-1/2+1/m}[1 - (1 - S^{1/m})^m](1 - S^{1/m})^{m-1}\Big]. \tag{7.20}$$

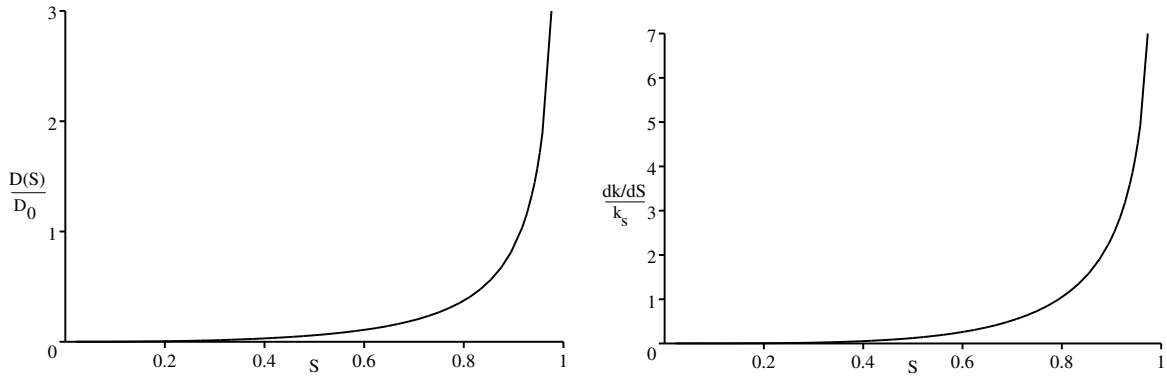

Figure 7.4: Normalised soil water diffusivity $D(S)/D_0$ with $D_0 = k_s\rho g(1-m)/(\mu\alpha m)$ and convection $\frac{dk}{dS}\frac{1}{k_s}$ after equations (7.19) and (7.20) for $m = 0.5$ which is typical for loam soils (see Table 7.1).

7.4.1 Root Surface Boundary Condition

Derivation of Pseudo Equilibrium Root Surface Boundary Condition

In section 7.2.1 we noted that the volume of water taken up per unit root surface area per unit time is given by equation (7.1). However, it is usually taken at face value and the derivation of it has not always been presented. We now aim to justify the use of this boundary condition.

Neglecting the osmotic pressure effects on water uptake by plant roots and assuming that we know the value of the water diffusivity in the root cortex, then for a root surface membrane with the inner boundary at a_x and an outer boundary at the root surface a, the water pressure distribution inside this membrane is given after Molz [84] by a solution to the equation

$$\frac{\partial p_m}{\partial t} = \frac{D}{r}\frac{\partial}{\partial r}(r\frac{\partial p_m}{\partial r}), \tag{7.21}$$

with boundary conditions given for example by

$$p_m = p \quad \text{on} \quad r = a, \quad \text{and} \quad p_m = p_r \quad \text{at} \quad r = a_x, \tag{7.22}$$

where p_m is the water pressure in the root cortex tissues, p is the water pressure at the root surface, p_r is the water pressure in the xylem, D is the water diffusivity in the cortical tissues, a is the radius of the root and $a - a_x$ is the thickness of the cortex, i.e., a_x is the location of the root surface membrane inner boundary.

Molz [84] estimates the water diffusivity in the cortex using a circuit analog model and finds that it is approximately of order $D = 1.26 \times 10^{-6}$ cm^{2}s^{-1}. Non-dimensionalising the above equation with typical timescale $[t]$ and root radius a, we

find that the dimensionless problem becomes

$$\frac{a^2}{D[t]}\frac{\partial p_m}{\partial t} = \frac{1}{r}\frac{\partial}{\partial r}(r\frac{\partial p_m}{\partial r}), \tag{7.23}$$

with

$$p_m = p \quad \text{on} \quad r = 1, \quad \text{and} \quad p_m = p_r \quad \text{at} \quad r = a_x/a = r_x. \tag{7.24}$$

Given that the average radius of the maize root is of order 0.02 cm, then for timescales $[t] >> a^2/D \approx 5$ min the water pressure distribution profile is at pseudo steady state, i.e., the time derivative term in the equation (7.23) is small, and the steady state solution is given by

$$\begin{aligned} p_m &= \frac{p - p_r}{-\ln(r_x)}\ln(r) + p \\ &\approx \frac{p - p_r}{1 - r_x}(r - 1) + p \quad \text{for} \quad r_x < r < 1, \end{aligned} \tag{7.25}$$

Hence, in dimensional terms the flux of water through the unit of root surface area is given approximately by

$$D\frac{\partial p_m}{\partial r}|_{r=a} = \frac{D}{a - a_x}(p - p_r). \tag{7.26}$$

The quantity $k_r = D/(a - a_x)$ is generally known as a root surface membrane hydraulic conductivity and it is measured experimentally for different roots. Hence assuming that a_x/a is constant for roots of different radii [83], and we only know the value of $k_r(a)$ for root with radius a, we can calculate it for the other values of root radii using $k_r(a_i) = k_r(a)a/a_i$.

Using the continuity of water pressure across the root surface we can write the boundary condition also in terms of water pressure in the soil assuming that the water pressure in the soil is changing slowly in time so that the pseudo-equilibria derivation presented above is valid. As a boundary condition we then have

$$\frac{k(S)}{\mu}\frac{\partial p}{\partial r} = k_r(p - p_r) \quad \text{at} \quad r = a, \tag{7.27}$$

where p is the water pressure in the soil, p_r is the water pressure in the root xylem, k_r is the radial conductivity of root surface membrane, a is the radius of the root, and $k(S)$ is the soil water permeability.

Water Movement in the Xylem Longitudinally Upwards to the Shoot

The water movement in the xylem is classically calculated from the steady Navier-Stokes' equation for a circular tube (xylem) at constant water density and viscosity. The solution to $\mu\nabla^2\mathbf{u} = \nabla p - \rho g\widehat{\mathbf{k}}$, where $\mathbf{u}$ is the water speed profile in the tube with non-slip boundary condition, is given by $u(r) = \dfrac{r^2 - R^2}{4\mu}[\dfrac{\partial p_r}{\partial z} - \rho g]$, where R is the radius of the xylem tube and μ is the viscosity of water. The total flux across the section $(z, z + dz)$ of this tube is then given in terms of the pressure drop across this section, i.e.,

$$q^* = \int_0^R 2\pi r u(r) dr[\frac{\partial p_r}{\partial z} - \rho g] = -\frac{\pi R^4}{8\mu}[\frac{\partial p_r}{\partial z} - \rho g]. \tag{7.28}$$

Hence, for n xylems inside the root we have the total flux across the cross sectional area $q = nq^*$. Therefore the total water flux upwards is given by

$$q = -k_x[\frac{\partial p_r}{\partial z} - \rho g], \tag{7.29}$$

where $k_x = \pi n R^4/(8\mu)$ is, in the soil science literature, called the root axial conductivity and typically measured experimentally for different root orders. It has been shown that the agreement between the measured axial conductivity and calculated one using the geometrical properties of xylem elements is good [43]. We will return to the calculation of axial conductivity for roots of different order in Chapter 8 when we discuss the axial conductivity of a root branching structure.

Conservation of Water Inside the Root

Considering a unit length of the root, and assuming that there is a balance between the water flow into the xylem, i.e., across the root surface membrane, and out of this unit length of the root along the xylem we find that

$$2\pi a k_r(p - p_r) = \frac{\partial q}{\partial z}, \tag{7.30}$$

where a is the radius of the root and q is the longitudinal flux of water. This results in an ordinary differential equation for p_r as a function of z, i.e.,

$$2\pi a k_r(p - p_r) = -k_x \frac{\partial^2 p_r}{\partial z^2}, \tag{7.31}$$

which we can solve subject to boundary conditions

$$p_r = T \quad \text{at} \quad z = 0, \quad \text{and} \quad \frac{\partial p_r}{\partial z} = 0 \quad \text{at} \quad z = L, \tag{7.32}$$

where L is the length of the root and T is the average pressure at the top of the root, i.e., at the root-shoot boundary. One of the first papers to propose this model as a description for root internal pressure variations along the root was Landsberg and Fowkes [73].

7.4.2 Radial and Axial Root Conductivities

Radial and axial conductivities are generally difficult to measure. However, North and Noble [92] have successfully managed this for the cactus plant *Opuntia fiscus-indica* L. for different parts of the root tissue. They report that the radial conductivity of the endodermis k_r is of order 2×10^{-7} to 10^{-6} m s^{-1}MPa^{-1}, and that the xylem axial conductivity k_x is of order 10^{-11} to 4×10^{-11} m^{4}s^{-1}MPa^{-1}.

Frensch and Steudle [43] found that the radial conductivity of maize roots with radius 5×10^{-4} m was of order 2.5×10^{-7} m s^{-1}MPa^{-1}, and axial conductivity of order 10^{-9} m^{4}s^{-1}MPa^{-1}.

As discussed in the previous Section 7.4.1, the radial conductivity of a root of different radius is given in terms of the measured one by

$$k_r(a_i) = \frac{a k_r(a)}{a_i}, \quad \text{but} \quad 2\pi a_i k_r(a_i) = 2\pi a k_r(a) = \text{constant}, \tag{7.33}$$

where a is the radius of the root that the measurement of $k_r(a)$ was performed for, and a_i is the radius of the root we wish to find the conductivity for.

Doussan et al. [33] model the pressure distribution inside the maize root system assuming a constant external soil pressure. They use the value 2×10^{-7} ms^{-1}MPa^{-1} for root radial conductivity k_r, and 5×10^{-11} m^{4}s^{-1}MPa^{-1} for xylem conductivity k_x for all roots, i.e., for all three orders. However, this might result in error, since the difference in the radius of zero and second order roots can be tenfold, hence resulting in at least a tenfold difference in k_x and k_r.

7.5 Model for Water Flow Inside the Root at Constant Soil Pressure

Assuming that the external pressure in the soil is constant, i.e., $p = P$ we have for the water pressure inside the root system the equation

$$2\pi a k_r (P - p_r) = -k_x \frac{\partial^2 p_r}{\partial z^2}. \tag{7.34}$$

We non-dimensionalise the equation with

$$z = L z^* \quad \text{and} \quad p_r = T p_r^*, \tag{7.35}$$

where z^* and p_r^* are the dimensionless length and pressure respectively. The dimensionless equation becomes (after dropping *s)

$$\kappa^2 (P_0 - p_r) = -\frac{\partial^2 p_r}{\partial z^2}, \tag{7.36}$$

where $P_0 = P/T$ and $\kappa^2 = 2\pi a k_r L^2/k_x$ is the dimensionless water uptake coefficient.

The solution to this problem with boundary conditions (7.32), i.e., with

$$p_r = 1 \quad \text{at} \quad z = 0, \quad \text{and} \quad \frac{\partial p_r}{\partial z} = 0 \quad \text{at} \quad z = 1, \tag{7.37}$$

is given by

$$\begin{aligned} p_r &= P_0 + \exp(\kappa z)\frac{1}{2}\Big[(P_0 - 1)\tanh(\kappa) - P_0 + 1\Big] \\ &+ \exp(-\kappa z)\frac{1}{2}\Big[-(P_0 - 1)\tanh(\kappa) - P_0 + 1\Big], \end{aligned} \tag{7.38}$$

with $P_0 = P/T$ and $\kappa^2 = 2\pi a k_r L^2/k_x$. The graph of this solution in dimensional terms is shown on Figure 7.5 for a typical value $\kappa^2 \approx 4.36$.

This solution was probably first found by Landsberg and Fowkes [73] who, amongst other things, used this model to determine the water efflux, i.e., flux of water out from the roots into the stems and leaves, for given soil water saturation profiles.

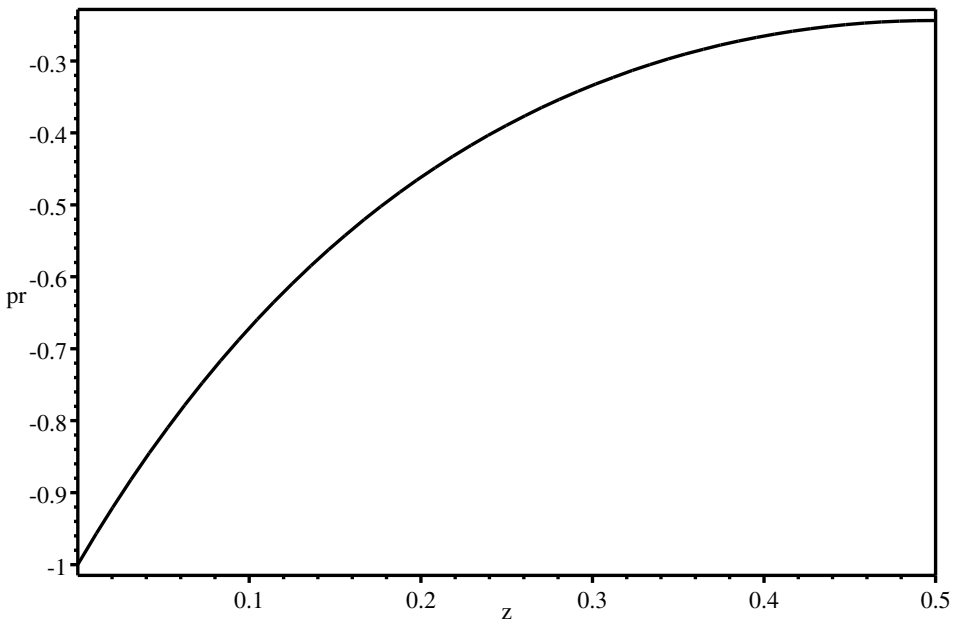

Figure 7.5: Pressure inside the root p_r [MPa] as a distance from the root-shoot boundary (i.e., from the base) z [m] with external soil pressure set to $P = 0$ [MPa], $k_r = 2.5 \times 10^{-7}$ [$\mathrm{m^3 m^{-2} s^{-1} MPa^{-1}}$], $k_x = 4.5 \times 10^{-11}$ [$\mathrm{m^4 s^{-1} MPa^{-1}}$], $a = 5 \times 10^{-4}$ [m], $L = 0.5$ [m], and $T = -1$ [MPa].

7.6 Model for Water Flow in the Soil with Constant Root Internal Pressure

Now that we have found out the influence of constant soil water pressure on root internal water pressure we will investigate the influence of constant root internal water

pressure on water distribution in the soil. Writing equations (7.14) and (7.15) in terms of the cylindrical polar coordinate r, where $r = \sqrt{x^2 + y^2}$, we get the following model

$$(\phi_{l,s} - \phi_{l,r})\frac{\partial S}{\partial t} = \frac{1}{r}\frac{\partial}{\partial r}(D(S)r\frac{\partial S}{\partial r}) \tag{7.39}$$

with root surface boundary condition given by

$$D(S)\frac{\partial S}{\partial r} = k_r[p(S) - P_r] \quad \text{at} \quad r = a, \tag{7.40}$$

where P_r is the constant pressure inside the root, and

$$D(S) = \frac{k_s\rho g}{\mu}\frac{(1-m)}{\alpha m}S^{1/2-1/m}[(1 - S^{1/m})^{-m} + (1 - S^{1/m})^m - 2], \tag{7.41}$$

$$p(S) = -\frac{\rho g}{\alpha}(S^{-1/m} - 1)^{1/n}. \tag{7.42}$$

We take the far-field soil water content to be given by a constant S_∞, i.e.,

$$S \to S_\infty \quad \text{as} \quad r \to \infty. \tag{7.43}$$

7.6.1 Non-dimensionalisation

We non-dimensionalise this model by choosing the following time and length scales

$$t = [t]t^* = \frac{(\phi_{l,s} - \phi_{l,r})\alpha m a^2 \mu}{(1-m)k_s\rho g}t^*, \quad r = ar^*, \quad p = \frac{\rho g}{\alpha}p^*, \tag{7.44}$$

and the dimensionless model becomes (after dropping *s)

$$\frac{\partial S}{\partial t} = \frac{1}{r}\frac{\partial}{\partial r}(rD(S)\frac{\partial S}{\partial r}), \tag{7.45}$$

with

$$D(S) = S^{1/2-1/m}[(1 - S^{1/m})^{-m} + (1 - S^{1/m})^m - 2]. \tag{7.46}$$

The dimensionless boundary condition is

$$D(S)\frac{\partial S}{\partial r} = \lambda_w[p(S) - p_r] \quad \text{at} \quad r = 1, \quad \text{with} \quad p(S) = -(S^{-1/m} - 1)^{1/n}, \tag{7.47}$$

where dimensionless parameters λ_w and p_r are given by

$$\lambda_w = \frac{k_r\rho g m a}{(1-m)K_s} \quad \text{with} \quad K_s = \frac{k_s\rho g}{\mu} \quad \text{and} \quad p_r = \frac{P_r\alpha}{\rho g}. \tag{7.48}$$

The far-field boundary condition is still

$$S \to S_\infty \quad \text{as} \quad r \to \infty, \tag{7.49}$$

as S and S_∞ are already dimensionless. The numerical values for different soil types and for maize plant according to [33] and [130] are shown in Table 7.2.

Parameter	$[t]$	λ_w	p_r
Units	sec	-	-
Hygiene Sandstone	2.93×10^{-3}	3.03×10^{-7}	-79
Touchet Silt Loam G.E.3	9.69×10^{-4}	6.95×10^{-8}	-50
Silt Loam G.E.3	8.28×10^{-3}	7.39×10^{-7}	-42.3
Guelph Loam (drying)	3.9×10^{-3}	1.13×10^{-7}	-115

Table 7.2: Values of dimensionless parameters for $a = 2 \times 10^{-4}$ m, $P_r = -1$ MPa, $k_r = 5 \times 10^{-11}$ $\mathrm{m^4 s^{-1} MPa^{-1}}$ and other soil parameter values presented in Table 7.1.

7.6.2 Approximations

Table 7.2 shows that the water uptake coefficient $\lambda_w \sim O(10^{-7})$ and also $-\lambda_w p_r \sim O(10^{-5})$ are very small. Therefore we expect small water content gradients in the soil due to water uptake. Hence at the leading order the water uptake is constant, i.e., $F \approx \lambda_w[p(S_\infty) - p_r]$.

However, over long time-scales there might be changes in the root surface water content and hence we are interested in the correction term to this constant water uptake. Therefore, looking for a higher order solution in the form $S(r,t) = S_\infty + s(r,t)$ where $s(r,t)$ is the disturbance to the uniform water content profile S_∞ due to the water uptake by the root, the equation becomes

$$\frac{\partial s}{\partial t} = \frac{1}{r}\frac{\partial}{\partial r}\Big(rD(S_\infty + s)\frac{\partial s}{\partial r}\Big), \tag{7.50}$$

with boundary condition

$$D(S_\infty + s)\frac{\partial s}{\partial r} = \lambda_w\Big(p(S_\infty + s) - p_r\Big) \quad r = 1, \tag{7.51}$$

and

$$s \to 0 \quad \text{as} \quad r \to \infty. \tag{7.52}$$

Outer Solution

As in Chapter 2 we will now rescale into the outer region far away from the root, i.e., $r = R/\sigma$ and $t = \tau/\sigma^2$ with $\sigma << 1$. Taking into account that far away from the root the disturbance to the uniform concentration profile is small, i.e., $s << 1$, we approximate the soil water diffusivity by expanding it in Taylor series and using the highest order term only. Hence we have

$$D(S_\infty + s) \approx D(S_\infty) + O(s). \tag{7.53}$$

Therefore the highest order outer problem is

$$\frac{\partial s}{\partial \tau} = \frac{1}{R}\frac{\partial}{\partial R}(RD(S_\infty)\frac{\partial s}{\partial R}), \tag{7.54}$$

with

$$s \to 0 \quad \text{as} \quad r \to \infty. \tag{7.55}$$

The outer similarity type solution is given by (using the similarity variable $\eta = r^2/(4t)$)

$$S = S_\infty + s = S_\infty + BE_1(\frac{r^2}{4tD(S_\infty)}), \tag{7.56}$$

where B is the matching constant, which will be determined by matching this inner solution with the outer solution. We will also relax this constraint and allow B to be a slowly varying function in time, i.e., $B = B(t)$ with $B'(t)/B(t) << 1$.

Inner Solution

Rescaling back in space to the inner region near the root the inner problem becomes

$$\sigma^2 \frac{\partial s}{\partial \tau} = \frac{1}{r}\frac{\partial}{\partial r}(rD(S_\infty + s)\frac{\partial s}{\partial r}), \tag{7.57}$$

with

$$\begin{aligned} \frac{\partial s}{\partial r} &= \lambda_w \frac{p(S_\infty + s)}{D(S_\infty + s)} - \lambda_w \frac{p_r}{D(S_\infty + s)} \quad \text{at} \quad r = 1, & (7.58)\\ &\approx \frac{\lambda_w}{D}(p(S_\infty) - p_r) + \frac{p'D - D'(p - p_r)}{D^2}\Big|_{S_\infty} s + O(s^2) \quad r = 1, & (7.59)\\ & & (7.60) \end{aligned}$$

where $D = D(S_\infty)$ and $D' = \partial D(S)/\partial S|_{S=S_\infty}$. Hence, as long as $S(1,t) \sim S_\infty$ we have $|s| << S_\infty$ and therefore the leading order inner problem is

$$\frac{1}{r}\frac{\partial}{\partial r}(rD(S_\infty)\frac{\partial s}{\partial r}) = 0, \tag{7.61}$$

with the leading order boundary condition corresponding to constant flux, i.e.,

$$\frac{\partial s}{\partial r} = \frac{\lambda_w}{D(S_\infty)}(p(S_\infty) - p_r) \quad \text{at} \quad r = 1. \tag{7.62}$$

The leading order inner solution is therefore given by

$$S = S_\infty + s_1 + \frac{\lambda_w[p(S_\infty) - p_r]}{D(S_\infty)} \ln r. \tag{7.63}$$

Matching

To match the leading order inner solution to the leading order outer solution we adopt exactly the same procedure as used in Chapter 2 and 3. Hence expanding the exponential integral for small argument we find that the outer solution becomes

$$S \approx S_\infty + B\{-2\ln r + \ln[4e^{-\gamma}D(S_\infty)t] + \ldots\}. \tag{7.64}$$

Matching $O(\ln r)$ terms in the inner and outer expansion gives that

$$B = -\frac{\lambda_w[p(S_\infty) - p_r]}{2D(S_\infty)}, \tag{7.65}$$

and matching $O(1)$ terms gives

$$S_\infty + s_1 = S_\infty - \frac{\lambda_w[p(S_\infty) - p_r]}{2D(S_\infty)}\ln[4e^{-\gamma}D(S_\infty)t], \tag{7.66}$$

and using a small initial time adjustment so that $s_1 = 0$ at $t = 0$ we get that

$$s_1 = -\frac{\lambda_w[p(S_\infty) - p_r]}{2D(S_\infty)}\ln[4e^{-\gamma}D(S_\infty)t + 1]. \tag{7.67}$$

Hence we can now do an adjustment to the leading order constant flux by including this s_1 in the flux calculation, i.e., the flux of water into the root is given by

$$F_w(t) = \lambda_w[p(S_\infty + s_1) - p_r], \tag{7.68}$$

where s_1 is given by equation (7.67). This expression is valid up until the time when $s_1 \sim -S_\infty$, i.e., to times approximately $t_c \sim \exp(\frac{2S_\infty D(S_\infty)}{\lambda_w[p(S_\infty)-p_r]}) \sim \exp(10^5) \ggg .. \ggg 1$ when $|p(S_\infty)| << |p_r|$.

However, when $p(S_\infty)$ is comparable in magnitude to p_r then, from the equation (7.67) $t_c = \exp(\frac{2S_\infty D(S_\infty)}{\lambda_w[p(S_\infty)-p_r]})/[4e^{-\gamma}D(S_\infty)]$ might be smaller than order $\exp(10^5)$. We can see on the Figure 7.6 that in this case t_c is less than order 4 months[8] (plant vegetational time-scale) when $S_\infty \lesssim 0.1$. However, $S_\infty \lesssim 0.1$ implies that the plant is growing in extremely dry soil, where the assumption of constant root radius is probably not going to hold due to the effects of root shrinking [94] and the water uptake has probably stopped since root has started to bleed out water.

7.7 Model for Water Flow Inside and Outside the Root

In this section we will consider the two previous cases, i.e., water flow inside and outside the root, simultaneously. We begin by recalling the dimensional equation for the water flow in the soil.

[8] 4 months in dimensional terms corresponds to dimensionless time of order 10^{10}.

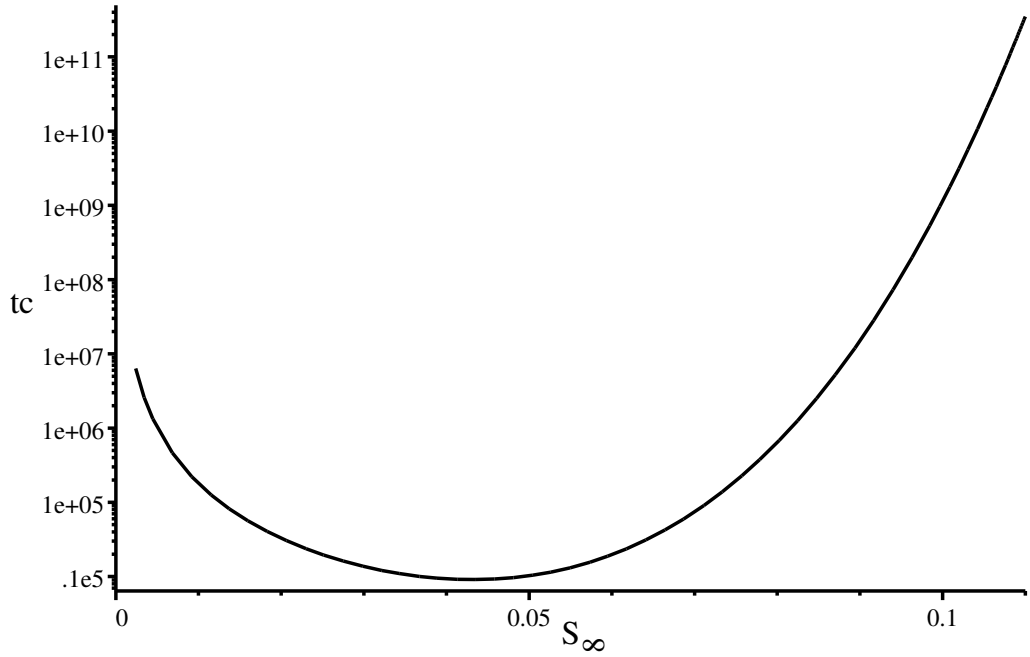

Figure 7.6: Time t_c when $S(1, t_c) \approx 0$ as a function of initial water saturation S_∞, i.e., solution to the equation (7.67) with $s_1 = -S_\infty$. Parameters are $\lambda_w = 10^{-7}$, $p_r = -100$ and $n = 2$ thus $m = 1 - 1/n = 0.5$.

Model for Flow in the Soil

The flow of water in the soil using the Darcy-Richards-van Genuchten model was in previous section found to be given for cylindrical symmetry and vertical variation by

$$(\phi_{l,s} - \phi_{l,r})\frac{\partial S}{\partial t} = \frac{1}{r}\frac{\partial}{\partial r}(rD(S)\frac{\partial S}{\partial r}) + \frac{\partial}{\partial z}(D(S)\frac{\partial S}{\partial z}) - \frac{\rho g}{\mu}\frac{\partial k(S)}{\partial z}, \tag{7.69}$$

where

$$D(S) = \frac{k_s \rho g(1-m)}{\mu \alpha m} S^{1/2-1/m}[(1 - S^{1/m})^m + (1 - S^{1/m})^{-m} - 2], \tag{7.70}$$

$$k(S) = k_s S^{1/2}[1 - (1 - S^{1/m})^m]^2 \quad \text{for} \quad m = 1 - 1/n \quad 0 < m < 1. \tag{7.71}$$

Root Radial Boundary Conditions

Far away from the root we expect the solution to the concentration to be undisturbed by the root uptake, hence we take

$$\frac{\partial S}{\partial r} \to 0 \quad \text{as} \quad r \to \infty. \tag{7.72}$$

However, the boundary condition at the root surface needs to be modified to include the longitudinal variations in the root internal and external pressure. This can be

determined by solving equation (7.31) at $r = a$, i.e., we need to solve

$$2\pi a k_r[p(r,z) - p_r(z)] = -k_x \frac{\partial^2 p_r}{\partial z^2} \quad \text{at} \quad r = a, \tag{7.73}$$

with boundary conditions

$$p_r = T \quad \text{at} \quad z = 0, \quad \text{and} \quad \frac{\partial p_r}{\partial z} = 0 \quad \text{at} \quad z = L. \tag{7.74}$$

The solution to the equation (7.73) for $p_r(z)$ is given in terms of integrals of $p(r,z)$ at $r = a$. Hence we will have a mixed differential-integral boundary condition at the root surface, i.e.,

$$\frac{K(p)}{\rho g}\frac{\partial p}{\partial r} = k_r[p - p_r(z)] \quad \text{at} \quad r = a \quad \text{for} \quad 0 < z < L, \tag{7.75}$$

where L is the length of the root. However, before we proceed to find the exact form of the root surface boundary condition (7.75) we will first non-dimensionalise the full problem.

7.8 Non-dimensionalisation

Non-dimensionalising the z directional length with the maximum length of the root L, the r directional length with the root radius a, and choosing the time-scale $[t]$ such that the time-derivative term balances the radial diffusion term, i.e., by choosing

$$z = Lz^*, \quad r = ar^*, \quad p = \frac{\rho g}{\alpha}p^*, \quad t = [t]t^* \quad \text{with} \quad [t] = \frac{(\phi_{l,s} - \phi_{l,r})\mu\alpha m a^2}{\rho g k_s(1-m)}, \tag{7.76}$$

the dimensionless equation becomes (after dropping *s)

$$\frac{\partial S}{\partial t} = \frac{1}{r}\frac{\partial}{\partial r}(rD(S)\frac{\partial S}{\partial r}) + \epsilon_0\epsilon_1\frac{\partial}{\partial z}(D(S)\frac{\partial S}{\partial z}) - \epsilon_0\frac{\partial k(S)}{\partial z}, \tag{7.77}$$

where

$$\epsilon_0 = \frac{\alpha m a^2}{L(1-m)}, \quad \epsilon_1 = \frac{1-m}{\alpha m}\frac{1}{L}, \tag{7.78}$$

$$D(S) = S^{1/2-1/m}[(1 - S^{1/m})^m + (1 - S^{1/m})^{-m} - 2], \tag{7.79}$$

$$k(S) = S^{1/2}[1 - (1 - S^{1/m})^m]^2 \quad \text{for} \quad m = 1 - 1/n \quad 0 < m < 1. \tag{7.80}$$

The values of ϵ_0 and ϵ_1 for different soils are shown in Table 7.3.

The dimensionless boundary conditions become

$$D(S)\frac{\partial S}{\partial r} = \lambda_w[p(S) - p_r(z)] \quad \text{at} \quad r = 1, \quad 0 < z < 1. \tag{7.81}$$

Parameter	$\frac{1-m}{\alpha m}$	ϵ_0	ϵ_1
Hygiene Sandstone	13.32	5.98×10^{-7}	0.266
Touchet Silt Loam G.E.3	33.05	2.42×10^{-7}	0.661
Silt Loam G.E.3	223.03	3.58×10^{-8}	4.461
Guelph Loam (drying)	84.42	9.43×10^{-8}	1.688
Guelph Loam (wetting)	28.41	2.82×10^{-7}	0.5
Beit Netofa Clay	2.58×10^{-4}	0.031	5×10^{-5}

Table 7.3: Values of the dimensionless parameters ϵ_0 and ϵ_1 for the soil parameter values presented in Table 7.1 and $a = 2 \times 10^{-4}$ [m] and $L = 0.5$ [m].

$$\frac{\partial S}{\partial r} \to 0, \quad \text{i.e.,} \quad S \to S_\infty \quad \text{as} \quad r \to \infty, \tag{7.82}$$

where $\lambda_w = k_r \mu m a/(k_s(1-m))$ is the dimensionless water uptake parameter and S_∞ is the constant far-field water content.

The internal root pressure in terms of external root pressure is given as a solution to the dimensionless analogue of the equation (7.73) with boundary conditions (7.74), i.e., by non-dimensionalising $p_r = \frac{\rho g}{\alpha} p_r^*$ and $p = \frac{\rho g}{\alpha} p^*$ we get (after dropping $*$s)

$$-\frac{\partial^2 p_r}{\partial z^2} = \kappa^2 [p(1,z) - p_r(z)], \tag{7.83}$$

with

$$p_r = T_0 \quad \text{at} \quad z = 0 \quad \text{and} \quad \frac{\partial p_r}{\partial z} = 0 \quad \text{at} \quad z = 1, \tag{7.84}$$

where $\kappa = L\sqrt{2\pi a k_r/k_x} \approx 1.1$ for the root xylem and radial conductivity parameters presented in section 7.4.2, and $T_0 = \dfrac{T\alpha}{\rho g}$.

Hence, the solution in the Green's function form becomes

$$p_r(z) = T_0 + \kappa^2 \int_0^1 G(z,\xi)[p(1,\xi) - T_0]\, d\xi, \tag{7.85}$$

with

$$G(z,\xi) = \begin{cases} -\frac{1}{\kappa}\sinh(\kappa z)[\cosh(\kappa\xi) - \tanh(\kappa)\sinh(\kappa\xi)] & 0 \le z \le \xi \le 1, \\ -\frac{1}{\kappa}\sinh(\kappa\xi)[\cosh(\kappa z) - \tanh(\kappa)\sinh(\kappa z)] & 0 \le \xi \le z \le 1. \end{cases} \tag{7.86}$$

7.8.1 Timescales

As we see, the overall system is highly complex and in general requires extensive and complicated numerical simulations. However, we notice that $\epsilon_0 << 1$, with $\epsilon_1 \lesssim 1$. This implies that processes in z-direction are happening on a very different timescale compared to processes in r-direction. Specifically, it means that water transport occurs much faster in the dimensionless radial direction than in the dimensionless vertical direction due to the different length-scales in the horizontal and radial directions.

7.8.2 Approximations

We begin the analysis of this dimensionless model by considering the system at the leading order only, i.e., neglecting all $O(\epsilon_0)$ terms, and assuming that as $r \to \infty$ the relative moisture condition is given by a constant that is independent of z and t, i.e., we take $S \to S_\infty$ as $r \to \infty$. Hence the problem to be solved becomes

$$\frac{\partial S}{\partial t} = \frac{1}{r}\frac{\partial}{\partial r}(rD(S)\frac{\partial S}{\partial r}), \tag{7.87}$$

with

$$D(S)\frac{\partial S}{\partial r} = \lambda_w[p_1 - p_r(p_1)] \quad \text{at} \quad r = 1, \tag{7.88}$$

$$S \to S_\infty \quad \text{as} \quad r \to \infty, \tag{7.89}$$

and

$$-\frac{\partial^2 p_r}{\partial z^2} = \kappa^2[p_1 - p_r(p_1)], \tag{7.90}$$

with

$$p_r = T \quad \text{at} \quad z = 0, \quad \text{and} \quad \frac{\partial p_r}{\partial z} = 0 \quad \text{at} \quad z = 1, \tag{7.91}$$

where p_1 is the soil water pressure at the surface of the root.

The water uptake parameter λ_w is the same as presented in Table 7.2, i.e., $\lambda_w << 1$. Hence using the similar asymptotic analysis for $\lambda_w << 1$ as presented in Section 7.6.2 we arrive at (see also equation (7.66))

$$S_1 = S_\infty - \frac{F}{2D(S_\infty)}\ln[4e^{-\gamma}D(S_\infty)t + 1], \tag{7.92}$$

where S_1 is the moisture condition at the surface of the root and F is the water flux into the root. However, we know that

$$S_1 = \frac{1}{[1 + (-p_1)^n]^m}, \quad \text{and} \quad F = \lambda_w[p_1 - p_r(p_1)]. \tag{7.93}$$

From equation (7.90) we know that

$$p_1 = p_r - \frac{1}{\kappa^2}\frac{\partial^2 p_r}{\partial z^2}, \tag{7.94}$$

and hence using these three relations we can write equation (7.92) in terms of p_r only, i.e.,

$$\frac{\partial^2 p_r}{\partial z^2}\Big[1 + \Big(\frac{1}{\kappa^2}\frac{\partial^2 p_r}{\partial z^2} - p_r\Big)^n\Big]^m \frac{\lambda_w L(t)}{2D(S_\infty)\kappa^2} + S_\infty\Big[1 + \Big(\frac{1}{\kappa^2}\frac{\partial^2 p_r}{\partial z^2} - p_r\Big)^n\Big]^m - 1 = 0, \tag{7.95}$$

where $L(t) = \ln[4e^{-\gamma}D(S_\infty)t + 1]$. This equation needs to be solved for p_r subject to the boundary conditions

$$p_r = T_0 \quad \text{at} \quad z = 0, \quad \text{and} \quad \frac{\partial p_r}{\partial z} = 0 \quad \text{at} \quad z = 1, \tag{7.96}$$

where $T_0 = T\alpha/(\rho g)$ is the dimensionless water pressure at the base of the root. For $\lambda_w << 1$ the leading $O(1)$ solution for p_r is given by the same solution as found for the case where external water pressure is constant. Hence at the leading order the water uptake by the root does not influence the distribution of water in the soil, i.e., the leading order solution is

$$\begin{aligned} p_r(z) &= -(S_\infty^{-1/m} - 1)^{1/n}[1 + \tanh(\kappa)\sinh(\kappa z) - \cosh(\kappa z)] - \\ &- T[\tanh(\kappa)\sinh(\kappa z) - \cosh(\kappa z)] + O(\lambda_w). \end{aligned} \tag{7.97}$$

The result for various different far-field values S_∞ are presented in Figure 7.7. Hence the water uptake $F(z)$ along the root is simply given by

$$F(z) = -\frac{\lambda_w}{\kappa^2}\frac{\partial^2 p_r}{\partial z^2} + O(\lambda_w^2), \tag{7.98}$$

and the total uptake of water by this root is given at the leading order by

$$F_{\text{tot}} = 2\pi\int_0^1 F(z)\,dz = -\frac{2\pi\lambda_w}{\kappa^2}\frac{\partial p_r}{\partial z}\Big|_{z=0}^{z=1} = \frac{2\pi\lambda_w}{\kappa^2}\frac{\partial p_r}{\partial z}\Big|_{z=0}. \tag{7.99}$$

As we can see the overall water uptake by root is determined by the internal water pressure gradient at the base of the root. Negative flux on Figure 7.8 implies that the root is bleeding out water. We see that this happens only at very low relative moisture levels.

7.9 Conclusions

In this chapter we started by modelling the water uptake by a cylindrical root in an infinite extent of soil. According to our analysis we can now reword the original Nye-Tinker-Barber model assumption concerning the water content. Barber [6] states that the nutrient uptake model is applicable only if *"moisture conditions are maintained essentially constant near field capacity"*. However, in this chapter we have shown that the water uptake by a single cylindrical root in the absence of competition does not influence very much the overall water content in the soil even when the soil moisture content is less than full saturation. Hence, we can now say that the Nye-Tinker-Barber model holds even for non-saturated soils provided that the dimensionless water uptake parameter $|\lambda_w p_r|$ is small. For all available experimental data on root tissue conductivities and agricultural soils $|\lambda_w p_r| << 1$. Hence the expression derived in Chapter 2 for nutrient uptake by single cylindrical root in infinite extent of soil holds for all realistic values of volumetric moisture content ϕ_l.

As we can see water uptake by a plant root in an infinite extent of soil does not influence the water saturation profile in the soil very much. Doussan et al.

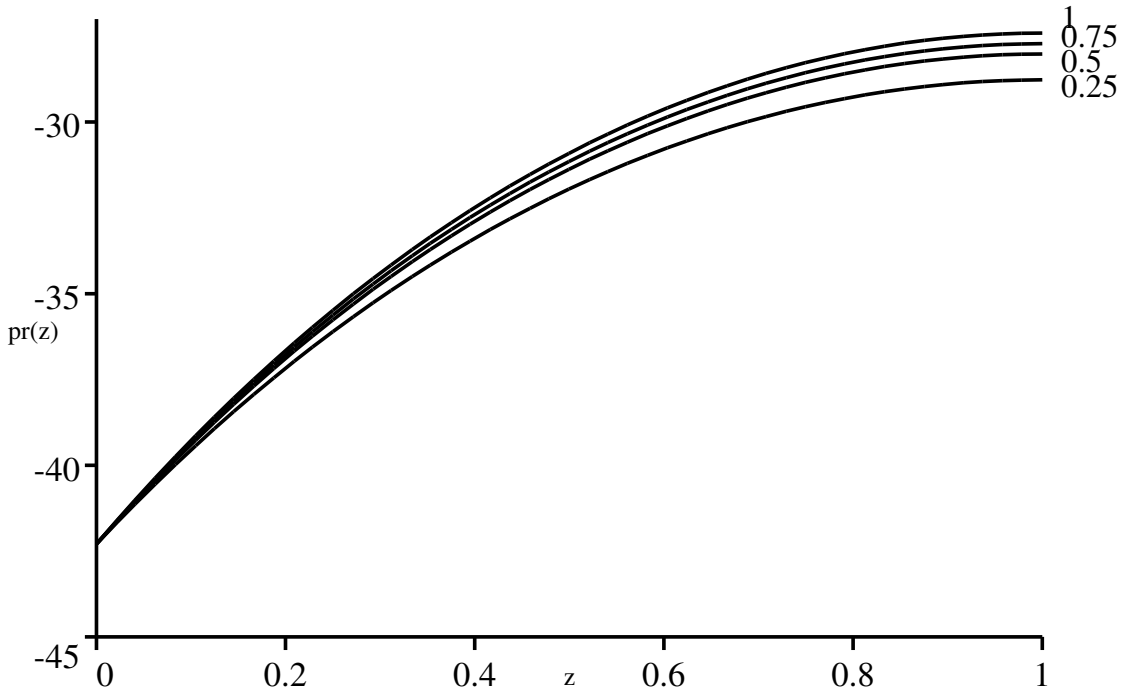

Figure 7.7: Vertical distribution of dimensionless pressure inside the root for various different far-field relative moisture contents S_∞ given by equation (7.97). Other parameters $T = -42.3$, $n = 2$, $m = 1 - 1/n = 0.5$.

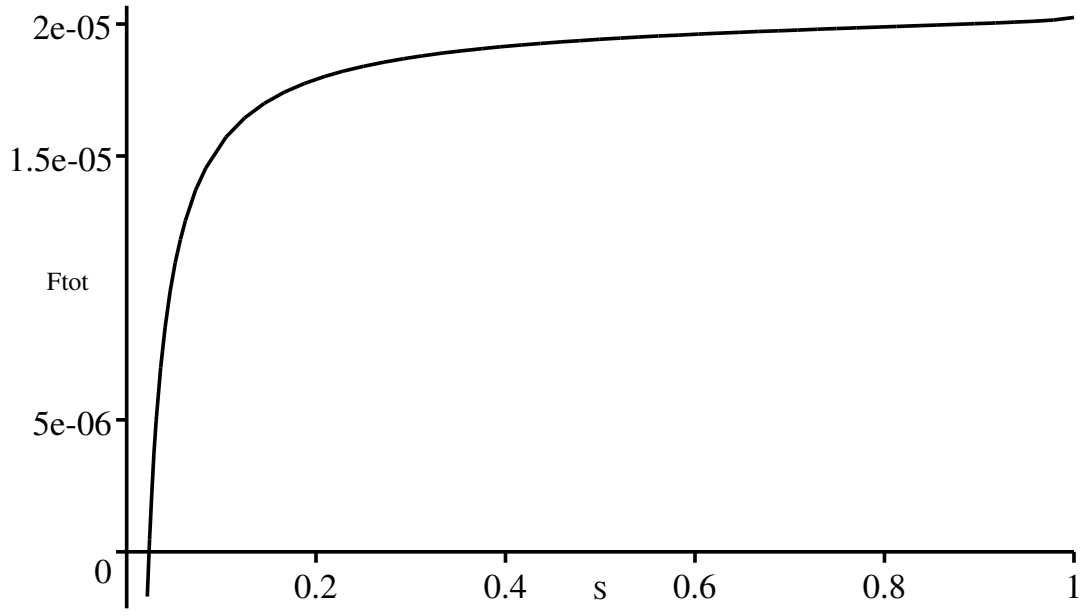

Figure 7.8: Total dimensionless water uptake by the root as a function of far-field relative water content S_∞ given by equation (7.99). Other parameters $T = -42.3$, $n = 2$, $m = 1 - 1/n = 0.5$.

[33], Landsberg and Fowkes [73] and Molz [86] have also found from their analyses and numerical solutions that the water saturation profile around the root is nearly constant. However, we saw that there are noticeable water pressure gradients inside the root, and therefore we can conclude that the dominant limiting factor for the water uptake by the plant root in this situation is the water transport within the root. This agrees with the conclusions made by Nye in [94] where he also finds that the limiting factor in the water uptake is the root tissue conductivity and not the transport of water in the soil even in the case of root shrinking in non-saturated soil.

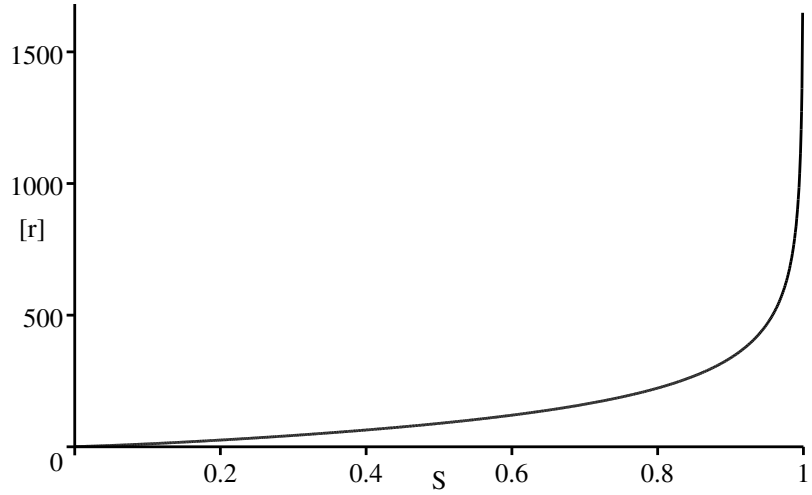

Figure 7.9: Diffusional length scale $[r]$ in cm for different values relative saturation S.

The roots however, are not growing in the infinite extent of soil, but are part of extensive root branching networks. Hence the competition for water in this situation will become strong if the water diffusional length scale is much larger than the inter root distance. The water diffusional length scale at the relative water saturation S corresponding to a plant growth timescale of 1 month is given by

$$[r] = \sqrt{\frac{D(S)[t]}{\phi_{l,s} - \phi_{l,r}}}. \tag{7.100}$$

For Silt loam G.E. 3 we find that for $[t] = 1$ month the diffusional length scale is given by $[r] = 364\sqrt{S^{1/2-1/m}[(1 - S^{1/m})^{-m} + (1 - S^{1/m})^m - 2]}$ [cm] with $m = 0.5$. The value of $[r]$ for different S is shown on Figure 7.9.

As we can see the diffusional length scale is very long. Over time of order 1 month the small disturbance will spread for $S > 0.5$ over 1 m or more. This is much more than the average inter-root distance (approximately of order 1 cm) of the root system. Therefore we can expect strong competition for water uptake between

the sub-branches of the root system, which will result in fast reduction of local water content inside the root system. Hence, we expect that the water content in the rooting region will be reduced quite rapidly. A model for water uptake by a root branching system will be presented in next Chapter 8.

Chapter 8

Water Uptake by a Growing Root System

In the previous chapter we dealt with the water uptake by a cylindrical root in an infinite extent of soil. We found that the water uptake is so small that it does not greatly influence the water saturation profile around the root. We also found that for average/above average relative saturation levels the water diffusional length-scale is much larger than the average inter-root distance. In that regime we expect the competition between the sub-branches to be very strong. However, because of the small water uptake term the water saturation profile between two neighbouring roots is nearly flat. This suggests that water uptake is limited by water transport within the roots and by the long range water movement within the soil.

In this chapter we will address the issue of water uptake by developing root systems. We will treat the cases of continuous rainfall, given by average seasonal rainfall, and no rainfall. The case of stochastic rainfall will also briefly be discussed.

8.1 Anatomical Properties of Root Branching Network and Xylem Network

In the previous chapter we assumed that the root axial conductivity was constant along the root. This assumption does not make any difference to the water saturation profile around a single cylindrical root in an infinite extent of the soil. However, it might play an important part when there is a competition for water between the sub-branches. Thus in this chapter we will need to take into account aspects of root morphology, more particularly the structure of xylem vessels.

In their excellent review article on water movement into and within roots, Steudle and Peterson [117] distinguish between three types of xylems: protoxylem, early metaxylem and late metaxylem (see Figure 8.1).

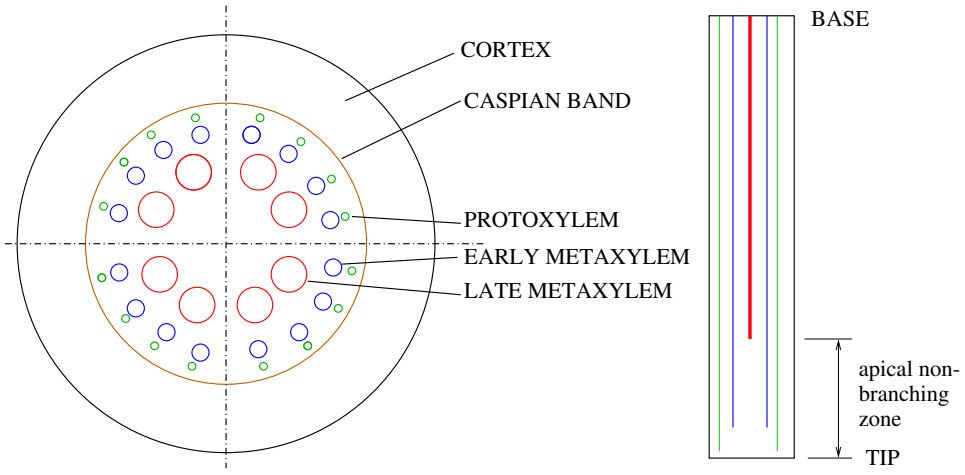

Figure 8.1: Root cross-sectional structure with all three types of xylems after [117].

In Table 8.1 we present the properties of the different xylem elements for zero order roots after [43], [133] and first order roots after [132].

Protoxylem tubes (green circles on Figure 8.1) are the smallest xylem elements in the zero order root with an approximate diameter of 4 ± 1 μm. There are on average 20 protoxylem tubes per cross section of the root[1] [43]. Protoxylems are thought to be active for the whole length of the root.

Early metaxylem tubes (blue on Figure 8.1) are the second largest ones in the root with an average diameter of 22 ± 3 μm. The number of early metaxylem tubes per cross section of the root is approximately $17 - 18$ [43], [133]. According to [43] and [117] early metaxylems become fully active and open for water movement approximately 2.5 cm from the tip of the root.

Late metaxylem tubes (red on Figure 8.1) are the largest xylem elements with an average diameter of order 92 μm and there are approximately 5-7 of them per cross section of the root [133]. Late metaxylems vessels are thought to become active approximately 20 cm (depending on the growth conditions) from the tip [117].

In this chapter we neglect the protoxylem elements since (a) their relative importance in overall hydraulic conductance is large only in the very small region near the root tip, and (b) there is very little data available for protoxylems of the lateral branches.

We notice that the largest xylem elements, i.e., late metaxylem elements, become active in the region where the zero order root, under normal circumstances, develops lateral branches. This is intuitively understandable by the argument that if the plant

[1]The number of xylem elements per cross section of the root is obtained by cutting the root perpendicular to its axis and counting the number of xylem vessels that are visible under the microscope.

is investing its carbon resources into developing lateral branches, which will contribute to the water and nutrient uptake, then it is only reasonable that there will be also extra "piping" made available to deal with the increased water flux into the main zero order root. On the other hand, the reason why they are not open near the tip might be to minimise the overall "risk" to a plant. As the large xylem vessels are closed near the root tip any damage caused to the tip, by insects for example, will result in water and nutrient loss from the smaller xylem elements only. Thus the overall risk of resource loss through the tip would be greater if the largest xylem elements were open near the tip of the root.

There is considerably less data on the morphology of first order branches. The only extensive and detailed study is that conducted by Varney et al. [132]. The authors divide the branch roots of maize into four different categories according to their radius. They determine which xylem elements are functioning using rhodamine B(0.001%) staining and epifluorescence. By conducting metric analysis of the micrographs presented, I was able to extract the data on xylem elements of first order roots. As we can see in Table 8.1, the variation in the axial hydraulic conductivity of first order branch roots can be very large, varying from 10^{-14} to 10^{-9} $\mathrm{m^4 s^{-1} MPa^{-1}}$. However, Varney et al. [132] note that the majority of first order branches fall into Class 1 and 2 (approximately 76% of total number of roots measured). They also mention that sometimes the Class 1 first order lateral roots can have one large late metaxylem element, thus making them similar to Class 2 first order lateral branches.

Order	$d = 2a$	d_E	n_E	d_L	n_L	$k_{x,E}$	$k_{x,E+L}$	Ref.
	μm	μm		μm		$\mathrm{m^4 s^{-1} MPa^{-1}}$	$\mathrm{m^4 s^{-1} MPa^{-1}}$	
Zero	1000	27.4	16.2	92.3	6.6	1.875×10^{-10}	1.198×10^{-8}	[43],[133]
First								
Class 1	200	5	3	-	-	4.6×10^{-14}	4.6×10^{-14}	[132]
Class 2	350	9.7	5	20	1	10^{-12}	5×10^{-12}	[132]
Class 3	525	13	6	55	1	4.2×10^{-12}	2.28×10^{-10}	[132]
Class 4	625	27	9	61	3	1.2×10^{-10}	10^{-9}	[132]

Table 8.1: Properties of xylem elements of zero and first order roots. First order roots are divided into four different classes as in [132], where a is the radius of the root, i.e., $d = 2a$ is the diameter of the root, d_E is the diameter of early metaxylem elements, n_E is the number of early metaxylem elements per cross sectional area, d_L is the diameter of late metaxylem elements, n_L is the number of late metaxylem elements, $k_{x,E}$ is the hydraulic conductivity calculated using Poiseuille law (see Section 7.4.1 Chapter 7) assuming that only early metaxylem elements are functioning, and $k_{x,E+L}$ is the hydraulic conductivity calculated assuming that early and late metaxylem elements are all functioning.

8.2 Root System Internal Pressure Variation

We begin by modelling the pressure distribution inside the root branching structure. For simplicity we consider the root branching structure to consist of two orders of roots only, i.e., zero and first order. It is possible to extend this theory to include more orders, but this would make the analysis more complicated and less transparent. It must also be noted that there are few data available on the morphological properties of second order branches and the xylems within them. Varney et al. [132], who conducted the study into the structure of first order lateral branches, note that there were not very many second order branches present in soil grown maize plants.

8.2.1 First Order Root Internal Pressure and Water Uptake

To model the pressure variation inside the first order roots we assume that the xylem tubes of first order roots connect up to the xylem tubes of zero order roots in such a way that the pressure is continuous across the branch-point. We will also hypothesise that similarly to the zero order roots, the first order lateral branch late metaxylem elements are not active in their apical non-branching region. As discussed earlier, this has been shown to be true for zero order branches and nodal roots [43], [117].

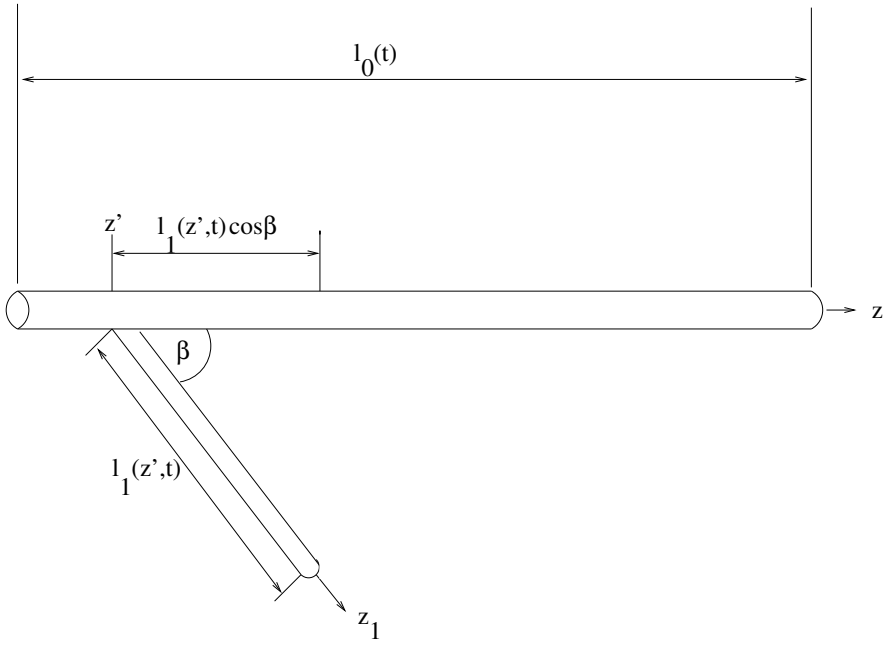

Figure 8.2: Root branching structure, where β is the branching angle, l_0 and l_1 are the length of zero and first order root respectively, and z' is the branch-point.

The pressure variation along the first order root growing out from branch point at $z = z'$ in direction z_1 (see Figure 8.2) is given, by analogy with the model presented in Chapter 7 for a single root, by

$$2\pi a_1 k_{r,1}(p - p_{r,1}) = -k_{x,1}\frac{\partial^2 p_{r,1}}{\partial z_1^2}, \tag{8.1}$$

where $p_{r,1}$ is the water pressure inside the first order root, p is the water pressure in the soil, $k_{r,1}$ and $k_{x,1}$ are the radial and axial conductivities of first order roots. The axial conductivity is given by

$$k_{x,1} = \begin{cases} k_{x,E+L} & \text{for} \quad 0 \le z_1 < l_1(z',t) - l_{a,1} \\ k_{x,E} & \text{for} \quad l_1(z',t) - l_{a,1} \le z_1 \le l_1(z',t) \end{cases} \tag{8.2}$$

where $k_{x,E}$ and $k_{x,E+L}$ are the values of conductivity for first order roots presented in Table 8.1. The boundary conditions for equation (8.1) are given by

$$p_{r,1} = p_{r,0}(z',t) \quad \text{at} \quad z_1 = 0 \quad \text{and} \quad \frac{\partial p_{r,0}}{\partial z_1} = 0 \quad \text{at} \quad z_1 = l_1(z',t). \tag{8.3}$$

Writing $z_1 = (z - z')/\cos\beta$ we get that

$$2\pi a_1 k_{r,1}(p - p_{r,1}) = -k_{x,1}\cos^2\beta\frac{\partial^2 p_{r,1}}{\partial z^2}, \tag{8.4}$$

with

$$p_{r,1} = p_{r,0}(z',t) \quad \text{at} \quad z = z' \quad \text{and} \quad \frac{\partial p_{r,0}}{\partial z} = 0 \quad \text{at} \quad z = z' + l_1(z',t)\cos\beta, \tag{8.5}$$

where $l_1(z',t)$ is the length of the first order branch emerging from the branching point at z' at time t. As in Chapter 6 it is given by

$$l_1(z',t) = K_1\Big[1 - e^{-r_1 t/K_1}(1 - \frac{z' + l_{a,0}}{K_0})^{-\frac{r_1 K_0}{r_0 K_1}}\Big] \quad \text{for} \quad t \ge t_0(z'), \tag{8.6}$$

where $t_0(z')$, the time of creation of first order branch at position z', is given by

$$t_0(z') = -\frac{K_0}{r_0}\ln(1 - \frac{z' + l_{a,0}}{K_0}). \tag{8.7}$$

Dimensionless First Order Equation

To obtain the dimensionless equation for first order internal pressure we choose the length scale to be equal to the maximum length of the zero order root, and the pressure scales for $p_{r,1}$ and p to be the same, i.e., we choose

$$z = K_0 z^*, \quad p = [p]p^*, \quad p_{r,1} = [p]p^*_{r,1}, \quad p_{r,0} = [p]p^*_{r,0}. \tag{8.8}$$

Use of this gives the following dimensionless equation after dropping the stars(*)

$$\frac{\kappa_1^2}{\cos^2\beta}[p - p_{r,1}] = -\frac{\partial^2 p_{r,1}}{\partial z^2}, \tag{8.9}$$

where $\kappa_1^2 = 2\pi a_1 k_{r,1} K_0^2 / k_{x,1}$ is the dimensionless first order root water uptake parameter. The different values of κ_1^2 for non-branching zones and branching zone are presented in Table 8.2, i.e.,

$$\kappa_1^2 = \begin{cases} \kappa_{1,E+L}^2 & \text{for} \quad z' \le z < z' + [l_1(z',t) - l_{a,1}]\cos\beta \\ \kappa_{1,E}^2 & \text{for} \quad z' + [l_1(z',t) - l_{a,1}]\cos\beta \le z \le z' + l_1(z',t)\cos\beta \end{cases} \tag{8.10}$$

First order classes	$\kappa_{1,E}^2$	$\kappa_{1,E+L}^2$
1	4240	4240
2	195	39
3	46	0.86
4	1.625	0.195

Table 8.2: Dimensionless parameters κ_1^2 for apical and basal regions of the different classes of first order maize plants using the data for axial conductivity presented in Table 8.1.

The dimensionless boundary conditions are

$$p_{r,1} = p_{r,0} \quad \text{at} \quad z = z', \quad \text{and} \quad \frac{\partial p_{r,1}}{\partial z} = 0 \quad \text{at} \quad z = z' + l_1(z',t)\cos\beta. \tag{8.11}$$

We note that $\kappa_1^2 >> 1$ for class 1 and 2 roots, but can be order one or less for class 3 and 4 roots. However, Varney et al. [132] point out that approximately 76% of the 3510 branches they measured fell into class 1 and 2. Thus, class 3 and 4 roots are very rare, and we will neglect them in this chapter [2].

The water diffusional length-scale over 1 day for relative soil water saturation levels $S >> 0.01$ is much larger than maximum length (8 cm) of a first order branch. Thus we can assume that along each first order root the relative water saturation is approximately constant. Therefore we solve the above equation for $p_{r,1}$ analytically for p constant and find that first order lateral branch internal pressure is given by

$$\begin{aligned} p_{r,1}(z) &= p(z) + \frac{\sinh(\frac{\kappa_1}{\cos\beta}(z - z'))}{\sinh(\frac{\kappa_1}{\cos\beta}(l_1 - l_{a,1}))}\Big[\cosh(\frac{\kappa_1}{\cos\beta}(l_1 - l_{a,1}))(p(z) - p_{r,0}(z')) + \\ &+ A - p(z)\Big] + (p_{r,0}(z') - p(z))\cosh(\frac{\kappa_1}{\cos\beta}(z - z')), \\ &\quad \text{for} \quad z' < z < (l_1 - l_{a,1})\cos\beta \end{aligned} \tag{8.12}$$

[2] When $\kappa_1^2 l_1^2 << 1$, as for Class 3 and 4 roots, then at the leading order $-\frac{\partial^2 p_{r,1}}{\partial z^2} \approx 0$ and thus $p_{r,1}(z) \approx p_{r,0}(z')$, i.e., in this case the first order root internal pressure is equal to the zero order internal pressure at the branch-point.

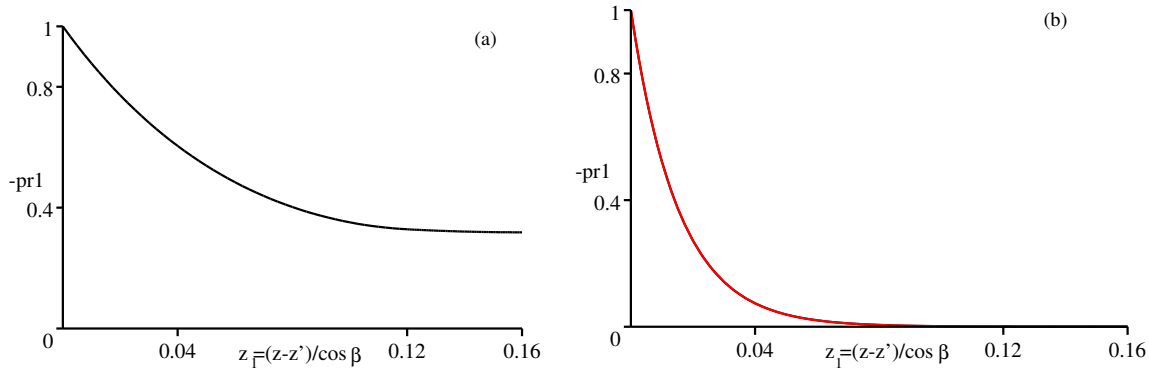

Figure 8.3: Solution of equation (8.9) for first order branch for $p = 0$ everywhere in soil and $p_{r,0} = -1$ at the branch-point at $z = z'$. (a) is the solution for class 2 branches, i.e., for $\kappa_{1,E} = 195$ and $\kappa_{1,E+L} = 39$. (b) is the solution for class 1 branches with $\kappa_{1,E} = \kappa_{1,E+L} = 4240$; black line shows the solution given by equations (8.12)-(8.13) and the red line is the boundary layer solution given by (8.17). The dimensionless length $z_1 = (z - z')/\cos\beta = 0.16$ corresponds to a dimensional length of 8 cm.

and

$$\begin{aligned} p_{r,1}(z) &= p(z) + (p(z) - A)\sinh(\frac{\kappa_{11}}{\cos\beta}(z - z'))\frac{(e^{2\kappa_{11}l_1} - 1)e^{-\kappa_{11}(l_1 - l_{a,1})}}{1 + e^{2\kappa_{22}l_{a,1}}} - \\ &- (p(z) - A)\cosh(\frac{\kappa_{11}}{\cos\beta}z)\frac{e^{-\kappa_{11}(l_1 - l_{a,1})}(e^{2\kappa_{11}l_1} + 1)}{1 + e^{2\kappa_{11}l_{a,1}}}, \\ &\text{for} \quad (l_1 - l_{a,1})\cos\beta < z < l_1\cos\beta, \end{aligned} \tag{8.13}$$

where A is determined from patching the slope of the solutions at $z = (l_1 - l_{a,1})\cos\beta$, i.e., from $\left[\frac{\partial p_{r,1}}{\partial z}\right]_-^+ = 0$ at $z = (l_1 - l_{a,1})\cos\beta$. The solution for Class 2 roots is shown on Figure 8.3 (a).

For Class 1 first order lateral branches we can derive an even simpler expression for the internal pressure[3] using the fact that $\kappa_1^2 l_0^2/\cos^2\beta >> 1$. Thus, at the leading order $p_{r,1}(z) \approx p(z)$, except at the thin boundary layer region near the branch-point $z = z'$ (see Figure 8.3 (b) for solution when $p = 0$ everywhere). Changing to the boundary layer variable $\xi = (z - z')/\epsilon_\kappa$, where $\epsilon_\kappa = \cos\beta/\kappa_1 << 1$, the boundary layer equation becomes

$$-\frac{\partial^2 p_{r,1}}{\partial\xi^2} = p(z) - p_{r,1}(\xi), \tag{8.14}$$

with

$$p_{r,1} = p_{r,0} \quad \text{at} \quad \xi = 0, \quad p_{r,1} \to p \quad \text{as} \quad \xi \to \infty. \tag{8.15}$$

[3]We cannot derive the simplified expression for Class 2 first order lateral branches since in this case $\kappa_1^2 l_0^2/\cos^2\beta \sim O(1)$.

Thus for $p(z) \sim p(z') + O(\epsilon_\kappa)$ in equation (8.14) we find, that the leading order solution to $p_{r,1}$ is given by

$$p_{r,1}(\xi) = p(z) + [p_{r,0}(0) - p(0)]e^{-\xi}, \tag{8.16}$$

i.e.,

$$p_{r,1}(z) = p(z) + [p_{r,0}(z') - p(z')]e^{-(z-z')/\epsilon_\kappa}. \tag{8.17}$$

We also note that the boundary layer thickness is of order $\cos\beta/\kappa_1 \approx 7.6 \times 10^{-3}$ which is less than the dimensionless inter-branch distance $\approx 1.4 \times 10^{-2}$. Thus, at any interval $(z, z + dz)$ along the zero order root there is only one Class 1 branch contributing to the overall water uptake.

For both Class 1 and 2 first order lateral branches, the dimensional flux of water across $z = z'$, i.e., from first order into the zero order, is given approximately by

$$f_1 \approx \frac{k_{x,1}}{K_0}\frac{\partial p_{r,1}}{\partial z}\Big|_{z=z'} = -\frac{k_{x,1}}{\epsilon_\kappa K_0}[p_{r,0}(z') - p(z')]. \tag{8.18}$$

We can see that most of the water uptake occurs near the branch point. This is due to the limitations for water transport along the root. With the decrease in the root radius, the radial conductivity of first order root increases, thus making the water flow into the root easier, but the axial conductivity decreases (i.e., overall κ_1 increases) making the transport of water along the root more difficult. This gives rise to a water movement limitation inside the root system resulting in reduced water uptake near the tip region. Thus most of the water gets taken up in the region where it is easiest to transport it axially, i.e., near the branch point from where the water can be transported into the zero order root with larger radius and larger xylem elements.

8.2.2 Zero Order Root Internal Pressure

The zero order root internal water pressure $p_{r,0}$ was given in Chapter 7 by equation (7.34). In the derivation of this equation we only included the water flowing into the root from the soil. In the case of the root system we have to account also for the contribution of water flowing from first order roots into the zero order root. The contribution by a sub-branch at position z' is approximately given by equation (8.18) and thus the inflow of water into a zero order root is given by $2\pi a_0 k_{r,0} + \psi_1(z)f_1(z)$, where $\psi_1(z)$ is the distribution of first order branch-points on zero order root and $f_1(z)$ is the inflow of water from first order branch at z into the zero order root. Thus, the equation for the zero order internal pressure becomes,

$$[2\pi a_0 k_{r,0} + \psi_1(z)\frac{k_{x,1}}{\epsilon_\kappa K_0}](p - p_{r,0}) = -k_{x,0}\frac{\partial^2 p_{r,0}}{\partial z^2}, \tag{8.19}$$

where a_0 is the radius of the zero order root, p is the water pressure in the soil, and $k_{r,0}$ and $k_{x,0}$ are the radial and axial conductivities of zero order roots respectively. The quantity $\psi_1(z)$ describes the piece-wise continuous distribution of first order lateral branch-points on the zero order root, i.e., in branching region $\psi_1 = 1/l_{n,0}$, where $l_{n,0}$ is the inter-branch distance, and $\psi_1 = 0$ in non-branching regions. The boundary conditions for zero order roots are given by

$$p_{r,0} = T \quad \text{at} \quad z = 0 \quad \text{and} \quad \frac{\partial p_{r,0}}{\partial z} = 0 \quad \text{at} \quad z = l_0(t), \tag{8.20}$$

where T is the water pressure at the base of the root and l_0 is the length of the zero order root. As in Chapters 4-6, the length of the zero order root, $l_0(t)$, is given by

$$l_0(t) = K_0(1 - e^{-r_0 t/K_0}), \tag{8.21}$$

where K_0 is the maximum length of the zero order root and r_0 is the initial growth rate of a zero order root[4].

Dimensionless Zero Order Equation

Use of the same scaling (8.8) as for first order roots results in the following dimensionless equation for the zero order root internal pressure variation

$$[\kappa_0^2 + \kappa_{00}^2 \psi(z)](p - p_{r,0}) = -\frac{\partial^2 p_{r,0}}{\partial z^2}, \tag{8.22}$$

with

$$p_{r,0} = \frac{T}{[p]} \quad \text{at} \quad z = 0, \quad \frac{\partial p_{r,0}}{\partial z} = 0 \quad \text{at} \quad z = l_0(t) = 1 - e^{-\nu_0 t}, \tag{8.23}$$

where $\kappa_0^2 = 2\pi a_0 k_{r,0} K_0^2 / k_{x,0}$ is the dimensionless water uptake parameter for zero order roots, and $\kappa_{00}^2 = k_{x,1} K_0 / (\epsilon_\kappa k_{x,0} l_{n,0})$ is the first order root water contribution dimensionless parameter, where $l_{n,0}$ [cm] is the first order inter-branch distance. The dimensionless piece-wise constant branch-point distribution is given by $\psi(z) = 1$ for the branching region and $\psi(z) = 0$ for non-branching regions. The zero order root dimensionless elongation parameter is $\nu_0 = r_0[t]/K_0$, where $[t]$ is the time-scale to be specified later.

Using data presented in Table 8.1 we find that $\kappa_0^2 \approx 0.016$ in the branching region and $\kappa_0^2 \approx 0.871$ in the apical non-branching region. For Class 1 first order

[4]The elongation rate at time t is given by $dl_0/dt = r_0(1 - l_0(t)/K_0)$, where $l_0(t)$ is the length of the root at time t.

branches $\kappa_{00}^2 \approx 0.035$ and for Class 2 branches $\kappa_{00}^2 \approx 0.375$. Thus the value of overall conductivity in different regions for zero order root with Class 1 branches is

$$\kappa_0^2 + \psi(z)\kappa_{00}^2 = \begin{cases} 0.052 & \text{for} \quad 0 \leq z < l_0(t) - l_{a,0}, \\ 1.04 & \text{for} \quad l_0(t) - l_{a,0} \leq z \leq l_0(t), \end{cases} \tag{8.24}$$

and with Class 2 branches

$$\kappa_0^2 + \psi(z)\kappa_{00}^2 = \begin{cases} 0.537 & \text{for} \quad 0 \leq z < l_0(t) - l_{a,0}, \\ 1.04 & \text{for} \quad l_0(t) - l_{a,0} \leq z \leq l_0(t). \end{cases} \tag{8.25}$$

Approximations to $p_{r,0}$

As we can see the two water uptake parameters, κ_0 and κ_{00}, for zero order roots are of order 1 or less. This makes the analysis of the model somewhat more complicated. However, if we map the moving boundary given by $z = l_0(t)$ into the fixed boundary at $\zeta = z/l_0(t) = 1$ we transform the above equation into

$$-\frac{\partial^2 p_{r,0}}{\partial \zeta^2} = l_0^2(t)[\kappa_0^2 + \kappa_{00}^2 \psi(\zeta)](p - p_{r,0}), \tag{8.26}$$

with

$$p_{r,0} = \frac{T}{[p]} \quad \text{at} \quad \zeta = 0, \quad \frac{\partial p_{r,0}}{\partial \zeta} = 0 \quad \text{at} \quad \zeta = 1. \tag{8.27}$$

Let us assume that there are no first order lateral branches, i.e., $\psi(z) = 0$ everywhere. Then for times such that $l_0^2\kappa_0^2 << 1$, the leading order approximation to the equation (8.26) is given by $-\frac{\partial^2 p_{r,0}}{\partial \zeta^2} \approx 0$, and thus $p_{r,0} \approx T/[p]$ (see also Figure 8.4 for solution to $p_{r,0}$ for $p = 0$ and $T/[p] = -1$, where $\psi(z)$ is piecewise constant).

However, when $l_0^2\kappa_0^2 \approx 1$ the relative water saturation, and hence also water pressure, in the soil will start influencing the root internal water pressure. Thus, we will solve the equation for zero order root internal pressure numerically simultaneously with the numerical solution to water movement in the soil.

8.2.3 Water Uptake per Unit Volume of Soil

In the previous sections of this chapter we described how to calculate the first and zero order internal pressure as a function of soil water pressure p. Using this information we are now in a position to describe the water uptake by plant root distributions, when the internal pressure distribution and the length density of roots are known. We will consider the variation in root length density and resulting water uptake in the direction of soil depth only, i.e., z, and take the volume element dV in that direction to be given by $dV = \pi(a_0 + K_1 \cos\beta)^2 dz$, were a_0 is the radius of zero order root, K_1

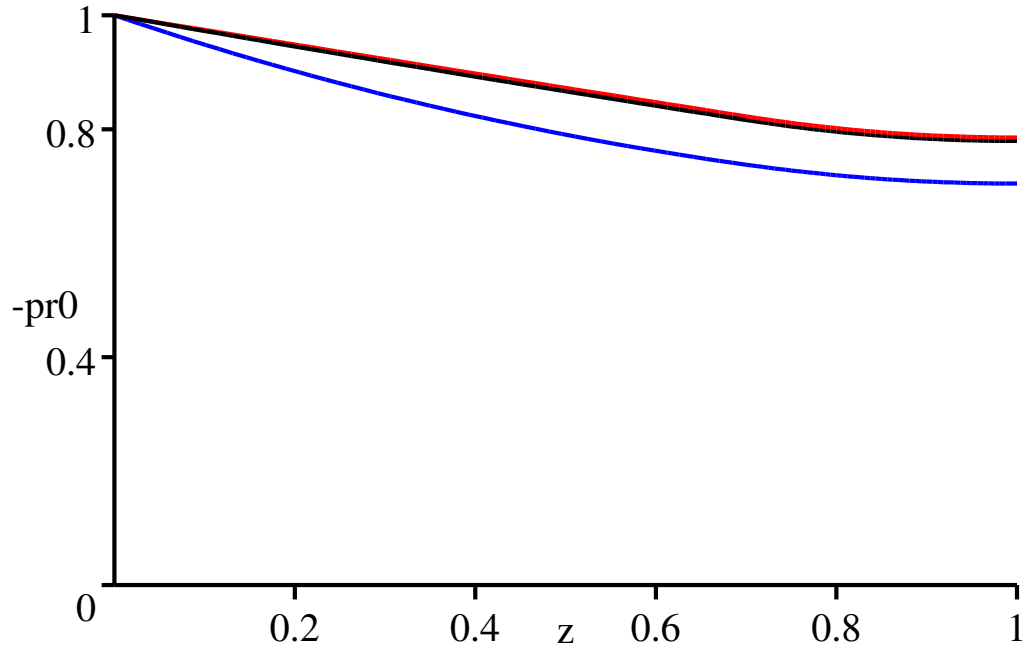

Figure 8.4: Zero order root internal pressure $p_{r,0}$ for uniform external pressure $p = 0$. Red line shows the solution in absence of lateral branches, black line shows the solution in presence of Class 1 first order lateral branches and blue line shows the solution in presence of Class 2 lateral branches.

is the length of the zero order root and β is the branching angle (see the Figure 6.6 in Chapter 6 for graphical description of this). This situation corresponds to a field crop in which case there is very little horizontal variation in the root length density.

As discussed in Chapter 7, Section 7.9, the water profile around each individual root is almost flat, but the small disturbance due to the water uptake will spread over a large region since the water diffusional length scale is very large (much larger than inter-root distance). Thus the competition for water between sub-branches is very strong. Since the profile is flat around each root, the limiting factor in the root system water uptake is expected to be the long range water movement within the rooting region in the soil. Therefore, we can take the uptake by zero and first order branches to be proportional to $(p - p_{r,0})$ and $(p - p_{r,1})$, respectively. Analogously to the results presented in Chapter 6 for the nutrient uptake by the developing root system, we find that for vertical variation in the root length density (see Chapter 6, Section 6.3, Figure 6.6) the water uptake by zero order roots will be given by

$$F_0(z) = \frac{2\pi a_0 dz k_{r,0}(p - p_{r,0})}{dV} = \frac{2\pi a_0 k_{r,0}(p - p_{r,0})}{\pi(a_0 + K_1 \cos\beta)^2}, \tag{8.28}$$

where $2\pi a_0 dz$ is the surface area of zero order root per unit volume of soil dV. For first order branches we have to integrate over all branches reaching position z, i.e.,

similarly to nutrient calculation presented in Chapter 6 we write

$$F_1(z) = \frac{2\pi a_1 k_{r,1}}{\pi(a_0 + K_1 \cos\beta)^2 \cos\beta} \int_{\hat{z}}^{z} [p(z) - p_{r,1}(z, z')]\psi_1(z')\, dz', \tag{8.29}$$

where $p_{r,1}$ in general is given by equations (8.12)-(8.13).

For zero order roots, with only Class 1 first order lateral branches, the above equation simplifies even further since we found that the thickness of the boundary layer where the water uptake occurs, i.e., the layer where $p_{r,1} \not\approx p$, is an order of magnitude less than the average inter-branch distance. Thus, at $(z, z + dz)$ the only contribution to water uptake is from the branch-point in that section. Since in the boundary layer $p_{r,1} \approx p_{r,0}$ we have

$$F_1(z) \approx \frac{2\pi a_1 k_{r,1}\psi_1(z)}{\pi(a_0 + K_1 \cos\beta)^2 \cos\beta}[p(z) - p_{r,0}(z)], \tag{8.30}$$

and therefore for a zero order root with only Class 1 first order lateral branches the overall water uptake F by the plant is given by

$$F = F_0 + F_1 = \Big[\frac{2\pi a_0 k_{r,0}}{\pi(a_0 + K_1 \cos\beta)^2} + \frac{2\pi a_1 k_{r,1}\psi_1}{\pi(a_0 + K_1 \cos\beta)^2 \cos\beta}\Big](p(z) - p_{r,0}(z)). \tag{8.31}$$

8.3 Darcy-Richard's Equation

According to the conservation of water per unit volume of soil with the volumetric sink, F, representing the water uptake by the roots per unit volume of soil, we have the following dimensional equation for the relative water saturation in the soil (see Chapter 8)

$$\phi\frac{\partial S}{\partial t} = \frac{\partial}{\partial z}[D_0 D(S)\frac{\partial S}{\partial z}] - K_s\frac{\partial k(S)}{\partial z} - F(S, z, t), \tag{8.32}$$

where

$$D_0 = \frac{\rho g k_s}{\mu}\frac{(1-m)}{\alpha m} \quad \text{and} \quad K_s = \frac{\rho g k_s}{\mu} \quad \text{and,} \tag{8.33}$$

$$D(S) = S^{1/2-1/m}[(1 - S^{1/m})^{-m} + (1 - S^{1/m})^m - 2] = m^2 S^{1/2+1/m} + m^2 S^{1/2+2/m} + \cdots, \tag{8.34}$$

$$k(S) = S^{1/2}[1 - (1 - S^{1/m})^m]^2 = m^2 S^{1/2+2/m} - m^2(\frac{2}{3} - m)S^{1/2+3/m} + \cdots. \tag{8.35}$$

In the above equations ϕ is the porosity of the soil[5], k_s is the conductivity of saturated soil, μ is the viscosity of water, K_s is the hydraulic conductivity of soil, α

[5]For simplicity we will take the relative water saturation S in the soil to be given by $S = \phi_l/\phi$, i.e., we neglect the minimum residual water content ϕ_r as used in Chapter 7, since it is generally quite low and thus negligible.

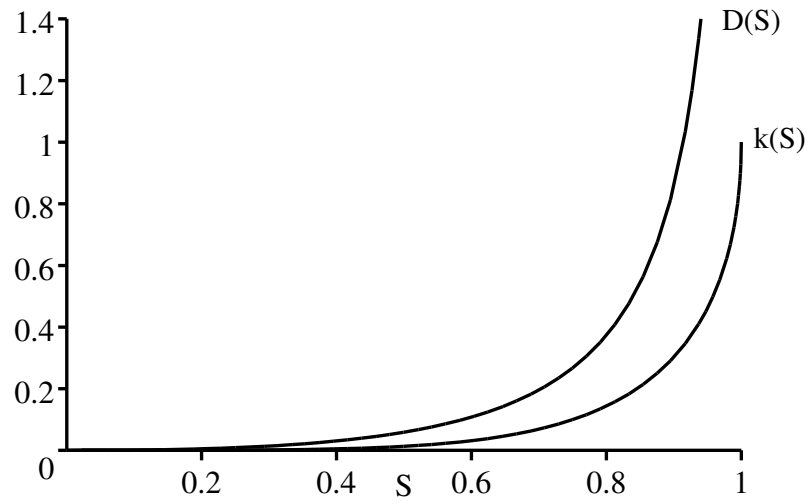

Figure 8.5: Soil water diffusivity $D(S)$ and convection $k(S)$, given by equations (8.34) and (8.35) respectively, as a function of water saturation for typical Loam soil (as used in numerical experiments presented in Figure 8.7).

and m are the suction characteristic parameters, i.e., soil water pressure p is assumed to be given by the van Genuchten expression $p = -(\rho g/\alpha)[S^{-1/m} - 1]^{1/n}$, where ρ is the density of water, g is the gravitational constant, and $F(S, z, t)$ is the volume of water removed by the root system per unit volume of soil at position z.

Boundary Condition

At the surface of the soil we will prescribe the rate of rainfall W to be equal to the flux of water into the soil, i.e., we neglect surface water evaporation at this stage. Thus,

$$-D_0 D(S)\frac{\partial S}{\partial z} + K_s k(S) = W_{\mathrm{DIM}} \quad \text{at} \quad z = 0, \tag{8.36}$$

where W_{DIM} is the volume flux of water per unit soil surface area per unit time.

Next we have to specify the boundary condition at the bottom of the soil (or at the bottom of the experimental growth box). Many ground-water textbooks deal with models for determining the position of the water table, i.e., the position of the fully saturated soil, from the geological description of the soil and surrounding geophysical profile [8], [9]. However, as a simpler alternative we can use the zero flux or full saturation boundary condition at the bottom of the growing box. Both of these boundary conditions are motivated by experimental conditions: (a) zero flux corresponds to the plant growth pot that is sealed at the bottom so that no water leaks in or out from the pot [44]; (b) full saturation boundary condition corresponds to an experiment where the growing pot is seated in the water reservoir which is constantly topped up so that the soil at a given level is always fully saturated [45].

The zero flux boundary condition at the bottom boundary of the growing box [44] is given by

$$-D_0 D(S)\frac{\partial S}{\partial z} + K_s k(S) = 0 \quad \text{at} \quad z = l_w, \tag{8.37}$$

and constant saturation at the bottom of the growing box [45] or in the field [134], is given by

$$S = 1 \quad \text{at} \quad z = l_w. \tag{8.38}$$

For simplicity we will investigate the problem with a zero flux boundary condition (8.37) only, since this means that we will be studying the interaction between rainwater and water uptake by roots only. This implies that we will be neglecting the additional component of water flux into the rooting region from the groundwater.

In this thesis we set out to study the nutrient uptake by plant roots and possible pollution of ground water by residual fertiliser. Thus we will be concerned with the fluxes of water and nutrient from top of the soil to bottom and not *vice versa*.

Initial Condition

We take the initial saturation profile to be constant, i.e.,

$$S = S_\infty \quad \text{for} \quad 0 < z < l_w. \tag{8.39}$$

8.3.1 Non-dimensionalisation

We non-dimensionalise the system by choosing the length-scale to be equal to the length of the longest root in the system, i.e., the maximum length of the zero order root $K_0 = 50$ cm. Hence, by choosing

$$z = K_0 z^*, \quad t = [t]t^* \quad \text{with} \quad [t] = \frac{\phi\alpha m K_0^2}{K_s(1-m)}, \quad p_{r,i} = |T|p^*_{r,i} \quad i = 0, 1, \quad p = |T|p^*, \tag{8.40}$$

where $K_s = k_s\rho g/\mu$ is the hydraulic conductivity of fully saturated soil, we get the resulting dimensionless equation

$$\frac{\partial S}{\partial t} = \frac{\partial}{\partial z}[D(S)\frac{\partial S}{\partial z} - \epsilon k(S)] - F(S, z, t), \tag{8.41}$$

where

$$D(S) = S^{1/2-1/m}[(1 - S^{1/m})^{-m} + (1 - S^{1/m})^m - 2], \tag{8.42}$$

$$k(S) = S^{1/2}[1 - (1 - S^{1/m})^m]^2. \tag{8.43}$$

As before the parameter $\epsilon = \alpha(n-1)K_0$ for typical loam soil and maximum root length 50 cm is of order $0.2 - 1.51$ (see Table 8.3).

8.3.2 Dimensionless Boundary Conditions

The boundary condition at the top of the soil becomes

$$-D(S)\frac{\partial S}{\partial z} + \epsilon k(S) = W \quad \text{on} \quad z = 0, \tag{8.44}$$

where $W = W_{\rm DIM} K_0 \alpha m/[K_s(1-m)]$ is the dimensionless rate of rainfall.

At the bottom boundary we simply have

$$-D(S)\frac{\partial S}{\partial z} + \epsilon k(S) = 0 \quad \text{on} \quad z = l_w^* = l_w/K_0. \tag{8.45}$$

8.3.3 Dimensionless Water Uptake $F(S,z)$

In the case of a zero order root with first order lateral branches that fall into the Class 1 category[6] only, the dimensionless water uptake term is given by

$$F = \lambda_w[p - p_{r,0}], \quad \text{with} \quad p = -\epsilon_0(S^{-1/m} - 1)^{1/n}, \tag{8.46}$$

where $\epsilon_0 = \rho g/(\alpha|T|)$ and

$$\begin{aligned} \lambda_w &= |T|\frac{2\pi a_0 k_{r,0} l_{n,0}\cos\beta + 2\pi a_1 k_{r,1} K_0}{\pi(a_0 + K_1\cos\beta)^2 l_{n,0}\cos\beta}\Big[\frac{\alpha m K_0^2}{K_s(1-m)}\Big], \\ &= \frac{2a_0 k_{r,0}(l_{n,0}\cos\beta + K_0)|T|}{(a_0 + K_1\cos\beta)^2 l_{n,0}\cos\beta}\Big[\frac{\alpha m K_0^2}{K_s(1-m)}\Big], \end{aligned} \tag{8.47}$$

since $a_0 k_{r,0} = a_1 k_{r,1}$ =constant.

The root internal pressure $p_{r,0}$ in above equation satisfies equation (8.22) with boundary condition (8.23) at $z = 0$ calculated with $[p] = |T|$, i.e.,

$$[\kappa_0^2 + \kappa_{00}^2\psi(z)](p - p_{r,0}) = -\frac{\partial^2 p_{r,0}}{\partial z^2}, \tag{8.48}$$

$$p_{r,0} = -1 \quad \text{at} \quad z = 0, \quad \frac{\partial p_{r,0}}{\partial z} = 0 \quad \text{at} \quad z = l_0(t) = 1 - e^{-\nu_0 t}, \tag{8.49}$$

8.4 Values of Dimensionless Parameters

The dimensionless Darcy-Richard-van Genuchten model has the following dimensionless parameters in it: ϵ is the convection parameter that quantifies the relative importance of convection with respect to diffusion; W is the dimensionless rainfall parameter which in general can be either very small or very large depending on the climatic

[6]The Class 1 category of first order lateral branches is characterised by the absence of open functioning late metaxylem vessels. Thus there are only early metaxylem vessels present in those roots (see also Table 8.1). Early metaxylem vessels are much thinner than late metaxylem vessels, and therefore their axial conductivity is lower. Dimensionless conductivity of Class 1 branches is $\kappa_1 l_1 >> 1$, thus they take up water only near the branch point.

conditions; l_w^* is the dimensionless ground-water depth; λ_w is the dimensionless water uptake parameter for root system with Class 1 first order lateral branches only; ϵ_0 is the dimensionless van Genuchten parameter, i.e., $S = [1 + (-p/\epsilon_0)^n]^{-m}$.

Parameter	ϵ	λ_w	ϵ_0
Hygiene Sandstone	3	2.272	1.27×10^{-2}
Touchet Silt Loam G.E.3	1.51	0.329	2×10^{-2}
Silt Loam G.E.3	0.22	2.949	2.36×10^{-2}
Guelph Loam (drying)	0.59	1.131	8.7×10^{-3}
Guelph Loam (wetting)	1.76	3.645	5×10^{-3}
Beit Netofa Clay	1.9×10^5	10.31	6.58×10^{-2}

Table 8.3: The values of dimensionless parameters for the soil parameter values presented in Table 7.1 and $a_0 = 5 \times 10^{-4}$ [m], $a_1 = 2 \times 10^{-4}$ [m], $l_{n,0} = 10^{-2}$ [m] and $L = 0.5$ [m].

8.4.1 Dimensionless Rate of Rainfall

The magnitude of the dimensionless rainfall parameter $W = W_{\rm DIM}\frac{K_0\alpha(n-1)}{K_s}$ depends on the average rainfall rate W. For example the average rainfall in England is less than 1 m year^{-1}, i.e., on average $W \approx O(10^{-2}) - O(10^{-3})$. However, during storm events $W_{\rm DIM}$ is much larger than average, and thus W can be large, resulting in ponding at the surface of the soil. When ponding occurs, then ideally, we should model the surface ponding and derive the boundary condition by considering the balance between surface runoff, accumulation of rainwater in the pond and vertical infiltration. However, since this chapter is concerned with the development of a mathematical model for the water uptake by root branching structures we will simplify this surface ponding calculation so that once the surface of the soil has become fully saturated due to the rainfall we take it to stay so, i.e., we modify the boundary condition given by (8.44) to

$$S = 1 \quad \text{at} \quad z = 0. \tag{8.50}$$

8.5 Numerical Experiments and Analytic Approximations

Due to complicated non-linearities in this model, we need to solve this system numerically. Without loss of generality we will present the results for the root system which has zero order roots with only Class 1 first order lateral branches. The water uptake by a root system that has only Class 1 first order lateral branches on a zero order root is less than the uptake by a root system that has only Class 2 branches, since the Class 2 branches have bigger xylem elements and thus can take up more water than Class 1 branches. Therefore, any behaviour in the system that is present in the root system with Class 1 first order lateral branches is also going to be present in a root system with Class 2 lateral branches, but it will occur on a shorter time-scale. However, since the model for the root system with Class 2 first order lateral branches is much more complicated, we will do the analysis and numerical simulations only for a root system with only Class 1 first order lateral branches.

Thus we recall that for Class 1 lateral branches the model in the rooting region is given by

$$\frac{\partial S}{\partial t} = \frac{\partial}{\partial z}[D(S)\frac{\partial S}{\partial z} - \epsilon k(S)] - F(S), \tag{8.51}$$

with

$$-D(S)\frac{\partial S}{\partial z} + \epsilon k(S) = W \quad \text{on} \quad z = 0. \tag{8.52}$$

In the non-rooting region, i.e., $z > l_0(t)$, where l_0 is the length of the zero order root, the sink term is zero, i.e., $F = 0$.

The form of $D(S)$, $k(S)$ and $F(S) = \lambda_w[-\epsilon_0(S^{-1/m} - 1)^{1/n} + 1]$ is shown on Figures 8.5 and 8.6. In soil science the term "permanent wilting point" is often used to describe the moisture conditions in the soil. It corresponds to the relative saturation in the soil when the test plant has wilted under defined conditions, such that it does not recover unless it is watered [3]. Typical values for the wilting point are in the range $p \approx -1.5$ MPa, i.e., corresponding to the relative saturation level $S \approx 0.01$ [51]. We see that the permanent wilting point corresponds approximately to the level of saturation when the water uptake by the plant stops, and the plant starts bleeding out water (see Figure 8.6).

Root internal pressure $p_{r,0}$ will be calculated from

$$-\frac{\partial^2 p_{r,0}}{\partial z^2} = [\kappa_0^2 + \kappa_{00}^2\psi(z)](p(S) - p_{r,0}), \tag{8.53}$$

with

$$p_{r,0} = -1 \quad \text{at} \quad z = 0, \quad \frac{\partial p_{r,0}}{\partial z} = 0 \quad \text{at} \quad z = l_0(t). \tag{8.54}$$

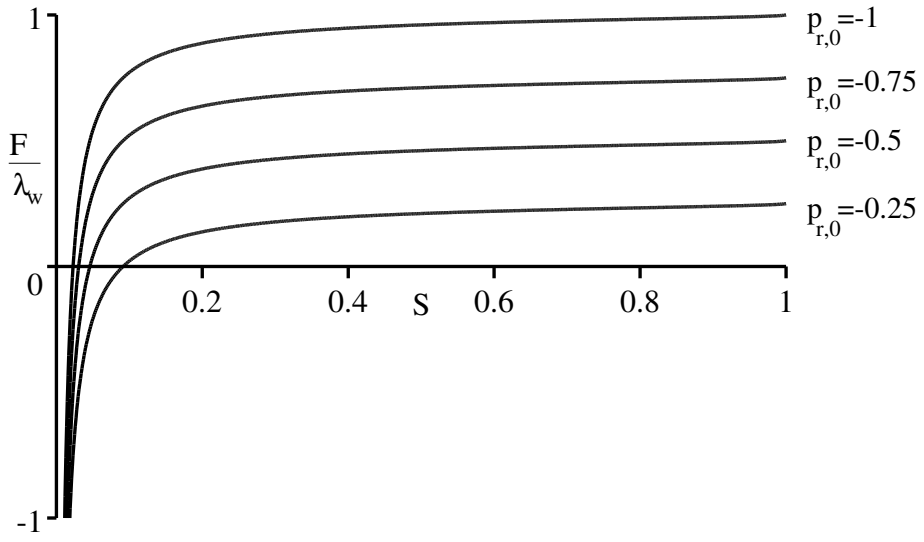

Figure 8.6: Water uptake term $F(S)$ as a function of water saturation for typical loam soil (as used in numerical experiments presented in Figure 8.7). Typical value of the permanent wilting point for plants is approximately $p \approx -1.5$ MPa, corresponding to $S \approx 0.01$ [51].

As a first approximation we are going to investigate the case when the rate of rainfall is constant, i.e., by averaging over a suitably chosen time period we can estimate the average rainfall during that period and thus investigate how it influences the water uptake by plant roots.

In Figures 8.7 and 8.8 we have presented the numerical solutions for two different rainfall W regimes and for various different initial saturation levels (red lines on Figure 8.7) for root system with zero order root and Class 1 first order lateral branches only. For numerical computation, we use the finite difference scheme with a central difference approximation to the diffusion term and upwind approximation to the convection term [87]. The non-linearity of diffusion is handled by introducing an extra iteration loop inside the main time iteration loop.

8.5.1 Low Water Mobility

To analyse this model we first determine at which water saturation level does the water diffusivity become smaller than the water uptake term[7] $\lambda_w|p_{r,0,\max}|$, i.e., when is $D(S) << \lambda_w|p_{r,0,\max}|$. For loam soil this is at the level $S << S_{\text{dif}} = 0.565$. Similarly we can ask when is the water uptake term larger than the convection term, i.e., when is $\epsilon k(S) << \lambda_w|p_{r,0,\max}|$, and for loam soil it is at the level $S << S_{\text{conv}} = 0.733$. Thus, for water saturation levels $S << S_{\text{dif}}$ (since $S_{\text{dif}} < S_{\text{conv}}$) the Darcy-Richard's

[7]See also Figures 8.5 and 8.6 for graphs of $F(S)$, $D(S)$ and $k(S)$ for different saturation levels S.

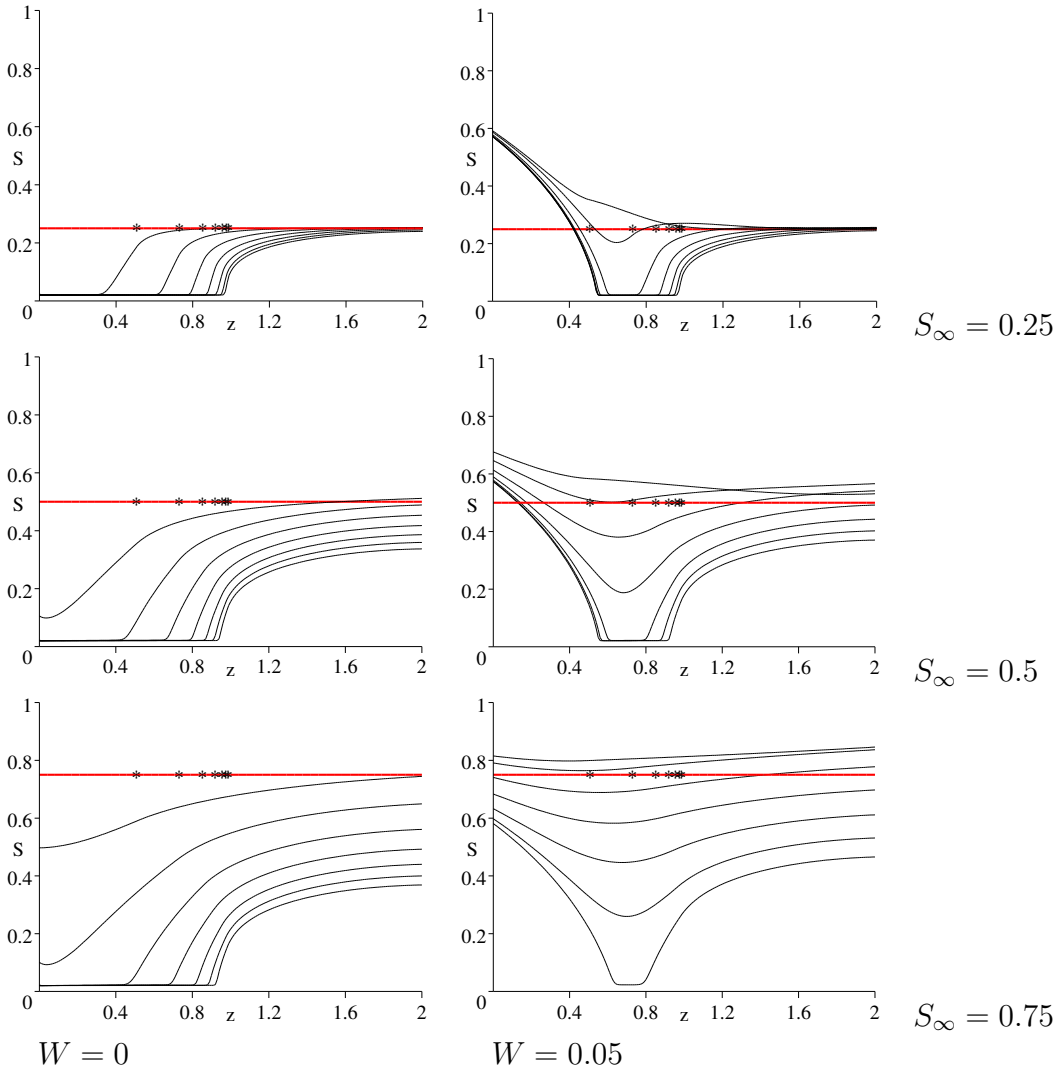

Figure 8.7: Water profile due to water uptake by a developing root system for different rainfall patterns, i.e., $W = 0$ corresponding no rainfall, and $W = 0.05$ corresponding to high average seasonal rainfall. The red line shows the initial condition, black lines correspond to times $t = 0.2$, 0.4, 0.6, 0.8, 1, 1.2, 1.4 months. Parameters are $\epsilon = 0.1$, $\lambda_w = 0.1$, $\epsilon_0 = 0.02$. The position of the zero order root tip is marked by $*$ for each relative saturation curve.

equation (8.51) simplifies at leading order to an ordinary differential equation for S, i.e.,

$$\frac{\partial S}{\partial \tau} \approx -\lambda_w[-\epsilon_0(S^{-1/m} - 1)^{1/n} - p_{r,0}], \tag{8.55}$$

with

$$S = S_\infty \quad \text{at} \quad \tau = 0, \tag{8.56}$$

where τ is time measured from the time the root tips have reached the position z.

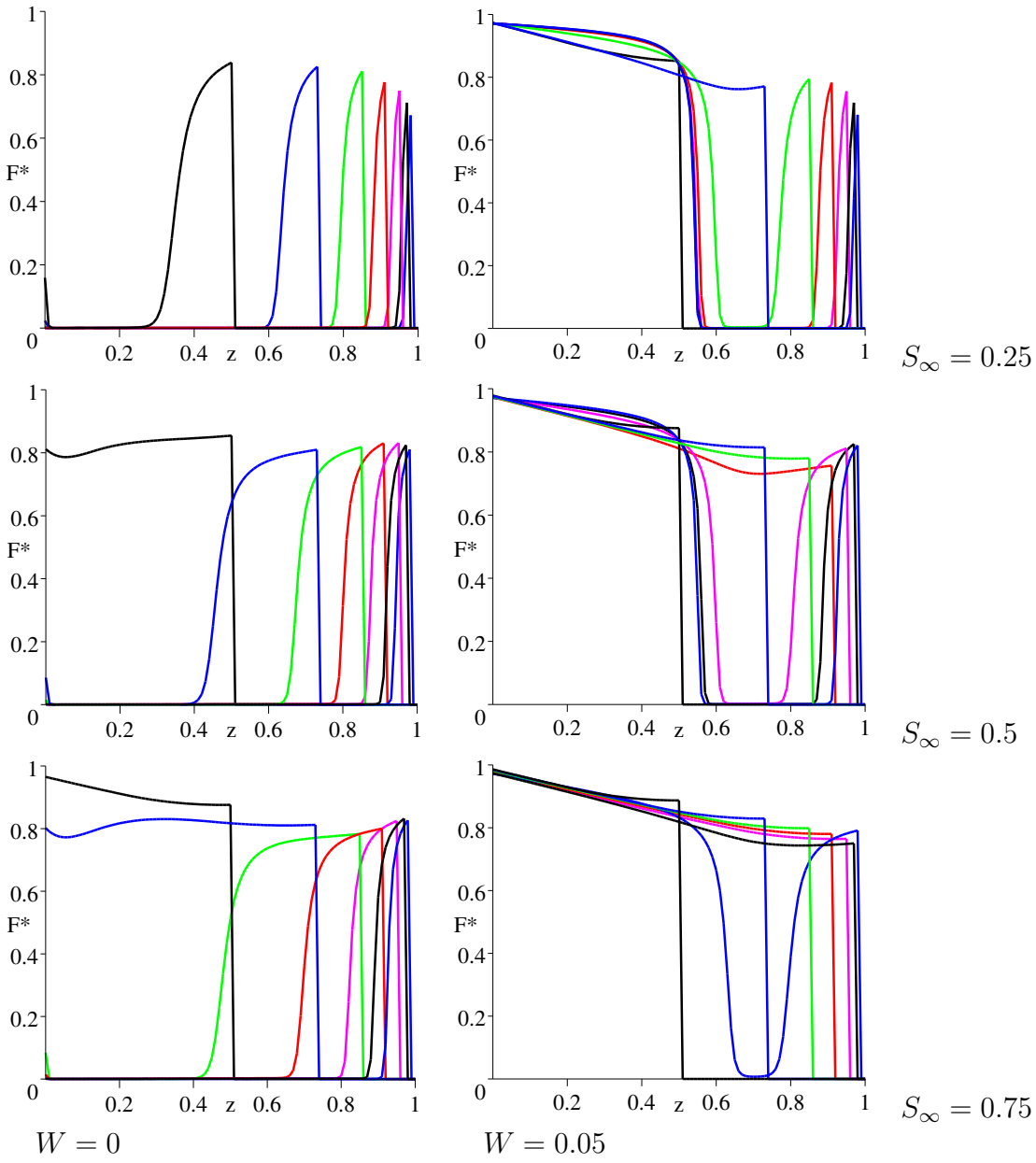

Figure 8.8: Dimensionless relative rate of water uptake $F^* = F/\lambda_w = -\epsilon_0(S^{-1/m} - 1)^{1/n} - p_{r,0}$ at times $t = 0.2$, 0.4, 0.6, 0.8, 1, 1.2, 1.4 months (black, blue, green, red, purple, black, blue lines respectively) for different rates of rainfall. See also soil water relative saturation profiles in Figure 8.7. Parameters are $\epsilon = 0.1$, $\lambda_w = 0.1$, $\epsilon_0 = 0.02$.

Thus the leading order solution in this case is given by

$$\int_{S_\infty}^{S} \frac{ds}{\lambda_w[\epsilon_0(s^{-1/m} - 1)^{1/n} + p_{r,0}]} = \tau, \tag{8.57}$$

for $p_{r,0} \approx -1$ at the leading order as found in Section 8.2.2. The solution given by (8.57) is shown in Figures 8.9 and 8.10. As we observe, after a time of about 1

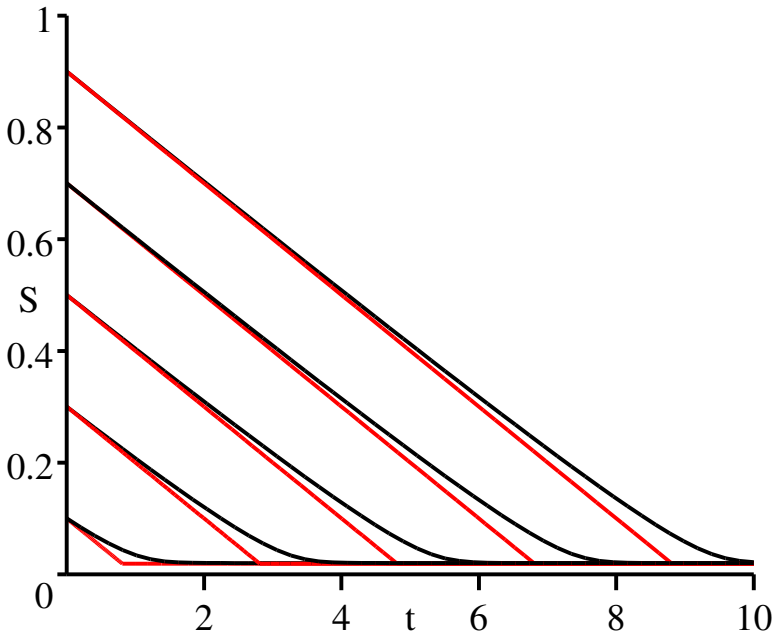

Figure 8.9: Comparison between solution (8.57) (black lines) and piece-wise linear solution (red lines) given by $S = S_\infty - \lambda_w(-p_{r,0})t$ for $t < t^*$ and $S = S^*$ for $t > t^*$, i.e., $\tau = t$.

week, the water saturation has reached a pseudo-equilibria given approximately by the saturation

$$S^* \approx [1 + (-p_{r,0}/\epsilon_0)^n]^{-m}, \quad \text{i.e.} \quad \left.\frac{\partial S}{\partial \tau}\right|_{S^*} \approx 0. \tag{8.58}$$

The time-scale τ^* over which this level S^* is reached as a function of initial concentration can be calculated from the following simple minded calculation. At short times $\partial S/\partial \tau = -\lambda_w(-p_{r,0})$ which implies that $S \approx S_\infty - \lambda_w(-p_{r,0})\tau$, thus $\tau^* \approx (S_\infty - S^*)/[\lambda_w(-p_{r,0})]$. The comparison between the full solution (8.57) and piece-wise continuous solution given by $S = S_\infty - \lambda_w(-p_{r,0})\tau$ for $\tau < \tau^*$ and $S = S^*$ for $\tau > \tau^*$ is shown on Figure 8.9.

Thus, in a situation when there is an inadequate supply of water to the rooting region, the water uptake stops within approximately 1 week.

On Figure 8.10 we have presented the comparison between the numerical solution to the full model and the analytic approximation given by equation (8.57) taking into account the time at which the roots have reached position at z, i.e., $\tau = -(1/\nu_0)\ln[(1-z)/(1-l_0(0))]$ for $z > l_0(0)$ and $\tau = 0$ for $z < l_0(0)$, where $l_0(0)$ is the starting length of zero order root. We see that this solution agrees well with the numerical solution in the main rooting region away from $z = 0$. However, near $z = 0$ there is a "boundary layer" region. We will discuss the properties of it, i.e., the

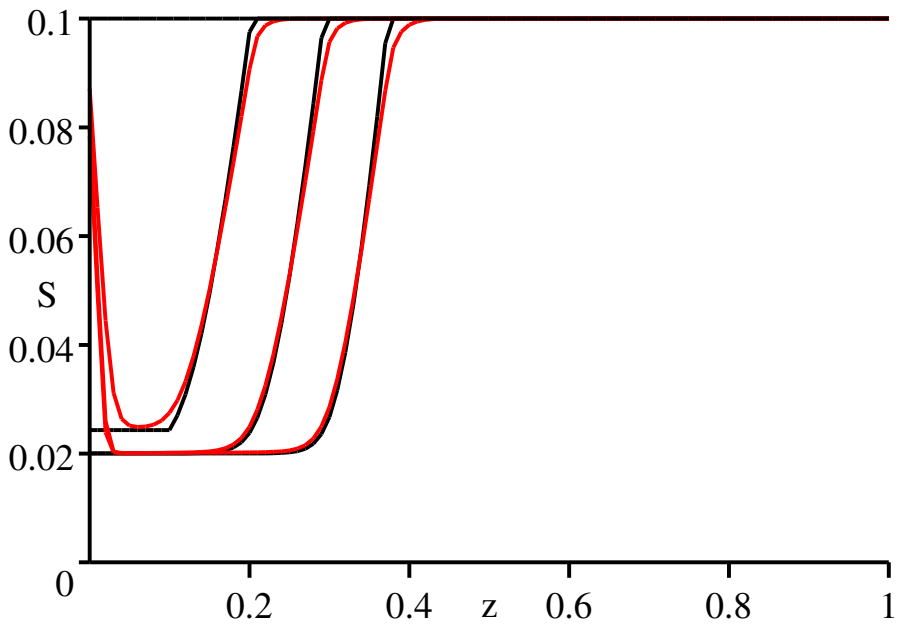

Figure 8.10: Water saturation profile for initial relative saturation $S_\infty = 0.1$ and $W = 0.001$. Black lines represent the analytic approximation given by equation (8.57) and red lines show the result from numerical simulations with the full diffusion convection model. Curves plotted for times $t = 1, 2, 3$ days.

thickness, in the next section where we find that for all non-zero values of W there will be a "pseudo-equilibrium" developing near the surface of the soil.

8.5.2 Pseudo-Steady State

As we can see from Figure 8.7 the region near the surface of the soil at $z = 0$ eventually settles into a pseudo-steady state, i.e., the water saturation profile will change very slowly after the initial fast transients. We define the width of this pseudo-equilibrium region to be z^*, i.e., for $0 < z < z^*$

$$\frac{\partial}{\partial z}\left[D(S)\frac{\partial S}{\partial z} - \epsilon k(S)\right] - F(S) = 0, \tag{8.59}$$

with boundary condition

$$-D(S)\frac{\partial S}{\partial z} + \epsilon k(S) = W \quad \text{at} \quad z = 0, \tag{8.60}$$

and

$$S = S^* \quad \text{at} \quad z = z^*, \tag{8.61}$$

where S^* and z^* are determined from the equations

$$F(S^*) = 0 \quad \text{and} \quad W = \int_0^{z^*} F(S)dz. \tag{8.62}$$

The first of equations (8.62) describes the level of the relative water saturation in the soil when the water uptake stops[8], and the second one describes the balance of water in this pseudo-equilibrium region, i.e., all the water coming into the soil at $z = 0$ is taken up by the roots within the region $0 < z < z^*$. Thus, the solution to equations (8.59)-(8.62) specifies the values of all three unknowns $S(z)$, S^* and z^*.

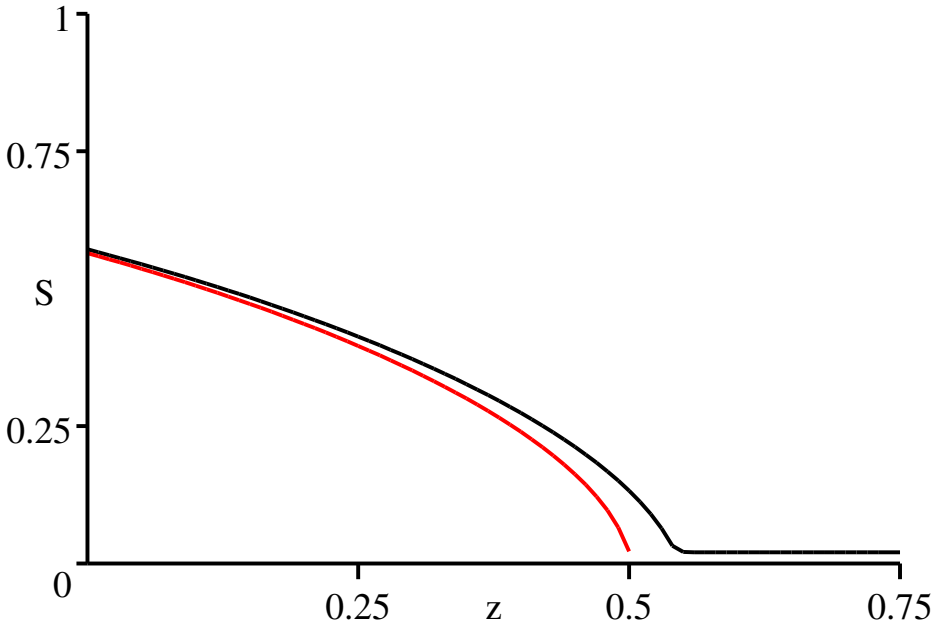

Figure 8.11: Comparison between numerical experiments with full model (black line) at time $t = 1$ month and pseudo-equilibrium calculation for $W = 0.05$ and initial relative water saturation given by $S_\infty = 0.25$.

Since at the leading order $p_{r,0}$ is constant and $F \sim \lambda_w(-p_{r,0}) + O(\epsilon_0\lambda_w)$ then the leading order approximation to z^* is calculated as

$$W = \int_0^{z^*} F\, dz \approx \lambda_w(-p_{r,0})z^*, \quad \text{thus} \quad z^* \approx \frac{W}{\lambda_w(-p_{r,0})}. \tag{8.63}$$

We can now define the critical rate of rainfall W_c for which the full length of the root is inside the pseudo-equilibrium region and thus is taking up water. This is approximately given by $W_c = \lambda_w(-p_{r,0})l_0$, where l_0 is the length of the zero order root. Thus, in dimensional terms, the critical rate of rainfall for fully grown maize root system with 50 cm long zero order roots, is approximately $W_{c,\mathrm{DIM}} \approx 4.69$ cm day^{-1}. Therefore, if the rate of rainfall is more than 4.69 cm day^{-1} then the full maize root system is taking up water, since the dry region does not develop. If however, the rate of rainfall is less than that, only the region at the top of the soil and near the

[8]Since at that low saturation level also the diffusion term and convection term is very small the water is very immobile for this relative saturation regime.

tip is taking up water, because of the "dry" region that develops in the middle of the rooting region.

8.6 Stochastic Rate of Rainfall W

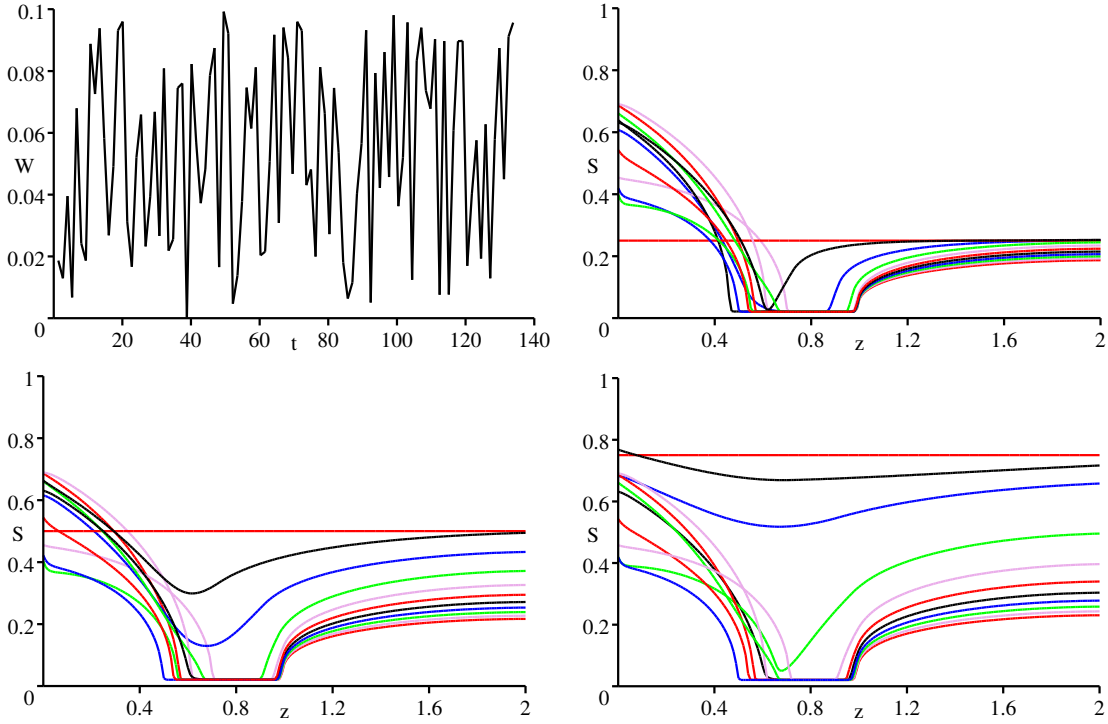

Figure 8.12: Rate of rainfall is a random number drawn every 1.2 days from the interval $(0, 0.1)$, such that the average rate of rainfall over the period is $W = 0.05$, i.e., the same as used in calculations presented in Figure 8.7. Coloured lines corresponding to $t = 0, 0.1, 0.2, 0.3..$ etc months. Colour ordering in time: red, black, blue, green, plum, red, black etc.

One of the most striking features in the numerical experiments presented above is the existence of wet region at the top of the soil and a dry region in the rooting zone. We have discussed the mechanisms of their formation in previous sections. However, we assumed that the rate of rainfall was constant. As one observes in everyday life, the rainfall pattern can be very unpredictable. Thus, in this section we will investigate what happens to these wet and dry band regions in the soil when we introduce a stochastic rainfall pattern. Will they still exist and what is their average width?

We define the rainfall to be given by the uniformly distributed random number drawn from the interval $(0, 2W)$ after equal time interval of 1.2 days, so that the average rainfall is still W as used in the previous sections. The results of numerical simulations are presented in Figure 8.12.

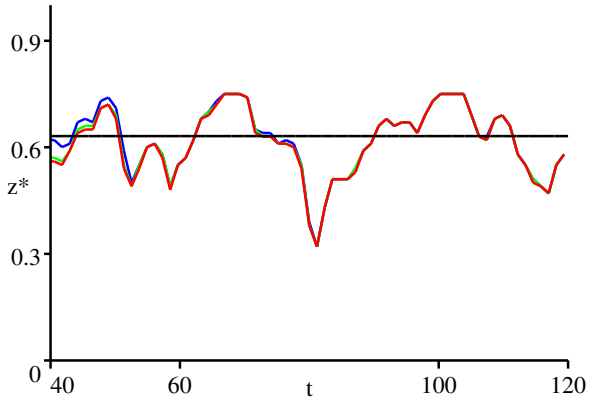

Figure 8.13: Position of wet-dry boundary z^* for the stochastic rate of rainfall calculated for different initial water saturations $S_\infty = 0.25$ (red line), $S_\infty = 0.5$ (green line) and $S_\infty = 0.75$ (blue line) and the average position (black line) of z^* calculated over the time period from 50 days to 120 days, i.e., after the initial transient time. Position of z^* was determined numerically to be the point where S becomes less than 0.0225. Corresponding value for z^* when $W = \text{constant} = 0.05$ is $z^* \approx 0.55$.

As we can see, the wet and dry bands still exist, however the position of the interface follows with smoothing the changes in the rate of rainfall, but the average position of the interface is of order $z^* \approx 0.6$. In Section 8.5.2 for constant rainfall the similar value of the boundary position is approximately $z^* \approx 0.55$ (measuring it in similar way as for stochastic case). Thus, the average in the case of stochastic rainfall is slightly higher than in the case of constant rainfall, however, the difference is not very big. This difference might be attributed to the existence of strong storm events in the case of stochastic rainfall which push the boundary downwards.

8.7 Conclusions

In this chapter we have modelled the water uptake by a growing root branching structure and the resulting changes in the relative water saturation in the soil. The changes in the water content calculated in this chapter are in agreement with the calculations conducted by Bengough [10], which report that after initial fast transients, the water saturation equilibrates and thus uptake by roots stops in the soils where there isn't any resupply of water (see Figure 8.7 for $W = 0$). Similar water saturation profiles presented in Figure 8.7 for $W = 0$ and in Bengough [10] have been measured experimentally by Davis [26].

In the case of average seasonal rainfall two pseudo-equilibrium regions can develop (see Figure 8.7). The first one is near the surface of the soil and it forms because of the rate of rainfall balancing the rate of water uptake within that region. The second

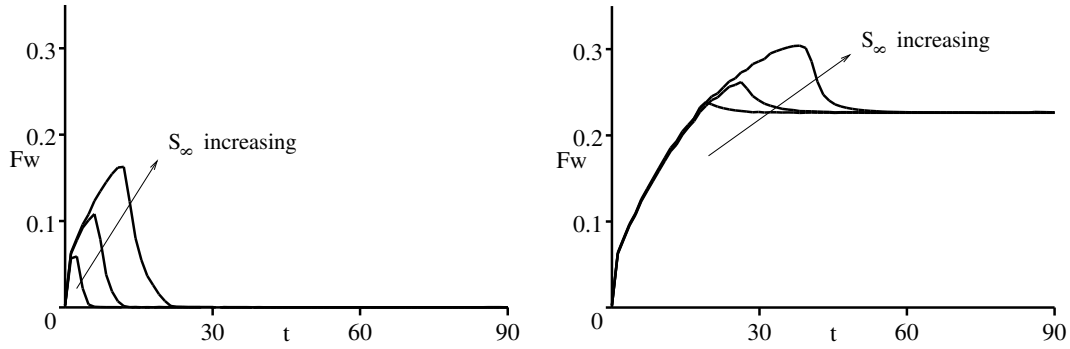

Figure 8.14: Overall rate of water uptake Fw by the full plant in litres per day for $S_\infty = 0.25, 0.5$ and 0.75 for $W = 0$ (graph on left) and $W = 0.05$ (graph on right). Time t in days.

pseudo-equilibrium region, if it exists, is just below the first one. In that region the rates of uptake and relative saturation have dropped to a very low level, thus resulting in water becoming relatively immobile in the soil.

The modelling presented in this chapter helps to address the question of where the main sites of water uptake by plant root systems are. This question has been of great interest to experimental and theoretical biologists [131], [34]. Experimental studies have found that most of the water uptake by a zero order root occurs near the tip of the root [131]. This has been explained assuming a variation in root radial conductivity, since younger tissues of root epidermis are thought to have higher radial conductivity [34]. We indeed confirm the fact that there is, in addition to the local maximum in water uptake near the base, also a local maximum for water uptake at the root tip. However, it is not because of variation in the internal root conductivity, but because of the long range water movement limitations in the soil. The tip of the root is constantly growing into soil which is less depleted of water and thus the tip region is able to take up more water (see Figure 8.8). Because of the highly non-linear diffusion and convection of water in the soil, the fast reduction in soil water content in the middle part of the rooting region causes the diffusion to become much slower there than near the tip region, therefore making the flow of water into this region of low saturation harder. Thus we find that at low levels of rainfall the middle part of the root system is taking up a negligible amount of water.

In the case of high rainfall there will be another local maximum for water uptake near the top of the soil $z = 0$. Indeed, when the rate of rainfall satisfies $W > W_c \approx \lambda_w(-p_{r,0})l_0$, then there is more water being supplied from the top than is taken up by the root and thus the saturation remains relatively high throughout the rooting zone. In that situation the dominant site for water uptake is near the base of the stem from where it is easiest to transport it to stem and leaves.

Based on the analysis we can also conclude that when the plant is very young and thus, the root system very short, all of the root will be getting the benefits of rainfall. However, as roots grow into deeper layers in the soil the amount of water taken up increases, and once the water uptake becomes larger than the rate of rainfall, a pseudo-equilibrium starts developing, resulting in a formation of a dry zone behind the pseudo-equilibrium wet zone where the soil is still relatively highly saturated with water.

We see from Figure 8.14 that when there is no water flux from the surface of the soil, then the water uptake by the plant stops after about 10-30 days depending on the initial condition. However, when the water flux at the surface of the soil is non-zero then the rate of water uptake by the plant reaches a constant level. This constant level is determined directly by the pseudo-equilibrium that develops near the soil surface. The speed at which it develops is dependent on the initial water saturation in the soil.

Many plant scientists have also been concerned with defining the critical value of soil moisture that is needed for successful functioning and growth of plants. This led in the early part of the 20th century to experimental measurements of the so called *permanent wilting point*. It is defined as the moisture content of the soil when the leaves of plants growing in the soil first reach a stage of wilting from which they do not recover unless they are watered [3]. As such, the permanent wilting point is generally thought to be a very badly defined property of plant and soil, since clearly, the water saturation in the soil is not uniform. However, the value for the permanent wilting point has still been measured extensively for different plant and soil combinations. The calculations presented in this chapter might be able to provide more detailed definition to the permanent wilting point or perhaps provide the way of replacing it with other characteristic parameters describing the available water in the soil. This could be for example the critical rate of rainfall when the rate of water uptake by plant is below a certain critical level which might be defined to be proportional to the amount of water evaporating to the atmosphere through the leaves.

Chapter 9

Simultaneous Water and Nutrient Uptake

In the previous chapters we have modelled the nutrient uptake by root branching structures in the absence of water movement in the soil (Chapters 2 to 6). In Chapters 7 and 8 a model for water movement and uptake by root branching structures was described. In this final modelling chapter, a model for simultaneous water and nutrient movement together with simultaneous uptake of water and nutrients by the root branching structure will be presented. This is done with a view of quantifying the extent of groundwater pollution due to fertiliser application.

9.1 Fertiliser Application and Pollution

Groundwater is an important source of clean water for industry, agriculture and domestic users. The amount of pollutants in the water, i.e., inorganic and organic residues, is therefore an important concern to everyone. This has led to international and national organisations and governments producing a large number of legislative controls on pollution levels. The World Health Organisation (WHO) Guidelines for Drinking Water Quality on Chemicals of Health Significance in Drinking-water (see WHO web page `www.who.int`) list the guideline values for nineteen inorganic and thirty organic compounds. For example, the allowed level of plant nutrient nitrogen compounds in drinking water as nitrate (NO_3^-) is 50 mg per litre. For nitrite (NO_2^-), the guidelines specify that the average concentration must not exceed 0.2 mg per litre and that the concentration must never exceed 3 mg per litre. These values for nitrite and nitrate are also used by the European Community (EC) in their legislation on drinking water quality. However, the United States of America and Canada place a limit on nitrate in drinking water that is five times lower than that of WHO and EC.

Nitrogen based compounds are by far the most regulated compounds from the point of view of water pollution. This is a result of the excessive use of nitrate fertilisers leading to its leakage into drinking water reservoirs. The reason why nitrogen compounds, such as nitrate (NO_3^-) and nitrite (NO_2^-), have been under such scrutiny is their link to various medical problems, such as methemoglobinemia (blue-baby) syndrome in infants [53], [52], [37]. Higher than average nitrate uptake by expectant mothers has also been linked to childhood diabetes, however, the precise mechanism is still under scrutiny [37]. High levels of nitrite and nitrate in the drinking water can also be linked to bladder cancer, non-Hodgkin's lymphoma, gastric and prostate cancer, spontaneous abortion, thyroid enlargement etc. Oral consumption of nitrite results in it being transformed to nitric oxide by stomach acids; nitric oxide in turn is known as a vasodilatory molecule that is important to regulation of blood pressure and blood flow [37]. Therefore, it is thought to be important in diseases involving heart and circulation malfunction. An excellent extensive overview of the clinical symptoms of nitrite and nitrate overconsumption is presented by Ellis et al. [37].

Nitrogen pollution has also been linked to large scale changes in aquatic ecosystems. One famous case is the effect nitrate fertilisers in the Mississippi River have had on the Gulf of Mexico. Fertiliser residues in the river are transported to the Gulf of Mexico where they are thought to give rise to large hypoxic regions, i.e., regions in the gulf where the dissolved oxygen content is lower than 2 mg per litre [48]. Such hypoxic regions can be fatal to marine wildlife, particularly to those with lower mobility.

Another nitrogen containing compound, ammonia (NH_3^+), is a very toxic substance which can seriously damage eyes, skin, respiratory tract, and gut. Therefore, the allowed level of it in water has been set very low. For example in the US 0.03 mg per litre are considered to be toxic over the short term, but for long term exposure the toxicity level has been set to 0.002 mg per litre.

Nitrogen is applied to agricultural and forest land in most countries as urea. Although, urea can be taken up directly by the plants [80], it transforms in the soil into ammonia (NH_4^+), which in turn transforms by the process of nitrification by chemolithotropic bacteria of the family *Nitrobacteraceae* into nitrite (NO_2^-). Nitrite in turn is highly transient and is oxidised very rapidly to nitrate (NO_3^-) [81]. Plants take up most of the nitrogen in the form of ammonia and nitrate [80].

Nitrogen fertilisation is extremely important in the areas where the soils have a very low level of organic matter. However, since nitrogen compounds are very mobile in the soil this can lead to major problems of pollution of groundwater and rivers. For example, the average yearly nitrogen application to maize fields in Spain is 510 kg N per hectare per year [39]. The average surface runoff per year is in the range

of 5 kg per hectare (7% of total fertiliser applied), and average leaching per year has been 3 kg per hectare (4% of total applied) [135]. However, nutrient losses as high as 50% have been recorded [17].

In comparison to nitrogen containing compounds, very little research has been concerned with phosphate pollution. However, substantial amounts of phosphate fertiliser are applied in areas with highly weathered soil like the West African Savannah, Malaya, and South Australia [93]. Even when the intensity of phosphate fertilisation is high, there are virtually no governmental or international regulations on its levels in groundwater and rivers. According to [13] this might be because phosphate is not toxic. However, during recent years concerns have mounted over the effect of phosphate on aquatic ecosystems. For example, an increase of 10 parts per billion phosphate-phosphorus in the Kuparuk River in Alaska resulted in an immediate increase of algal growth by 20 fold in a region of 10 kilometres down from the phosphate placement site [102]. Indeed, in some cases phosphate fertiliser has been used to increase the productivity of fisheries. This type of practice has motivated the start of the process of formalising the allowed levels of phosphate in aquatic ecosystems. For example the United States Environmental Protection Agency is considering a guideline value for phosphate in drinking water in the range 0.025 to 0.1 mg P per litre [13].

Another example of potentially negative effects of phosphate can be observed in plant ecosystems. Ingerpuu et al. [59] present the results of a 30 year fertilisation study of the wooded meadow Laelatu on the west coast of Estonia. This site has found to be one of the most species rich sites[1] in temperate Eurasia. Amongst the things they measured was the response of species richness to the application of nitrate-phosphate-potassium fertiliser. They found that fertilisation increases the coverage and decreases the number of different vascular plants, e.g. grasses, but has the opposite effect on byrophytes, e.g. mosses. Caldwell et al. [18] have also found that the phosphate levels in soil influenced greatly the competitiveness of different grass species in respect to their ability to acquire phosphate from the soil. Thus, the fertilisation can have huge effects on the plant ecosystems and can make some of the less adapted species almost extinct since their root systems might not be well adapted to changes in the phosphate levels in the soil [63].

In this chapter a model for simultaneous water and nutrient uptake by the plant root system will be discussed.

[1]It is the most species rich site on the small scale, i.e., the number of different plant species detected on 10 m^2 plot is up to 68. Overall number of different plant species found in Laelatu is approximately 371.

9.2 Model for Simultaneous Water and Nutrient Uptake by Root Branching Structure

We recall that water movement and uptake by a root branching structure is governed by the equations (8.32)-(8.37) presented in Chapter 8, i.e., the relative water saturation S in the soil is given by

$$\phi\frac{\partial S}{\partial t} = \nabla \cdot [D_0 D(S)\nabla S - K_s k(S)\hat{\mathbf{k}}] - F_w(S, z, t), \tag{9.1}$$

where $D(S)$ and D_0 characterise the water diffusivity, and $k(S)$ and K_s characterise the conductive water movement due to gravity. The functional form of $D(S)$ and $k(S)$ are given by Chapter 8 equations (8.33)-(8.35). The water uptake F_w by root branching structure is also described in Chapter 8 Section 8.2.2.

The nutrient movement in the soil and uptake of it by the root branching structure was described in Chapter 6. We use the same equation by writing the water content in the soil ϕ_l in terms of porosity ϕ and relative water saturation S, $\phi_l = \phi S$, i.e., we get

$$\frac{\partial}{\partial t}[(b + \phi S)c] + \nabla \cdot [c\mathbf{u}] = \nabla \cdot [D_f \phi^{d+1} S^{d+1} \nabla c] - F(c, S, t), \tag{9.2}$$

where we have taken the nutrient diffusivity in the non-saturated soil to be given by $D_f\phi^d S^d$, i.e., the impedance factor f, presented in Chapter 2, is given by $f = \phi^d S^d$, where the parameter d is according to [6], [95] in the range $1 \leq d \leq 2$. The nutrient uptake term F describes the amount of nutrient removed by the plant root system per unit soil volume in unit time and the form of it will be described in Sections 9.5.1 and 9.5.2 after we have non-dimensionalised the model.

In this chapter we will assume that the buffer power of the soil does not change when the moisture conditions change. This is supported by experimental measurements conducted by Kuchenbuck et al. [70] where they found that the buffer power variation with soil moisture conditions is negligible in comparison to the changes in impedance factor. This may be realistic in the sense that all soil particles will retain a water film over them even in dry soils. This water film is where exchange between the two phases occurs. Thus, we take all change in the nutrient ion mobility due to the changes in the soil moisture conditions to occur only due to the diffusion limitation, i.e., impedance factor $f(S) = S^d$.

The speed of water movement $\mathbf{u}$ in the soil is given by the Darcy law for water flow in unsaturated porous media and can be written in terms of relative water saturation as

$$\mathbf{u} = -D_0 D(S)\nabla S + K_s k(S), \tag{9.3}$$

where D_0, $D(S)$, K_s and $k(S)$ are the same water diffusivity and conductivity parameters and functions as in the water movement equation (9.1) (see also Chapter 8 equations (8.33)-(8.35) and Figure 8.5). Thus the equation for nutrient movement in the soil becomes

$$\frac{\partial}{\partial t}[(b+\phi S)c] = \nabla \cdot \left\{ D_f \phi^{d+1} S^{d+1} \nabla c + c[D_0 D(S) \nabla S - K_s k(S) \hat{\mathbf{k}}] \right\} - F(c, S, t), \quad (9.4)$$

where $\hat{\mathbf{k}}$ is the unit vector pointing vertically downwards into the soil.

9.2.1 Soil Surface Boundary Condition

As in Chapter 8, we will assume that there is a flux of water due to rainfall at the top of the soil, i.e.,

$$-D_0 D(S) \frac{\partial S}{\partial z} + K_s k(S) = W_{\text{dim}} \quad \text{at} \quad z = 0, \quad (9.5)$$

where W_{dim} [cm s^{-1}] is the volume flux of water per unit soil surface area in unit time.

We take the rate of fertiliser application to be given by ϱ_{dim} [μmol cm^{-2} s^{-1}] and thus the boundary condition for the nutrient at the top of the soil is given by

$$-D_f \phi^{d+1} S^{d+1} \frac{\partial c}{\partial z} - c[D_0 D(S) \frac{\partial S}{\partial z} - K_s k(S)] = \varrho_{\text{dim}} \quad \text{at} \quad z = 0. \quad (9.6)$$

Taking into account the rainfall boundary condition for water, the nutrient boundary condition simplifies to

$$-D_f \phi^{d+1} S^{d+1} \frac{\partial c}{\partial z} + W_{\text{dim}} c = \varrho_{\text{dim}} \quad \text{at} \quad z = 0. \quad (9.7)$$

9.2.2 Boundary Condition in the Bottom of the Soil

To calculate the fertiliser movement into the groundwater and from there to the lakes and rivers, the boundary condition at the groundwater level would need to be derived from the model for large scale groundwater movement. However, in this section we will use the same approach as in Chapter 8, i.e., we prescribe the zero flux of water and nutrient at a given distance l_w. This will correspond to the pot experiment where the pot has an impermeable bottom. The benefit of this approach is, that it enables us to calculate the nutrient and water movement in the rooting region only without any influence of the nutrient and water from the groundwater.

Thus, at the bottom of the soil we assume that there is no flux of water and nutrient out of the soil, i.e., we choose

$$-D_0 D(S) \frac{\partial S}{\partial z} + K_s k(S) = 0 \quad \text{at} \quad z = l_w, \quad (9.8)$$

and

$$-D_f\phi^{d+1}S^{d+1}\frac{\partial c}{\partial z}=0 \quad \text{at} \quad z=l_w. \tag{9.9}$$

This corresponds to the case when there is an impermeable layer of rock at depth l_w.

9.3 Non-dimensionalisation of the Model

We non-dimensionalise the model by choosing the timescale to balance the convective nutrient movement, i.e., we choose

$$c=K_m c^*, \quad z=K_0 z^*, \quad t=[t]t^* \quad \text{with} \quad [t]=\frac{bK_0^2}{D_0}, \tag{9.10}$$

where K_0 is the maximum length of the longest root, i.e., zero order root, in the root system. We will consider the nutrient movement in the soil depth direction, i.e., in the z direction, only. The dimensionless model for water and nutrient movement in the soil, including the dimensionless expressions for water and nutrient uptake, F_w and F respectively, is now given by

$$\delta\frac{\partial S}{\partial t}=\frac{\partial}{\partial z}\Big[D(S)\frac{\partial S}{\partial z}-\epsilon k(S)\Big]-F_w, \tag{9.11}$$

$$\frac{\partial}{\partial t}\Big[(1+\delta S)c\Big]=\frac{\partial}{\partial z}\Big[(D(S)\frac{\partial S}{\partial z}-\epsilon k(S))c+RS^{d+1}\frac{\partial c}{\partial z}\Big]-F, \tag{9.12}$$

or alternatively, using the water equation to simplify the nutrient equation, we get

$$(1+\delta S)\frac{\partial c}{\partial t}-\Big[D(S)\frac{\partial S}{\partial z}-\epsilon k(S)\Big]\frac{\partial c}{\partial z}=R\frac{\partial}{\partial z}\Big[S^{d+1}\frac{\partial c}{\partial z}\Big]-F+F_w c, \tag{9.13}$$

where the dimensionless time-derivative parameter δ is given by $\delta=\phi/b$, the dimensionless nutrient diffusivity parameter is $R=D_f\phi^{d+1}/D_0$, and the dimensionless water and nutrient convectivity parameter is $\epsilon=K_sK_0/D_0$ (it is the same ϵ as used in Chapter 8 and its values are presented in Table 8.3).

Similarly the dimensionless boundary conditions will be given by

$$-D(S)\frac{\partial S}{\partial z}+\epsilon k(S)=W \quad \text{at} \quad z=0, \tag{9.14}$$

$$W\,c-RS^{d+1}\frac{\partial c}{\partial z}=\varrho \quad \text{at} \quad z=0, \tag{9.15}$$

and

$$-D(S)\frac{\partial S}{\partial z}+\epsilon k(S)=0 \quad \text{at} \quad z=l_w, \tag{9.16}$$

$$RS^{d+1}\frac{\partial c}{\partial z}=0 \quad \text{at} \quad z=l_w, \tag{9.17}$$

where the dimensionless rate of fertiliser application ϱ is given in terms of the dimensional fertiliser application, ϱ_{dim}, by $\varrho=\varrho_{\text{dim}}K_0/(D_0K_m)$, and the dimensionless rate of rainfall, W, is given by $W=W_{\text{dim}}K_0/D_0$.

9.4 Values of Dimensionless Parameters

In the nutrient movement equation (9.13) the parameters of most interest to us are R and ϵ. The parameter R quantifies the relative importance of nutrient diffusion in the soil pore water with respect to movement of nutrient due to water movement in the soil. Typically, the value of this parameter for Silt loam G.E.3 is of the order of 5×10^{-5}. This implies that the effect of nutrient diffusion on the root system length scale is very small. Thus, most of the nutrient in the soil is moving due to large scale water movement.

The parameter ϵ describes the importance of convective flux of water due to gravity in comparison to water movement due to unsaturated soil pore water gradient. Again, for typical Silt loam G.E.3 this is small, i.e., $\epsilon \approx 0.224$. Thus, most of the nutrient movement in the soil is driven by the water movement down the water saturation gradient.

The dimensionless rate of rainfall W is the same as used in Chapter 8, i.e., the average value for W ranges from 0 to 10^{-2} (see Chapter 8 Section 8.4.1), but during the storm events it can be bigger.

The dimensionless rate of fertiliser application is $\varrho = \varrho_{\text{dim}} K_0/(D_0 K_m)$. As discussed in Chapter 5, the phosphate application rate ϱ_{dim} is $\approx 1.35 \times 10^{-7}$ μmol cm^{-2}s^{-1}. Thus, the typical value for the dimensionless rate of fertiliser application is $\varrho \approx 0.1$ for Silt loam G.E.3. The typical potassium application rate is $\varrho_{\text{dim}} \approx 3.397 \times 10^{-7}$ μmol cm^{-2}s^{-1} giving a dimensionless rate of fertiliser application of $\varrho = 0.094$.

For nitrate ϱ_{dim} is $\approx 5.48 \times 10^{-6}$ μmol cm^{-2}s^{-1} corresponding to 120 kg of nitrate per hectare applied over six moth period. Thus, the nitrate dimensionless fertiliser application rate is $\varrho \approx 0.8$.

9.5 Two Time-Scales

In the above equation the parameter δ multiplying the time derivative term in the water movement equation (9.11) quantifies the difference in the water and nutrient movement time-scales. For phosphate and potassium the buffer power $b >> 1$, i.e., 239 and 39 respectively, which implies that the parameter $\delta = \phi/b$ for those nutrients is very small, i.e., $\delta << 1$. Thus, the water saturation relaxes rapidly to a pseudo-equilibrium on the timescale of phosphate and potassium movement in the soil, i.e., $t \sim \delta$. In the nutrient movement equation the time-derivative term reduces at the leading order from $(1 + \delta S)\partial c/\partial t$ to $\partial c/\partial t$, since $\delta << 1$ and $S < 1$.

9.5.1 Nutrient Uptake Term F when $\delta << 1$

In Chapters 7-8 we showed that the water saturation in the soil around each individual root is, at the leading order, locally constant in space. Therefore, we can use the formula for nutrient flux into a single cylindrical root derived in Chapter 2.

We recall that the nutrient uptake by a single cylindrical root with radius a was found in Chapter 2 to be given by the equation (2.120), i.e., the dimensional uptake of nutrient [μmol cm^{-2}s-1] is given by

$$F_{\text{dim}} = \frac{2F_m c/K_m}{1 + c/K_m + L(t) + \sqrt{4c/K_m + (1 - c/K_m + L(t))^2}}, \tag{9.18}$$

where

$$L(t) = \frac{\lambda}{2} \ln[\alpha(t - t_0) + 1] \tag{9.19}$$

and dimensionless uptake parameter λ and timescale parameter α are given by

$$\lambda = \frac{F_m a}{D_f \phi^{d+1} S^{d+1} K_m}, \quad \text{and} \quad \alpha = 4e^{-\gamma} \frac{D_f \phi^{d+1} S^{d+1}}{a^2 b(1 + \delta S)}. \tag{9.20}$$

F_m [μmol cm^{-2}s-1] describes the maximum rate of nutrient uptake.

In Chapter 6 we developed a model for nutrient uptake by root branching structures in the absence of water movement. The nutrient uptake per unit of soil volume was taken there to be the sum of uptake by all zero and first order roots at a given location, i.e., by $F_0 + F_1$, where F_0 is the nutrient uptake by the zero order roots and F_1 is the nutrient uptake by first order lateral branches.

Zero order nutrient uptake F_0 for zero order root with initial length $l_0(0)$ is given, similar to Chapter 6 Sections 6.2.3.1 and 6.3, by

$$F_0 = \Lambda_0 \frac{2c}{1 + c + L_0(z,t) + \sqrt{4c + (1 - c + L_0(z,t))^2}}, \tag{9.21}$$

where

$$L_0(z,t) = \begin{cases} \frac{\lambda_0}{2S^{d+1}} \ln\left[(\alpha_0 t + \alpha_{00} \ln(1 - z)) \frac{S^{d+1}}{1+\delta S} + 1\right], & \text{for} \quad z > l_0(0), \\ \frac{\lambda_0}{2S^{d+1}} \ln\left[\alpha_0 t \frac{S^{d+1}}{1+\delta S} + 1\right], & \text{for} \quad 0 < z < l_0(0), \end{cases} \tag{9.22}$$

with

$$\lambda_0 = \frac{F_m a_0}{D_f \phi^{d+1} K_m}, \quad \alpha_0 = 4e^{-\gamma} \frac{D_f \phi^{d+1}}{a_0^2 b}[t], \quad \alpha_{00} = 4e^{-\gamma} \frac{D_f \phi^{d+1}}{a_0^2 b} \frac{K_0}{r_0}, \tag{9.23}$$

and

$$\Lambda_0 = \frac{2a_0 F_m K_0^2}{(a_0 + K_1 \cos\beta)^2 K_m D_0}. \tag{9.24}$$

The nutrient uptake F_1 by first order lateral branches is, after Chapter 6 Sections 6.2.3.1 and 6.3, given by

$$F_1 = \Lambda_1 \int_{\hat{z}}^{z} \frac{2c\psi(z')dz'}{1 + c + L_1(z,t;z') + \sqrt{4c + (1 - c + L_1(z,t;z'))^2}}, \tag{9.25}$$

with

$$L_1(z,t;z') = \frac{\lambda_1}{2S^{d+1}} \ln\Big\{[\alpha_1 t + \alpha_{11} \ln(\frac{1 - (z' + l_{a,0})}{1 - l_0(0)}) + \alpha_{111} \ln(1 - \frac{z - z'}{K_1 \cos\beta})]\frac{S^{d+1}}{1 + \delta S} + 1\Big\}, \tag{9.26}$$

where

$$\alpha_1 = 4e^{-\gamma}\frac{D_f\phi^{d+1}}{a_1^2 b}[t], \quad \alpha_{11} = 4e^{-\gamma}\frac{D_f\phi^{d+1}}{a_1^2 b}\frac{K_0}{r_0}, \quad \alpha_{111} = 4e^{-\gamma}\frac{D_f\phi^{d+1}}{a_1^2 b}\frac{K_1}{r_1}, \tag{9.27}$$

$$\Lambda_1 = \frac{2a_1 F_m K_0^3}{\cos\beta(a_0 + K_1\cos\beta)^2 D_0 K_m l_{n,0}}, \quad \lambda_1 = \frac{F_m a_0}{D_f\phi^{d+1}K_m}, \tag{9.28}$$

where $l_0(0)$ is the length of the zero order root at time $t = 0$ and the dimensionless first order root branch point distribution on the zero order root is $\psi(z') = 1$ in the branching region and $\psi(z') = 0$ in the non-branching region.

Similarly to previous chapters, the dimensionless length of the zero order root is given by

$$l_0(t) = 1 + (l_0(0) - 1)e^{-\nu t}, \tag{9.29}$$

where $\nu = r_0[t]/K_0$ is the dimensionless zero order root elongation parameter.

The integration interval $(\hat{z}, z)$ in equation (9.25) is, as in Chapter 6, defined to be the interval from where the first order lateral branches will reach at least the depth z, i.e., $\hat{z}$ is a solution to equation (6.8) as discussed in Chapter 6 Section 6.2.2.

The values of various different nutrient uptake parameters λ_i, Λ_i, α_i, α_{ii} and α_{iii} are presented in Table 9.1 for phosphate and potassium.

	Λ_0	Λ_1	λ_0	λ_1	α_0	α_{00}	α_1	α_{11}	α_{111}	ν	$[t]$ [days]
P	0.733	4.335	43	17	111	5.196	694	34.5	1.6	21.4	505.5
K	2.532	16.55	167	67	198	32	675	199	10	3.4	82.5
NO_3^-	0.452	25	-	-	-	-	-	-	-	0.08952	2.12

Table 9.1: Dimensionless nutrient uptake parameters for phosphate, potassium and for simplified nitrate model in Silt loam G.E.3 soil.

9.5.2 Nitrate Uptake, i.e., $\delta \lesssim 1$

For nitrate the buffer power b is 1 and thus $\delta = \phi/b \approx \phi \lesssim 1$. Clearly, in the case of nitrate the water movement occurs on a similar timescale to the nitrate movement. Thus, we cannot use the nutrient uptake expression found in Chapter 2, since water saturation is not in pseudo-equilibrium in comparison to the nitrate movement. Therefore, in general, one would need to solve again the single cylindrical root coupled water and nutrient uptake models with the reflection boundary condition at the half distance between the roots. However, instead, we will use the information obtained in the previous Chapters 5 and 6 when we considered the nitrate uptake by the root system in the fully saturated soil.

We found in the earlier chapters that the nitrate concentration profile is relatively flat around each individual root. Initially it was flat around each root because of the relatively high level of nutrient in the soil in comparison to the amount taken up by the root ($\lambda/c_\infty << 1$). However, this small nutrient uptake will eventually cause the local concentration of nutrient to decrease. By the time when the nutrient concentration has dropped to a level where the uptake would considerably influence the nutrient concentration around each root, the diffusional length-scale has become comparable to the inter-root distance. Therefore, over long-timescale the diffusion will maintain the flat profile between the sub-branches. Thus we found that for all times in the saturated soil the nitrate uptake per unit of root surface area can approximately taken to be given by $F_m c/(K_m + c)$, where c is the local nutrient concentration per unit volume of soil. We assume that this holds at the leading order also for non-saturated soil and therefore we take the dimensionless zero order root nitrate uptake to be given by

$$F_0 = \frac{\Lambda_0 c}{1 + c}, \tag{9.30}$$

and first order nitrate dimensionless uptake is given by

$$F_1 = \frac{\Lambda_1 c}{1 + c} \int_{\hat{z}}^{z} \psi(z')\, dz'. \tag{9.31}$$

The values of this simplified nitrate model for different nutrient uptake parameters Λ_i, are presented in Table 9.1.

We will use the above expressions in this chapter, however, we will also point out that more modelling effort is needed to describe the uptake of nitrogen containing compounds by plant roots. In particular, one should probably include the details of the nitrogen cycle in the soil.

Throughout this thesis, we have only dealt with one nitrogen containing compound, i.e., nitrate. As mentioned earlier, nitrogen is applied to agricultural land in

the form of urea, which in turn changes into ammonia and then via nitrification into nitrite and nitrate. Over the years, considerable effort has been put into modelling these changes in nitrate containing compounds in absence of the uptake by plant roots. For example McLaren [81] found that all four (urea, ammonia, nitrite, nitrate) are present in the top layer of the soil with thickness approximately 1 meter. Below 1 meter, only nitrate was present. Thus, even in the absence of the nutrient uptake by the root, the nitrate level in the soil changes quite considerably in soil depth. Starr et al. [116] found that the profile of ammonia and nitrite reaches equilibrium within 40 days. However, they also found that in the topmost layer of the soil both fractions, ammonia and nitrate, were present in substantial quantities. Since plants take up at least three types of nitrogen containing compounds, urea, ammonia and nitrate, and according to Xu et al. [136], each of them at very different rates, the model for nitrogen uptake by plant roots presented in this chapter is lacking in important details. However, as a first approximation, we will present the results of nitrate uptake by root branching systems without including the urea-ammonia-nitrite-nitrate cycle.

9.6 Simple Analysis of the Model

The simplest questions one can ask when analysing this model for simultaneous water and nutrient uptake by a plant root system is: when does the soil surface nutrient concentration start increasing due to fertiliser application, thus increasing the risk of surface runoff, since high levels of nutrient at the top layers of soil are vulnerable to be washed away by heavy storms. The simple minded answer to this can be derived by considering the soil surface boundary condition

$$Wc - RS^{d+1}\frac{\partial c}{\partial z} = \varrho \quad \text{at} \quad z = 0. \tag{9.32}$$

Clearly, when $\varrho - Wc(0,t) > 0$ then $\partial c/\partial z|_{z=0} < 0$ and thus the nutrient concentration at the soil surface is higher than in immediate neighbourhood in the soil. However, when $\varrho - Wc(0,t) < 0$ the soil surface concentration is less than that in the immediate soil environment. We see that for phosphate ($\varrho = 0.1$, $c_\infty \approx 1$) the concentration of nutrient at the root surface starts increasing for most realistic rates of rainfall, i.e., for $W \leq 0.05$.

The nitrate ($\varrho = 0.8$, $c_\infty \approx 200$) starts accumulating on the surface of the soil if the rate of rainfall W is less than 3×10^{-3}. However, when $W > 3 \times 10^{-3}$ the nitrate is washed very fast into the soil, and thus the concentration on the surface of the soil starts decreasing.

Similarly, for any given soil nitrate level and rate of rainfall one could define the critical rate of fertilisation when the soil surface concentration starts increasing or decreasing.

In this modelling chapter we neglect the surface water movement due to unexpected heavy storm events, which can lead to surface runoff of fertilisers. Instead, we will say that if the nutrient root surface concentration starts increasing due to fertilisation the possibility of surface runoff also increases.

The groundwater pollution due to the fertilisation can be quantified as the proportion of fertiliser that could be carried past the rooting region in the soil.

9.7 Numerical Computation

Due to the high level of non-linearity in the nutrient and water movement terms and in the nutrient uptake term, we need to solve this model numerically. We will use the same numerical codes as in Chapters 6 and 8 by combining all the relevant water and nutrient interaction terms.

The initial condition for relative water saturation will be chosen to be, as in Chapter 8, given by constant water saturation in the soil, i.e., $S = S_\infty$ at $t = 0$. In the nutrient uptake calculations in Chapters 5-6 the constant nutrient initial condition $c = c_\infty$ at $t = 0$ was used. However, in those chapters, the soil was considered to be fully saturated. Thus in order to compare the results in this chapter to the previous ones, we have to have the same amount of nutrient initially in the soil pore water for unsaturated soil as for saturated soil. Therefore in this section the initial condition for nutrient will be taken to be given by $c = c_\infty/S_\infty$ at $t = 0$, so that $S_\infty c_\infty$ =constant at $t = 0$ for all S_∞. The results of the numerical calculations for the phosphate are presented in Figure 9.1 and 9.2 for $S_\infty c_\infty = 0.5$.

9.7.1 Numerical Results for Phosphate Uptake

The results for calculations of phosphate uptake with a constant rate of rainfall and constant fertilisation are shown on Figure 9.1. We can see that the concentration at the soil surface is approximately 2 (see Figure 9.1 (a)). This value can be explained by considering the boundary condition at the soil surface and neglecting the small diffusion term, since $R << 1$, i.e.,

$$Wc - \varrho = RS^{d+1}\frac{\partial c}{\partial z} << 1 \quad \text{thus} \quad c \approx \frac{\varrho}{W} \quad \text{at} \quad z = 0. \tag{9.33}$$

For $W = 0.05$ and $\varrho = 0.1$ we get $c(0, t) \approx 2$.

We also see that the fertiliser moves relatively slowly into the main rooting region (see Figure 9.1 (a)). The speed of this movement can be determined from the nutrient movement equation (9.13). Neglecting the small $O(R)$ diffusion term, we find that the leading order equation is the following hyperbolic partial differential equation

$$(1+\delta S)\frac{\partial c}{\partial t} - \Big[D(S)\frac{\partial S}{\partial z} - \epsilon k(S)\Big]\frac{\partial c}{\partial z} = -F + F_w c, \tag{9.34}$$

which has characteristic nutrient movement speed given by

$$\frac{\mathrm{d}z}{\mathrm{d}t} = -\Big[D(S)\frac{\partial S}{\partial z} - \epsilon k(S)\Big]\frac{1}{1+\delta S}. \tag{9.35}$$

At the water pseudo-steady state (see Chapter 8 Section 8.5.2) this characteristic speed expression simplifies to

$$\frac{\mathrm{d}z}{\mathrm{d}t} = \frac{W}{1+\delta S^*}, \tag{9.36}$$

where S^* is the pseudo-steady state water saturation profile. Thus, for $W = 0.05$, $\delta = 1.67 \times 10^{-3}$ and $S^* \approx 0.6$ the distance between the curves plotted on Figure 9.1 (a) should be of order $dz = 0.05 \times dt = 10^{-3}$ for dimensionless time interval $dt = 12[\text{days}]/505[\text{days}]$, which is what one observes also numerically[2]. Thus, in dimensional terms, the phosphate fertiliser moves into the soil at approximate speed of 4×10^{-3} cm per day, i.e., during the full 4 month long growing season fertiliser would move only to 0.5 cm depth in the soil. Thus, any effect of phosphate fertiliser on groundwater will occur on a long time-scale. However, because of its accumulation at the soil surface, the risk of river pollution due to surface runoff is quite considerable.

The small scale changes in the phosphate concentration profile due to the simultaneous water and nutrient uptake in the rooting region are presented in Figure 9.1 (b). As we see, the resulting concentration profiles are quite complex, however, they can be explained by the effective nutrient sink/source term in the equation (9.13). The effective sink/source term for nutrient in that equation is given as a balance between the nutrient uptake and rise in nutrient concentration due to the water uptake, i.e., by $-F + c\,F_w$. Thus, if the water uptake is large enough, then the nutrient concentration will increase, however, if it is small then the nutrient concentration will decrease due to the nutrient uptake. The characteristic step profile observed in the region $0 < z < 0.1$ develops because the initially uniform uptake of nutrients in this region is over balanced by the non-uniform water uptake[3]. We also observe the effect of the apical non-branching zone in the region $0.5 < z < 1$ where initially due to the water uptake the concentration increases but once the pseudo-steady state in the

[2]Estimating the distance between the curves numerically at $c = 1$ on Figure 9.1 (a) we find that it varies between 1.1×10^{-3} and 7.6×10^{-4}.

[3]We are modelling the simultaneous water flow inside the root system and outside in the soil.

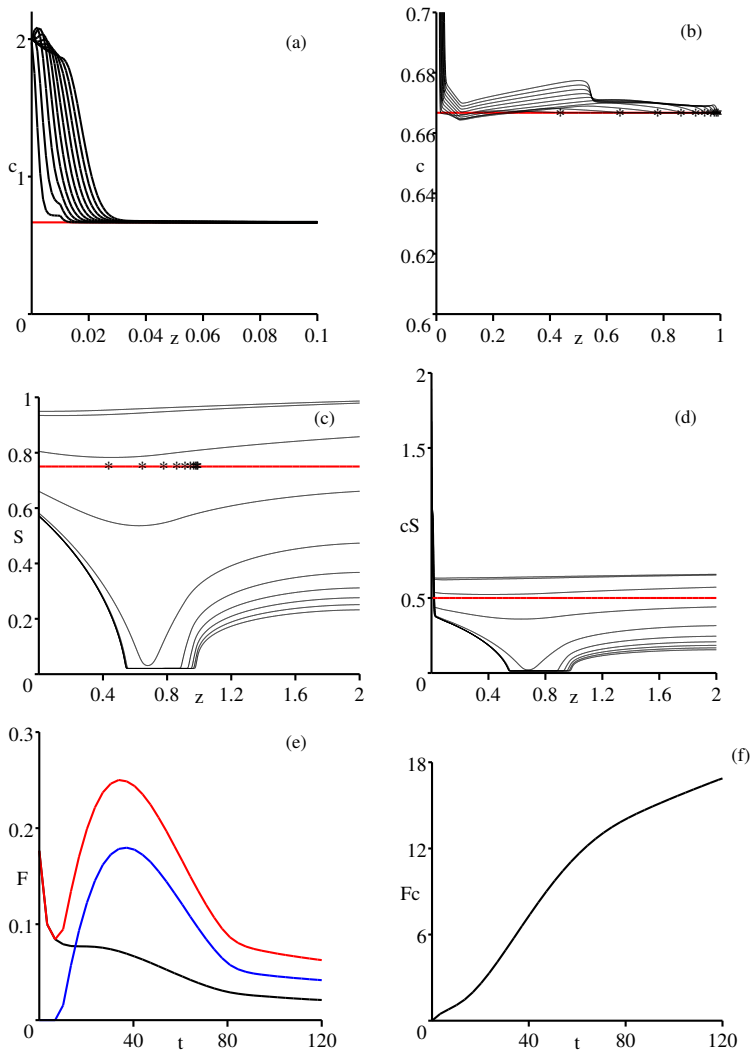

Figure 9.1: Numerical solution for phosphate uptake with initial water saturation profile $S_\infty = 0.75$. Corresponding initial condition for $S_\infty c_\infty = 0.5$ is $c_\infty = 0.66$ at $t = 0$. Calculations are for constant rate of rainfall $W = 0.05$ and rate of fertiliser application $\varrho = 0.1$. Red lines show the initial conditions, black lines present the numerical solution after equal time intervals of 12 days. (a) the change in phosphate concentration due to the fertiliser movement near the soil surface; (b) change in phosphate concentration on the larger spatial scale ($*$ shows the successive positions of zero order tip); (c) the water saturation profile in the soil; (d) the total amount of soluble phosphate in the soil; (e) the rate of phosphate uptake [μmol day^{-1}] by the root system as a function of time [days] (black line shows the uptake by zero order root, blue line shows the uptake by first order lateral branches and red line shows the total uptake of phosphate by the root system); (f) shows the cumulative uptake [μmol] as a function of time [days].

water saturation has developed and thus the water uptake in that "dry region" stops (see also Figure 9.1 (c) for water saturation profile), the nutrient uptake by the roots will start decreasing the nutrient concentration.

The total amount of phosphate available for plant uptake in the soil pore water is shown in Figure 9.1 (d). We observe that the total amount of phosphate available to the plant increases as the water saturation increases and *vice versa*. This is due to the fast equilibration between phosphate in solid and liquid fractions.

The rate of phosphate uptake is shown on Figure 9.1 (e). The rate of phosphate uptake by first order lateral sub-branches is at least twice as much as the rate of uptake by zero order roots. We also see that maximum rate of uptake occurs during the main growing season on about the 40th day from planting.

The results on Figure 9.1 were presented for a constant rate of rainfall and for a constant fertiliser application rate. However, the rate of rainfall can be very unpredictable. The fertiliser is also not applied continuously to the soil over the full growing season. Instead it is applied maybe once in spring. Thus, on Figure 9.2 we present the results of numerical computation for random rainfall events, i.e., rate of rainfall is a random number drawn from the uniform distribution in interval $0 < W < 0.1$ with the average rate of rainfall given by $\widehat{W} = 0.05$. We also consider that there is only a single fertilisation event with duration of 1 day, i.e., $\varrho = 12$ for $0 < t < 1$ [day] such that the overall amount of fertiliser applied over 4 month period is the same as in the case of constant fertilisation.

As we see on Figure 9.2 (a), due to the single fertilisation event, the phosphate concentration at the soil surface rises initially quite high. However, at later times, when there is no fertilisation, the phosphate concentration at the soil surface falls to a low level due to the removal of it by the plant roots and due to the vertical infiltration of water. As we see, the influence of fertiliser does not reach out into the deeper layers in the soil (Figure 9.2 (a) and (b)). In this situation the rate of phosphate uptake by plant roots is strongly dependent on the rate of rainfall. The interesting feature to note here is that in comparison to zero order root phosphate uptake, the uptake by first order lateral branches is much more sensitive to the changes in rainfall. However, the first order lateral branches still take up most of the phosphate.

9.7.2 Numerical Results for Nitrate Uptake

The numerical solution to the simplified nitrate model is presented in Figure 9.3. The aspect to note here is the relatively faster rate of fertiliser movement into the soil and its accumulation near the boundary of the soil surface water pseudo steady state, i.e., near $z = z^* \approx 0.5$.

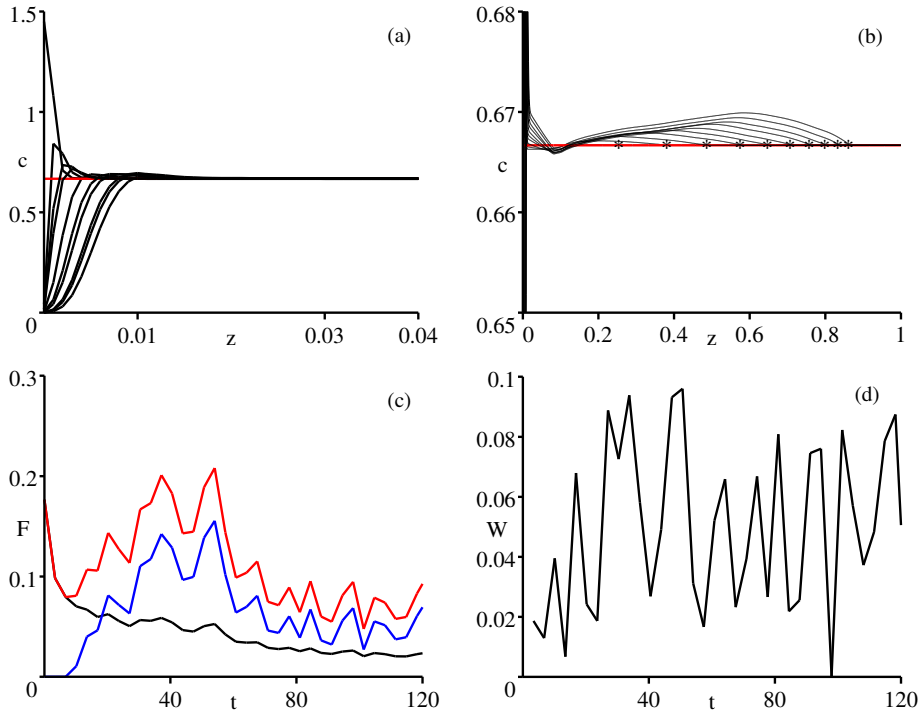

Figure 9.2: Numerical solution for phosphate uptake for uniformly distributed random rainfall with average $\widehat{W} = 0.05$ and single fertilisation event in the beginning of growing season, i.e., $\varrho = 12$ for time $0 < t < 1$ [day] and $\varrho = 0$ for the rest of time. Thus, the overall amount of fertiliser applied is the same as in the case of constant rate of fertilisation calculations presented in Figure 9.1. Lines shown after equal time interval 3 days. (a) the changes in phosphate levels near the soil surface due to the single fertilisation event and phosphate uptake by the plant roots; (b) changes in the phosphate concentration levels in the main rooting region ($*$ shows the position of the zero order root tip); (c) the rate of phosphate uptake [μmol day^{-1}] by the plant root system as a function of time [days] (black line shows the zero order root uptake, blue line shows the first order root uptake, and red line shows total phosphate uptake); (d) the rainfall pattern $W(t)$.

As mentioned in the case of phosphate fertiliser movement, the characteristic speed of fertiliser movement at the water pseudo-equilibria is given approximately by $\mathrm{d}z/\mathrm{d}t \approx W/(1 + \delta S^*)$. In dimensional terms, this corresponds to nitrate fertiliser movement of 0.95 cm per day, which is also what one observes in the numerics presented on Figure 9.3.

Thus, nitrate is highly mobile in the soil, mimicking the movement of water with the exception that it can start accumulating at the water "wet region" pseudo-equilibrium boundary at $z = z^*$, since behind it in the "dry region" the water mobility is very low. This accumulation effect has not been reported in the literature. However, we have neglected urea-ammonia-nitrite-nitrate cycle in the soil which might

provide an explanation for the lack of experimental evidence. However, the tentative conclusion we would like to draw from this calculation is that due to the high mobility of nitrate the development of a "dry" zone might serve as a barrier for fertiliser movement into the deeper layers of the soil, thus decreasing the risk of pollution. However, when the crop is harvested and the water uptake in the soil stops, this fertiliser will rapidly be transported to the deeper layers in the soil.

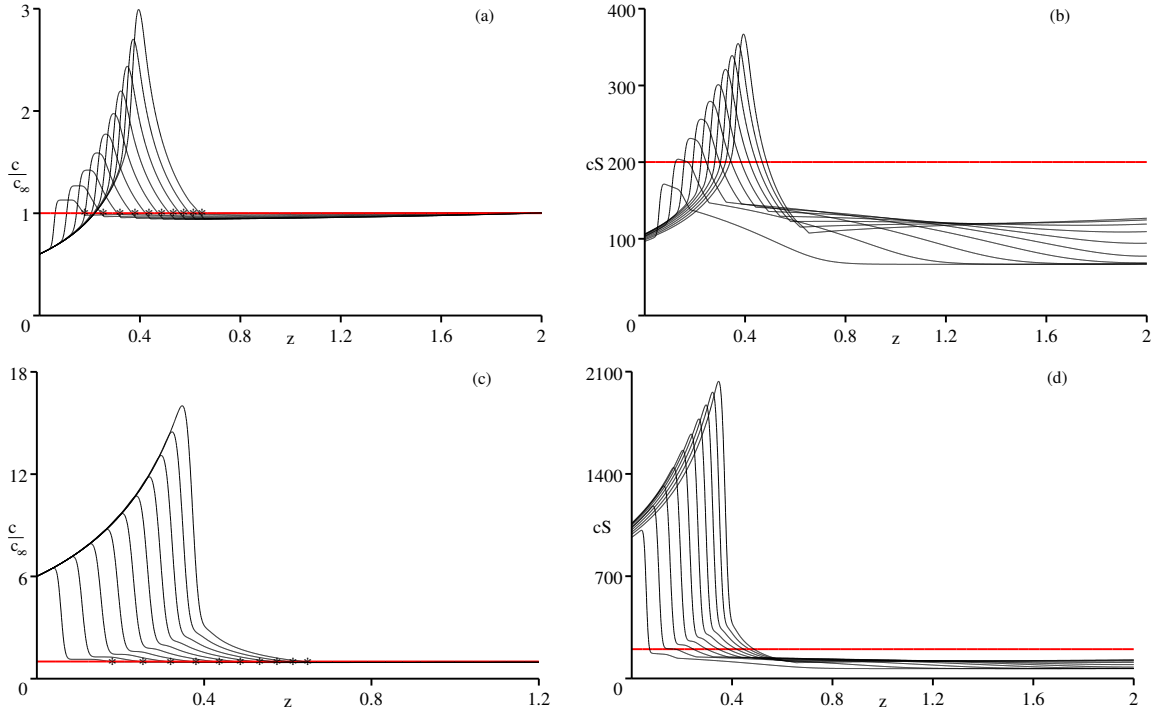

Figure 9.3: Nitrate concentration profiles in the soil for two different nitrate fertiliser regimes (a) and (b) for $\varrho = 0.8$ and (c) and (d) for $\varrho = 80$. (a) and (c) show the concentration profile of nitrate in the soil, and (b) and (d) show the overall amount of nitrate in the soil pore water. The rate of rainfall is $W = 0.05$, initial water saturation is $S = 0.75$ and initial nitrate concentration $c_\infty = 200/0.75$. Curves printed after equal time interval 2.4 days.

9.8 Conclusions

In this chapter we presented a model for simultaneous water and nutrient uptake by plant root systems. We found that phosphate, due to its large buffer power, remains relatively immobile in the soil despite large scale water movement. The risk of surface runoff due to the phosphate fertiliser application was found to be considerable since due to the continuous fertiliser application, nutrient started accumulating on the surface of the soil. However, when the continuous fertiliser application was replaced

by the spot fertilisation, the risk of surface runoff was reduced. The groundwater pollution with phosphate is strongly dependent on water movement and the soil's ability to resupply phosphate from the solid fraction, i.e., buffer power. Thus, if there is a substantial increase in the soil moisture, then more phosphate is released from the solid fraction and carried to the deeper layers in the soil.

The most interesting result of the phosphate uptake calculation is found by comparing the cumulative uptake in the absence of water movement to that when water movement is included (see Figure 9.4). We observe that the nutrient uptake in the latter case is lower than in the former case. This is because water uptake leads to the reduction in relative water saturation in the soil and thus a reduction in the phosphate available for uptake. As we will now discuss, this suggests an explanation for why the Barber model only agrees with some of the experimental measurements and not others.

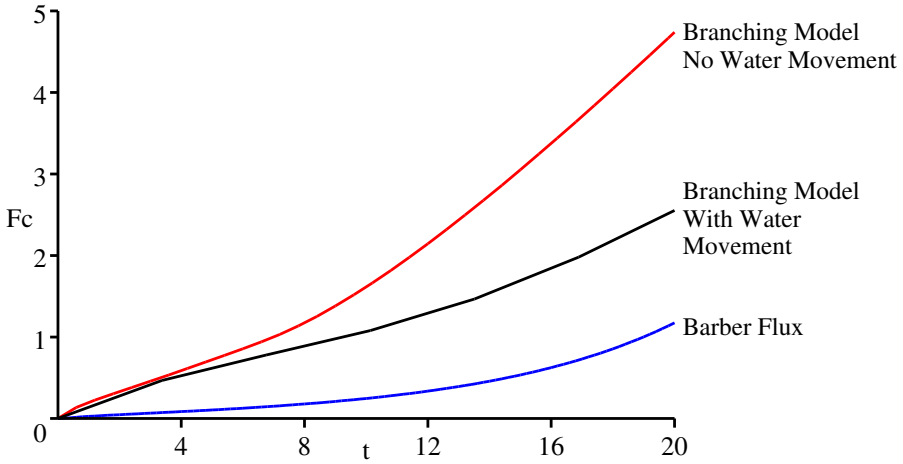

Figure 9.4: Cumulative uptake of phosphate [μmol] by the root branching structure as a function of time [days]. Model for nutrient uptake by branching system in absence of competition is presented in Chapter 6. Model for nutrient uptake by branching structure was presented in this chapter, i.e., Chapter 9. Barber calculation is assuming the single cylindrical root with volume averaged root radius, i.e., neglecting branching structure, and ignoring the water movement in the soil.

In this thesis it has been shown that the classical Barber volume averaged and exponentially growing[4] [6], [111], [112] phosphate uptake calculation will typically underestimate the phosphate uptake when there are low levels of phosphate in the soil. However, the Barber calculation has often been found to agree with the experimental measurements in situations when there is a high level of phosphate in the soil. Barber

[4]Barber neglects the root branching structure and water movement in his models, however, he constantly tops up the nutrient levels in the soil.

explains this discrepancy between the measured and predicted uptake of phosphate at low soil phosphate values by the absence of root hair and mychorrizae influence in his model and because he neglects "additional chemical effects"[5]. However, there are reasons to doubt each of these three explanations. Firstly, the discrepancy between measured and predicted uptake cannot be due to the neglect of root hairs, since the plant root nutrient uptake parameters were measured using the roots that do have root hairs. Thus all the effect of root hair presence has been "absorbed" into the experimentally measured values of Michaelis-Menten nutrient uptake coefficients F_m and K_m. Secondly, Barber often heated the soil for 6 days at 70°C in order to "stabilise" the phosphate conditions. However, because of this procedure it is unlikely that substantial quantities of fungi and their spores survived in this soil. Thus in the beginning of the experiment the probability that there was any fungi left in the soil is low, however it cannot be ruled out completely. One way of verifying the hypothesis that the mycorrhizae are important would be to actually look for mycorrhizae in the soil. Thirdly, the additional chemical effect of root exudates on nutrient uptake is quite controversial and all the phenomena observed are qualitative and not quantitative. I think that the differences between Barber's measured and predicted phosphate uptake can be explained by the failure of Barber's model to take into account the root branching structure and effects of water uptake.

The results on cumulative uptake of phosphate by a root branching structure are presented in Figure 9.4. We see that the Barber calculation clearly underestimates the uptake of phosphate from the soil. Inclusion of the branching structure and root competition to the classical cylindrical root model, presented in Chapter 6, will indeed correct the estimate of phosphate uptake "upwards". However, the inclusion of water movement in the model corrects the estimate of phosphate uptake "downwards".

We now need to discuss why Barber's model agrees so well with experimental measurements at high phosphate values, but underestimates the uptake at low phosphate values. Barber found in his experiments on root morphology and nutrient uptake [112] that the overall mass of roots in the case of high phosphate content was much higher than in the case of low phosphate content. When the root mass is higher then the water uptake is higher and therefore the water movement correction "downwards" in comparison to the branching correction "upwards" might well be such that it causes the Barber calculation to agree with the measured uptake. However, if the root mass is lower, as it is in the case of low phosphate soil, the water uptake "downward" correction is smaller and thus the Barber calculation does not agree with the experimental measurements, instead it underestimates it.

[5]He probably means that these "additional chemical effects" are linked to the root exudates that are present on the root surface.

In order to clarify these problems with nutrient uptake by root systems, more accurate simultaneous measurements of nutrient and water uptake together with root branching structure development should be carried out. Technically these experiments are not very difficult, however, they are very time-consuming and labour-intensive. In order to get conclusive experimental verification of different mechanisms that control plant nutrient uptake this consistent experimental effort has to be made in order to determine if the error rises from inaccuracies in the single root model (i.e. Nye-Tinker-Barber model), as argued by Barber and coworkers, or from neglecting water movement and not treating the root branching structure adequately.

Chapter 10

Final Conclusions and Future Developments

In this thesis I set out to develop a modelling framework for calculating the nutrient uptake by realistic plant root networks. The major aspect of this research was to show how to go from small cylindrical root scale behaviour to the larger root branching structure scale.

Up until now, the problem of nutrient uptake by plant root systems has been addressed using a computational model for a single cylindrical root. Attempts at extending this approach to three dimensional root branching structure simulations have been made. This approach relies heavily on the recent rapid increase in computational power. However, these computational models suffer from several problems: large computational errors in upscaling the cylindrical computation model to 3D computational branching structure model; problems with its comparison to experimental measurements, since in experiments the quantity measured is likely to be some average level of nutrient in the soil, i.e., volume average, as oppose to exact nutrient concentration around specific 3D root branching structure.

In this thesis I describe an alternative approach to the three dimensional computational simulations, i.e., space averaged modelling of nutrient uptake by root branching networks. The aim is to address the real life problems of nutrient delivery to roots of agricultural plants and to identify the possible "bottle necks" in this system and the ways of overcoming them.

I began the modelling in Chapter 2 by presenting the derivation of the Nye-Tinker-Barber model for the nutrient uptake by one cylindrical root in an infinite extent of soil. The nutrient was considered to be diffusing in the soil pore water and taken up by the root according to a non-linear nutrient uptake law. Previously the non-linear uptake law has led to the model being solved numerically and only for the simplest root geometry, a single semi-infinite straight root. The increase in

numerical complexity on extending the model to three dimensional root distributions had prevented the extension of this model to more realistic root distributions. In Chapter 2, I present the derivation of an approximate analytic solution to this model. The simplicity and transparency of this analytic approximation provides us with a very powerful tool for tackling the nutrient uptake by more complicated root systems, i.e., root branching structures.

Before proceeding to consider the root branching systems, I considered two complications to the nutrient uptake by cylindrical roots: root hairs and mycorrhizae. I present this in Chapter 3. Root hairs are small, thin, unicellular extensions of root surface cells that can be many times longer than the radius of the root itself. Thus, when present, they are thought to be very important for nutrient uptake. I extend the cylindrical root model, presented in Chapter 2, to calculate the nutrient uptake by root hairs and derive an analytic solution. Use of the analytic formula enables me to suggest future experiments on the importance of the root hairs. One of the most important experiments to be conducted would involve the use of genetically modified plants. It is well understood in developmental biology that, using genetic modification, one can get mutant roots which develop no root hairs, develop root hairs from every cell on root epidermis, and develop intermediate number of root hairs (wild type plants) [32], [31]. The length of root hairs is also thought to be controllable. Thus, an experiment that measures the removal of nutrients from the soil by bald, hairy and wild type roots would validate the root hair model presented in Chapter 3.

Mycorrhizae are fungi that grow in the soil and form symbiotic links with roots, i.e., mycorrhizae take up nutrients from soil distant from the root and transport it to the root where they exchange the nutrients for carbon compounds which they need for their own functioning. In Chapter 3, I develop a model to quantify the importance of mycorrhizae to the root. Based on this, I suggest more detailed experiments aimed at analysing the mycorrhizal influence on soil nutrient levels and plant nutrition. Essentially, there are two alternative experimental ways of approaching the mycorrhizal nutrient uptake problem. The first approach would be to make more accurate measurements of mycorrhizal length density around each individual root. However, since mycorrhizae are very small this approach might prove experimentally very difficult. An alternative way would involve studying the mycorrhizal development patterns and measuring the dependence of elongation rates and branching densities on the soil and nutrient environment. This approach would probably be the most efficient one, since it will also, in addition to addressing aspects of plant nutrition, address the aspects of fungal development and branching.

In Chapter 4, I extend the model for nutrient uptake by a single cylindrical root to developing, branching root systems. Roots branch by developing lateral branches

from the side of a parent root at a discrete set of branching points. I develop a model for calculating the overall length of each sub-branch in the root system for three different orders of lateral branches using the measured properties of the maize root system. As a first approximation, I then calculate the nutrient uptake by this developing branching structure in the absence of competition between sub-branches. Using this calculation I discuss inaccuracies in earlier interpretations of experimental results. In particular, the assumption of constant average root radius of branching root population is shown to be erroneous, resulting in inaccuracies in nutrient uptake calculations for immobile nutrients, i.e., mainly for phosphate and potassium. This clarifies previously "unexplained discrepancies" in experimental data on nutrient uptake by developing root systems.

As some nutrients are highly mobile in the soil, e.g., nitrate, it is important to account for inter-root competition in the soil. This is first addressed in Chapter 5 for static root distributions and later in Chapter 6 for the developing root branching systems. Starting from the simplest case, i.e., a time independent root system, I develop a model for nutrient uptake by a root system in the presence of competition between sub-branches and the parent root. To calculate the local nutrient uptake I use the analytical solution for one cylindrical root found in Chapter 2 to estimate the spatial dependence of the local nutrient concentration inside the rooting region.

However, root systems of agricultural plants grow actively for most of their life span. Thus, for more realistic estimates of nutrient uptake by agriculturally important plants, such as maize, beans etc., the effect of root growth on nutrient levels in the soil needs to be incorporated in the model. Building on the understanding developed during the work presented in Chapters 4 and 5, I expand my model to include a root branching structure that develops in time and space. This enables me to calculate the changes in local soil nutrient concentration due to the depletion by the growing root system.

In Chapters 5 and 6 I show that in a fully saturated soil in the absence of vertical water movement the fertiliser that is applied at the soil surface occupies only a very small region of soil near the surface. This is because of the diffusion of nutrient ions in the soil pore water is very slow. This suggests the need for modelling the nutrient uptake simultaneously with water movement in the soil and water uptake by root branching system.

Therefore, in Chapters 7 and 8, I introduce a model for water movement in the soil and uptake by the root system. Experimental observations have shown that water and nutrient uptake are often inter-related. I develop a water uptake model using the same methodology used for the nutrient uptake model, i.e., I first calculate the water uptake by a single cylindrical root in an infinite extent of soil (Chapter

7) and then expand the model to calculate the water uptake by the root branching structure (Chapter 8). I also include the longitudinal transport of water along the root to the shoot by solving the relevant transport equations for water flow inside the root. Again, as in the nutrient uptake case, using asymptotic analysis techniques I developed an analytic formula for the water flux into one cylindrical root in the infinite extent of soil. In addition, I also quantify the flow of water along the root and the resulting water pressure variations inside the root.

Based on the analytic expressions developed for a single root in Chapter 7, I extend the model to include the developing root branching structure in Chapter 8. One important complication of the model for water uptake by plant roots was the need to model the water flow inside the root branching network, i.e., the water taken up by lateral branches flows into the main parent root and influences the overall water flow speed in there. I treat this by considering the mass and flow balances inside the root branching network and in the soil. Using asymptotic analysis techniques I show that when there is a flux of water into the soil from the top due to rainfall, the water flow can develop two regions of pseudo-equilibrium saturation. The first pseudo-equilibrium region characterises the so called "wet region" near the soil surface, where due to the rainwater the soil has a higher moisture level than in the rest of the soil immediately below it. The second pseudo equilibrium region characterises the so called "dry region" in the soil, where the water saturation has dropped to a very low level due to water uptake by the roots and where rainwater cannot reach since all of it gets taken up by the roots within the wet region.

Since we found in Chapter 8 that considerable water saturation differences in the soil can be present, their influence on the nutrient movement in the soil needs investigation. In Chapter 9 a complete model for simultaneous water and nutrient movement in the soil and uptake by root system is presented based on the systematic theoretical developments presented in the previous chapters. Using ecologically realistic rates of rainfall and fertiliser application rates I calculate the rate of nutrient uptake by the root system of a typical agricultural plant.

Previous crop models for determining the optimum fertiliser application rates have used heuristic statistical models validated using experimental observations to predict the rate of fertiliser uptake by plants. However, the model that I have built provides more insight into the limiting mechanisms in that process. Another possible agricultural application of the model is to guide genetic modification of crops. Genetic modification holds the promise of being able to engineer plants for different environmental conditions. However, without a model for the effect of any modification, improvements will be due to trial and error, and thus slower and more costly. A related, but more academic application for the model is the explanation of different root

morphologies. Evolution can be considered to be the optimisation of benefit relative to cost. The model will enable ecologists to quantify the efficiency of nutrient uptake by morphologically different root systems, both those that exist in nature and those that do not, and therefore determine what morphology is optimum for any specific set of soil conditions. This has not been feasible with previous computational models due to their complexity and computational inefficiency.

At this final stage of a theoretical thesis, the author usually outlines the possible ways of extending the modelling of the problem they have tackled. However, I will not do so, since the most vital thing that needs to be done is the consistent experimental verification of all the models presented in this thesis. There are many nutrient uptake measurements presented in the literature. In general there is a lack of simultaneous nutrient and water uptake measurements by the root branching structures whose morphology has been determined in detail. In experimental measurements of nutrient uptake by plant root systems, the most common measurement of root structure is the overall length and weight of roots in the end of the experiment. However, as I show in this thesis, models using this measure of the root network size, neglecting the root branching structure, can lead to a difference of approximately 30% between the measured and predicted nutrient uptake. Thus, there is a clear need for experiments that measure simultaneously the overall nutrient uptake by the root branching structure and the morphological properties of the root system, i.e., number and size of the sub-branches together with the elongation rates. This way the models presented in this thesis can be properly calibrated.

The second area of experiments that needs attention, and which can lead to future modelling developments, are the measurements of nutrient uptake in relation to internal nutrient status of the plant. In Chapters 7-8, the model for water uptake by plant roots is described in relation to water movement inside the root and outside. Thus with the use of modern experimental techniques, the Michaelis-Menten nutrient uptake law should be reviewed and re-derived based on basic molecular chemistry principles. I have shown in this thesis how one would treat this type of system considering water flow. However, when the information becomes available, one can re-derive the model for nutrient uptake by branching structure using similar techniques.

Finally, as discussed in Chapter 9, a model considering more detailed nitrogen cycle in the soil is needed. In this thesis an illustrative example of nitrate uptake by root branching structure was presented. However, nitrogen containing compounds are usually applied to the soil as urea, which will via ammonia and nitrite turn into nitrate. All those compounds, even the very short lived ones, are available for plant uptake. Therefore more detailed modelling would clarify the processes that limit the transport and dynamics of nitrogen containing compounds in the soil.

Bibliography

[1] M. Abramowitz and J. A. Stegun. *Handbook of Mathematical Functions*. Dover Publications Inc., 1969.

[2] B. Acock and Ya. A. Pachepsky. Convective-diffusive model of two-dimensional root growth and proliferation. *Plant and Soil*, **180**:231–240, 1996.

[3] M. Allaby. *A Dictionary of Plant Sciences*. Oxford University Press, 1998.

[4] C. W. N. Anderson, R. R. Brooks, R. B. Stewart, and R. Simcock. Harvesting a crop of gold in plants. *Nature*, **395**:553, 1998.

[5] J.P. Baldwin, P.B. Tinker, and P.H. Nye. Uptake of solutes by multiple root systems from soil. II The theoretical effects of rooting density and pattern on uptake of nutrients from soil. *Plant and Soil*, **36**:693–708, 1972.

[6] S. A. Barber. *Soil Nutrient Bioavailability. A Mechanistic Approach*. A Wiley-Interscience Publication, New York, 1984.

[7] G.M. Barrow. *Physical Chemistry*. McGraw-Hill Kogakusha Ltd., 4th edition, 1971.

[8] J. Bear. *Dynamics of fluids in porous media*. Dover, 1988.

[9] J. Bear and A. Verruijt. *Modelling groundwater flow and pollution*. Reidel, Dordrecht, 1987.

[10] A. G. Bengough. Modelling rooting depth and soil strength in a drying soil profile. *Journal of Theoretical Biology*, **186**:327–338, 1997.

[11] K. K. S. Bhat and P. H. Nye. Diffusion of phosphate to plant roots in soil. I Qualitative autoradiography of the depletion zone. *Plant and Soil*, **38**:161–175, 1973.

[12] K. K. S. Bhat, P. H. Nye, and J. P. Baldwin. Diffusion of phosphate to plant roots in soil. IV The concentration distance profile in the rhizosphere of roots with root hairs in the rhizosphere of roots with root hairs in a low-P soil. *Plant and Soil*, **44**:63–72, 1976.

[13] D. Binkley, H. Burnham, and H. L. Allen. Water quality impacts of forest fertilization with nitrogen and phosphorus. *Forest Ecology and Management*, **121**:191–213, 1999.

[14] P. Bonfante-Fasolo. Anatomy and morphology of VA mycorrhizae. In Ll. C. Powell and D.J. Bangyaraj, editors, *VA Mycorrhiza*, pages 5–33. CRC Press, Inc., Boca Raton, Florida, 1984.

[15] K. Borch, T. J. Bouma, J. P. Lynch, and K. M. Brown. Ethylene: a regulator of root architectural responses to soil phosphorus availability. *Plant, Cell and Environment*, **22**:425–431, 1999.

[16] D. J. F. Bowling. *Uptake of Ions by Plant Roots*. Chapman and Hall, A Halstead Press, John Wiley and Sons, Inc., 1976.

[17] A. Buston, R. Roman, R. Caballero, J. A. Díes, M. C. Cartagena, A. Vallejo, and A. Caballero. Water and solute movement under conventional corn in central Spain. II Salt leaching. *Soil Science Society of America Journal*, **60**:1536–1540, 1996.

[18] M. M. Caldwell, D. M. Eissenstat, and J. H. Richards. Competition for phosphorus: differential uptake from dual-isotope-labelled soil interspaces between shrub and grass. *Science*, **229**:384–386, 1985.

[19] H. S. Carslaw and J. C. Jaeger. *Conduction of Heat in Solids*. Oxford University Press, 1959.

[20] D-X. Chen and J. H. Lieth. Two dimensional model of water transport in the root zone and plant for container-grown crysanthemum. *Agricultural and Forest Meterology*, **59**:129–148, 1992.

[21] N. Claassen and S. A. Barber. A method for characterizing the relation between nutrient concentration and the flux into roots of intact plants. *Plant Physiology*, **54**:564–568, 1974.

[22] D. T. Clarkson. Root structure and sites of ion uptake. In Y. Waisel, U. Kafkafi, and A. Eshel, editors, *Plant Roots: The Hidden Half*, pages 483–510. Marcel Dekker Inc, New York, 2 edition, 1996.

[23] V. Clausnitzer and J. W. Hopmans. Simultaneous modelling of transient three-dimensional root growth and soil water flow. *Plant and Soil*, **164**:299–314, 1994.

[24] V. Clausnizer, J. W. Hopmans, and J. L. Starr. Parameter uncertainty analysis of common infiltration models. *Soil Science Society of America Journal*, **62**:1477–1487, 1998.

[25] P. R. Darrah. Interactions between root exudates, mineral nutrition and plant growth. In H. Lambers, H. Porter, and M. M. I. Van Vuuren, editors, *Inherent variation in plant growth. Physiological mechanisms and ecological consequences.*, pages 159–181. Backhuys Publishers, Leiden, The Netherlands, 1998.

[26] C. H. Davis. Absorption of soil moisture by maize roots. *Botanical Gazette*, **101**:791–805, 1940.

[27] C. Dawson. Fertiliser statistics. *The Fertiliser Review 1998*, 1998.

[28] A. J. Diggle. ROOTMAP - a model in three-dimensinal coordinates of the growth and structure of fibrous root systems. *Plant and Soil*, **105**:169–178, 1988.

[29] S. R. Dodge. An even more humongous fungus. Press Release, July 24th 2000. Pacific Northwest Research Station/USDA Forest Service, `http://www.fs.fed.us/pnw/news/fungus.htm`.

[30] L. Dolan, K. Janmaat, V. Willemsen, P. Linstead, S. Poething, K. Roberts, and B. Scheres. Cellular organisation of the *Arabidopsis thaliana* root. *Development*, **119**:71–84, 1993.

[31] L. Dolan and K. Okada. Signalling in cell type specification. *Seminars in Cell and Developmental Biology*, **10**:149–156, 1999.

[32] L. Dolan and B. Scheres. Root pattern: Shooting in the dark? *Seminars in Cell and Developmental Biology*, **9**:201–206, 1998.

[33] C. Doussan, L. Pagès, and G. Vercambre. Modelling of the hydraulic architecture of root systems: An integrated approach to water absorption- model description. *Annals of Botany*, **81**:213–223, 1998.

[34] C. Doussan, G. Vercambre, and L. Pagès. Modelling of the hydraulic architecture of root systems: An integrated approach to water absorption- distribution of axial and radial conductances in maize. *Annals of Botany*, **81**:225–232, 1998.

[35] M. C. Drew and L. R. Saker. Nutrient supply and the growth of the seminal root system in barley. *Journal of Experimental Botany*, **29**:435–451, 1978.

[36] R. Edwards. Heat your greens. *New Scientist*, (2147):21, August 1998.

[37] G. Ellis, I. Adatia, M. Yazdanpanah, and S. K. Makela. Nitrite and nitrate analyses: a clinical biochemistry perspective. *Clinical Biochemistry*, **31**(4):195–220, 1998.

[38] A. Fahn. *Plant Anatomy*. Pergamon Press, 4 edition, 1990.

[39] J. E. Fernándes, J. M Murillo, F. Moreno, F. Cabrera, and E. Fernández-Boy. Reducing fertilization for maize in southwest Spain. *Communications in Soil Science and Plant Analysis*, **29**:2829–2840, 1998.

[40] E. L. Fiscus, A. Klute, and M. R. Kaufman. An interpretation of some whole plant water transport phenomena. *Plant Physiology*, **71**:810–817, 1983.

[41] A. C. Fowler. *Mathematical Models in the Applied Sciences*. Cambridge University Press, 1997.

[42] R. A. Freeze and J. A. Cherry. *Groundwater*. Prentice-Hall, Inc., 1979.

[43] J. Frensch and E. Steudle. Axial and radial hydraulic resistance to roots of maize (*Zea mays* l.). *Plant Physiology*, **91**:719–726, 1989.

[44] W. R. Gardner. Relation of root distribution to water uptake and availability. *Agronomy Journal*, **56**:41–45, 1964.

[45] W. R. Gardner and C. F. Ehlig. Some observations on the movement of water to plant roots. *Agronomy Journal*, **54**:453–456, 1962.

[46] Z. Ge, G. Rubio, and J. P. Lynch. The importance of root gravitropism for inter-root competition and phosphorus acquisition efficiency: results from a geometric simulation model. *Plant and Soil*, **218**:159–171, 2000.

[47] E. George, E. Häussler, S. K. Kothari, X.-L. Li, and H. Marschner. Contribution of mycorrhizal hyphae to nutrient and water uptake of plants. In D. J. Read, D. H. Lewis, and A. H. Fitter, editors, *Mycorrhizas in Ecosystems*, pages 42–47. CAB International, 1992.

[48] D. A. Goolsby. Mississippi basin nitrogen flux believed to cause gulf hypoxia. *EOS Transactions, American Geophysical Union*, **81**(29), 2000.

[49] P. Grabarnik, L. Pagès, and A. G. Bengough. Geometrical properties of simulated maize root systems, consequences for length density and intersection density. *Plant and Soil*, **200**:157–167, 1998.

[50] D. J. Greenwood and T.V. Karpinets. Dynamic model for the effects of K-fertiliser on crop growth, K-uptake and soil-K in arable cropping. 1. Description of the model. *Soil Use and Management*, **13**:178–183, 1997.

[51] P. J. Gregory. Water and crop growth. In A. Wild, editor, *Russell's Soil Conditions and Plant Growth*, pages 338–377. Academic Press, 1988.

[52] S. K. Gupta, R. C. Gupta, A. B. Gupta, A. K. Seth, J. L. Bassin, and A. Gupta. Recurrent acute respiratory tract infections in areas with high nitrate concentration. *Environmental Health Perspectives*, **108**(4):363–366, 2000.

[53] S. K. Gupta, R. C. Gupta, A. K. Seth, A. B. Gupta, J. L. Bassin, and A. Gupta. Methaemoglobinaemia in areas with high nitrate concentration in drinking water. *National Medical Journal of India*, **13**(2):58–61, 2000.

[54] C. Hackett and D. A. Rose. A model of the extension and branching of a seminar root of barley, and its use in studying relations between root dimensions, I The model. *Austalian Journal of Biological Science*, **25**:669–679, 1972.

[55] C. Hackett and D. A. Rose. A model of the extension and branching of a seminar root of barley, and its use in studying relations between root dimensions, II Results and inferences from manipulation of the model. *Austalian Journal of Biological Science*, **25**:681–690, 1972.

[56] E. J. Hinch. *Perturbation Methods*. Cambridge University Press, Cambridge, 1991.

[57] R. M. Hofer. Root hairs. In Y. Waisel, U. Kafkafi, and A. Eshel, editors, *Plant Roots: The Hidden Half*, pages 111–126. Marcel Dekker Inc, New York, 2 edition, 1996.

[58] F. Hoppensteadt. *Mathematical Methods of Population Biology*. Cambridge Studies in Mathematical Biology. Cambridge University Press, 1982.

[59] N. Ingerpuu, K. Kull, and K. Vellak. Bryophyte vegetation in a wooded meadow: relationships with phanerogam diversity and responses to fertilisation. *Plant Ecology*, **2**(134):163–171, 1998.

[60] S. Itoh and S. A. Barber. A numerical solution of whole plant nutrient uptake for soil-root systems with root hairs. *Plant and Soil*, **70**:403–413, 1983.

[61] S. Iwata, T. Tabuchi, and B. P. Warkentin. *Soil Water Interactions*. Marcel Dekker Inc., 1988.

[62] M. B. Jackson, W. J. Davies, and M. A. Else. Pressure-flow relationships, xylem solutes and root hydraulic conductance in flooded tomato plants. *Annals of Botany*, **77**:17–24, 1996.

[63] R. B. Jackson, J. H. Manwaring, and M. M. Caldwell. Rapid physiological adjustment of roots to localised soil enrichment. *Nature*, **344**:58–59, 1990.

[64] I. Jakobsen and A. D. Abbott, L. K. Robson. External hyphae of vesicular-arbuscular mycorrhizal fungi associated with *Trifolium subterraneum* L. 1. Spread of hyphae and phosphorus inflow into the roots. *New Phytologist*, **120**:371–380, 1992.

[65] I. Jakobsen and A. D. Abbott, L. K. Robson. External hyphae of vesicular-arbuscular mycorrhizal fungi associated with *Trifolium subterraneum* L. 2. Hyphal transport ^{32}P over defined distances. *New Phytologist*, **120**:509–516, 1992.

[66] E. J. Joner and I. Jakobsen. Growth and extracellular phosphatase activity of arbuscular mycorrhizal hyphae as influenced by soil organic matter. *Soil Biology and Biochemistry*, **27**(9):1153–1159, 1995.

[67] A Jungk and N. Claassen. Ion diffusion in the soil-root system. *Advances in Agronomy*, **61**:53–110, 1997.

[68] J. Kevorkian and J. D. Cole. *Perturbation methods in applied mathematics*. Springer-Verlag, 1981.

[69] J. M. H. Knops, D. Tilman, N. M. Haddad, S. Naeem, C. E. Mitchell, J. Haarstad, M. E. Ritchie, K. M. Howe, P. B. Reich, E. Siemann, and J. Groth. Effects of plant species richness on invasion dynamics, disease outbreaks, insect abundances and diversity. *Ecology Letters*, **2**:286–293, 1999.

[70] R. Kuchenbuch, N. Claassen, and A. Junk. Potassium availability in relation to soil moisture I. Effect of soil moisture on potassium diffusion, root growth and potassium uptake by onion roots. *Plant and Soil*, **95**:221–231, 1986.

[71] F. Lafolie, L. Bruckler, and F. Tardieu. Modelling root water potential and soil-root water transport. I Model Presentation. *Soil Science Society of America Journal*, **55**(5):1203–1212, 1991.

[72] F. Lafolie, L. Bruckler, and F. Tardieu. Modelling root water potential and soil-root water transport. II Field Comparisons. *Soil Science Society of America Journal*, **55**(5):1212–1220, 1991.

[73] J. J. Landsberg and N. D. Fowkes. Water movement through plant roots. *Annals of Botany*, **42**:493–508, 1978.

[74] P. Leadley. Interspecific plant competition for soil nutrient: the importance of diffusion limitations in the soil and fine scale heterogeneity in root distributions. Personal communication and talk given at GCTE Focus 3 conference Food and Forestry, Global Challenges, 20-23.09.1999, the University of Reading.

[75] V. G. Levich. *Physiochemical Hydrodynamics*. Prentice-Hall, 1962.

[76] M. Loreau and N. Behera. Phenotypic diversity and stability of ecosystem processes. *Theoretical Population Biology*, **56**:29–47, 1999.

[77] D. R. Lungley. The growth of root systems- a numerical computer simulation model. *Plant and Soil*, **38**:145–159, 1973.

[78] J. P. Lynch, K. L. Nielsen, R. D. David, and A. G. Jablokow. *SimRoot*: Modelling and visualization of root systems. *Plant and Soil*, **188**:139–151, 1997.

[79] L. A. Mackie-Dawson and D. Atkinson. Methodology for the study of roots in field experiments and the interpretation of results. In D. Atkinson, editor, *Plant root growth, an ecological perspective*, pages 25–48. Blackwell Scientific Publication, Oxford, 1991.

[80] H. Marschner. *Mineral Nutrition of Higher Plants*. Academic Press, 2 edition, 1995.

[81] A. D. McLaren. Temporal and vectorial reactions of nitrogen in soil: a review. *Canadian Journal of Soil Science*, **50**:97–109, 1970.

[82] R. B. Meagher. Phytoremediation of toxic elements and organic pollutants. *Current Opinion in Plant Biology*, **3**(5):153–162, 2000.

[83] D. M. Miller. Studies of root function in Zea mays. II Dimensions of the root system. *Canadian Journal of Botany*, **59**(5):811–818, 1981.

[84] F. J. Molz. Models of water transport in the soil-plant system. *Water Resources Research*, **17**(5):1245–1260, 1981.

[85] F. Y. Molz. Simulation of plant water uptake. In I. K. Iskander, editor, *Modelling wastewater renovation. Land treatment.*, pages 69–91. John Wiley and Sons, New York, 1981.

[86] F.J. Molz. Potential distributions in the soil-root system. *Agronomy Journal*, **67**:726–729, 1975.

[87] K. W. Morton and D. F. Mayers. *Numerical Solution of Partial Differential Equations*. Cambridge University Press, 1994.

[88] J. D. Murray. *Mathematical Biology*. Springer-Verlag, 2 edition, 1993.

[89] V. S. Myer and J. T. Ritchie. Resistance to water flow in the sorghum plant. *Plant Physiology*, **65**:33–39, 1980.

[90] E. I. Newman. Water movement through root systems. *Philosophical Transactions of Royal Society of London B*, **273**:463–478, 1976.

[91] M. N. Nimah and R. J. Hanks. Model for estimating soil water, plant and atmospheric interrelations. 1. Description and sensitivity. *Soil Science Society of America Proceedings*, **37**:522–527, 1973.

[92] G. B. North and P. S. Nobel. Radial hydraulic conductivity of individual root tissues of *Opuntia fiscus-indica* L. Miller as soil moisture varies. *Annals of Botany*, **77**:133–142, 1996.

[93] P. H. Nye. Towards the quantitative control of crop production and quality. II The scientific basis for guiding fertilizer and management practice, particularly in poorer countries. *Journal of Plant Nutrition*, **15**:1151–1173, 1992.

[94] P. H. Nye. The effect of root shrinkage on soil water inflow. *Philosophical Transactions of Royal Society of London B*, **345**:395–402, 1994.

[95] P.H. Nye and P.B. Tinker. *Solute Movement in the Soil-Root System*. Blackwell Scientific Publications, 1977.

[96] J. J. Oertli. Transport of water in the rhizosphere and in roots. In Y. Waisel, U. Kafkafi, and A. Eshel, editors, *Plant Roots: The Hidden Half*, pages 559–587. Marcel Dekker Inc., New York, 2 edition, 1996.

[97] L. Pagès, M. O. Jourdan, and D. Picard. A simulation model of the three-dimensional architecture of the maize root system. *Plant Soil*, **119**:147–154, 1989.

[98] L. Pagès and S. Pellerin. Evaluation of parameters describing the root system architecture of field grown maize plants *Zea mays L.* 2. Density, length and branching of first order lateral roots. *Plant and Soil*, **164**:169–176, 1994.

[99] J. B. Passioura. Water transport in and to roots. *Annual Review of Plant Physiology and Plant Molecular Biology*, **39**:245–265, 1988.

[100] S. Pellerin and L. Pagès. Evaluation of parameters describing the root system architecture of field grown maize plants *Zea mays L.* 1. Elongation of seminal and nodal roots and extension of their branched zone. *Plant and Soil*, **164**:155–167, 1994.

[101] S. Pellerin and L. Pagès. Evaluation in field conditions of a three-dimensional architectural model of the maize root system: comparison of simulated and observed horizontal root maps. *Plant and Soil*, **178**:101–112, 1996.

[102] B. Peterson, J. E. Hobbie, A. E. Hershey, M. A. Lock, T. E. Ford, J. R. Vestal, V. L. McKinley, M. C. Hullar, M. A. Miller, R. M. Ventullo, and G. S. Volk. Transformation of a tundra river from heterotrophy to autotrophy by addition of phosphorus. *Science*, **229**:1383–1386, 1985.

[103] C. L. Petrie, Z. J. Kabala, A. E. Hall, and J. Simunek. Water transport in an unsaturated medium to roots with differing local geometry. *Soil Science Society of America Journal*, **56**(6):1686–1694, 1992.

[104] D. Rimmel. Ultimate interface. *New Scientist, Inside Science*, (115):1–4, 1998.

[105] R. H. Ritchie and A. Y. Sakikura. Asymptotic expansions of solutions of the heat conduction equation in internally bounded cylindrical symmetry. *Journal of Applied Physics*, **27**(12):1453–1457, 1956.

[106] D. Robinson. Responses of plants to non-uniform supplies of nutrients. *New Phytologist*, **127**:635–674, 1994.

[107] H. R. Rowse, D. A. Stone, and A. Gerwitz. Simulation of the water distribution in soil. II The model for cropped soil and its comparison with experiment. *Plant and Soil*, **49**:533–550, 1978.

[108] U. M. Sainju and R. E. Good. Vertical root distribution in relation to soil properties in New Jersey Pilenlands Forest. *Plant and Soil*, **150**:87–97, 1993.

[109] F. E. Sanders. Modelling plant growth responses to vasicular arbuscular mycorrhizal infection. *Advances in Plant Pathology*, **9**:135–166, 1993.

[110] F. E. Sanders, P. B. Tinker, R. L. B. Black, and S. M. Palmerly. The development of endomycorrhizal root systems: I Spread of infection and growth promoting effects with four species of vesicular-arbuscular endophyte. *New Phytologist*, **78**:257–268, 1977.

[111] M. K. Schenk and S. A. Barber. Phosphate uptake by corn affected by soil characteristics and root morphology. *Soil Science Society of America Journal*, **43**:880–883, 1979.

[112] M. K. Schenk and S. A. Barber. Root characteristics of corn genotypes as related to P uptake. *Agronomy Journal*, **71**:921–924, 1979.

[113] S. E. Smith and D. J. Read. *Mycorrhizal Symbiosis*. Academic Press, 1997.

[114] S. Snapp, R. Koide, and J. Lynch. Exploitation of localised phosphorus-patches by common beans. *Plant and Soil*, **177**:211–218, 1995.

[115] L. Y. Spek. Generation and visualization of root-like structures in a three-dimensional space. *Plant Soil*, **197**:9–18, 1997.

[116] J. L. Starr, F. E. Broadbent, and D. R. Nielsen. Nitrogen transformations during continuous leaching. *Soil Science Society of America Proceedings*, **38**:283–289, 1974.

[117] E. Steudle and C.A. Peterson. How does water get through roots? *Journal of Experimental Botany*, **49**(322):775–788, 1998.

[118] F. Tardieu. Analysis of spatial variability of maize root density. 1. Effect of wheel compactation on the spatial arrangement of roots. *Plant and Soil*, **107**:259–266, 1988.

[119] F. Tardieu. Analysis of spatial variability of maize root density. 2. Distances between roots. *Plant and Soil*, **107**:267–272, 1988.

[120] F. Tardieu, L. Bruckler, and F. Lafolie. Root clumping may affect the root water potential and the resistance to soil-root water transport. *Plant and Soil*, **120**(2):291–301, 1992.

[121] H. M. Taylor and B. Klepper. Water uptake by cotton root systems. I An examination of assumptions in the single root model. *Soil Science*, **120**:57–67, 1975.

[122] D. Tennant. A test of a modified line intersect method of estimating root length. *Journal of Ecology*, **63**:995–1001, 1975.

[123] P. Thalier and L. Pagès. Modelling the influence of assimilate availability on root growth and architecture. *Plant and Soil*, **201**:307–320, 1998.

[124] P.G. Thorne. Fate of explosives in plant tissues contaminated during phytoremediation. Special Report 99-19, US Army Crops of Engineers, Cold Regions Research and Engineering Laboratory, December 1999.

[125] J. H. M. Thornley. Modelling water in crops and plant ecosystems. *Annals of Botany*, **77**:261–275, 1996.

[126] D. Timlin and Ya. A. Pachepsky. A modular soil and root process simulator. *Ecological Modelling*, **94**(1):67–80, 1997.

[127] P. B. Tinker. Soil chemistry of phosphorus and mycorrhizal effects on plant growth. In P. B. Tinker, editor, *Endomycorrhizas*, pages 353–371. Academic Press, 1975.

[128] P. B. Tinker. Transport of water to plant roots in soil. *Philosophical Transactions of Royal Society of London B*, **273**:445–461, 1976.

[129] P. B. Tinker and P. H. Nye. *Solute Movement in the Rhizosphere*. Oxford University Press, 2000.

[130] M. Th. van Genuchten. A closed-form equation for predicting the hydraulic conductivity of unsaturated soils. *Soil Science Society of America Journal*, **44**:892–898, 1980.

[131] G. T. Varney and M. J. Canny. Rates of water uptake into the mature root system of maize plants. *Plant Physiology*, **123**:775–786, 1993.

[132] G.T. Varney, M. J. Canny, X. L. Wang, and M.E. McCully. The branch roots of zea 1. 1st order branches, their number, sizes and division into classes. *Annals of Botany*, **67**:357–364, 1991.

[133] P. Weerathaworn, A. Soldati, and P. Stamp. Anatomy of seedling roots of tropical maize (*Zea mays*) L cultivars at low water supply. *Journal of Experimental Botany*, **43**(253):1015–1021, 1992.

[134] J. Wu, R. Zhang, and S. Gui. Modeling soil water movement with water uptake by roots. *Plant and Soil*, **215**:7–17, 1999.

[135] J. J. Wu and B. A. Babcock. Metamodelling potential nitrate water pollution in the central United States. *Journal of Environmental Quality*, **28**(6):1916–1928, 1999.

[136] Q. F. Xu, C. L. Tsai, and C. Y. Tsai. Interaction of potassium with the form and amount of nitrogen nutrition on growth of maize. *Plant Nutrition*, **15**(1):23–33, 1992.